CRWMS/M&O

Controlled Document Instructions

Complete only applicable items.

DATE		
08/02/93		
TO	COPY NO.	LOCATION NRC
ABRAMS CHARLOTTE	102066.0	WASHINGTON

Description of Document(s)

TITLE	DOCUMENT IDENTIFIER	EFFECTIVE DATE	NO. OF SHEETS
B00000000-01717-2200-00010 Rev. 0 A COMPARATIVE APPLICATION OF THE REPOSITORY INTEGRATION PROGRAM (RIP) TO TOTAL SYSTEM PERFORMANCE ASSESSMENT - 1991		07/16/93	

Instructions/Remarks

ISSUANCE OF:

A COMPARATIVE APPLICATION OF THE REPOSITORY INTEGRATION PROGRAM (RIP) TO TOTAL SYSTEM PERFORMANCE ASSESSMENT - 1991

YOU ARE NOW ON "MANAGED" DISTRIBUTION FOR THIS DOCUMENT

*** New issue - no obsolete material ***

see enclosure on shelf

12-106

original to Charlotte Abrams 4F3

Encl 1

102.3 WM-11 NH03

DUE BY: N/A

Receipt Acknowledgement

NAME	SIGNATURE	DATE
9310150268 930716 PDR WASTE WM-11 PDR		

Contact the Document Center staff member named below with any questions regarding these instructions.

BY	LOCATION	PHONE
DCC LAS VEGAS	TES3/423	(702) 794-5312

QAP-6-1

0029 (06/18/93)

WBS: 1.2.5.4.1
QA: N/A

Civilian Radioactive Waste Management System
Management & Operating Contractor

A COMPARATIVE APPLICATION OF THE REPOSITORY INTEGRATION PROGRAM (RIP) TO TOTAL SYSTEM PERFORMANCE ASSESSMENT - 1991

Document No. B00000000-01717-2200-00010-00

July 16, 1993

Prepared for:

U.S. Department of Energy
Yucca Mountain Site Characterization Project Office
P.O. Box 98608
Las Vegas, Nevada 89193-8608

Prepared by:

INTERA Inc.
101 Convention Center Drive
Las Vegas, Nevada 89109

Under Contract Number
DE-AC01-91RW00134

rec'd with letter dtd 7/16/93

WBS: 1.2.5.4.1
QA: N/A

Civilian Radioactive Waste Management System
Management & Operating Contractor

A COMPARATIVE APPLICATION OF THE REPOSITORY INTEGRATION PROGRAM (RIP) TO TOTAL SYSTEM PERFORMANCE ASSESSMENT - 1991

Document No. B00000000-01717-2200-00010-00

July 16, 1993

Prepared for:

U.S. Department of Energy
Yucca Mountain Site Characterization Project Office
P.O. Box 98608
Las Vegas, Nevada 89193-8608

Prepared by:

INTERA Inc.
101 Convention Center Drive
Las Vegas, Nevada 89109

Under Contract Number
DE-AC01-91RW00134

102 8

WBS: 1.2.5.4.1
QA: N/A

Civilian Radioactive Waste Management System
Management & Operating Contractor

A COMPARATIVE APPLICATION OF THE REPOSITORY INTEGRATION PROGRAM (RIP) TO TOTAL SYSTEM PERFORMANCE ASSESSMENT - 1991

Document No. B00000000-01717-2200-00010-00

July 16, 1993

Prepared for:

U.S. Department of Energy
Yucca Mountain Site Characterization Project Office
P.O. Box 98608
Las Vegas, Nevada 89193-8608

Prepared by:

INTERA Inc.
101 Convention Center Drive
Las Vegas, Nevada 89109

Under Contract Number
DE-AC01-91RW00134

ACKNOWLEDGEMENT

The Total System Performance Assessment (TSPA) analyses generated using the Repository Integration Program (RIP) were conducted by the staff of the Civilian Radioactive Waste Management System (CRWMS), Management and Operating (M&O) Contractor, Performance Assessment group, including (in alphabetical order) Carl Bruch, Tim Dale, Jerry McNeish, and B.S. RamaRao under the direction of Robert Andrews. Additional analyses of unsaturated zone flow and transport using Total System Performance Assessment Code (TOSPAC) and TRACR3D were performed by Noreen Baker with support from Mark Reeves. Reviews of this document have been performed by Suresh Pahwa and Abe Van Luik.

The results presented in this document reflect a comparison of the RIP methodology for total system performance with that used by Sandia National Laboratories (SNL) and its contractors in TSPA-1991 (Barnard et al., 1992). Preliminary results were presented to SNL staff in January 1993. Helpful comments were received from Mike Wilson, Rally Barnard, Holly Dockery, Felton Bingham (all SNL) and Jack Gauthier (Spectra) during this meeting. Several upgrades to RIP have been generated over the past months by Golder Associates Inc. staff including Ian Miller, Rick Kossik, and Joe Hachey. In addition, the Golder staff has been helpful in identifying approaches to more efficiently utilize RIP.

The work presented in this document was funded under WBS 1.2.5.4.1--Total System Performance Assessment by the U.S. Department of Energy (DOE) Office of Civilian Radioactive Waste Management--Yucca Mountain Project Office under contract #DE-AC01-91RW00134. The DOE Branch Chief responsible for this work is Jeremy Boak. The M&O Office Manager responsible for this work is Jean Younker. The support of these individuals and organizations is gratefully acknowledged.

EXECUTIVE SUMMARY

During Fiscal Year (FY) 1991 and FY 1992, SNL and Battelle Pacific Northwest Laboratory were assigned the responsibility to generate initial TSPAs of the Yucca Mountain site. The analyses performed by these organizations (called TSPA-1991) are reported in Barnard et al. (1992) and Eslinger et al. (1993). During this same time period, Golder Associates Inc. was assigned the task of generating a model capable of analyzing the total system performance of a high-level radioactive waste repository. The developed model, called RIP, is documented in Kossik and Hachey (1993), Miller et al. (1993), and Golder Associates Inc. (1993).

In FY 1993, the CRWMS M&O Contractor was assigned the responsibility to plan, coordinate, and contribute to the second iteration of TSPA-2. Prior to initiating the next TSPA iteration, it was decided that it would be valuable to evaluate the applicability of RIP for use in this iteration. Therefore, analyses were conducted to compare the results generated by RIP to those reported in TSPA-1991. In particular, the aim was to generate a RIP input data set as equivalent as possible to that documented in Barnard et al. (1992) and to analyze the total system performance (as well as the performance of the individual subsystem components of the waste package/Engineered Barrier System (EBS), unsaturated gaseous flow and transport, unsaturated aqueous flow and transport, saturated flow and transport, and disruptive processes/events). The performance measure for comparison with the results of TSPA-1991 is the cumulative release of radionuclides to the accessible environment over a 10,000-year period following closure normalized to the U.S. Environmental Protection Agency (EPA) release limits specified in 40 CFR 191.

While the main goal of this study is to "test" the ability of RIP to be used for future total system performance assessment iterations, it has the added benefit of "testing" the results presented in TSPA-1991 (Barnard et al., 1992). The approach used to approximate the individual subsystem components in RIP is sufficiently different from that used in TSPA-1991 (in particular, for the waste package/EBS and unsaturated aqueous flow and transport), that exercising RIP produces an independent "verification" of the TSPA-1991 results given the same conceptualizations and input data assumptions are used.

We have based our abstraction on the TSPA-1991 document prepared by SNL staff and contractors (Barnard et al., 1992). We have chosen the representations presented in TSPA-1991 because they describe the broad spectrum of domains likely to be required in any assessment of total system performance. As a result of the abstracted nature of the TSPA-1991 conceptual models and parameters, developing an equivalent RIP data set proved to be relatively straightforward. Once an initial RIP data set was created from the conceptual descriptions and parameter values provided in the TSPA-1991 document, we "tested" each individual domain to determine our ability to reproduce the TSPA-1991 results. In some instances this was a direct comparison with conditional Complementary Cumulative Distribution Functions (CCDFs) or some other measure of domain performance. In other cases, we ran expected values from the parameter distributions and compared time releases (in Ci/yr) at particular boundaries of the system (for example, the host rock at the edge of the EBS). Following the "test" of each domain, we conducted additional sensitivity analyses on individual domains as well as the combination of domains. These sensitivity analyses consisted of one-at-a-time sampling from parameter

distributions and conceptual model variations to determine the impact on the results. In order to gain additional insights on system and domain behavior, we also created scatter plots of the sampled input parameter versus the dependent variable (generally, the cumulative release to some boundary).

The principal differences between TSPA-1991 and our implementation of the same data set using RIP are enumerated below:

- RIP input has to be simplified to mimic the treatment of radionuclide inventories and solubilities adopted in TSPA-1991. RIP allows complete chains to be specified and tracked and allows for partitioning between radionuclides which compete for solubility-limited releases.

- Diffusive releases in RIP are assumed to be steady-state.

- RIP can approximate fracture-matrix coupling by a Markovian process, which requires definition of a Markov transition rate. Such an approach does not reproduce dispersive mass transport.

- Future states are simulated directly in RIP. We have conducted conditional simulations for comparison to TSPA-1991 by using the importance sampling option in RIP.

The following items summarize the principal results of the comparison between RIP and TSPA-1991:

- RIP has been successfully used to approximate the relevant processes in TSPA-1991, including the waste package failure rate, waste form alteration, radionuclide release and radionuclide transport to the accessible environment.

- The TSPA-1991 results for release from the waste package are higher than RIP for solubility-limited radionuclides and lower for alteration-limited radionuclides.

- The TSPA-1991 CCDF for release from the EBS is slightly higher than calculated by RIP. This discrepancy may be due to slight differences in the waste package failure distribution and solubilities used in RIP and TSPA-1991.

- Slight differences in RIP and TSPA-1991 results for gaseous releases to the accessible environment are likely due to small differences in the waste package failure distribution and the time-stepping algorithm used in RIP to approximate the breakthrough curve.

- Differences between RIP and TSPA-1991 exist in the analysis of aqueous releases from the unsaturated zone when the Markovian multi-mode transport algorithm is used. For representative Markov transition rates (about 1/L, where L is the layer thickness), good agreement exists. When the matrix flow layers are treated as single-mode transport units in RIP, good agreement also exists.

- RIP reproduces the saturated zone radionuclide transport presented in TSPA-1991.
- RIP reproduces the volcanic and human intrusion scenarios presented in TSPA-1991.

Based on the experience gained in this study, we feel confident that the RIP approach is a viable method for use in future iterations of total system performance assessment. Its advantages (notably, flexibility in handling numerous types of functional relationships) far outweigh the simple representations required to make the model efficient for multiple realizations (in particular, the Markovian approximation of multi-mode transport and the temporal approximation of theoretical breakthrough curves). The flexibility of the RIP approach should be used to advantage in the next TSPA iteration (TSPA-II) to account for temperature dependencies on water contact mode, waste package failure, waste form alteration and dissolution, radionuclide mobilization (solubility), the percent of water in contact with the waste, and the gaseous and aqueous phase velocities. These dependencies should be derived from expert judgment or more detailed process-oriented modeling.

TABLE OF CONTENTS

Page

ACKNOWLEDGEMENT ii

EXECUTIVE SUMMARY iii

1. INTRODUCTION 1-1

1.1 OBJECTIVES 1-2
1.2 APPROACH 1-2
1.3 GENERAL DESCRIPTION OF RIP 1-3

1.3.1 Waste Package/EBS Radionuclide Release Model 1-4
1.3.2 Far Field Flow and Radionuclide Transport Model 1-5
1.3.3 Disruptive Events Model 1-5

1.4 EPA SUM 1-5
1.5 PRESENTATION OF STOCHASTIC OUTPUT 1-6
1.6 TYPES OF INPUT PARAMETER DISTRIBUTIONS 1-7

2. WASTE PACKAGE 2-1

2.1 TSPA-1991 APPROACH TO WASTE PACKAGE 2-1
2.2 RIP APPROACH TO WASTE PACKAGE/ENGINEERED BARRIER SYSTEM 2-5
2.3 RESULTS OF WASTE PACKAGE/ENGINEERED BARRIER SYSTEM ANALYSES 2-8

2.3.1 Sensitivity of CCDF to Waste Package Failure 2-9
2.3.2 Sensitivity of CCDF to Inventory 2-9
2.3.3 Sensitivity of CCDF to Waste Alteration 2-9
2.3.4 Sensitivity of CCDF to Waste Package Release 2-10
2.3.5 Comparison of Individual Radionuclide Release from TSPA-1991 and RIP 2-11
2.3.6 Scatter Plots for Selected Parameters from CCDF Analyses 2-12

2.4 PARAMETER SENSITIVITY ANALYSIS 2-12

2.4.1 Sensitivity of Waste Package to Waste Alteration Parameters 2-13
2.4.2 Sensitivity of Waste Package to Release Parameters 2-14

3. AQUEOUS FLOW AND TRANSPORT TO THE ACCESSIBLE ENVIRONMENT 3-1

TABLE OF CONTENTS (Continued)

Page

3.1 PROBLEM DOMAIN 3-1
3.2 CONCEPTUALIZATION AND MATHEMATICAL MODEL (TSPA-1991) 3-2
3.3 RIP MODEL: FLOW AND TRANSPORT SIMULATION CAPABILITY 3-3
3.4 CONCEPTUALIZATION OF FLOW AND TRANSPORT IN RIP 3-4
3.5 RESULTS OF RIP SIMULATIONS 3-6

3.5.1 Distribution of Nuclide Releases 3-6
3.5.2 Sensitivity Studies 3-8
3.5.3 Additional Sensitivity to Infiltration Flux 3-9

4. UNSATURATED GASEOUS TRANSPORT 4-1

4.1 DETAILED DESCRIPTION OF TSPA-1991 4-1
4.2 RIP ANALYSIS 4-2
4.3 RESULTS 4-3

5. EXTERNAL EVENTS AND PROCESSES 5-1

5.1 VOLCANIC INTRUSION SCENARIO 5-1

5.1.1 Description of TSPA-1991 5-1
5.1.2 RIP Analysis 5-2
5.1.3 Results 5-3

5.2 HUMAN INTRUSION SCENARIO 5-4

5.2.1 Description of TSPA-1991 5-4
5.2.2 RIP Analysis 5-5
5.2.3 Results 5-6

6. CONCLUSIONS AND RECOMMENDATIONS 6-1

7. REFERENCES 7-1

APPENDIX A - DETAILED DESCRIPTION OF RIP WASTE PACKAGE IMPLEMENTATION A-1

APPENDIX B - RIP THEORY: NUMERICAL ILLUSTRATIONS B-1

APPENDIX C - COMPARISON OF UNSATURATED ZONE FLOW AND MASS TRANSPORT MODELED USING RIP, TOSPAC, AND TRACR3D C-1

LIST OF FIGURES

Page

1-1. Presentation of Stochastic Input and Output 1-8

2-1. TSPA-1991 Waste Package Schematic (taken from Golder Associates, Inc., 1993) 2-17

2-2. Histogram of Applied Infiltration Flux (q) 2-18

2-3. Histogram of Saturated Hydraulic Matrix Conductivity (k_0) 2-19

2-4. Histogram of Fraction of Containers in Seepage Areas (f_s) 2-20

2-5. Histogram of Flux Used for Advective Release (q_s) 2-21

2-6. TSPA-1991 CCDF for Waste Package/EBS Release (taken from Barnard et al., 1992) 2-22

2-7. TSPA-1991 Individual Radionuclide Release Curves (normalized) 2-23

2-8. RIP Waste Package Schematic (taken from Miller et al., 1993) 2-24

2-9. ^{234}U Release Assuming Competing Isotope Solubilities 2-25

2-10. ^{235}U Release Assuming Competing Isotope Solubilities 2-26

2-11. Weibull Waste Package Failure Distribution 2-27

2-12. Log-Uniform Waste Package Failure Distribution 2-28

2-13. Initial Conceptualization - CCDF 2-29

2-14. Waste Package with Log-Uniform Failure Distribution - CCDF 2-30

2-15. Inventory Reduced to Nine Radionuclides - CCDF 2-31

2-16. Increase ^{99}Tc and ^{135}Cs Base Solubility - CCDF 2-32

2-17. One Failure Time Per Realization - CCDF 2-33

2-18. F_s Implemented to Determine Waste Package Group Totals - CCDF 2-34

2-19. F_s Implemented to Determine Waste Package Group Totals - with Air Gap - CCDF 2-35

2-20. F_s Implemented with q_s with Air Gap - CCDF 2-36

LIST OF FIGURES (Continued)

Page

2-21. ^{99}Tc Implemented with q_s with Air Gap - CCDF 2-37

2-22. ^{129}I Implemented with q_s with Air Gap - CCDF 2-38

2-23. ^{239}Pu Implemented with q_s with Air Gap - CCDF 2-39

2-24. ^{79}Se Implemented with q_s with Air Gap - CCDF 2-40

2-25. ^{234}U Implemented with q_s with Air Gap - CCDF 2-41

2-26. TSPA-1991 Individual Radionuclide Release Curves (non-normalized) 2-42

2-27. Release Initiated at 300 Years - CCDF 2-43

2-28. Individual Radionuclide Release Curve (^{99}Tc) 2-44

2-29. Individual Radionuclide Release Curve (^{239}Pu) 2-45

2-30. Sensitivity of ^{99}Tc Release to Matrix Dissolution Rate 2-46

2-31. Sensitivity of ^{239}Pu Release to Effective Catchment Area 2-47

2-32. Sensitivity of ^{239}Pu Release to Geometric Diffusion Factor 2-48

2-33. Sensitivity of ^{135}Cs to Diffusion Coefficient 2-49

2-34. Sensitivity Curve of the Release of ^{99}Tc to the Accessible Environment as a Function of the Matrix Dissolution Rate 2-50

2-35. Sensitivity Curve of the Release of ^{99}Tc to the Accessible Environment as a Function of the Fraction of Waste Wetted 2-51

2-36. Sensitivity Curve of the Release of ^{99}Tc to the Accessible Environment as a Function of Technetium Solubility 2-52

2-37. Sensitivity Curve of the Release of ^{99}Tc to the Accessible Environment as a Function of Technetium Solubility (low values of S_{Tc}) 2-53

2-38. Sensitivity Curve of the Release of ^{126}Sn to the Accessible Environment as a Function of the Matrix Dissolution Rate 2-54

LIST OF FIGURES (Continued)

Page

2-39. Sensitivity Curve of the Release of ^{135}Cs to the Accessible Environment as a Function of the Repository Infiltration Rate 2-55

2-40. Sensitivity Curve of the Release of ^{99}Tc to the Accessible Environment as a Function of the Volume of Water Contacting the Matrix 2-56

2-41. Sensitivity Curve of the Release of ^{135}Cs to the Accessible Environment as a Function of the Volume of Water Contacting the Matrix 2-57

2-42. Sensitivity Curve of the Release of ^{126}Sn to the Accessible Environment as a Function of the Volume of Water Contacting the Matrix 2-58

3-1. Map of the Boundary of Potential Repository at Yucca Mountain (taken from Barnard et al., 1992) 3-10

3-2. Schematic Cross-Section of Unsaturated-Zone Stratigraphy (taken from Barnard et al., 1992) 3-11

3-3. Stratigraphies of the Six Vertical Columns Used for the Simulation of Unsaturated Flow (taken from Barnard et al., 1992) 3-12

3-4. Apportionment of a Flow Rate to Matrix and Fractures: A Conceptualization 3-13

3-5. CCDFs for Nuclide Releases (EPA Sum) for the Case $\lambda = 0.1\ m^{-1}$ 3-14

3-6. CCDFs for EPA Sum and Ratios for ^{99}Tc and ^{129}I for the Case $\lambda = 0.1\ m^{-1}$ . . . 3-15

3-7. CCDFs for EPA Sum for $\lambda = 0.1, 0.01\ m^{-1}$, and from TSPA-1991 3-16

3-8. Sensitivity of CCDFS for EPA Sum to Poisson Transition Rate 3-17

3-9. CCDFs for the EPA Sum: Layers 3 and 5 Treated as Single Mode Media in RIP ($\lambda = 0.1\ m^{-1}$ for other layers) 3-18

3-10a. Time History of Release Rate to Accessible Environment for ^{99}Tc 3-19

3-10b. Time History of Release Rate to Accessible Environment for ^{129}I 3-20

3-10c. Time History of Release Rate to Accessible Environment for ^{237}Np 3-21

3-10d. Time History of Release Rate to Accessible Environment for ^{234}U 3-22

3-10e. Time History of Release Rate to Accessible Environment for ^{79}Se 3-23

LIST OF FIGURES (Continued)

Page

3-11. Release Rates to Accessible Environment for Radionuclides Released Using Composite Porosity Flow Model (taken from Barnard et al., 1992) 3-24

3-12. Scatter Plot of EPA Sum versus Infiltration Rate (all other parameters at mean value) 3-25

3-13. Scatter Plot of EPA Sum versus Infiltration Rate (all parameters are sampled) 3-26

3-14. Scatter Plot of EPA Sum versus Matrix Hydraulic Conductivity of Layer 3 3-27

3-15. Scatter Plot of EPA Sum versus Poisson Transition Rate 3-28

3-16a. CCDF for Infiltration - Run 3.2 3-29

3-16b. CCDF for Infiltration - Run 3.3 3-30

3-16c. CCDF for Infiltration - Run 3.4 3-31

3-16d. CCDF for Infiltration - Run 3.5 3-32

3-16e. CCDF for Infiltration - Run 3.1 3-33

3-17a. CCDF for EPA Sum - Run 3.2 3-34

3-17b. CCDF for EPA Sum - Run 3.3 3-35

3-17c. CCDF for EPA Sum - Run 3.4 3-36

3-17d. CCDF for EPA Sum - Run 3.5 3-37

4-1. Cross-Section Through Yucca Mountain (taken from Barnard et al., 1992) 4-5

4-2. Gas-Flow Path Lines within Yucca Mountain with the Repository at Ambient Temperature Conditions (300 K) (taken from Barnard et al., 1992) 4-6

4-3. Gas-Flow Path Lines within Yucca Mountain with the Repository at a Temperature of 330 K (taken from Barnard et al., 1992) 4-7

LIST OF FIGURES (Continued)

Page

4-4. Travel-Time Distributions for ^{14}C Transport (taken from Barnard et al., 1992) 4-8

4-5. ^{14}C Unit-Velocity Distribution for a Repository Temperature of 360 K 4-9

4-6. ^{14}C Unit-Velocity Distribution for a Repository Temperature of 330 K 4-10

4-7. ^{14}C Unit-Velocity Distribution for a Repository Temperature of 315 K 4-11

4-8. ^{14}C Unit-Velocity Distribution for a Repository Temperature of 300 K 4-12

4-9. ^{14}C Mass and Velocity Distributions per RIP Pathway 4-13

4-10. Conditional CCDF for Gaseous Releases (taken from Barnard et al., 1992) . . . 4-14

4-11. Conditional CCDF for Gaseous Releases from RIP 4-15

4-12. Scatter Plot of Modeled ^{14}C Inventory versus Total Normalized Release to the Accessible Environment 4-16

4-13. Scatter Plot of ^{14}C Prompt Fraction versus Total Normalized Release to the Accessible Environment 4-17

4-14. Scatter Plot of the Retardation/Permeability Factor versus Total Normalized Release to the Accessible Environment 4-18

5-1. Conceptualization of Volcanic Intrusion Interaction with the Repository (taken from Barnard et al., 1992) 5-8

5-2. Probability Density Function of the Dike Width (taken from Barnard et al., 1992) 5-9

5-3. Probability Density Function of the Erosion Depth (taken from Barnard et al., 1992) 5-10

5-4. Dike Orientation and Length within the Repository for a Selected Number of Realizations (taken from Barnard et al., 1992) 5-11

5-5. Probability Density Function of the Dike Width 5-12

5-6. Probability Density Function of the Fraction Entrained (taken from Barnard et al., 1992) 5-13

LIST OF FIGURES (Continued)

Page

5-7. Probability Density Function of the Wall-Rock Fraction 5-14

5-8. Conditional CCDF for Normalized Total Release to the Accessible Environment for Volcanic Intrusion Methods One and Two, Not Including the Probability of Occurrence (taken from Barnard et al., 1992) 5-15

5-9. Conditional CCDF for Normalized Total Release to the Accessible Environment for Volcanic Intrusion Methods One and Two, Including the Probability of Occurrence (taken from Barnard et al., 1992) 5-16

5-10. RIP Conditional CCDF for Normalized Total Release to the Accessible Environment for Volcanic Intrusion Methods One and Two, Including the Probability of Occurrence 5-17

5-11. Scatter Plot of Dike Length versus Total Normalized Release to the Accessible Environment for Method One 5-18

5-12. Scatter Plot of Erosion Depth versus Total Normalized Release to the Accessible Environment for Method One 5-19

5-13. Scatter Plot of Eruptive Volume versus Total Normalized Release to the Accessible Environment for Method Two 5-20

5-14. Scatter Plot of Wall-Rock Fraction versus Total Normalized Release to the Accessible Environment for Method Two 5-21

5-15. Scatter Plot of Fraction of Dike within Repository versus Total Normalized Release to the Accessible Environment for Method Two 5-22

5-16. Probability Density Function of the Saturated Tuff Ground-Water Velocity . . . 5-23

5-17. Probability Density Function of the Saturated Tuff Bulk Porosity 5-24

5-18. Probability Density Function of the Saturated Tuff Longitudinal Dispersivity 5-25

5-19. Probability Density Function of the Saturated Tuff Uranium Distribution Coefficient 5-26

5-20. Probability Density Function of the Saturated Tuff Neptunium Distribution Coefficient 5-27

LIST OF FIGURES (Continued)

Page

5-21. Probability Density Function of the Carbonate Aquifer Ground-Water Velocity 5-28

5-22. Probability Density Function of the Carbonate Aquifer Bulk Porosity 5-29

5-23. Probability Density Function of the Carbonate Aquifer Longitudinal Dispersivity 5-30

5-24. Probability Density Function of the Carbonate Aquifer Plutonium Distribution Coefficient 5-31

5-25. Probability Density Function of the Carbonate Aquifer Uranium Distribution Coefficient 5-32

5-26. Probability Density Function of the Carbonate Aquifer Neptunium Distribution Coefficient 5-33

5-27. Conditional CCDF for Normalized Total Release to the Accessible Environment for the Human Intrusion into the Tuff Aquifer, Not Including the Probability of Occurrence (taken from Barnard et al., 1992) 5-34

5-28. RIP Conditional CCDF for Normalized Total Release to the Accessible Environment for Human Intrusion into the Tuff Aquifer, including the Probability of Occurrence 5-35

5-29. Scatter Plot of Ground-Water Velocity versus Total Normalized Release to the Accessible Environment for the Human Intrusion into the Tuff Aquifer 5-36

5-30. Scatter Plot of Longitudinal Dispersivity versus Total Normalized Release to the Accessible Environment for the Human Intrusion into the Tuff Aquifer 5-37

5-31. Scatter Plot of the Distribution Coefficient for Uranium versus Total Normalized Release to the Accessible Environment for the Human Intrusion into the Tuff Aquifer 5-38

5-32. Scatter Plot of the Distribution Coefficient for Neptunium versus Total Normalized Release to the Accessible Environment for the Human Intrusion into the Tuff Aquifer 5-39

LIST OF FIGURES (Continued)

Page

5-33. Conditional CCDF for Normalized Total Release to Accessible Environment for the Human Intrusion into the Carbonate Aquifer, not including the Probability of Occurrence (taken from Barnard et al., 1992) 5-40

5-34. RIP Conditional CCDF for Normalized Total Release to the Accessible Environment for Human Intrusion into the Carbonate Aquifer, including the Probability of Occurrence 5-41

5-35. Scatter Plot of Ground-Water Velocity versus Total Normalized Release to the Accessible Environment for the Human Intrusion into the Carbonate Aquifer 5-42

5-36. Scatter Plot of Longitudinal Dispersivity versus Total Normalized Release to the Accessible Environment for the Human Intrusion into the Carbonate Aquifer 5-43

5-37. Scatter Plot of the Distribution Coefficient for Plutonium versus Total Normalized Release to the Accessible Environment for the Human Intrusion into the Carbonate Aquifer 5-44

5-38. Scatter Plot of the Distribution Coefficient for Uranium versus Total Normalized Release to the Accessible Environment for the Human Intrusion into the Carbonate Aquifer 5-45

5-39. Scatter Plot of the Distribution Coefficient for Neptunium versus Total Normalized Release to the Accessible Environment for the Human Intrusion into the Carbonate Aquifer 5-46

B-1. Nuclide Release Rate for Layer 1, Column 1: No Coupling Case - RIP Theory B-6

B-2. Nuclide Release Rate for Layer 1, Column 1: Full Coupling Case - RIP Theory B-7

B-3. Nuclide Release Rate through Layer 2, Column 1: No Coupling Case - RIP Theory B-8

B-4. Nuclide Release Rate through Layer 2, Column 1: Full Coupling Case - RIP Theory B-9

B-5. Nuclide Release Rate through Layer 1, Column 1: No Coupling Case - RIP Simulations B-10

LIST OF FIGURES (Continued)

Page

B-6. Nuclide Release Rate through Layer 1, Column 1: Full Coupling Case - RIP Simulations B-11

B-7. Nuclide Release Rate at the Bottom of Column 1: No Coupling Case - RIP Simulations B-12

B-8. Nuclide Release Rate at the Bottom of Column 1: Full Coupling Case - RIP Simulations B-13

B-9. Nuclide Release Rate Through Layer 1, Column 6: No Coupling Case - RIP Simulations B-14

B-10. Nuclide Release Rate Through Layer 1, Column 6: Full Coupling Case - RIP Simulations B-15

B-11. Nuclide Release Rate at the Bottom of Column 6: No Coupling Case - RIP Simulations B-16

B-12. Nuclide Release Rate at the Bottom of Column 6: Full Coupling Case - RIP Simulations B-17

B-13. Effect of λ on Breakthrough Curves at the Bottom of Layer 1: $\lambda = 1.0\ m^{-1}$ B-18

B-14. Effect of λ on Breakthrough Curves at the Bottom of Layer 1: $\lambda = 0.1\ m^{-1}$ B-19

B-15. Effect of λ on Breakthrough Curves at the Bottom of Layer 1: $\lambda = 0.05\ m^{-1}$ B-20

B-16. Effect of λ on Breakthrough Curves at the Bottom of Layer 1: $\lambda = 0.025\ m^{-1}$ B-21

B-17. Effect of λ on Breakthrough Curves at the Bottom of Layer 1: $\lambda = 0.01\ m^{-1}$ B-22

B-18. Effect of λ on Breakthrough Curves at the Bottom of Layer 1: $\lambda = 10^{-3}\ m^{-1}$ B-23

B-19. Effect of λ on Breakthrough Curves at the Bottom of Column 1: $\lambda = 10^{4}\ m^{-1}$ B-24

LIST OF FIGURES (Continued)

Page

B-20. Effect of λ on Breakthrough Curves at the Bottom of Column 1: $\lambda = 100\ m^{-1}$ B-25

B-21. Effect of λ on Breakthrough Curves at the Bottom of Column 1: $\lambda = 10\ m^{-1}$ B-26

B-22. Effect of λ on Breakthrough Curves at the Bottom of Column 1: $\lambda = 1.0\ m^{-1}$ B-27

B-23. Effect of λ on Breakthrough Curves at the Bottom of Column 1: $\lambda = 0.1\ m^{-1}$ B-28

B-24. Effect of λ on Breakthrough Curves at the Bottom of Column 1: $\lambda = 10^{-2}\ m^{-1}$ B-29

B-25. Effect of λ on Breakthrough Curves at the Bottom of Column 1: $\lambda = 10^{-3}\ m^{-1}$ B-30

C-1. Composite Hydraulic Conductivity of Topopah Springs Welded Unit C-4

C-2. Composite Capillary Pressure Head of Topopah Springs Welded Unit C-5

C-3a. Saturation Profile for Column 1: TOSPAC Simulations C-6

C-3b. Saturation Profile for Column 1: TRACR3D Simulations C-7

C-4a. Velocity Profile for Column 1: TOSPAC Simulations C-8

C-4b. Velocity Profile for Column 1: TRACR3D Simulations C-9

C-5a. Nuclide Release Rate Through Matrix and Fracture at the Bottom of Layer 1, Column 1: No Coupling Case - TOSPAC-TRANS C-10

C-5b. Nuclide Release Rate Through Matrix and Fracture at the Bottom of Layer 1, Column 1: Full Coupling Case - TOSPAC-TRANS C-11

C-5c. Total Nuclide Release Rate at the Bottom of Layer 1, Column 1: No Coupling Case - TOSPAC C-12

C-5d. Total Nuclide Release Rate at the Bottom of Layer 1, Column 1: Full Coupling Case - TRACR3D C-13

LIST OF FIGURES (Continued)

Page

C-6a. Nuclide Release Rate at the Bottom of Layer 1, Column 1: No Coupling Case - RIP C-14

C-6b. Nuclide Release Rate at the Bottom of Layer 1, Column 1: Full Coupling Case - RIP C-15

C-7a. Total Nuclide Release Rate at the Bottom of Column 1: TOSPAC C-16

C-7b. Total Nuclide Release Rate at the Bottom of Column 1: TRACR3D C-17

C-8a. Nuclide Release Rate at the Bottom of Column 1: No Coupling Case - RIP C-18

C-8b. Nuclide Release Rate at the Bottom of Column 1: Full Coupling Case - RIP C-19

C-8c. Nuclide Release Rate at the Bottom of Column 1 (Layers 3 and 5 in Single Mode): RIP Simulations C-20

LIST OF TABLES

Page

2-1. Inventory of Radionuclides for Various Analyses 2-59

2-2. Comparison of TSPA-1991 Container Parameters with RIP Parameters 2-60

2-3. Comparison of TSPA-1991 Inventory Parameters with RIP Parameters 2-61

2-4. Comparison of TSPA-1991 WP Failure Parameters with RIP Parameters 2-62

2-5. Comparison of TSPA-1991 Exposure Parameters with RIP Parameters 2-63

2-6. Comparison of TSPA-1991 Transport Parameters with RIP Parameters 2-64

2-7. Major Parameter Differences between RIP Simulations 2-65

2-8. Comparison of Peak Values for Individual Radionuclide Release (Ci/yr) 2-66

2-9. High-Solubility Radionuclides (^{99}Tc) Waste Alteration Sensitivity Analyses 2-67

2-10. Low-Solubility Radionuclides (^{239}Pu) Waste Alteration Sensitivity Analyses 2-67

2-11. High-Solubility Radionuclides (^{99}Tc) Release Parameter Sensitivity Analyses 2-68

2-12. Low-Solubility Radionuclides (^{239}Pu) Release Parameter Sensitivity Analyses 2-69

2-13. Correlation Coefficients for RUN 2.9 2-70

2-14. Correlation Coefficients for RUN 2.10 2-70

3-1. Hydrostratigraphy Used for Unsaturated-Zone Aqueous Problems (after Barnard et al., 1992) 3-38

3-2. Elevations of Layers at Selected Locations in Geohydrologic Problem Domain (after Barnard et al., 1992) 3-38

3-3. Elevations Used for the Composite-Porosity Model of the UZ (after Barnard et al., 1992) 3-39

LIST OF TABLES (Continued)

Page

3-4. Matrix Hydraulic Conductivity Distributions Used in TSPA-1991 and RIP (after Barnard et al., 1992) 3-40

3-5. Matrix Porosity Distributions Used in TSPA-1991 and RIP (after Barnard et al., 1992) 3-41

3-6. Fracture Porosity Distributions Used in TSPA-1991 and RIP 3-41

3-7. Infiltration Rate Distribution Used in TSPA-1991 and RIP 3-41

3-8. Parameters Used to Model the Saturated Zone in TSPA-1991 and RIP 3-42

3-9. Geohydrologic Units for Geochemistry in TSPA-1991 and RIP (after Barnard et al., 1992) (after Barnard et al., 1992) 3-42

3-10. K_d Probability Density Distributions Used in TSPA-1991 and RIP (after Barnard et al., 1992) 3-43

3-11. Additional Infiltration Distributions 3-44

4-1. TSPA-1991 ^{14}C Source Term Data (after Barnard et al., 1992) 4-19

4-2. TSPA-1991 ^{14}C Travel Time Specifications (after Barnard et al., 1992) 4-19

4-3. Comparison of TSPA-1991 and RIP Simulation Parameters 4-19

5-1. TSPA-1991 Volcanic Intrusion Method Two Parameters 5-47

5-2. TSPA-1991 K_d Beta Distributions for the Tuff Aquifer (Barnard et al., 1992) 5-47

5-3. TSPA-1991 Distribution Coefficients (mg/l) for the Human Intrusion Scenario into the Carbonate Aquifer (taken from Barnard et al., 1992) 5-48

5-4. TSPA-1991 Parameters for the Human Intrusion Scenarios (taken from Barnard et al., 1992) 5-48

5-5. Comparison of TSPA-1991 and RIP Parameters for the Tuff Saturated Aquifer 5-49

5-6. Comparison of TSPA-1991 and RIP Parameters for the Carbonate Aquifer 5-50

LIST OF TABLES (Continued)

		Page
B-1.	Fluxes and Velocities in Matrix for All Layers	B-31
B-2.	Fluxes and Velocities in Fractures for All Layers	B-31
B-3.	Travel Times Through Column 1	B-32
B-4.	Travel Times Through Column 6	B-32
C-1.	Total Releases at Bottom of Columns 1 and 6	C-21

1. INTRODUCTION

Yucca Mountain, Nevada is currently being characterized to determine its suitability as a potential site for a mined geologic repository for the permanent disposal of high-level radioactive waste. An important component in the determination of the suitability of Yucca Mountain is the prediction of the ability of the geologic and engineered barriers to contain and isolate the radioactive wastes. Performance Assessments (PAs) are conducted to evaluate the ability of the site as well as the repository and waste package designs to meet regulatory criteria. The post-closure regulatory criteria include the cumulative radionuclide release from the total system specified by the U.S. Environmental Protection Agency (EPA) in 40 CFR Part 191[1], and the Nuclear Regulatory Commission (NRC) criteria for the geologic setting (10 CFR 60.113 (a)(2)), the Engineered Barrier System (EBS) (10 CFR 60.113 (a)(1)(ii)(B)), and the waste package (10 CFR 60.113 (a)(1)(ii)(A)). The total system performance assessment combines the effects of the waste package, other engineered barriers, and the site to determine the release of radionuclides to the accessible environment due to all significant processes and events.

Several Total System Performance Assessments (TSPAs) have been conducted to provide preliminary indications of the likelihood that the proposed Yucca Mountain site and designs proposed for this site will meet the EPA regulatory requirements. The NRC staff completed a Phase 1 Iterative Performance Assessment in 1990. Electrical Power Research Institute (EPRI) completed a Phase 1 Total System PA in 1990 and a Phase 2 evaluation in 1992. Pacific National Laboratories (PNL) completed an initial assessment in 1988 (Doctor et al., 1992). Recent assessments have been performed by Sandia National Laboratories (SNL) (Barnard et al., 1992) and PNL (Eslinger et al., 1993). The recent assessment by SNL is called Total System Performance Assessment -1991 (TSPA-1991). These analyses use different levels of detail to describe the processes that affect total system performance.

Beginning in Fiscal Year 1993, the Management and Operating Contractor (M&O) for the Civilian Radioactive Waste Management System (CRWMS) was given the responsibility to plan, coordinate, and manage the next iteration of total system performance assessment for the Yucca Mountain Project Office (YMPO) of the Office of Civilian Radioactive Waste Management (OCRWM). This responsibility includes defining the scope of activities required to enhance the analyses conducted to date. The M&O responsibility also includes conducting a portion of the total system PA to complement the analyses being performed by other participants (principally SNL).

[1]Section 801 of the Comprehensive National Energy Policy Act of 1992 specifies that the EPA Standards promulgated under 40 CFR Part 191 do not apply to Yucca Mountain. This Act directed EPA to have the National Academy of Sciences (NAS) conduct a study to determine the reasonableness of different types of standards (notably, individual dose) to protect human health. Based on the NAS recommendations, EPA is directed to promulgate a new standard for Yucca Mountain and NRC is to modify 10 CFR Part 60 to be consistent with the revised EPA standard. Although the EPA standard is no longer directly applicable to Yucca Mountain, it is still a useful measure of total system performance and can be used as a surrogate for the suitability of the geologic disposal system until such time as a new standard is promulgated.

Before initiating the second total system performance assessment iteration (TSPA-II), it is prudent to review the applicability/representativeness of the conceptual models and parameters used in the analyses to date and to independently compare the results from different TSPA models to determine whether different approaches can be used to generate analogous results. In the following chapters we present a comparison of the TSPA results generated with the Repository Integration Program (RIP) developed by Golder Associates Inc. with those previously generated by SNL in their TSPA-1991, using, to the extent practicable, the same data set as was used in TSPA-1991.

RIP is a performance-assessment and site-characterization strategy-evaluation software developed by Golder Associates Inc. under contract to OCRWM in 1991 and 1992. RIP is a very flexible tool that allows the user to describe the different compartments affecting release of radionuclides to the accessible environment. RIP was designed to be at the top of the performance assessment "pyramid" of analyses in that it describes the system and incorporates as many of the system interdependencies as the user chooses to specify, but it does not explain the behavior of the physical-chemical processes acting in the system. More detailed process models are required to develop the physical understanding, while RIP can be used to describe this understanding and its impact on total system performance.

1.1 OBJECTIVES

The objective of the comparison of the TSPA results generated using RIP with those reported by SNL in TSPA-1991 (Barnard et al., 1992) is to evaluate the ability to abstract the parameters and functional relationships required in RIP from the data set presented in TSPA-1991. A related objective is to test the reasonableness of the results presented in TSPA-1991 by determining whether an abstract representation of the relevant processes (as contained in RIP) can be used to reproduce the CCDFS presented by Barnard et al. (1992). In essence, we are simultaneously testing the utility of RIP to be used in subsequent iterations of TSPA as well as the ability of an independent analysis group to reproduce the results presented in TSPA-1991.

In addition to the above principal objectives, we have a goal to extend the analyses presented to date by (1) conducting additional uncertainty analyses on some parameters believed to be important to the prediction of cumulative radionuclide release, and (2) evaluating the sensitivity of TSPA performance measures to variability in selected parameters.

1.2 APPROACH

The approach taken in this study was first to generate an initial input data set for RIP based on an abstraction from the information presented in TSPA-1991.

We have chosen RIP for this assessment because it uses a "top-down" TSPA approach which allows the user to incorporate varying levels of detail to describe the processes which occur within the different domains of the geologic disposal system (the waste packages/EBS, the unsaturated zone, the saturated zone, and external events and processes such as magmatism, tectonism, and human intrusion). RIP directly calculates the CCDF for cumulative release by propagating the uncertainty in parameters and processes through the abstract representations of

the system behavior. RIP is designed in a very flexible manner which allows the user to incorporate as much or as little detail as desired.

We have based our abstraction on the TSPA-1991 document prepared by SNL staff and contractors (Barnard et al., 1992). This document presents descriptions and justifications of the processes, conceptual models, and parameter values used to generate total system cumulative releases. We have chosen the representations presented in TSPA-1991 because they describe the broad spectrum of domains likely to be required in any assessment of total system performance. The conceptual models and parameter values used to describe the system represent the culmination of years of effort by SNL staff and contractors, including earlier PA exercises such as COVE-2a and PACE-90 as well as the development of waste package/EBS models by Lawrence Livermore National Laboratory (LLNL).

The data set presented in TSPA-1991 is somewhat abstracted already. The detailed chemical-physical processes which occur within the waste package domain are approximated by simplified time periods (rewetting, container breach, waste alteration, release concentration build-up and fall-off). The unsaturated zone (UZ) aqueous flow and transport is represented by a one-dimensional composite porosity model. The UZ gaseous flow and transport is derived by a one-dimensional representation of the gas phase travel time distributions generated by Ross et al. (1992). The treatment of volcanic and human intrusion events is based on simple geometric arguments. As a result of the abstracted nature of the TSPA-1991 conceptual models and parameters, developing an equivalent RIP data set proved to be relatively straightforward.

Once an initial RIP data set was created from the conceptual descriptions and parameter values provided in the TSPA-1991 document, we "tested" each individual domain to determine our ability to reproduce the TSPA-1991 results. In some instances this was a direct comparison with conditional CCDFs or some other measure of domain performance. In other cases, we ran expected values from the parameter distributions and compared time releases (in Ci/yr) at particular boundaries of the system (for example, the host rock at the edge of the EBS).

Following the "test" of each domain, we conducted additional sensitivity analyses on individual domains as well as the combination of domains. These sensitivity analyses consisted of one-at-a-time sampling from parameter distributions and conceptual model variations to determine the impact on the results. In order to gain additional insights on system and domain behavior we also created scatter plots of the sampled input parameter versus the dependent variable (generally the cumulative release to some boundary).

1.3 GENERAL DESCRIPTION OF RIP

The RIP repository performance assessment and strategy model is a computational tool for conducting probabilistic integrated total system performance assessments for geologic repositories. It is not a model in the normal sense of the word in that it does not explain the behavior of the system or its components but it attempts to describe the behavior. The description of the system is left entirely for the user to define by the use of simple or complex algebraic functional relationships. In a sense, the RIP program is similar to a spreadsheet. While the current version contains a large amount of built-in logic and calculational capabilities, the problem solved is

entirely defined by the user. The theory and capability of RIP are described in Miller et al., (1993). A user's guide for RIP has been published by Kossik and Hachey (1993).

The overall structure of RIP consists of a front-end, a back-end, and a post-processor. The front-end is where the parameter values and functional relationships are defined and sampled using a Monte Carlo-type sampling algorithm. The back-end is where the actual computation occurs. The back-end is run for each sampled realization created in the front end. The post-processor is used to display the results (whether as time histories or CCDFs) and conduct simple sensitivity analyses (one-and two-dimensional scatter plots and simple parameter correlations).

The computation part of RIP used in this report is divided into three primary domains: the waste package/EBS radionuclide release model, the near and far field radionuclide transport model, and the disruptive events model. These models are briefly described below.

1.3.1 Waste Package/EBS Radionuclide Release Model

The waste package/EBS component of RIP can be used to describe several processes which, if they occur, could lead to radionuclide releases to the geosphere. These include container failure, exposure of rapid release and bound radionuclides, and the mass transfer of radionuclides from the waste package to the host rock. Each of these processes may be dependent on the environmental parameters in the near field; in particular the temperature, geochemistry, and hydrology.

RIP allows the user to define multiple modes of container failure. These failure modes may be temperature or time dependent or dependent on the water contact mode adjacent to the waste package. The primary (container) and secondary (cladding or pour canister) containers may fail either sequentially or simultaneously.

Once the containers (primary and secondary) fail, the radionuclide inventory is exposed. RIP allows three inventories, a free inventory which is released instantaneously once the primary container fails, a gap inventory which is released instantaneously once the secondary container fails, and a matrix (i.e., bound) inventory which is released as the matrix is altered and dissolved. The exposure of bound radionuclides in the fuel or glass matrix is a function of the dissolution rate, the surface area exposed and the percent of surface area in contact with water.

Once radionuclides have been dissolved, they may be transferred to the host rock by advective transport, diffusive transport or a combination of advective-diffusive transport. Advective releases apply to all gaseous radionuclides. Aqueous-phase advective releases are a function of the radionuclide concentration in contact with the waste (which may or may not be solubility limited) and the flux past each waste package. Diffusive releases are a function of the radionuclide concentration, the effective diffusion coefficient and a geometric factor which embodies the effective cross-sectional area of the container surface through which diffusive releases may occur and the length of the diffusive path. Only steady-state diffusive releases can be handled in RIP. The release from the waste package is not dependent on the ability of the geosphere to transport the radionuclides.

1.3.2 Far Field Flow and Radionuclide Transport Model

RIP allows for a simplified description of radionuclide transport through the geosphere. The geosphere may be "discretized" into multiple pathways that are combined either in parallel or in series. These pathways may represent different flow regimes (aqueous vs gaseous), different flow domains (saturated or unsaturated zone), or different cross-sections of the repository. In addition, different flow modes may be applied to each pathway. A single-flow mode may be used to represent an equivalent porous media, while a multiple mode pathway may be used to describe fracture-matrix coupling in a dual porosity-dual permeability media. For single mode pathways, RIP uses an analytical solution to the one-dimensional advection-dispersion equation. For multiple mode pathways, RIP uses a modified Markovian process algorithm to predict the transition between the two modes. The details of the flow and transport solution schemes are described in Miller et al. (1993).

1.3.3 Disruptive Events Model

RIP assumes all disruptive events can be simulated as a Poisson process. The user simply defines the annual probability of the event occurring (as well as a description of the effects of the event on the other domains if it occurs), and RIP randomly determines if that event occurs during a particular time step of any given realization.

Once the event occurs, the effects may be either direct or indirect. Direct effects may include moving a certain percentage of the inventory (determined by geometric consideration such as interception ratios) either directly to the accessible environment (i.e., the surface) or to another pathway (i.e., the saturated zone). Indirect effects may include modifying the behavior and characteristics of the waste package or radionuclide transport pathways.

RIP allows for a particular sampling algorithm (called importance sampling) to increase the possibility of sampling infrequent events in a particular simulation. When importance sampling is used, all other realizations are weighted to account for the actual probability of occurrence.

1.4 EPA SUM

The remanded EPA standard (EPA, 1985) specifies probabilities that cumulative releases of radionuclides to the accessible environment shall not exceed certain levels within 10,000 years. The EPA sum is the sum of the ratios of the cumulative release of a radionuclide and the EPA-prescribed limit for that radionuclide, as given below:

$$M = \sum_i \frac{Q_i}{L_i} \qquad (1\text{-}1)$$

where M is the normalized cumulative release (the EPA sum), Q_i is the cumulative radioactivity of the *i*th radionuclide released to the accessible environment within 10,000 years, and L_i is the EPA limit for the *i*th radionuclide. The quotient Q_i/L_i is known as the EPA ratio for radionuclide i.

The EPA sum relates only to releases to the accessible environment. Accordingly, releases from EBS and unsaturated zones are not EPA sums.

1.5 PRESENTATION OF STOCHASTIC OUTPUT

The methodology used in this study to address the parameter uncertainty involves sampling parameter values from their probability distributions. Corresponding to one realization of such input parameters, obtained by sampling, the system is simulated and a measure of system performance is derived. For example, an important system performance measure in this study is the EPA sum, which is the normalized release to the accessible environment, explained in Section 1.4.

If a thousand Monte Carlo simulations of the system are performed, corresponding to a thousand realizations of the input vector, there would be one thousand results for the desired system performance, such as the EPA sum.

There are three alternative (and equivalent) options available to display such stochastic results. They are: (1) the Probability Density Function (PDF); (2) the Cumulative Distribution Function (CDF); and (3) the Complementary Cumulative Distribution Function (CCDF). The relationship between the three alternative forms of display is explained here.

The probability density function corresponds to a "histogram" for continuous variables. Figure 1-1a shows a PDF. The area under the PDF gives the probability. For example, the probability that a variable lies between X_1 and X_2 is given by the area under the PDF between X_1 and X_2 (Figure 1-1a). The total area under the PDF equals unity, denoting the certainty that the variable must lie between its lowest and highest limits.

If one defines the probability that the variable x is less than X, i.e. $P(x \leq X)$, it is evidently given by

$$F(X) = P(x \leq X) = \int_0^X p(x)dx \qquad (1\text{-}2)$$

(Negative values for x are not feasible here.) F(x) is called the CDF. Since total area under the PDF is unity, F(x) varies between zero and one. Figure 1-1b presents an example CDF, and shows that the probability that x (e.g., EPA sum) is less than or equal to a stated value X_1, is F_1.

The most popular form of presenting the stochastic results in the performance assessment context is by a CCDF, $F^*(x)$, defined simply by $F^*(x) = 1 - F(x)$. It denotes the probability that a variable x is greater than a stated value X, and may be called the probability of exceedance. Figure 1-1c presents an example CCDF and shows that the probability of x exceeding X_1 is given by F_1^* $(= 1 - F_1)$.

The complementary cumulative distribution function is chosen in this report as the most desirable form of displaying the output.

1.6 TYPES OF INPUT PARAMETER DISTRIBUTIONS

The stochastic input parameters are defined by their assumed probability density function. Some of the parameters are defined by normal, uniform, and log-uniform distributions. However, most of the stochastic input parameters in this study are defined by beta distributions. As the beta distribution is not as commonly known as the other distributions, the expression for this distribution is given below.

$$p(x) = c(x - a)^{\alpha} (b - x)^{\beta} \tag{1-3}$$

where	$p(x)$	=	probability density
	c	=	normalizing constant
	x	=	value of the random variable (input parameter)
	a	=	min [x]
	b	=	max [x]
	α,β	=	exponents

The exponents α, β in Equation (1-3) can be calculated based on the mean, standard deviation, and the minimum and maximum values of the distribution.

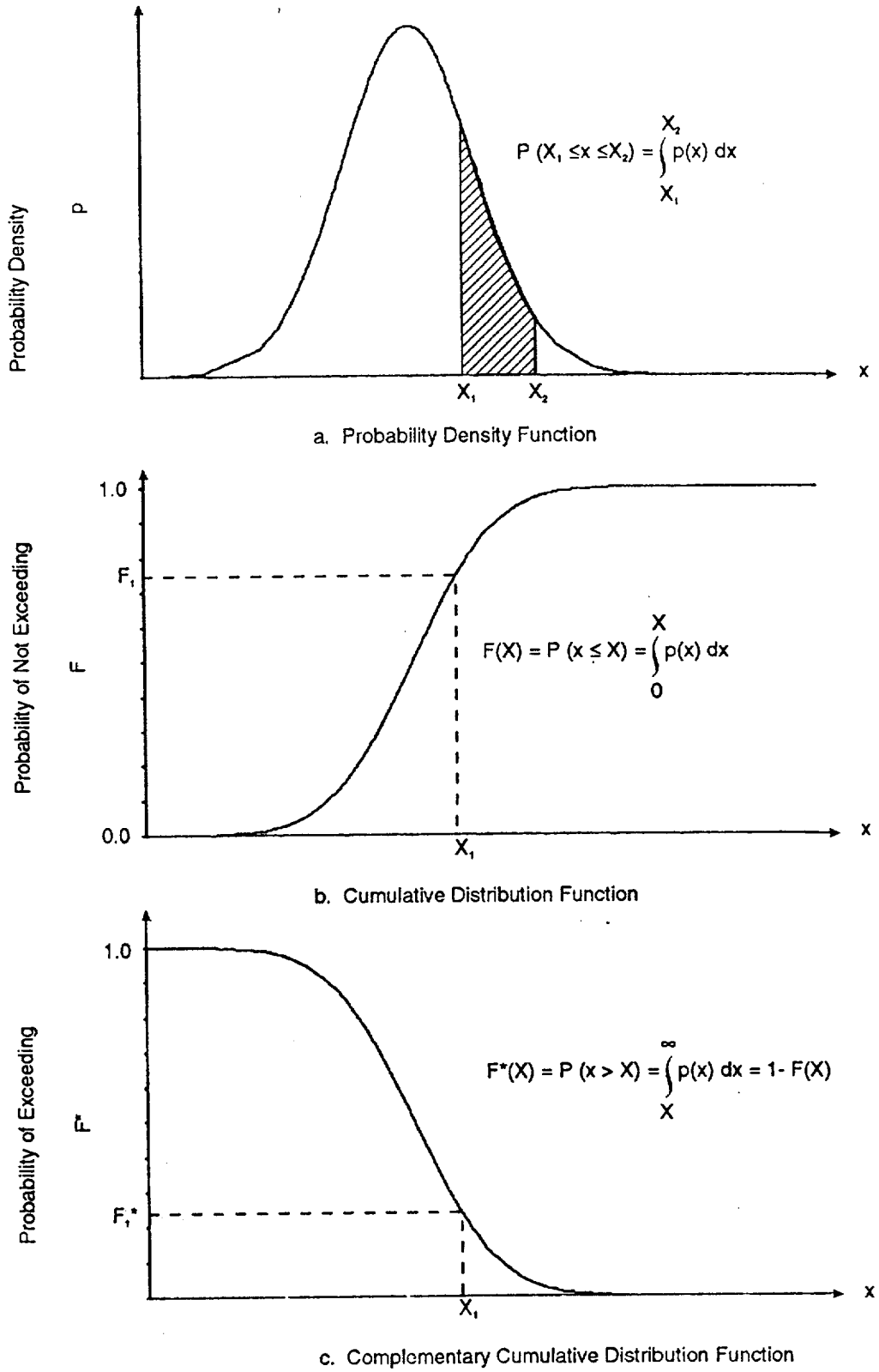

Figure 1-1. Presentation of Stochastic Input and Output

2. WASTE PACKAGE

The source term for all subsequent analyses of radionuclide release to the accessible environment is derived from the waste package/engineered barrier system. Thus, the accuracy of the total release to the accessible environment and any dose calculations are initially dependent on the appropriateness of the conceptualization of the waste package/engineered barrier system (WP/EBS).

The following discussion of the WP/EBS includes:

- Description of the TSPA-1991 conceptual model and parameter distribution
- Description of the RIP conceptual model and parameter distribution
- Comparison of CCDF results from TSPA-1991 and RIP
- Comparison of individual radionuclide release from TSPA-1991 and RIP
- Sensitivity of the radionuclide release to various WP features.

2.1 TSPA-1991 APPROACH TO WASTE PACKAGE

As noted, TSPA-1991 included a simplified waste package release model which assumed the reference container and repository layout as defined in the Yucca Mountain Site Characterization Plan (SCP) (DOE, 1988) and the Site Characterization Plan Conceptual Design Report (MacDougall et al., 1987). A schematic of the TSPA-1991 waste package (Barnard et al., 1992) is presented in Figure 2-1. The individual waste containers were assumed to be vertically emplaced with a 3 cm air gap separating the containers from the host rock. (MacDougall et al. (1987) used a 3.8 cm air gap). The effect of the cladding on the exposure of the fuel matrix was not considered in this conceptualization.

The radionuclide inventory used for the source term was dependent on the analyses conducted. For aqueous release analyses, 9 radionuclides were included; for volcanic events and human intrusion 39 radionuclides were included; and for gaseous release only ^{14}C was included. The volcanic events and human intrusion analyses simulate direct release to the surface, so all significant radionuclides are included. On the other hand, the aqueous release contains additional considerations such as velocity, retardation, and release rate. Some radionuclides are very insoluble and highly retarded, and thus provide a negligible contribution to total release. These are disregarded in the analyses. A summary of the radionuclides included in aqueous and gaseous release analyses is presented in Table 2-1.

For the aqueous release analyses, significant ingrowth of radionuclides was calculated up-front and included in the initial inventory of parent radionuclides. In particular, the initial inventories for ^{234}U and ^{237}Np were increased to account for their parents (notably ^{238}Pu, ^{241}Pu, and ^{241}Am) which were not simulated.

The 33,300 containers in the waste inventory were divided into two major categories based on data in the SCP (DOE, 1988): 60 percent pressurized-water-reactor (PWR) spent fuel and 40 percent boiling-water-reactor (BWR) spent fuel. TSPA-1991 assumed 2.1 metric tons of heavy metal per container, based on Apted et al. (1990). The only distinction between the two groups

was the assumed burnup value which was 33,000 megawatt-days per metric ton of heavy metal (MWd/MTHM) for PWR, and 27,500 MWd/MTHM for BWR. These values are used to calculate the "EPA ratio," the ratio of a radionuclide's release (radionuclide-specific cumulative release limit of 40 CFR Part 191 (EPA, 1985) (see Section 3.5.1, below)). A total repository of 70,000 MTHM of waste was assumed.

The processes included in the TSPA-1991 waste package/engineered barrier system included container wetting after the thermal dryout period, container failure, radionuclide mobilization, and radionuclide transport out of the container.

Rewetting: Rewetting means the re-occurrence of liquid-phase water into the host rock after the thermal period. It does not mean that saturated conditions are expected or will occur. There are two parts to the TSPA-1991 repository rewetting: (1) the actual time of wetting the waste packages being contacted by liquid water after the thermal pulse, and (2) the procedure to determine how many waste packages are contacted by liquid water. The system was assumed to be dry initially due to heat released from the waste. No thermal calculations were included. No waste was released during this time period. Container wetting was assumed to occur gradually, starting 300 years after emplacement and reaching equilibrium, with all packages "rewet," 1000 years later.

TSPA-1991 divided the waste packages into four categories depending on the water saturation of the waste packages. The saturation was directly related to the release mode of radionuclides from the containers. Four different modes of release were included: (1) advective only, (2) diffusive only, (3) advective and diffusive, and (4) none. Advective releases were assumed to occur if a waste package was in a locally wet (seepage area) part of the repository. A simple flow-through model was assumed in calculating the advective releases. Diffusive releases were assumed to occur if the air gap was partially filled with rubble. The height of the rubble in the air gap was assumed to be the same as the height of the water in the container, thus simplifying the estimate of the fraction of the spent fuel in a given container that contributes to diffusive releases. Advective and diffusive releases occurred when the containers were in locally wet areas and had rubble in the air gap. A fraction of the waste packages potentially were in dry areas with an intact air gap, and no release occurred from these packages.

The relative number of waste packages in each category was determined in the following manner. The fraction of containers in seepage areas is denoted by f_s and the fraction of containers with rubble filling at least part of the air gap is denoted f_r. The f_s fraction covers those containers experiencing advective releases, and the f_r fraction covers those containers with a failed air gap. The f_r fraction was a user supplied value. In TSPA-1991, half of the containers were assumed to be in the f_r fraction. The fraction of containers in the f_s fraction was calculated from the following equation:

$$f_s = P[q > q_0] = 0.5 \cdot \mathrm{erfc}\left(\frac{\ln q_o - u}{\sqrt{2}\,\sigma}\right) \qquad (2\text{-}1)$$

where: erfc = complementary error function (see Appendix A)
u = mean of the spatial flux distribution in log space
σ = standard deviation of the spatial flux distribution in log space
q = percolation rate
q_0 = flux carried by porous matrix (assumed equal to the saturated matrix hydraulic conductivity of the Topopah Springs (K_0), a tuff unit of Yucca Mountain that is the potential repository host rock).

The average flux for those containers subjected to seepage flow is given by:

$$q' = q \cdot f_s^{-1} \cdot 0.5 \cdot \text{erfc}\left(\frac{\ln q_0 - u - \sigma^2}{\sqrt{2}\,\sigma}\right) \qquad (2\text{-}2)$$

It is assumed that q_0 of that flux is carried by the porous matrix, so that the average flux available for seepage flow is given by:

$$q_s = q' - q_0 \qquad (2\text{-}3)$$

Figures 2-2 through 2-5 illustrate histograms of q, K_0, f_s, and q_s, respectively, generated with @RISK. It can be seen that f_s has a large number of values close to 0.0 (corresponding to no advective releases) and 1.0 (corresponding to advective releases). It bears noting that if f_s=0.5, then 25 percent of the waste packages would be in each of the four water contact and release modes.

Container Failure: The container failure distribution used in TSPA-1991 was based on the rewetting period and a time to failure given the repository is rewet with an assumed log-uniform distribution from 500 to 10,000 years. For a particular realization, a time was sampled from the distribution, and all containers were failed by the sampled time. If failures could not occur until 500 years after the container was wet, the initial releases should not occur until at least 800 years. However, a review of the individual radionuclide release curves (Barnard et al., 1992, Figure 4-47) shows that releases occurred starting at 300 years. (NOTE: There is some uncertainty regarding the interpretation of failure distributions used in TSPA-1991. We have used three different assumptions that are described in Section 2.3.1 below).

Radionuclide Mobilization: Before the radionuclides can be transported from the repository, the container must fail and the waste must be altered and mobilized. Alteration refers to chemical alteration (oxidation) of the UO_2 fuel matrix which frees the radionuclide for possible dissolution. The waste inventory was divided into alteration-limited (high solubility) and solubility-limited radionuclides. In TSPA-1991, 2 percent of the high-solubility radionuclide inventory (^{135}Cs, ^{129}I, ^{79}Se, and ^{99}Tc) was available for quick release once the container failed. This prompt inventory fraction is at the upper end of the values suggested, and the SCP goal is to achieve less than 0.02 (DOE, 1988). The matrix alteration rate (a_m), prompt alteration rate (a_p), and fraction of the

waste-form surface area wetted (f_{ws}) are included in the calculation of waste mobilized for advective releases. These are all input parameters in TSPA-1991 analyses. The matrix alteration is assumed to proceed at a certain rate, but only part of the waste is contacted by water and is releasing its waste to the water. The TSPA-1991 matrix alteration rate upper bound was based on laboratory experiments of spent fuel leaching (Apted et al., 1990). The lower bound was arbitrarily selected as 20 times lower to reflect the uncertainty in the parameter (Barnard et al., 1992). The prompt alteration rate was simply a small number to spread the release over 2 years, but is insignificant relative to the other time scales in the analyses (Barnard et al., 1992). The fraction of the waste form surface area wetted was simply set to the middle of the possible range (Barnard et al., 1992). For diffusive releases, f_{wd} is the fraction of the waste-form surface area wetted and participating in diffusive releases. This parameter was also set to the middle of the possible range (Barnard et al., 1992).

Radionuclide Transport: After the radionuclides have been mobilized, they are available for transport out of the waste containers. The TSPA-1991 calculation of advective release is different than that of diffusive release. Also, the treatment of transport of alteration-limited radionuclides is different from that of solubility-limited radionuclides.

For the advective-release model, TSPA-1991 assumed that water flows into the container at the top, and exits at the bottom. The time scale for this process is given by the volume of water in the container divided by the rate at which water flows through the container. The volume of water inside the waste container is given by:

$$V_1 = A \cdot d_{film} \cdot f_{ws} \tag{2-4}$$

where A = total surface area of the spent fuel rods in a container, d_{film} = thickness of the water film on the wetted part of the spent-fuel surface, and f_{ws} is the fraction of the waste-form surface area wetted.

The volume rate at which water flows through the container is given by:

$$V_2 = A_c \cdot f_{in} \cdot q_s \tag{2-5}$$

where A_c = the area around a waste container where water flux is gathered and funneled into the container (the "effective catchment area"), f_{in} = fraction of the flux through A_{cross} that actually gets into the waste package, and q_s is the average seepage flux in the vicinity of containers that have seepage flux.

For advective solubility-limited releases, the rate at which radionuclides are released is given by the rate of flow through the container multiplied by the maximum solubility of the radionuclide.

For diffusive releases across the rubble, two values of the diffusion coefficient were used, one for a wet container environment, and one for a moist container environment. Also, the diffusion time scales differ because the radionuclides have different retardation values. Combination advective-diffusive transport is handled differently for alteration-limited and solubility-limited cases. For alteration-limited radionuclide mobilization, the advective and wet-diffusive time scales are combined. The fastest process will dominate the mobilization. For solubility-limited

radionuclide mobilization, the advective and wet-diffusive releases are calculated separately, then added together.

TSPA-1991 results used for comparison purposes with RIP waste package results are presented in Figures 2-6 and 2-7. The CCDF of release from the WP/EBS is shown in Figure 2-6. Note that Figure 2-6 applies the EPA standard at the EBS/host-rock interface rather than at the accessible environment boundary as specified in the EPA's 40 CFR Part 191. This was done for ease of computation and for illustrative purposes only. Individual radionuclide release curves are presented in Figure 2-7 in terms of the ratios of their calculated release rates to the allowable release rates specified in the NRC's 10 CFR Part 60.

2.2 RIP APPROACH TO WASTE PACKAGE/ENGINEERED BARRIER SYSTEM

The RIP software is capable of simulating the primary concepts included in the TSPA-1991 waste package analyses. The following discussion divides the waste package concepts into five categories: container data, inventory, exposure of radionuclides to liquid water, transport of radionuclides, and air gap. Where appropriate, direct comparison of TSPA-1991 data with the RIP conceptualization are included in tables. Figure 2-8 shows a schematic of the processes which may be included in RIP waste package modeling.

Container Data: The container data used in RIP are directly comparable to the TSPA-1991. Table 2-2 details the comparison. Note that the RIP case of 2.1 MTHM/container only results in 69,930 MTHM in the repository, slightly less than the TSPA-1991 value of 70,000 MTHM.

Inventory: The waste inventory defined in TSPA-1991 can also be implemented within RIP, after units conversion. Table 2-3 shows the TSPA-1991 inventory for aqueous release analyses and the comparable RIP inventory. The RIP inventory was input as Ci/container, converted from Ci/MTHM as 2.1 MTHM/container. Prompt release fractions were included in the RIP data set as gap inventory, essentially free inventory within the secondary container. This is discussed in more detail in the "Exposure of Inventory" section. TSPA-1991 prompt alteration rate (calculated to take 2 years) is not included as such in RIP. RIP includes such release as rapid, or instantaneous release once the container fails. The TSPA-1991 prompt release time period is so small relative to the 10,000 year analysis period that it is insignificant.

Solubilities for the RIP data set were converted from TSPA-1991 moles/liter to g/m^3 according to the following formula:

$$\left(\frac{\text{mole}}{\text{liters}}\right) \cdot \left(\frac{\text{g}}{\text{mole}}\right) \cdot \left(\frac{1{,}000 \text{ liters}}{\text{m}^3}\right) = \frac{\text{g}}{\text{m}^3} \text{ of radionuclide} \qquad (2\text{-}6)$$

TSPA-1991 did not specify the solubilities for the alteration-limited radionuclides, essentially setting them to infinity (Wilson, 1993). In RIP, the solubilities for these radionuclides were set to values large enough to allow alteration rather than solubility to control the release rate.

Mobilization of Inventory: There are two aspects to mobilization of the radionuclides prior to transport. The inventory must be altered and the containers must fail. Table 2-4 lists the WP failure parameters. The TSPA-1991 rewetting time parameter values are based on thermal modeling of the spatial array of waste packages (Johnson and Montan, 1990). The 9,500-year range for container lifetime distribution was chosen for TSPA-1991 to reflect the significant uncertainty in container performance (Barnard et al., 1992). Table 2-5 lists the various parameters important to mobilization of the radionuclides. The TSPA-1991 fractions for containers with rubble in the air gap, fuel wet with seepage, and fuel wet and diffusing, were simply set to the middle of the possible range (Barnard et al., 1992). The source of TSPA-1991 matrix alteration rate and prompt alteration rate was discussed in Section 2.1. The TSPA-1991 value for spent fuel surface area per package was taken from design data tabulated in the SCP (DOE, 1988). The water film thickness on a spent fuel surface under unsaturated conditions is unknown, but will probably depend on surface roughness, capillarity, and water surface tension (Barnard et al., 1992). Many of the TSPA-1991 parameters are shown graphically on Figure 2-1.

The TSPA-1991 waste package failure distribution is described in Section 2.1. RIP simulation of WP failure requires the use of both container failures (primary and secondary) to adequately represent the TSPA-1991 WP failure. Resaturation was simulated by a uniform primary container failure of 800 - 1800 years. Once a package was contacted by liquid-phase water, the simulation of WP failure was initiated.

WP failure was simulated using the secondary container failure feature of RIP. To mimic the TSPA-1991 log-uniform distribution, the distribution used initially was a Weibull distribution. (*Note:* Initially, RIP did not allow for a log-uniform failure distribution. This was modified in subsequent versions of the software.) Other WP failure distributions are included in Table 2-4.

Within TSPA-1991, the fraction of seepage entering the container is combined with the water collection area. In RIP, these parameters are combined into an effective catchment area. The effective catchment area is only activated for the two water contact modes that have advective release (modes 1 and 2).

Many of the parameters in Table 2-5 help define the number of waste packages in each water contact mode. Within TSPA-1991, diffusive releases occur only in containers that have rubble in the air gap. Advective releases occur in containers that have fuel wet with seepage. Some containers have both diffusive and advective releases when fuel is wet and diffusing. The dry containers have no release.

RIP used the same four water contact modes defined in TSPA-1991, although with a different nomenclature. The advective-only release mode is called *wet-drip* in RIP. The advective and diffusive release mode is called *wet-feet* in RIP. The diffusive-only release mode is called *moist-continuous* in RIP. The no release mode is called *nominal* in RIP. Wet-drip and wet-feet occur when the fraction of containers in seepage areas (f_s) is equal to 1. Moist-continuous and nominal releases occur when f_s=0.0. When f_s=0.5, then 25 percent of the waste packages will be in each of the four water contact modes. It bears noting that for advective releases, only advective parameters are required (such as effective catchment area, seepage flux, and fraction of waste wet); for diffusive releases, only diffusive parameters are required (such as diffusion coefficient, geometric factor for diffusion, and the fraction of waste wet); while for the combined advective-

diffusive release both sets of parameters are required. It also bears noting that the diffusion coefficients for moist-continuous release is less than that for wet-feet releases due to the differences in tortuosity and effective area available for release when the media is partially saturated (see Conca, 1990).

Transport Parameters: The transport of exposed radionuclides is dependent on numerous parameters. Transport may be divided into advective and diffusive transport. Diffusive transport is further subdivided into moist and wet diffusion. Within RIP, the different diffusion coefficients are implemented by simulating release from each of the water contact modes differently. For water contact modes 1 and 2, the wet diffusion coefficient is used. For water contact mode 3, the moist diffusion coefficient is used. For water contact mode 4, no diffusive release is allowed. These parameters are detailed in Table 2-6. The TSPA-1991 diffusion coefficients are based on modifying the typical diffusion coefficient in water (3.0×10^{-2} m^2/yr) (Travis et al., 1984) to account for tortuosity and constrictivity effects. Also, under wet conditions the diffusion coefficient might be as high as it is in water (Barnard et al., 1992), but under moist conditions the effective diffusion coefficient is reduced by several orders of magnitude (Conca, 1990). The TSPA-1991 distribution of "wet" diffusion coefficients is a small range about the far-field value of 3.16×10^{-3} m^2/yr; the "moist" diffusion coefficient distribution is broader and its maximum is below the minimum wet values (Barnard et al., 1992).

The TSPA-1991 percolation rate distribution is based on distributions used in prior performance assessment analyses (PACE-90; SCP; Sinnock et al., 1984) and an exponential distribution was chosen to weight the range toward the low end of the distribution.

The TSPA-1991 effective diffusion area is equal to the waste container surface area reduced by the product of the effective porosity and the saturation of the rubble (Barnard et al., 1992).

The TSPA-1991 water collection area is subjective, based on expected drainage area for a single container. The fraction of seepage through the water collection area was set at the midpoint of the possible range (Barnard et al., 1992).

The TSPA-1991 rubble thickness is assumed to be 3 cm, based on Apted et al. (1990) and Ueng and O'Connell (1992).

Diffusive Release: RIP models diffusive releases through the waste package as a steady state process, with the transfer rate equal to the product of the effective diffusion coefficient, the concentration of the radionuclide in contact with the waste matrix, and a geometric factor. Several formulations of the geometric factor for diffusive mass transfer (w) exist. Assuming a spherical waste form of radius R, Chambre et al. (1985) define the geometric factor as

$$w = 4 \cdot \pi \cdot R \cdot n \cdot f \qquad (2\text{-}7)$$

where n = effective porosity of the degraded package, and f = percent of the waste in contact with a diffusive pathway. Assuming R = 0.9 m, n = 0.2 and f = 0.5, yields a geometric factor for diffusive mass transfer of about 1.0.

Air Gap: The TSPA-1991 air gap is implemented in RIP as a pathway, with an assigned transport velocity that is based on the arrival time for the 50 percent mass breakthrough given a diffusive release. The pathway is only accessed for releases from waste packages in water contact mode 3. The velocity is calculated as:

$$vel = D_{eff}/L \tag{2-8}$$

where D_{eff} = the effective diffusion coefficient and L = path length.

Additional Capabilities: RIP has additional capabilities not demonstrated in TSPA-1991 which increase the ability to simulate process complexity. These additional capabilities are primarily in the source term, decay, and effective solubility of radionuclides.

Source Term: RIP has three potential fractions of the source term (Free, Gap, and Bound) versus only two for TSPA-1991 (Prompt and Bound). This allows RIP to directly incorporate the effects of the cladding failure rate if the primary and secondary container failure modes are modeled as the sequential failure of the container and cladding. This was not done in this exercise.

Decay: RIP handles decay of radionuclides as the decay occurs. On the other hand, TSPA-1991 pre-calculated decay and then introduced the decay components into the source term. The RIP implementation produces a release inventory consistent with analytical calculations of decay products from the initial repository radionuclide inventory.

Effective Solubility: Another issue where RIP is more complex than TSPA-1991 involves the concept of effective solubilities. TSPA-1991 pre-calculates the impact of isotopes on solubility and partitions the solubility for particular isotopes. RIP calculates the effective solubility as additional isotopes are created due to radioactive decay. For example, in RIP the concept causes a decrease in the ^{234}U release relative to the TSPA-1991 ^{234}U release values, due to competing solubilities with other Uranium isotopes (e.g., ^{235}U). Figure 2-9 shows the result of including the effective uranium solubility in the calculation of release for ^{234}U. The ^{234}U plot in TSPA-1991 which does not include effective solubility reaches a plateau, while the RIP simulation shows that ^{234}U peaks and then declines as other uranium isotopes are produced due to radioactive decay and begin competing with the ^{234}U for solubility (Figure 2-10). Similar effects are seen for other radionuclides which have more than one isotope in the inventory.

2.3 RESULTS OF WASTE PACKAGE/ENGINEERED BARRIER SYSTEM ANALYSES

The RIP analyses of the waste package release involved incorporating increasing complexity into the conceptual model to obtain a waste package similar to the conceptual model of the waste package in TSPA-1991. The modifications dealt with:

- Waste package failure distribution
- Radionuclide inventory
- Solubility of radionuclides
- Infiltration-dependent water contact distribution
- Air gap around waste packages.

Table 2-7 indicates the primary differences between the RIP simulations. The initial case, RUN 2.1, was developed to simulate conditions contained within the TSPA-1991 waste package. The container failure distribution was a Weibull distribution, for gradual container failure beginning 500 years after container wetting and continuing for 9500 years. The inventory included the nine TSPA-1991 radionuclides along with their most significant decay products. The inventory for the daughter products was 0 Ci/container. However, within RIP, when radionuclides are present in the initial radionuclide list table, the possibility exists for ingrowth of the radionuclide. The solubility for alteration-limited radionuclides was initially taken to be the same distribution as in Golder Associates Inc. (1993) because the TSPA-1991 did not list actual solubilities for these radionuclides. The waste packages were divided evenly into 4 water contact modes, as identified in Section 2.2. Finally, the initial case did not include a diffusion gap for the 3 cm air gap simulated in TSPA-1991.

2.3.1 Sensitivity of CCDF to Waste Package Failure

The RIP initial waste package was set up to simulate failure of the waste packages with a Weibull distribution intended to mimic a log-uniform waste package failure distribution of 9,500 years. The Weibull distribution and the log-uniform distribution are shown in Figures 2-11 and 2-12. The Weibull distribution has more containers failing at early times than the log-uniform distribution. The CCDF for 1000 realizations using these two distributions demonstrates as expected that the Weibull failure distribution causes greater release than the log-uniform distribution. A CCDF of the WP case with the Weibull failure distribution is presented in Figure 2-13. A recent upgrade to RIP allowed use of a log-uniform distribution for WP failure. Figure 2-14 presents the CCDF for this case. Comparison of the 1.0, 0.1, 0.01, and 0.001 probability values on the CCDF show that the case with the log-uniform distribution consistently has lower release than the case with the Weibull distribution. These and other CCDF figures in this section should be compared to Figure 2-6, the TSPA-1991 composite porosity release from the EBS.

2.3.2 Sensitivity of CCDF to Inventory

As noted previously, the TSPA-1991 inventory for aqueous release included only nine radionuclides, and these radionuclides decayed but the decay products were not tracked. The initial RIP waste package (which included decay) was set up for 16 radionuclides (Table 2-1) which included the most significant daughter products from the nine TSPA-1991 radionuclides. The results of the initial case simulation with 16 radionuclides are included in Figures 2-13 and 2-14. Later RIP simulations reduced the inventory to nine radionuclides, not allowing any production of daughter products, but still calculating decay. This caused a significant decrease (a factor of 2) in the simulated release from the waste packages. The CCDF results for the reduced number of radionuclides are presented in Figure 2-15. The results are consistently lower than the case with 16 radionuclides primarily because daughter product production (especially ^{210}Pb and ^{226}Ra) does not occur in the case with nine radionuclides.

2.3.3 Sensitivity of CCDF to Waste Alteration

Solubility of Radionuclides: One parameter not specified in TSPA-1991 (Barnard et al., 1992) is the solubility of alteration-limited radionuclides such as ^{99}Tc. Wilson (1993) indicated the

solubilities were effectively infinite (>1000 kg/m^3). Solubility values were varied in RIP to find the value above which no additional release occurs. RIP solubilities for the alteration-limited radionuclides were then specified as greater than these values in the simulations presented in Figure 2-16. ^{99}Tc and ^{135}Cs were the only radionuclides given the high solubility values. The results indicate a slightly larger total release when essentially infinite solubilities are used for ^{99}Tc and ^{135}Cs.

2.3.4 Sensitivity of CCDF to Waste Package Release

Failure Time per Realization: TSPA-1991 waste package failures occurred according to the distribution described in Section 2.1. All previously presented RIP simulations failed the waste packages gradually through time for the duration of the 9500-year failure period. Figure 2-17 presents the results of simulations which implemented the TSPA-1991 failure characterization. This caused an increase in the release from the waste packages as shown on the CCDF, primarily because the waste package failures occurred earlier in time and were completed earlier than for the previous distribution (which had failure of all packages at 10,300 years).

Implementation of Relationship between Infiltration and Saturated Matrix Hydraulic Conductivity: Thus far, the number of waste packages in each water contact mode was equal to one quarter (25 percent) of the total number of waste packages. As noted in Section 2.1, TSPA-1991 used a functional relationship between infiltration and the saturated matrix hydraulic conductivity of the Topopah Springs to determine the number of waste packages in each of the water contact modes. In this waste package simulation, the f_s implementation described in Section 2.1 was simulated. Figure 2-18 shows the CCDF for this conceptualization. Comparison with the TSPA-1991 CCDF (Figure 2-6) shows that the RIP release is less than the TSPA-1991 release.

Air Gap: An additional factor in TSPA-1991 was the implementation of a 3-cm air gap at the edge of the waste packages. Within RIP, this was simulated as a 3-cm pathway that was only activated if releases were from the moist continuous waste packages and the diffusion coefficient value was the same as the moist diffusion coefficient. The dispersivity, a parameter required for a pathway in RIP, was arbitrarily selected as 1 m. Additional details are found in Appendix A. The results of adding the air gap to these simulations, which provide a waste package conceptual model very similar to the TSPA-1991 waste package are presented in Figure 2-19. Compared to Figure 2-18, the results are only slightly reduced. The air gap has the effect of delaying the release of the diffused radionuclides, leading to lower overall release.

Implementation of Average Flux Available for Seepage Flow: A final factor which TSPA-1991 included was an evaluation of whether or not the infiltration rate would cause fracture flow. In the cases where the flux is greater than the saturated matrix hydraulic conductivity of the Topopah Springs, fracture flow is assumed to be initiated. Only when fracture flow exists is there any possibility for waste packages to experience *wet-feet* or *wet-drip* water contact modes and the corresponding advective releases from the EBS. This q_s evaluation was included in RIP for the final waste package analysis to more precisely mimic the TSPA-1991 conceptualization. Results are shown in Figure 2-20. In general, as with the addition of the air gap to the conceptual model, the results show slightly lower releases than the previous simulations.

Additional CCDFs showing the results for individual radionuclide release are provided in Figures 2-21 through 2-25. These CCDFs present results for ^{99}Tc, ^{129}I, ^{239}Pu, ^{79}Se, and ^{234}U, respectively. Note the high ^{239}Pu release. It is to be noted again that all these CCDFs for WP/EBS releases are not calculations of the EPA standard's performance measure at the accessible environment boundary. These calculations apply that performance measure to the EBS-rock interface for illustrative purposes only.

2.3.5 Comparison of Individual Radionuclide Release from TSPA-1991 and RIP

The individual radionuclide release curves for the expected values of TSPA-1991 are presented in NRC-normalized form in Figure 2-7. The non-normalized results are presented in Figure 2-26. The peak values for TSPA-1991 and some of the RIP simulations are presented in Table-2-8. As noted in Section 2.1, the treatment of alteration-limited radionuclide release was different from solubility-limited release in TSPA-1991. In RIP, the radionuclides are treated identically, except that the solubility limit for a particular radionuclide will affect whether that nuclide has solubility-limited or alteration-limited release.

The TSPA-1991 peak values for the solubility-limited radionuclides are generally slightly higher than those from the RIP simulations. The expected value from the given TSPA-1991 solubility distribution is slightly lower when implemented in RIP for ^{243}Am, ^{237}Np, and ^{234}U. This difference, while slight, would cause a difference in the release for these radionuclides.

TSPA-1991 used partitioning of isotope solubility limits rather than calculate solubility limits as they changed through time. The partitioning factors at 10,000 years were used to adjust the solubility limits since they are higher than the ones at early time. RIP simulations used the same solubilities as TSPA-1991 over all times.

The TSPA-1991 peak values for the alteration-limited radionuclides are generally lower than those from the RIP simulations. The RIP results for the RUN 2.4 case alteration-limited radionuclides are very close to the TSPA-1991 values. Note the RUN 2.4 WP failure distribution produces less release at early time than the failure distribution in RUN 2.5 and RUN 2.8 because the WP failures in RUN 2.4 are spread out over 9,500 years after rewetting, while the WP failures in RUNs 2.5 and 2.8 are spread out from the time of rewetting to a value sampled from the log-uniform distribution of 0-9,500 years (mean of 3,170 years).

The description of TSPA-1991 individual radionuclide release indicates that rewetting starts at 300 years, continues uniformly for 1000 years, and no release occurs until at least 500 years after a container is wet (at least 800 years from waste emplacement). However, Wilson (1993) clarified that while the rewetting period was as we expected, the failure distribution was as follows. A maximum time of failure was sampled from a log-uniform distribution from 500 to 10,000 years. The expected value of this distribution is 3,170 years. The failure then was assumed to be uniform from 0 years after rewetting to the maximum failure time.

An additional RIP simulation was conducted to evaluate the impact of using 300 years as the start time for release. These CCDF results are presented in Figure 2-27. The release is slightly higher than Figure 2-20, the CCDF results for the RIP data set that resembles TSPA-1991 most closely. The individual radionuclide release curves are presented for a few of the radionuclides

(^{99}Tc and ^{239}Pu) in Figures 2-28 and 2-29. As expected, the release start time matches TSPA-1991 and the time of peak arrival occurs earlier than in Figure 2-20 and closer to the TSPA-1991 peak arrival.

2.3.6 Scatter Plots for Selected Parameters from CCDF Analyses

Limited sensitivity analyses were conducted to evaluate the importance of selected parameters on the release of certain radionuclides. These scatter plots were developed based on RUN 2.8. The effect of the dissolution value on ^{99}Tc release (1,000 realizations) is presented in Figure 2-30. Increasing the dissolution has a direct effect on the total ^{99}Tc release. The ^{239}Pu release as a function of the effective catchment area and geometric diffusion factor (100 realizations each) are shown in Figures 2-31 and 2-32. The release of ^{239}Pu is not directly affected by the effective catchment area value, while an increase in the geometric diffusion factor increases the total ^{239}Pu release. Finally, the effect of the diffusion coefficient on ^{135}Cs release (100 realizations) is presented in Figure 2-33. There is no apparent correlation between the increase in diffusion coefficient and ^{135}Cs release.

2.4 PARAMETER SENSITIVITY ANALYSIS

The release from the different waste packages is dependent on many variables. In an attempt to determine the sensitivity of the release to these parameters, we started with a base case with all the parameters set constant, usually to their expected values. The base case was a product of the comparison with TSPA-1991 discussed earlier. Multiple-realization runs were made with RIP varying one parameter at a time. This way, we were able to observe the effect of the various parameters without the stronger effects obscuring the more subtle effects.

Subsequently, simulations were made varying many parameters simultaneously. These combined runs allowed us to determine the relative importance of the different parameters to the release of radionuclides.

The release of radionuclides that we analyze falls into two categories: low-solubility (solubility-limited) and high-solubility (alteration-limited). The radionuclides ^{243}Am, ^{237}Np, ^{239}Pu, ^{126}Sn, and ^{234}U are in the former category, while ^{135}Cs, ^{129}I, ^{79}Se, and ^{99}Tc are in the latter category. The elements within each group have similar sensitivities, and for simplicity we present the results for ^{99}Tc and ^{239}Pu as being representative of high- and low-solubility radionuclides, respectively. Where there is variation within a category of radionuclides and it is not appropriate to consider a single "representative" radionuclide, the range of behaviors is discussed.

Four water contact modes were considered: wet-feet, moist-continuous, wet-drip, and nominal. The inventory was assumed to be divided equally among the four modes, but post-processing allowed us to independently analyze the waste packages in the different water contact modes. As there is no water contact for the nominal mode, no release occurs for these waste packages. Thus, none of the parameters of interest will affect the release of radionuclides from these containers, and we will not further discuss the nominal case.

2.4.1 Sensitivity of Waste Package to Waste Alteration Parameters

We first considered waste alteration parameters, including the matrix dissolution rate, the fraction of waste wetted, and the solubility of the radionuclides. The results for high- and low-solubility radionuclides are shown in Tables 2-9 and 2-10, respectively. These tables contain the parameter description, the range of the parameter analyzed, the expected value of the parameter, the sensitivity exhibited by the parameter (e.g., none, linear, or log-like), and the water contact modes responsible for the sensitivity. When the sensitivity was linear, the slope was represented by m, the standard convention (y=mx+b). In some cases, the sensitivity curve consisted of linear segments, each of different slope. For these cases, the slopes were designated by m_1 , m_2 , ... , from left to right for the respective segments. For simplicity, the water contact modes are abbreviated WF, WD, and MC for wet-feet, wet-drip, and moist-continuous, respectively.

It is seen that the high-solubility radionuclides are dependent on all the waste alteration parameters analyzed, exhibiting log-like behavior for the matrix dissolution rate (R_{dis}) and the fraction of waste wetted (f_w) (Figures 2-34 and 2-35) and linear behavior for the solubility. For all three cases, the wet-feet, wet-drip, and moist-continuous water contact modes are sensitive to changes in the waste alteration parameters.

The sensitivity curve for the solubility of ^{99}Tc is qualitatively different from the sensitivity curves discussed above (see Figures 2-36 and 2-37). For extremely low solubilities, the release increases linearly with great slope as the solubility increases. For a technetium solubility (S_{Tc}) of approximately 100, the slope of the sensitivity curve changes and the release then increases slowly, but linearly, as the solubility increases. Finally, at S_{Tc} approximately 9,000, there is another change in the slope of the sensitivity curve, and the release is constant with further increases in solubility. This behavior is simply explained. For a particular water contact mode, a low solubility means that the release is solubility-limited. As the solubility increases, the release increases until a critical solubility is reached. At this point, the release becomes alteration-limited and no increase in solubility can increase the release. The wet-feet and wet-drip water contact modes have approximately the same critical solubilities, while the moist-continuous mode has a significantly higher solubility. The sensitivity curve is a superposition of all the modes. In the first region, the releases from the wet-feet, wet-drip, and moist-continuous modes are increasing. In the second region, the releases from the wet-feet and wet-drip modes have plateaued, but the release from the moist-continuous mode is still increasing. In the third region, the release from the moist-continuous mode has plateaued, and the total release is constant.

Generally, the low-solubility radionuclides are not sensitive to the matrix dissolution rate or the fraction of waste wetted. For instance, only ^{126}Sn exhibits any sensitivity to changes in the matrix dissolution rate (Figure 2-38). In this case, the release rises linearly until it becomes constant. However, the increase is slight and considered insignificant. For the fraction of waste wetted, the releases of ^{234}U and ^{126}Sn rise linearly and become constant early in the sensitivity curve. This behavior is not very significant because of the low value at which the release becomes alteration-limited, and the magnitude of the overall increases (0.1% and 0.7% for ^{234}U and ^{126}Sn, respectively). Changes in solubility linearly affect the release of low-solubility radionuclides, as may be expected from our experience with the high-solubility radionuclides (at low solubilities, the release increases linearly).

2.4.2 Sensitivity of Waste Package to Release Parameters

The release parameters examined with sensitivity analyses are the repository infiltration rate, the volume of water contacting the matrix, the moist-continuous and wet-feet diffusion coefficients, the geometric factor for diffusion, and the effective catchment area. The results for the high- and low-solubility radionuclides are shown in Tables 2-11 and 2-12, respectively. As for Tables 2-9 and 2-10, these tables include the parameter description, the range over which the parameter was sampled, the expected value of the parameter, any sensitivities exhibited during the variation, and the water contact modes that were the cause for the sensitivities. In one case, the sensitivity was the "left-most point." This is in essence a linear rise followed by a constant region. However, because only the realization with the lowest parameter value (the left-most point on the curve) had a lower value for the release than the rest of the realizations that all had the same value, it was not possible to obtain a slope for the region of linear increase. For these cases, high-solubility radionuclides other than ^{99}Tc had different sensitivity curves. Some were always rising linearly, some increased linearly before they became constant, and some were always constant.

For both the geometric factor for diffusion (w) and the effective catchment area (A_c), the expected value is zero. This is because these variables are dependent on the water contact mode. For the former, w is zero for the wet-drip water contact mode, and it is non-zero for the moist-continuous and wet-feet water contact modes. For the latter, A_c is zero for the moist-continuous water contact mode, and it is non-zero for the wet-feet and wet-drip water contact modes. For the high-solubility radionuclides, the moist-continuous waste packages are sensitive to changes in w and the wet-drip waste packages are sensitive to changes in A_c.

The high-solubility radionuclides exhibited little or no sensitivity to the release parameters. The general pattern, exhibited by all but the wet-feet diffusion coefficient and the water volume contacting the matrix, was that of linear increase until the release was constant with further parameter increase (e.g., Figure 2-39). The point at which the transition occurs depends on the parameter and on the radionuclide. For a given parameter, there is usually a range of transition points corresponding to the different radionuclides. As an example, consider the repository infiltration rate (q_{inf}): ^{135}Cs has the transition point at 0.0002, so that there are enough points left of the transition that the linear behavior is apparent. ^{99}Tc has a lower transition point, so that there are fewer points showing on the plot. ^{129}I and ^{79}Se have the transition even lower, so that the only points plotted are above the transition--only the plateau is shown. The regions where the releases are sensitive to variations in q_{inf} are significantly less than the expected value of q_{inf}. Thus, near the expected values, the release of high-solubility radionuclides is insensitive to changes in the release parameters.

Whereas all the other sensitivity curves increase monotonically (or are constant), the dependence exhibited by the volume of water contacting the matrix is that of monotonic decrease. For high-solubility radionuclides ^{79}Se and ^{99}Tc, the curves are constantly decreasing. The shape of these curves indicates that the release is inversely related to the volume: release $\propto V^{-1}$ (Figure 2-40). For ^{135}Cs, the sensitivity curve was constant for volumes less than 0.11, and decreasing for greater volumes in a different manner than the other two high-solubility radionuclides discussed above (Figure 2-41). The behavior is due to the waste packages in the wet-feet, wet-drip, and moist-continuous water contact mode. The decrease is due to a change of the effective

concentration C(n) of the radionuclide in the water in contact with the matrix (Golder Associates Inc., 1993, p. 62). This concentration is defined as:

$$C(n) = \min\left[\frac{M_p(n)}{V}, C_s(n)\right] \tag{2-9}$$

where $M_p(n)$ is the average amount of exposed mass of radionuclide n in a failed waste package; V is the volume of water contacting the matrix; and $C_s(n)$ is the saturation concentration of radionuclide n. For small volumes of water contacting the matrix, the effective concentration is the saturation concentration. For sufficiently large volumes of water, the effective concentration is not controlled by solubility considerations ("i.e., the solubility is high and the concentration is determined by how much mass has been exposed and the volume of water into which it has dissolved" (Golder Associates Inc., 1993, p. 63).

The low-solubility radionuclides exhibited linear, non-trivial dependence on all the release parameters (Table 2-12) except the water volume contacting the matrix. These sensitivity curves were straight-forward and did not introduce any new insights. The sensitivity curves of the water volume contacting the matrix were, with one exception, expected. For ^{239}Pu and ^{237}Np, the release is insensitive to changes in the volume. For sufficiently large values of the water volume, the releases of ^{234}U and ^{243}Am decreased as the volume increased. This behavior is explained in the same fashion as in the discussion relating to Equation 2-9. The only irregularity was the sensitivity curve for ^{126}Sn: it has much more structure than any of the other sensitivity curves for the water volume contacting the matrix (Figure 2-42). This structure is exhibited by the wet-feet, wet-drip, and moist-continuous water contact modes. At this time, we do not have an explanation for the behavior of this sensitivity curve.

As we mentioned above, some simulations were made with multiple parameter variations. The coefficients of the correlation matrix were generated and analyzed. A negative correlation coefficient implies that as the parameter increases, the release decreases; a zero correlation coefficient means that there is no correlation between the release and a particular parameter; and a positive correlation coefficient means that as the parameter increases, the release increases. The larger the magnitude of the coefficient, the greater the correlation between a parameter and the release. Thus, when many parameters are varied, the parameters with the largest correlation coefficients have the most influence on the release of the radionuclides.

In the first multiple-parameter RIP RUN (RUN 2.9) we varied the moist-continuous diffusion coefficient ($D_{eff,mc}$), the matrix dissolution rate (R_{dis}), the fraction of waste wetted (f_w), and the solubility of technetium (S_{Tc}). The correlation coefficients for the 1000-realization run are shown in Table 2-13. Based on our discussion above, we conclude that for low-solubility radionuclides,

$$D_{eff,mc} >> R_{dis}\ ,\ f_w >> S_{Tc}\ .$$

By this, we mean that the effects from varying the moist-continuous diffusion coefficient ($D_{eff,mc}$) overwhelm any effects seen by varying R_{dis} or f_w , which in turn overwhelm any effects seen by varying S_{Tc} . Comparing with Tables 2-10 and 2-12, we see that this behavior

is consistent with our earlier results. Using the same nomenclature for high-solubility radionuclides,

$$R_{dis} > f_w > D_{eff,mc} ,$$

and for ^{99}Tc, in particular,

$$R_{dis} > f_w > S_{Tc} > D_{eff,mc} .$$

In the second multiple-parameter RIP RUN (RUN 2.10), we varied the moist-continuous diffusion coefficient ($D_{eff,mc}$), the wet-feet diffusion coefficient ($D_{eff,wf}$), the effective catchment area (A_c), the geometric factor for diffusion (w), the repository infiltration rate (q_{inf}), and the solubility of plutonium (S_{Pu}). The correlation coefficients for this 1,000-realization run are shown in Table 2-14. For the low-solubility radionuclides, the sensitivities are

$$w > D_{eff,wf} > A_c > q_{inf} >> D_{eff,mc} ,$$

and for ^{239}Pu, in particular,

$$S_{Pu} > w > D_{eff,wf} > A_c > q_{inf} >> D_{eff,mc} .$$

The high-solubility radionuclides do not exhibit as uniform behavior. ^{129}I and ^{79}Se have near-zero coefficients for all parameters in this run. ^{135}Cs has the following sensitivity:

$$D_{eff,mc} , w > q_{inf} > A_c >> S_{Pu} , D_{eff,wf} .$$

^{99}Tc has similar behavior:

$$D_{eff,mc} , w > q_{inf} > A_c , S_{Pu} , D_{eff,wf} .$$

We may combine the relations above to obtain series of relations which describe the relative importance of the different parameters for release of ^{239}Pu and ^{99}Tc. For ^{239}Pu,

$$S_{Pu} > w > D_{eff,wf} > A_c > q_{inf} >> D_{eff,mc} >> R_{dis} , f_w$$

For ^{99}Tc,

$$R_{dis} > f_w > S_{Tc} > D_{eff,mc} , w > q_{inf} > A_c , D_{eff,wf} .$$

From these two relations, it can be easily discerned which are the important parameters and which parameters are relatively unimportant for the release of ^{239}Pu and ^{99}Tc.

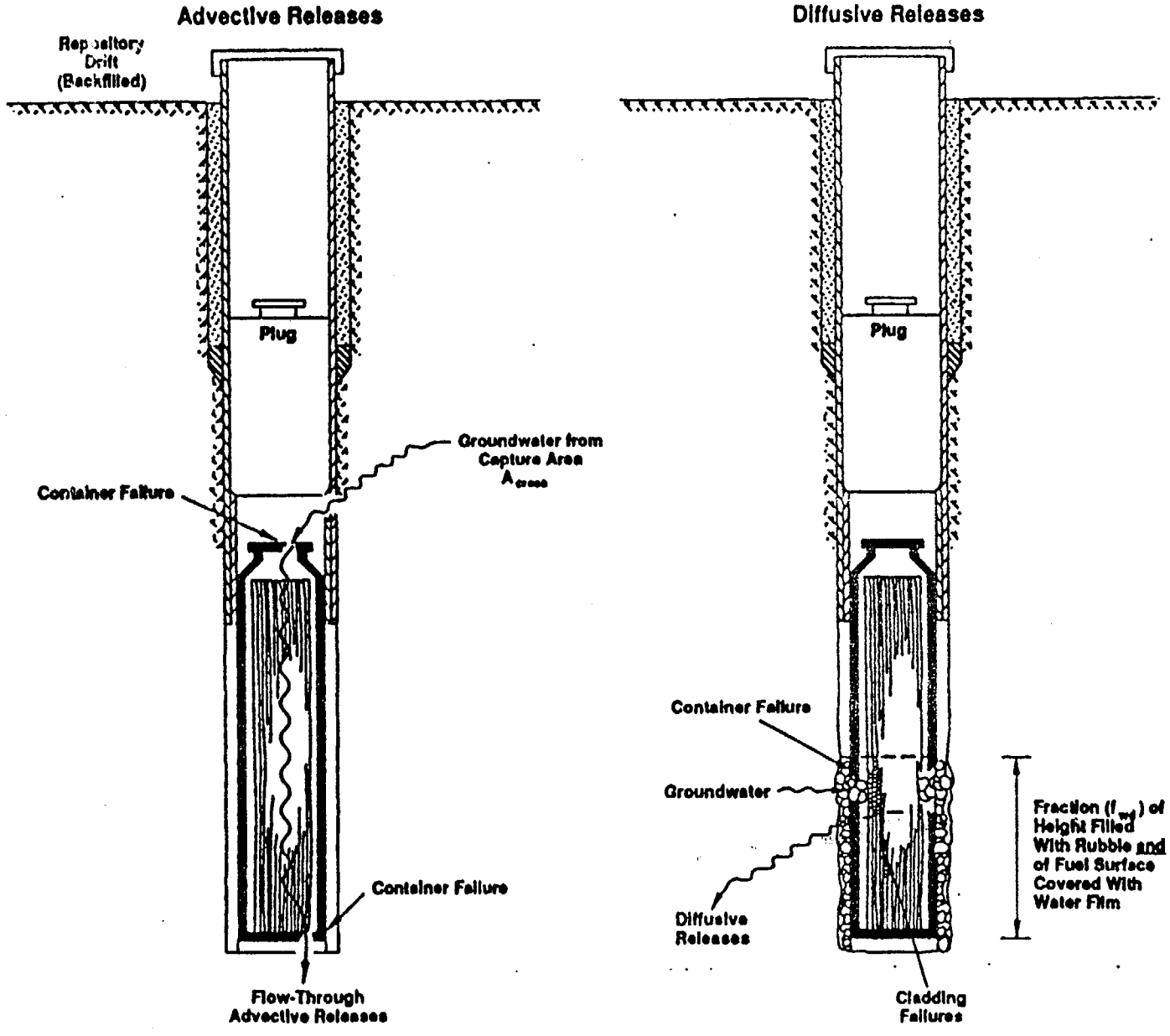

Figure 2-1. TSPA-1991 Waste Package Schematic (taken from Golder Associates, Inc., 1993)

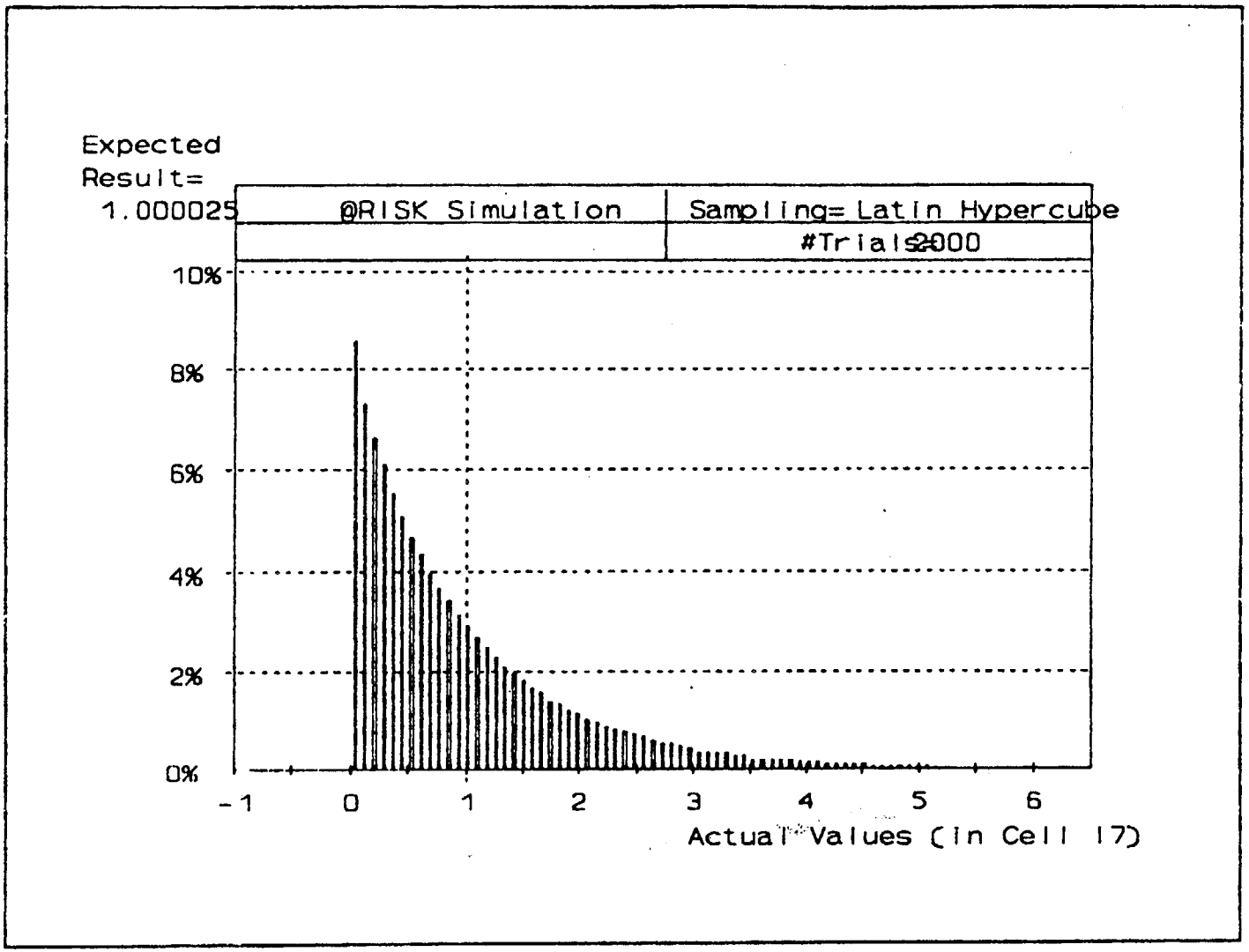

Figure 2-2. Histogram of Applied Infiltration Flux (q)

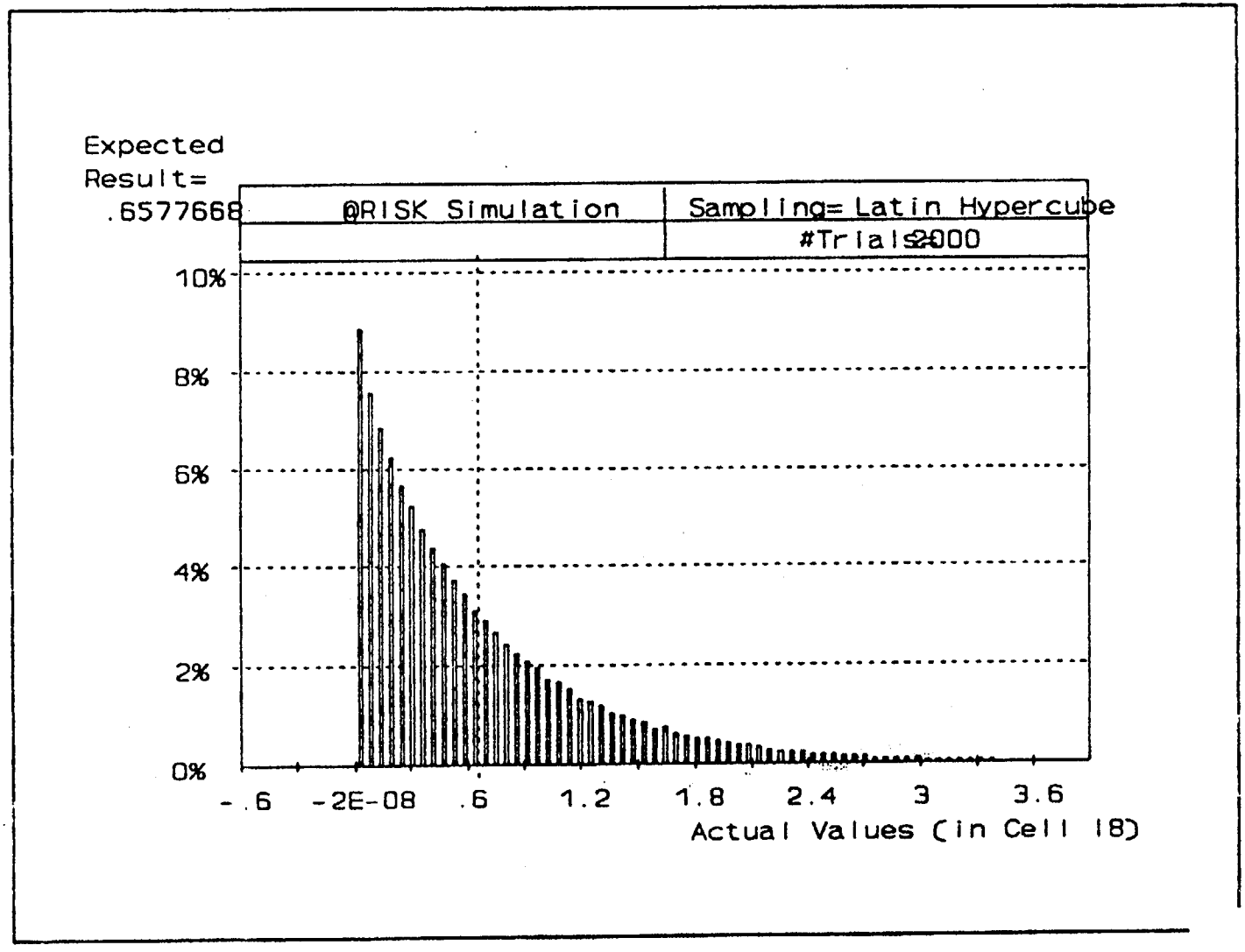

Figure 2-3. Histogram of Saturated Hydraulic Matrix Conductivity (k_0)

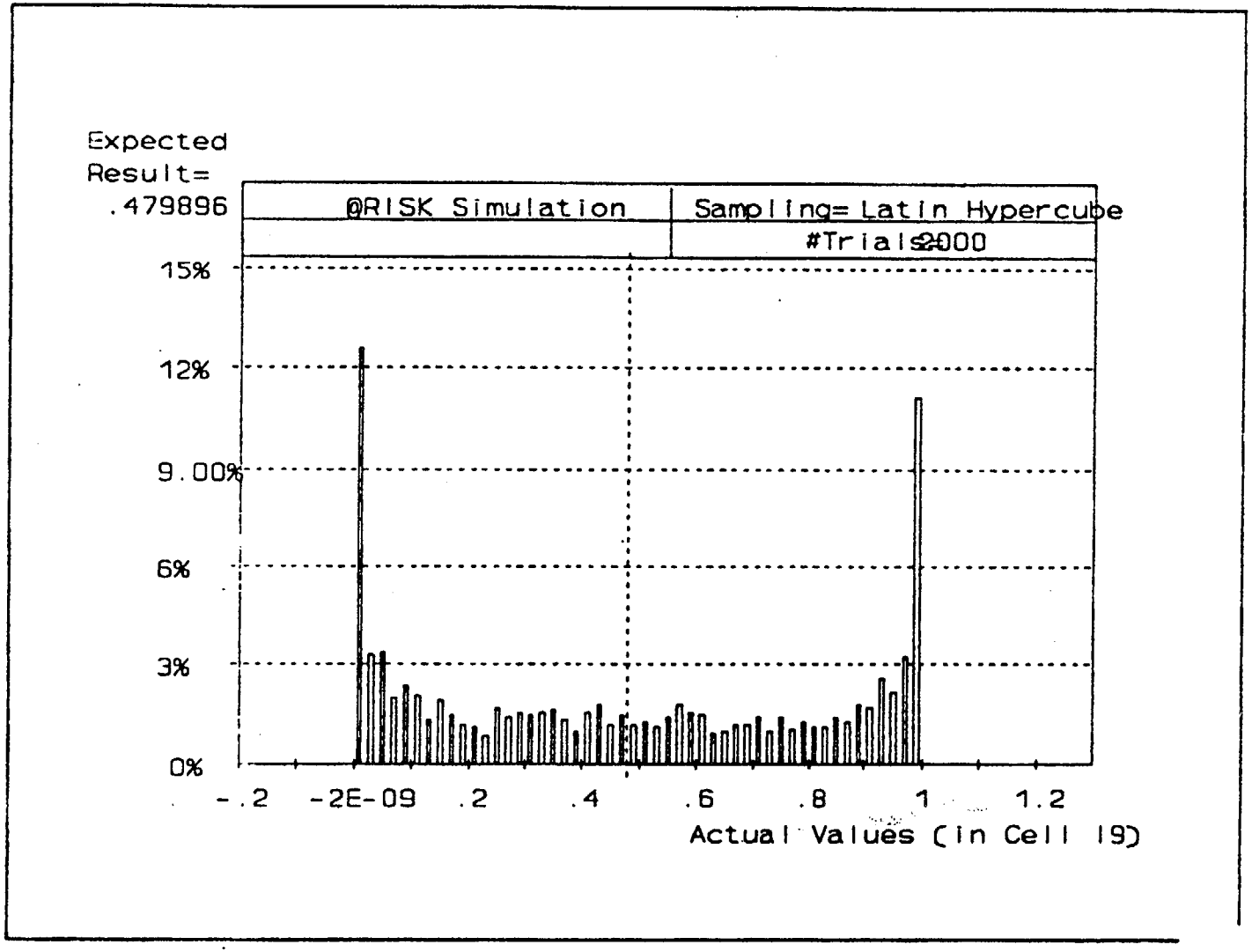

Figure 2-4. Histogram of Fraction of Containers in Seepage Areas (f_s)

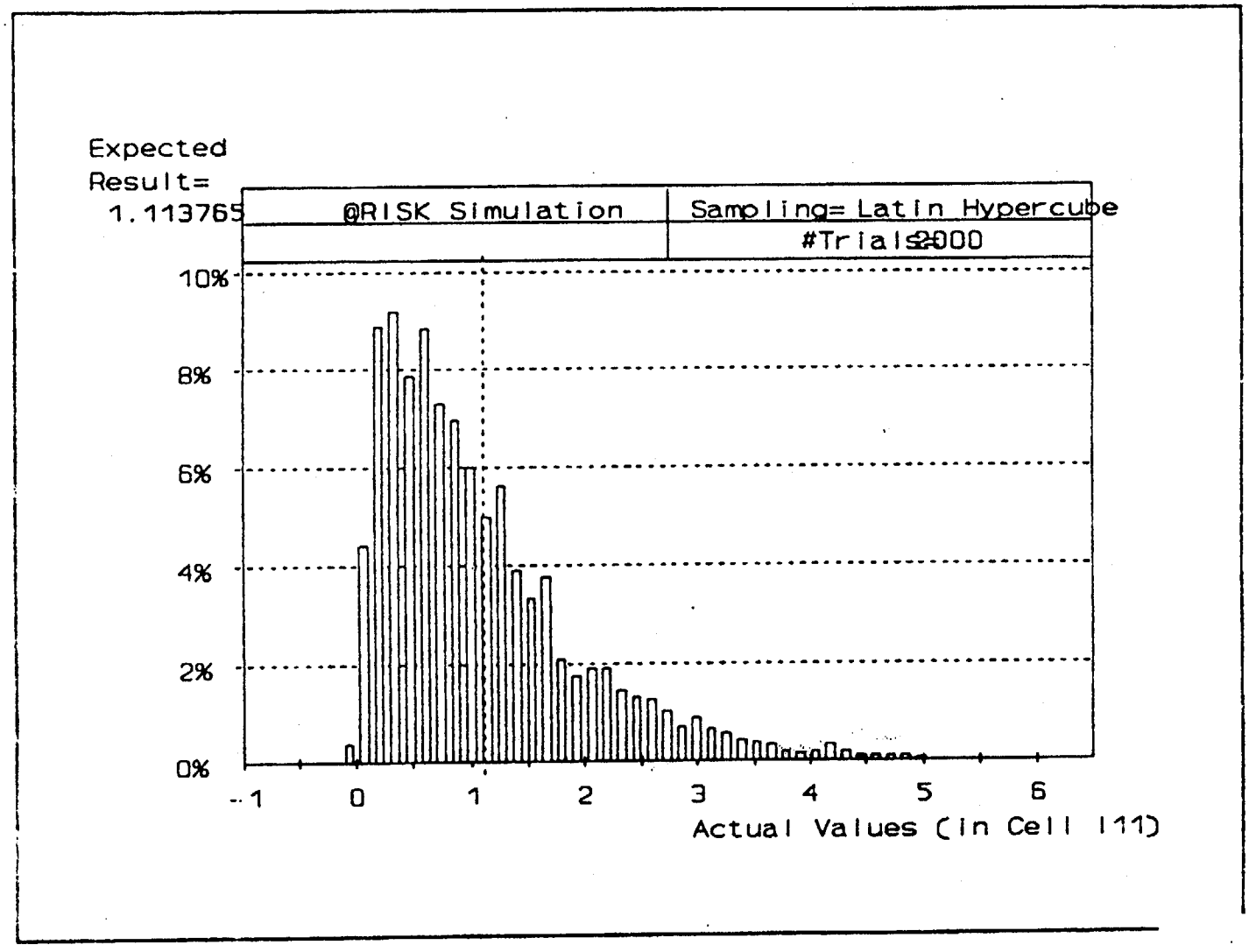

Figure 2-5. Histogram of Flux Used for Advective Release (q_s)

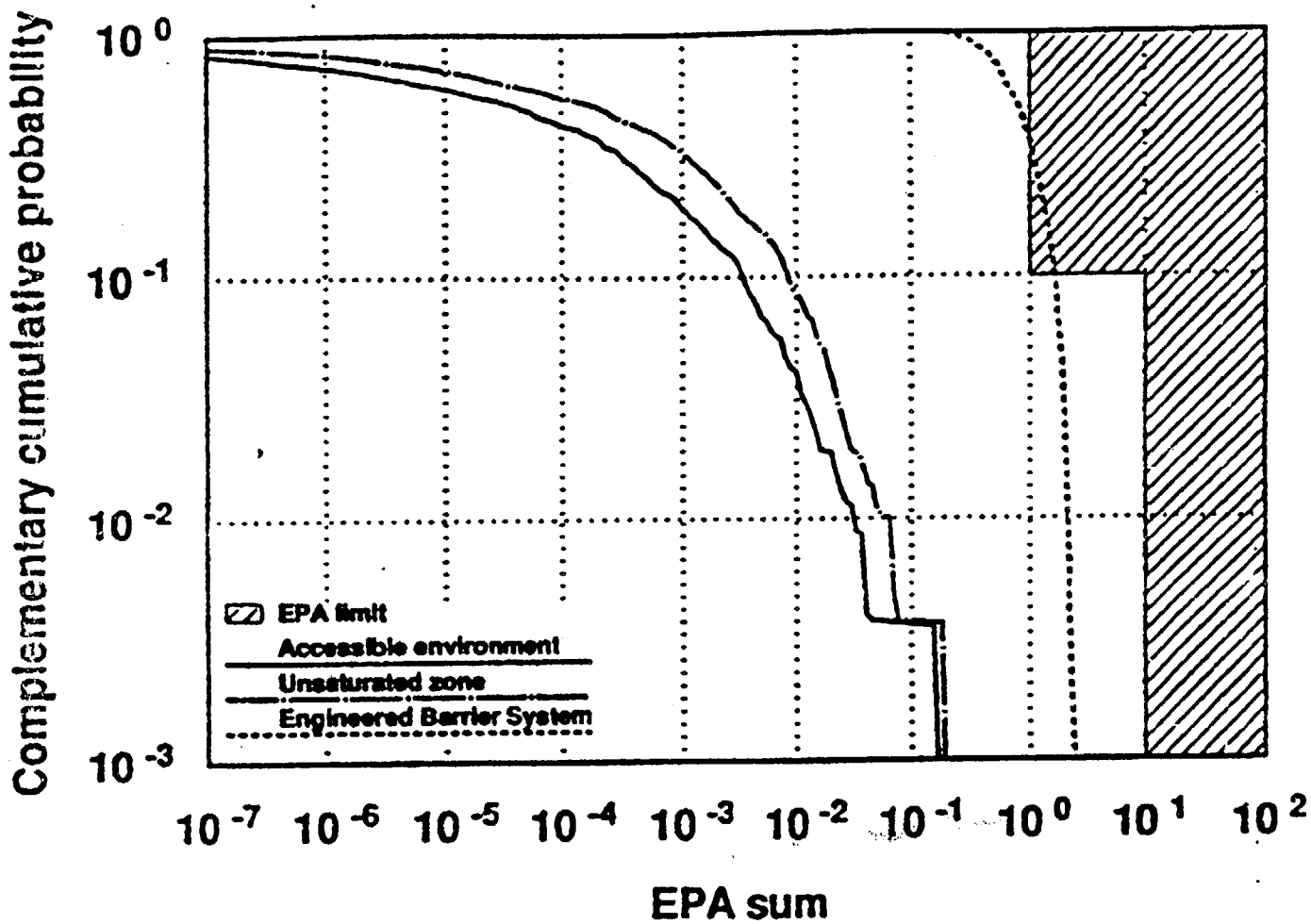

Figure 2-6. TSPA - 1991 CCDF for Waste Package/EBS Release (taken from Barnard et al., 1992)

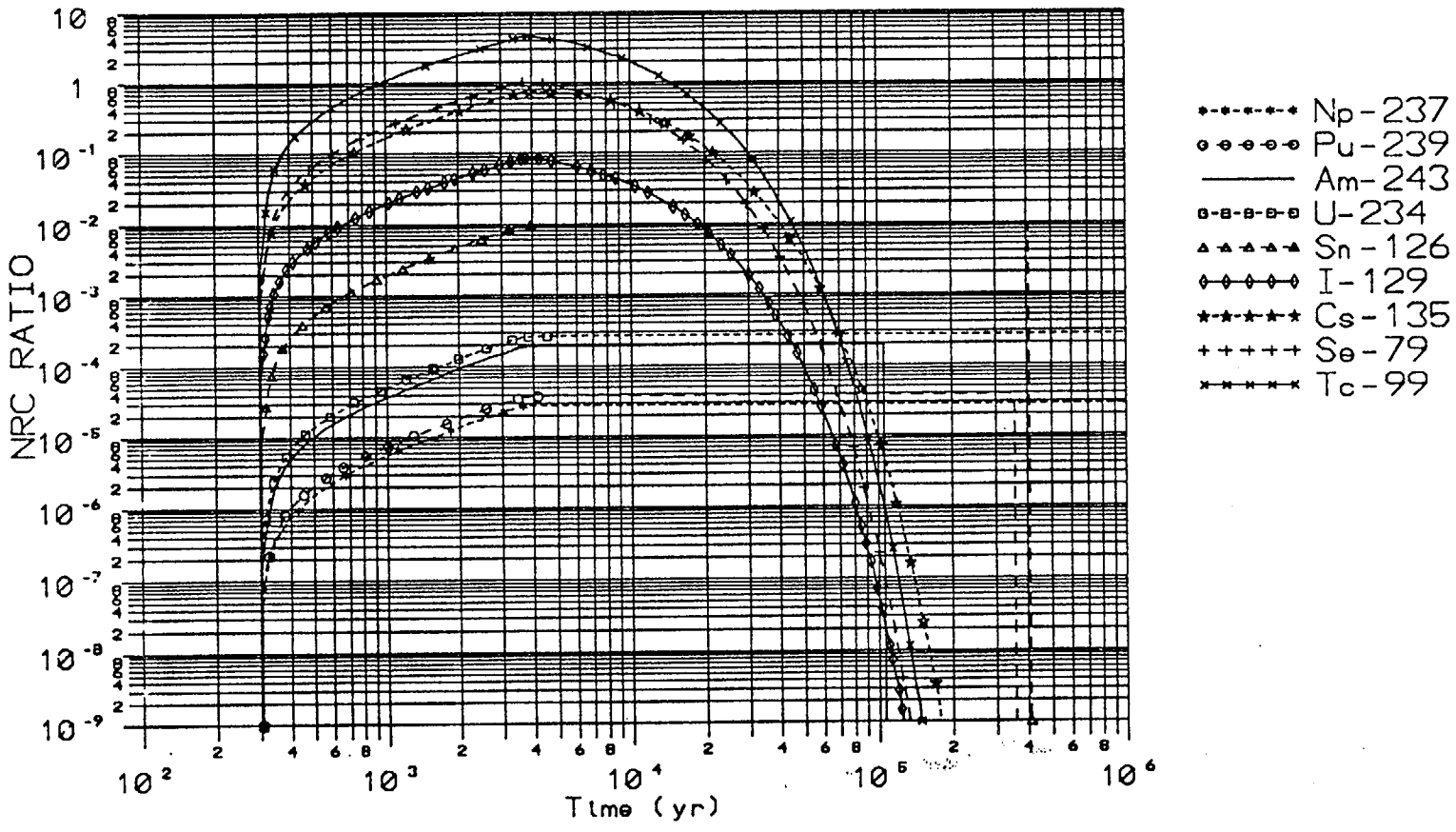

Figure 2-7. TSPA-1991 Individual Radionuclide Release Curves (normalized)

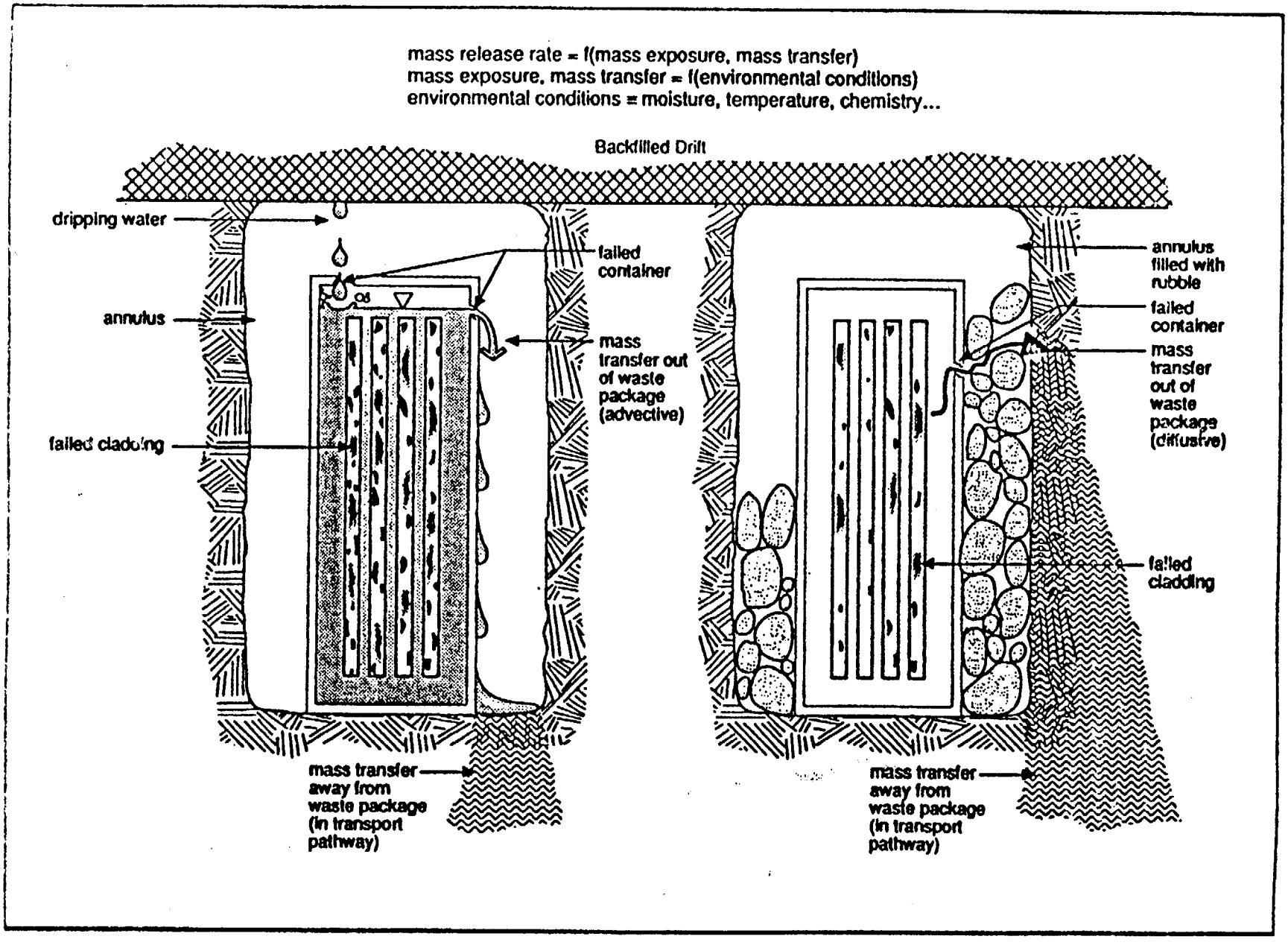

Figure 2-8. RIP Waste Package Schematic (taken from Miller et al., 1993)

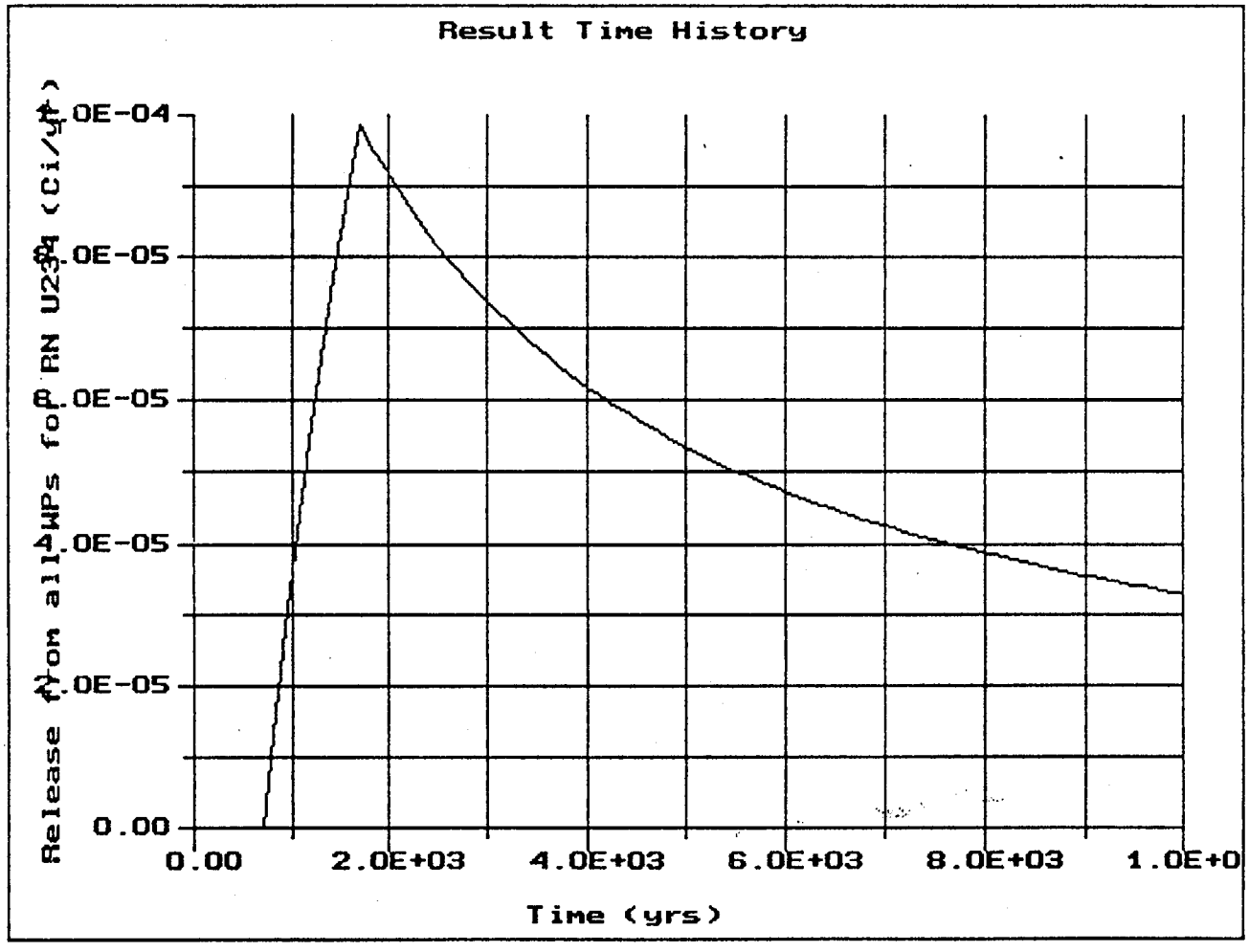

Figure 2-9. ^{234}U Release Assuming Competing Isotope Solubilities

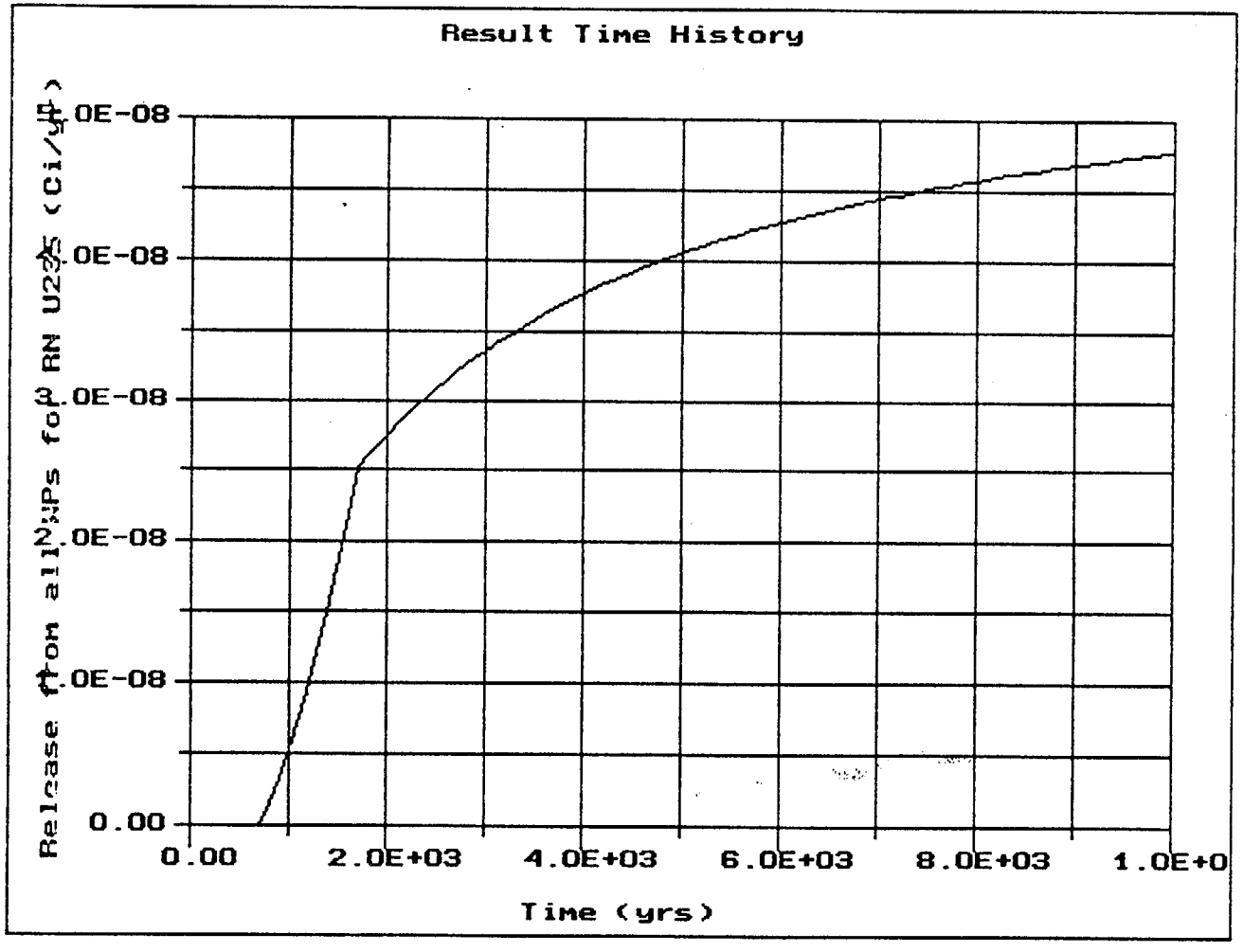

Figure 2-10. ^{235}U Release Assuming Competing Isotope Solubilities

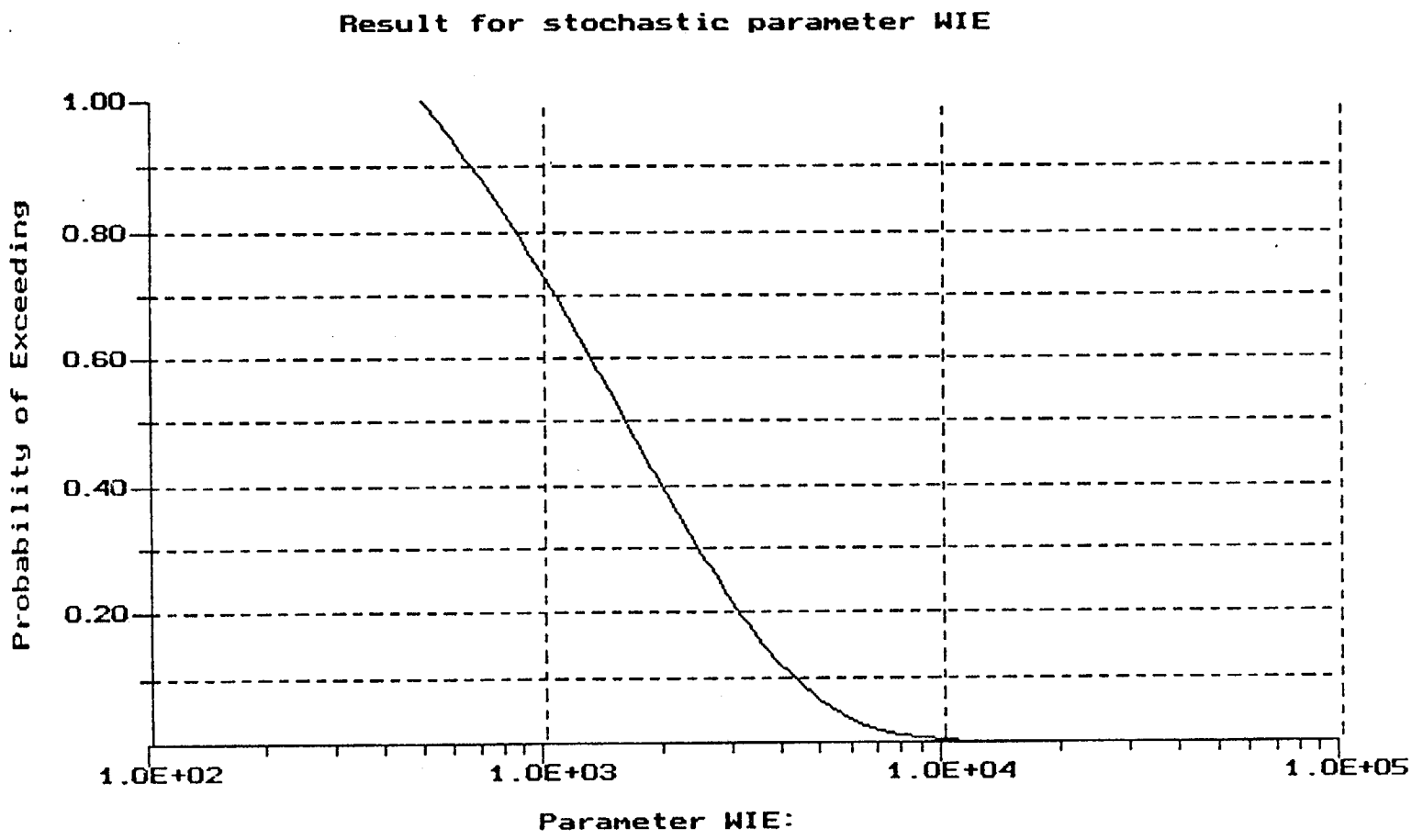

Weibull Distribution

Minimum = 5.000E+02

Slope = 1.000E+00

Mean - Min = 1.650E+03

Figure 2-11. Weibull Waste Package Failure Distribution

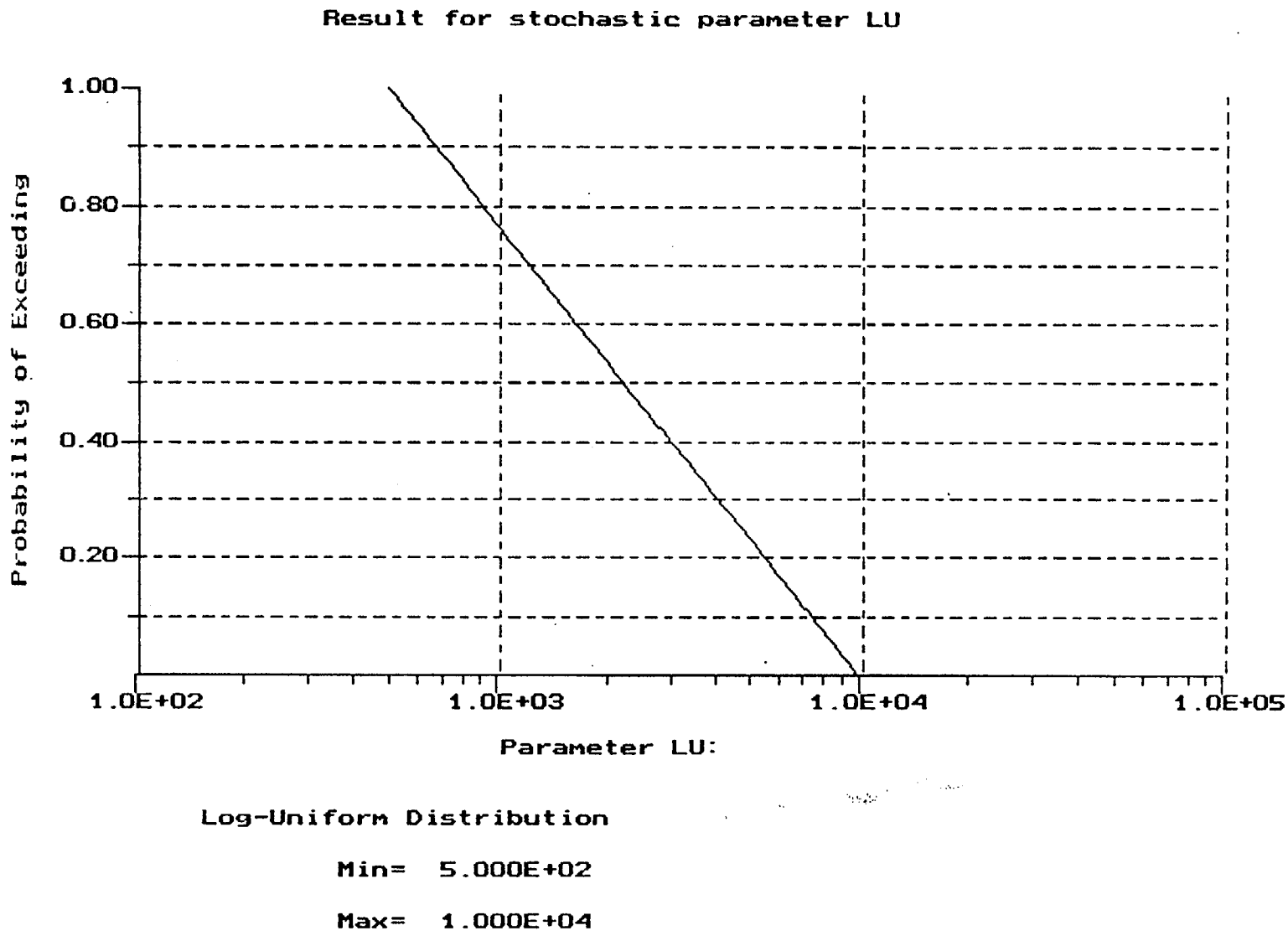

Figure 2-12. Log-Uniform Waste Package Failure Distribution

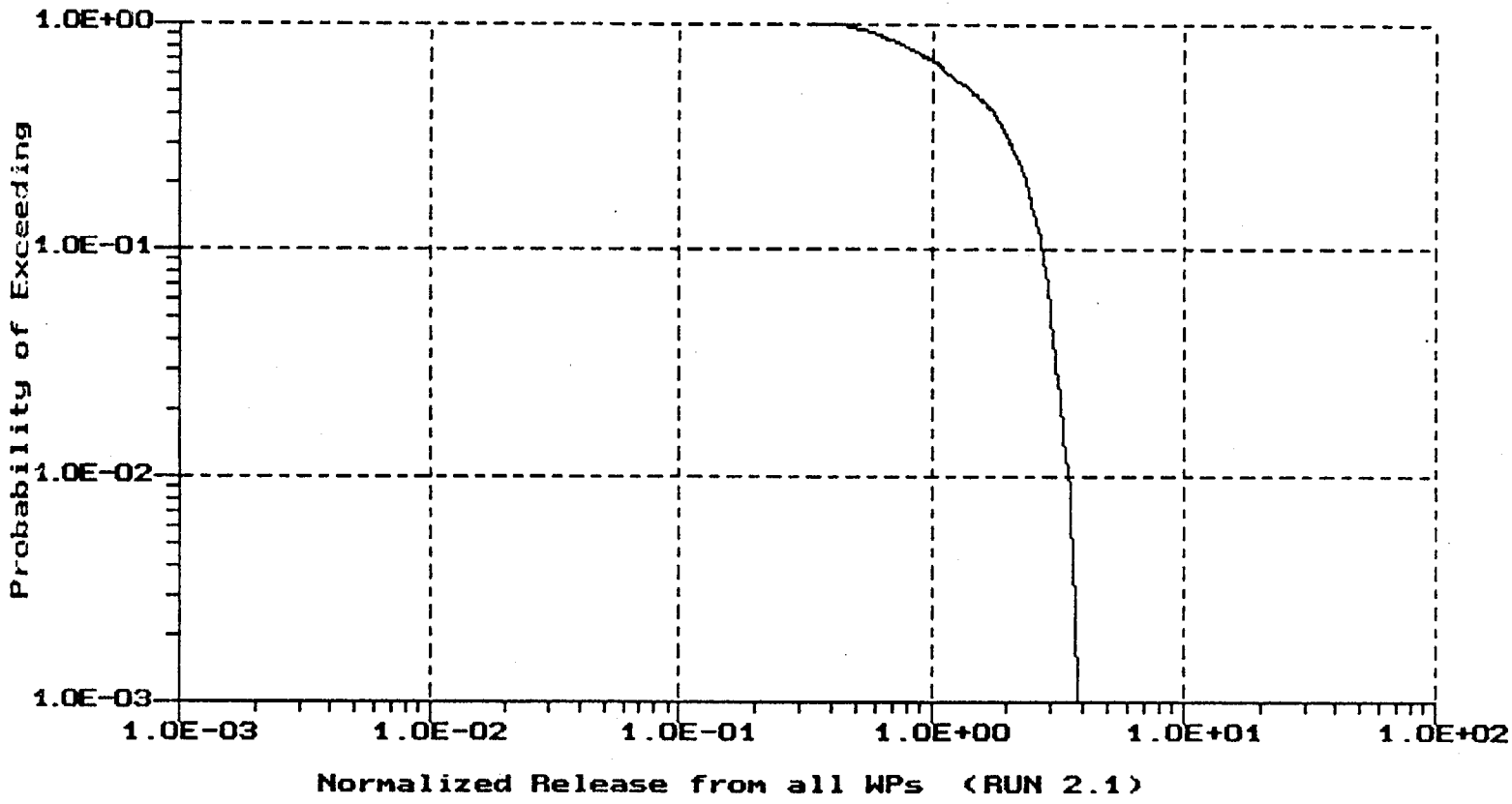

Distribution of Results

Mean= 1.585E+00

S.D.= 8.031E-01

Kurtosis= 2.204E+00

Skewness= 4.530E-01

Figure 2-13. Initial Conceptualization - CCDF

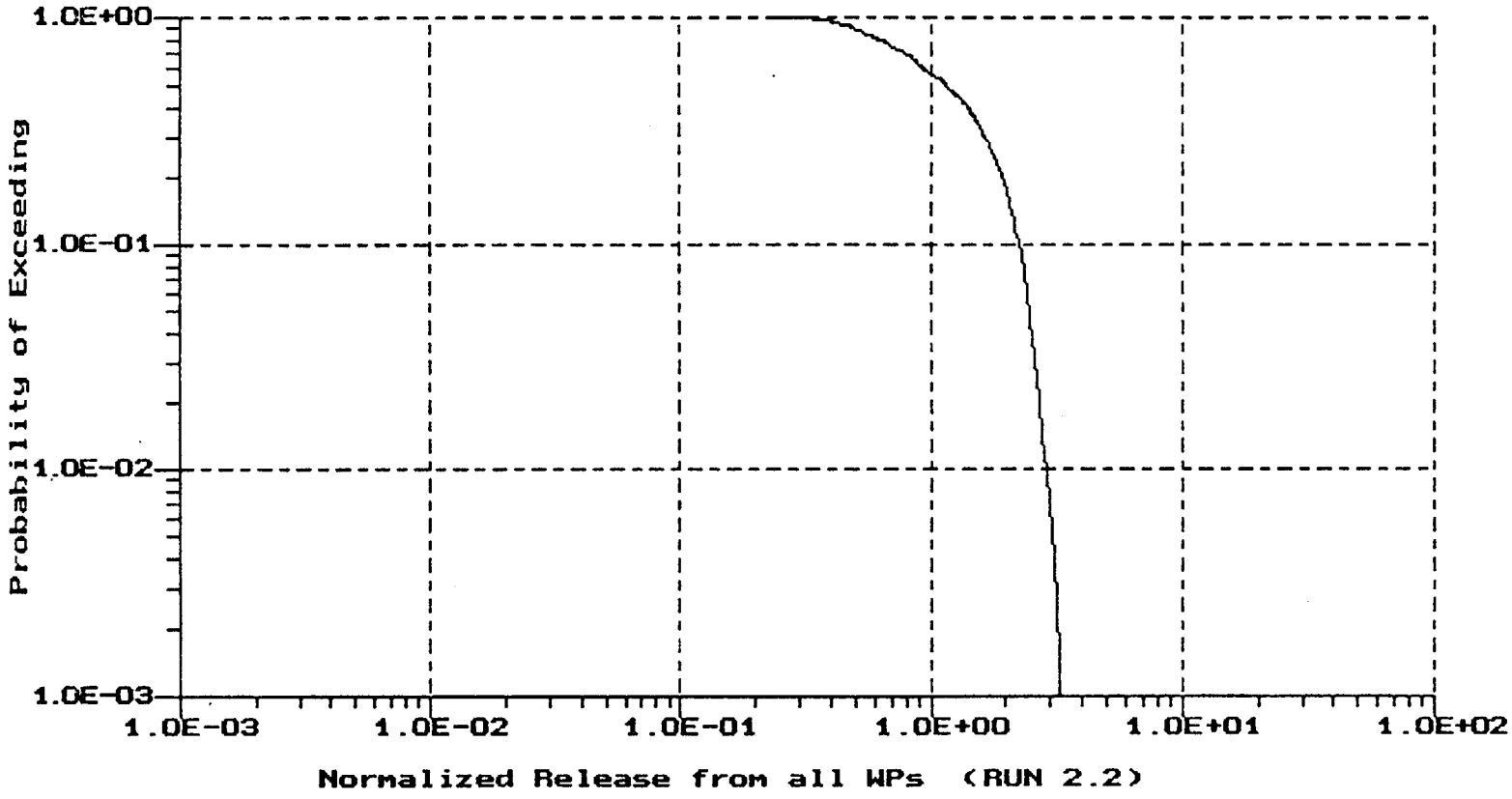

Distribution of Results

Mean= 1.287E+00

S.D.= 6.715E-01

Kurtosis= 2.282E+00

Skewness= 5.043E-01

Figure 2-14. Waste Package with Log-Uniform Failure Distribution - CCDF

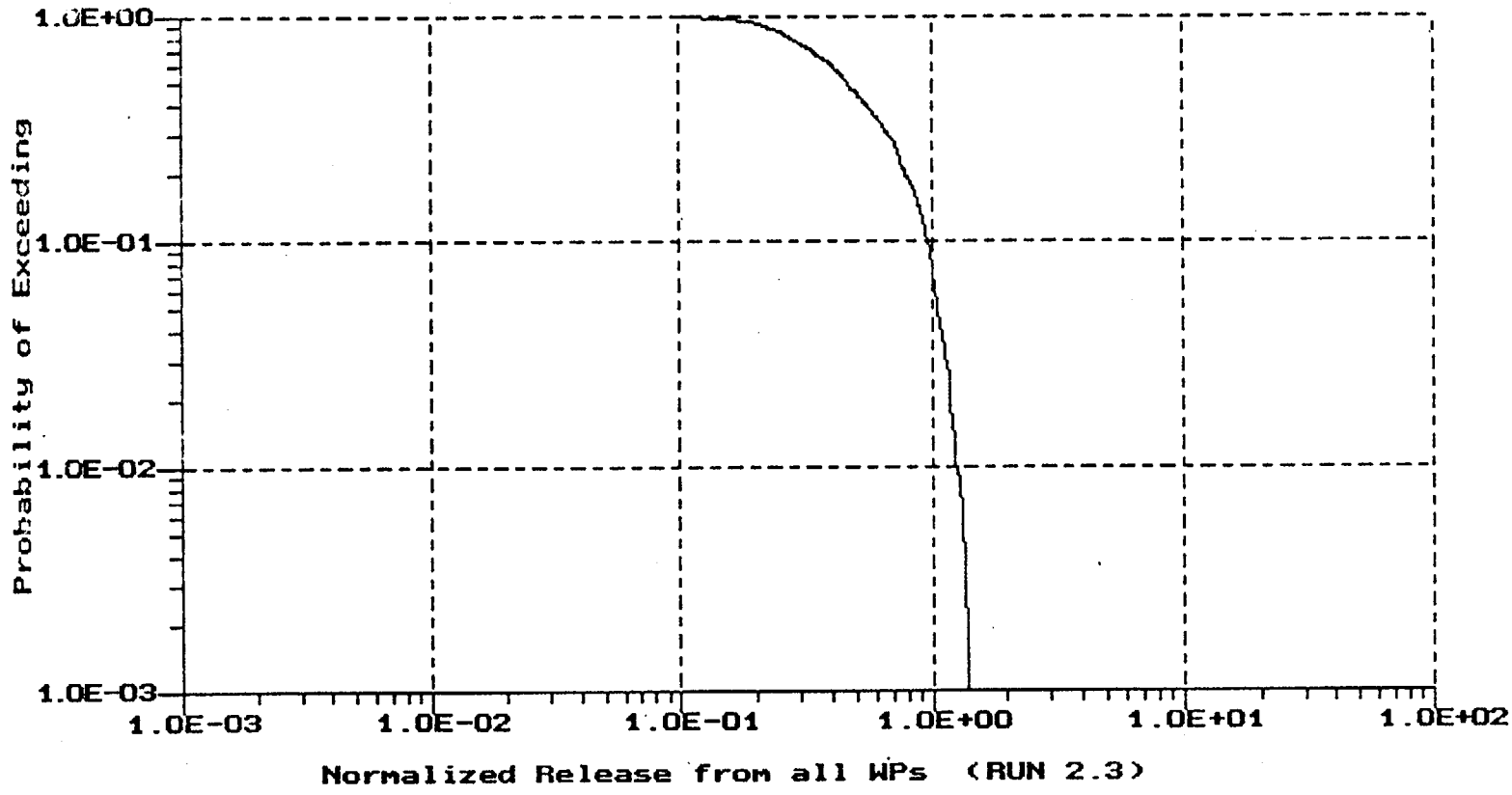

Distribution of Results

Mean= 5.368E-01

S.D.= 2.828E-01

Kurtosis= 2.655E+00

Skewness= 6.951E-01

Figure 2-15. Inventory Reduced to Nine Radionuclides - CCDF

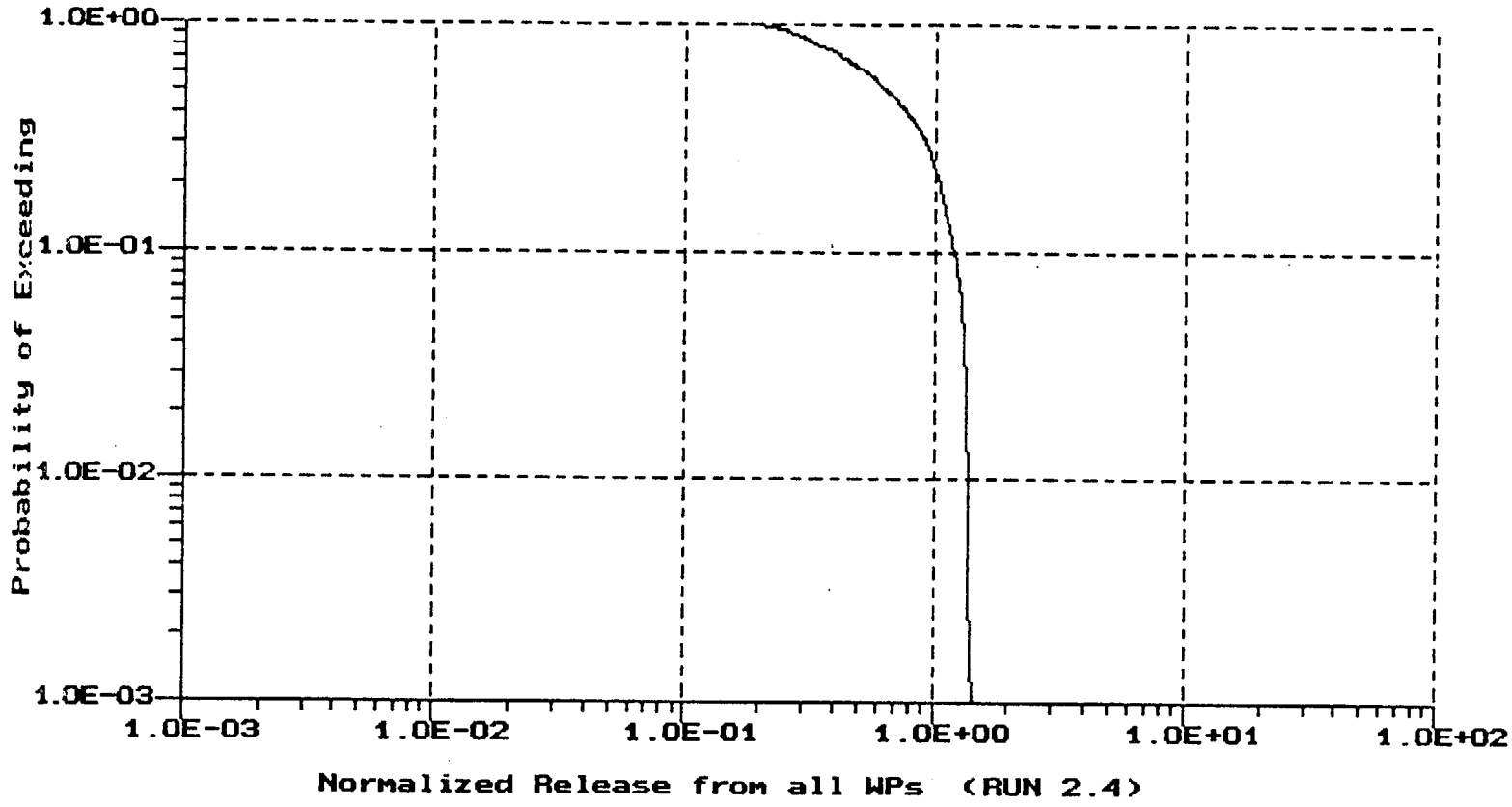

Distribution of Results

Mean= 7.027E-01

S.D.= 3.422E-01

Kurtosis= 1.910E+00

Skewness= 3.144E-01

Figure 2-16. Increase ^{99}Tc and ^{135}Cs Base Solubility - CCDF

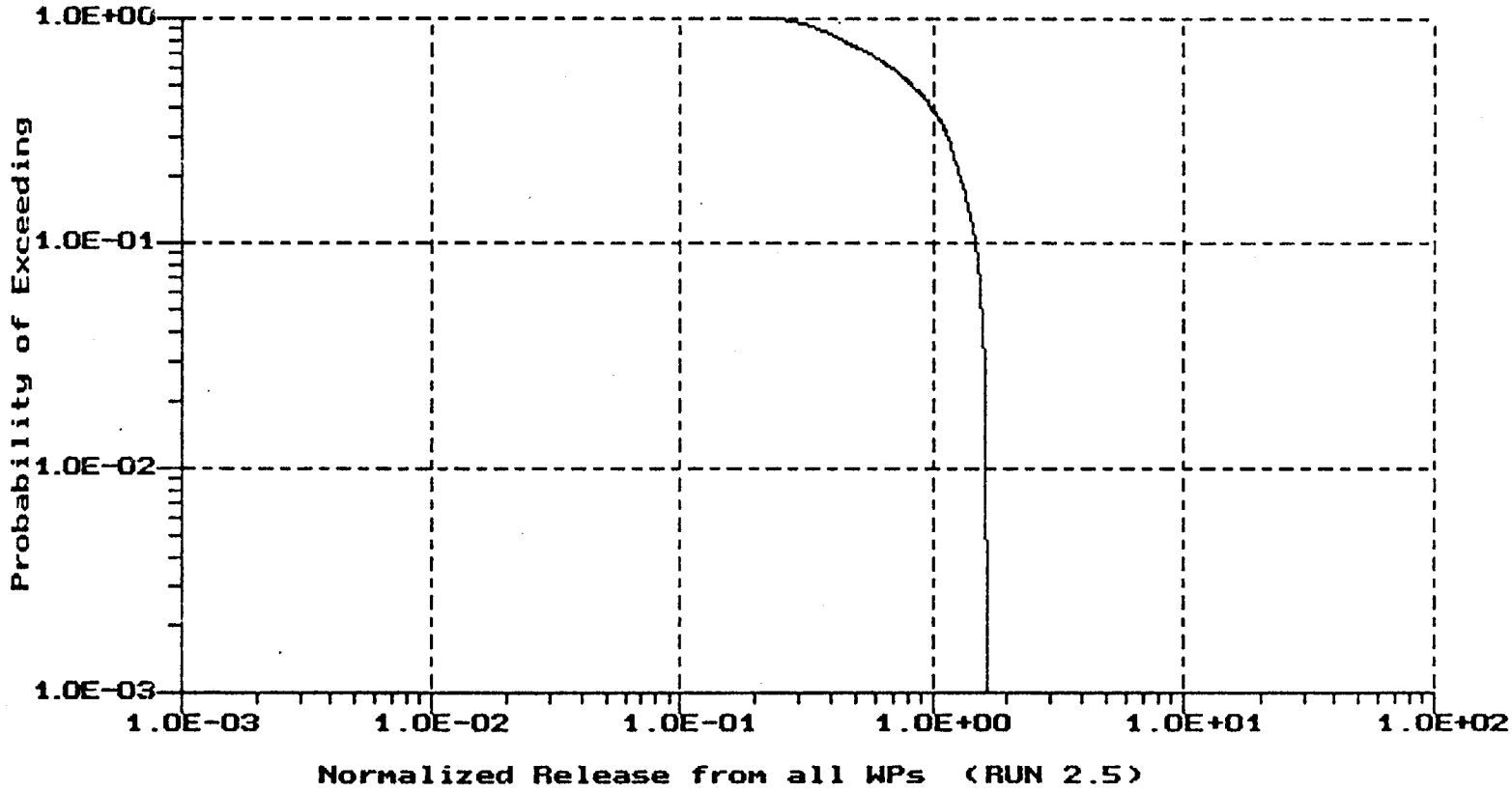

Distribution of Results

Mean= 8.757E-01

S.D.= 4.066E-01

Kurtosis= 1.827E+00

Skewness= 2.203E-01

Figure 2-17. One Failure Time Per Realization - CCDF

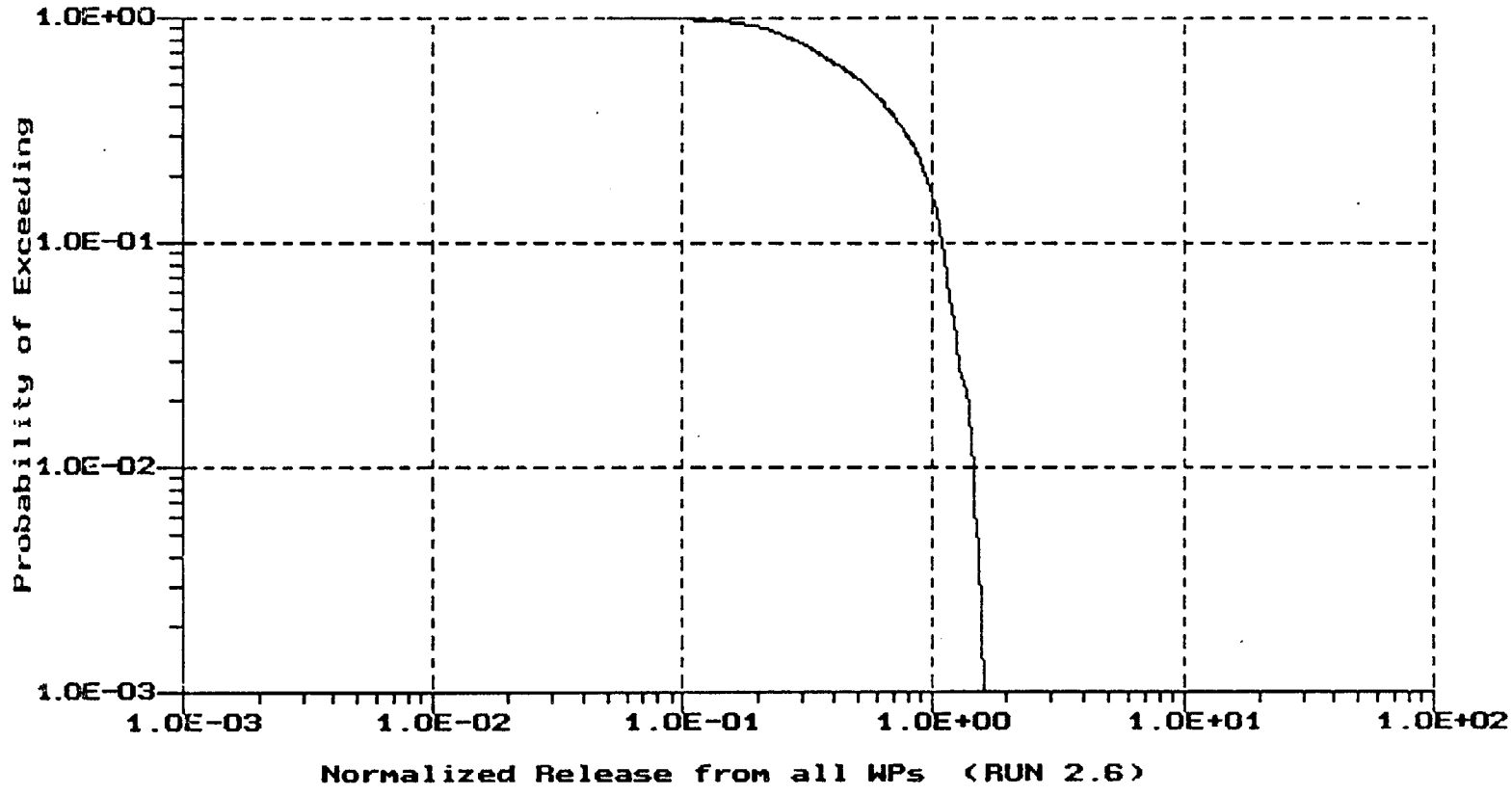

Distribution of Results

Mean= 6.064E-01

S.D.= 3.451E-01

Kurtosis= 2.388E+00

Skewness= 5.583E-01

Figure 2-18. F_s Implemented to Determine Waste Package Group Totals - CCDF

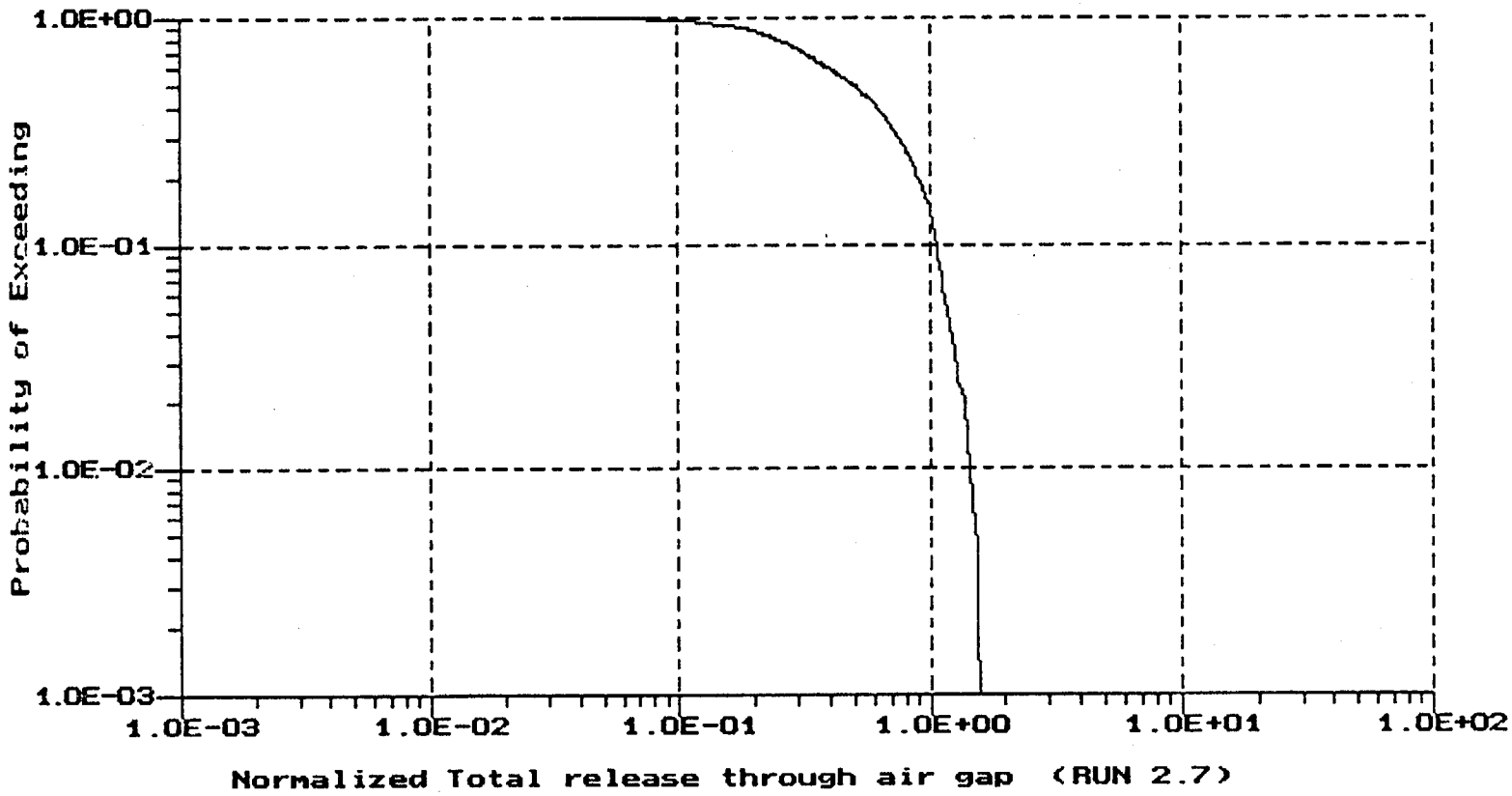

Distribution of Results

Mean= 5.722E-01

S.D.= 3.438E-01

Kurtosis= 2.507E+00

Skewness= 6.103E-01

Figure 2-19. F_s Implemented to Determine Waste Package Group Totals - with Air Gap - CCDF

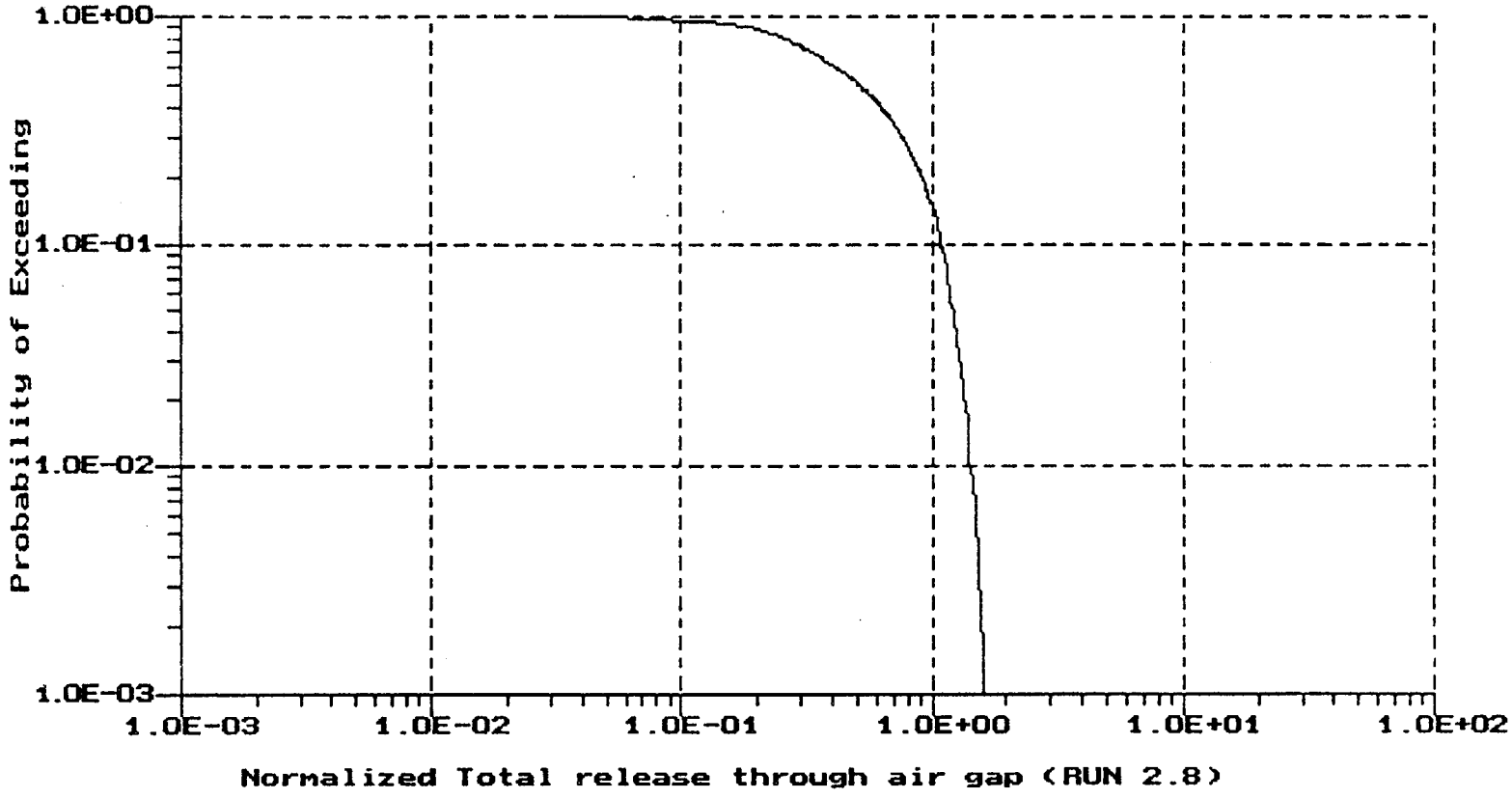

Distribution of Results

Mean= 5.819E-01

S.D.= 3.487E-01

Kurtosis= 2.505E+00

Skewness= 5.830E-01

Figure 2-20. F_s Implemented with q_s with Air Gap - CCDF

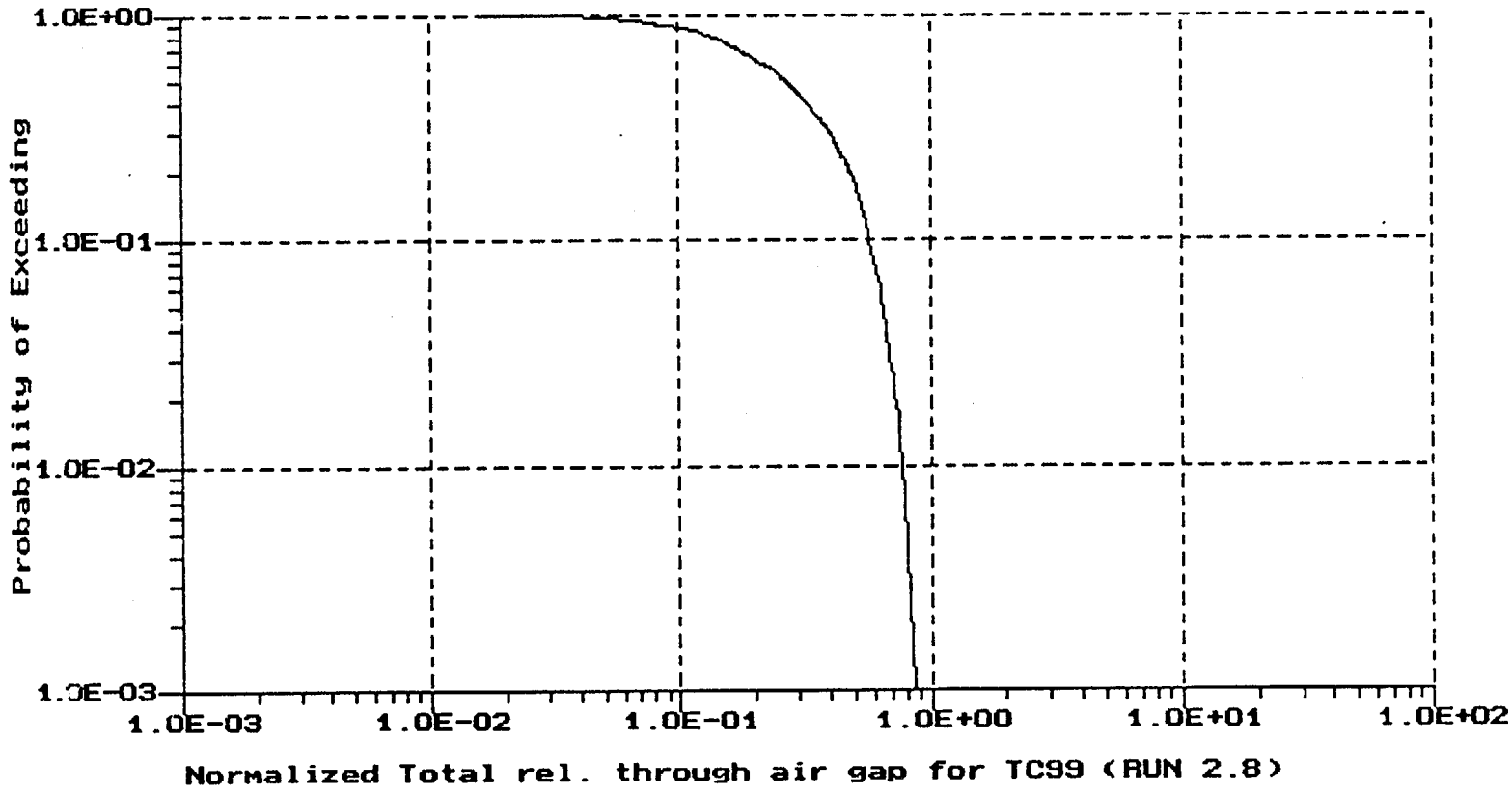

Distribution of Results

Mean= 3.081E-01

S.D.= 1.859E-01

Kurtosis= 2.534E+00

Skewness= 6.183E-01

Figure 2-21. ^{99}Tc Implemented with q_s with Air Gap - CCDF

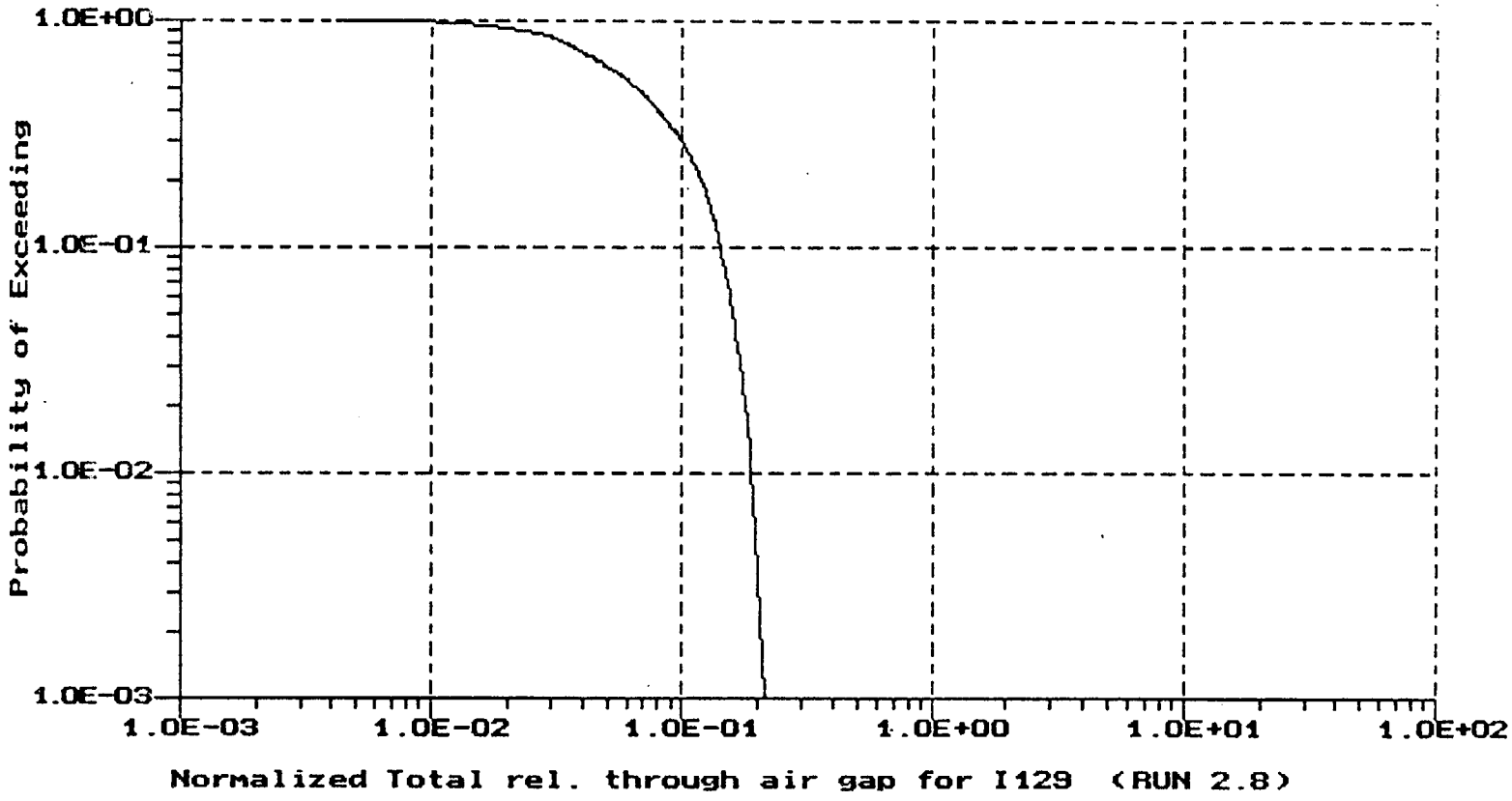

Distribution of Results

Mean= 7.553E-02

S.D.= 4.524E-02

Kurtosis= 2.520E+00

Skewness= 6.107E-01

Figure 2-22. ^{129}I Implemented with q_s with Air Gap - CCDF

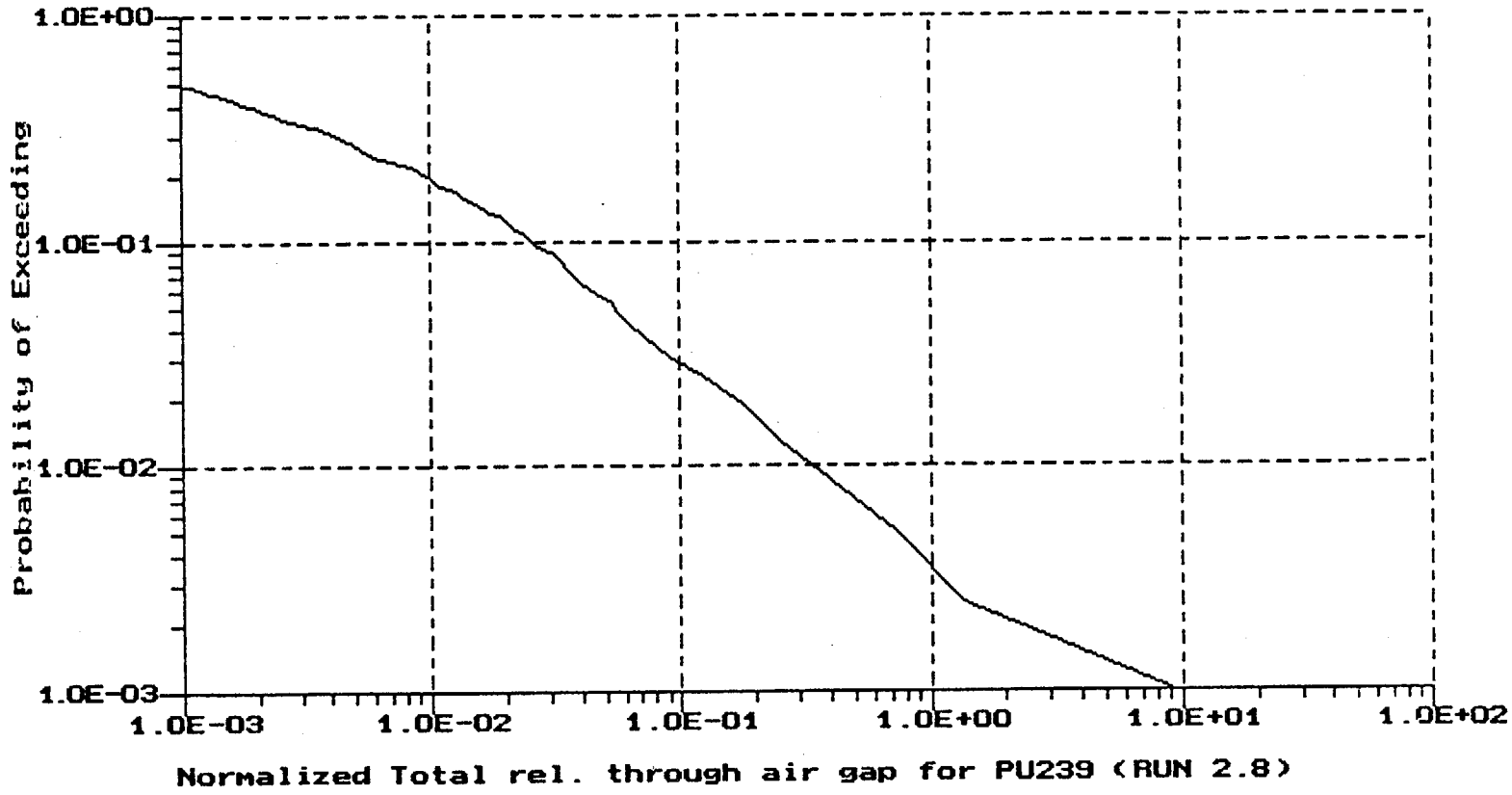

Distribution of Results

Mean= 6.970E-02

S.D.= 1.329E+00

Kurtosis= 7.592E+02

Skewness= 2.682E+01

Figure 2-23. ^{239}Pu Implemented with q_s with Air Gap - CCDF

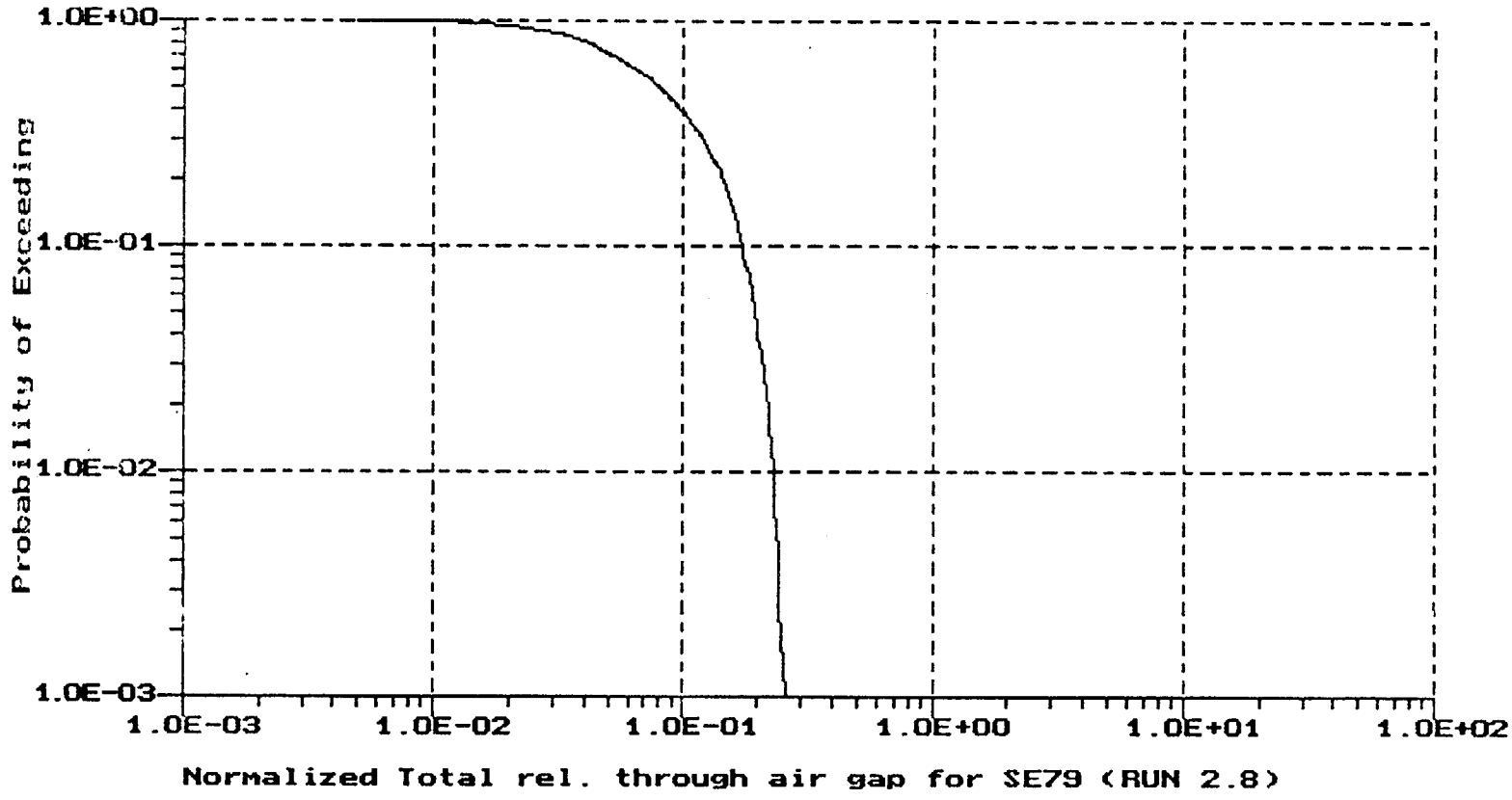

Distribution of Results

Mean= 9.195E-02

S.D.= 5.555E-02

Kurtosis= 2.565E+00

Skewness= 6.324E-01

Figure 2-24. ^{79}Se Implemented with q_s with Air Gap - CCDF

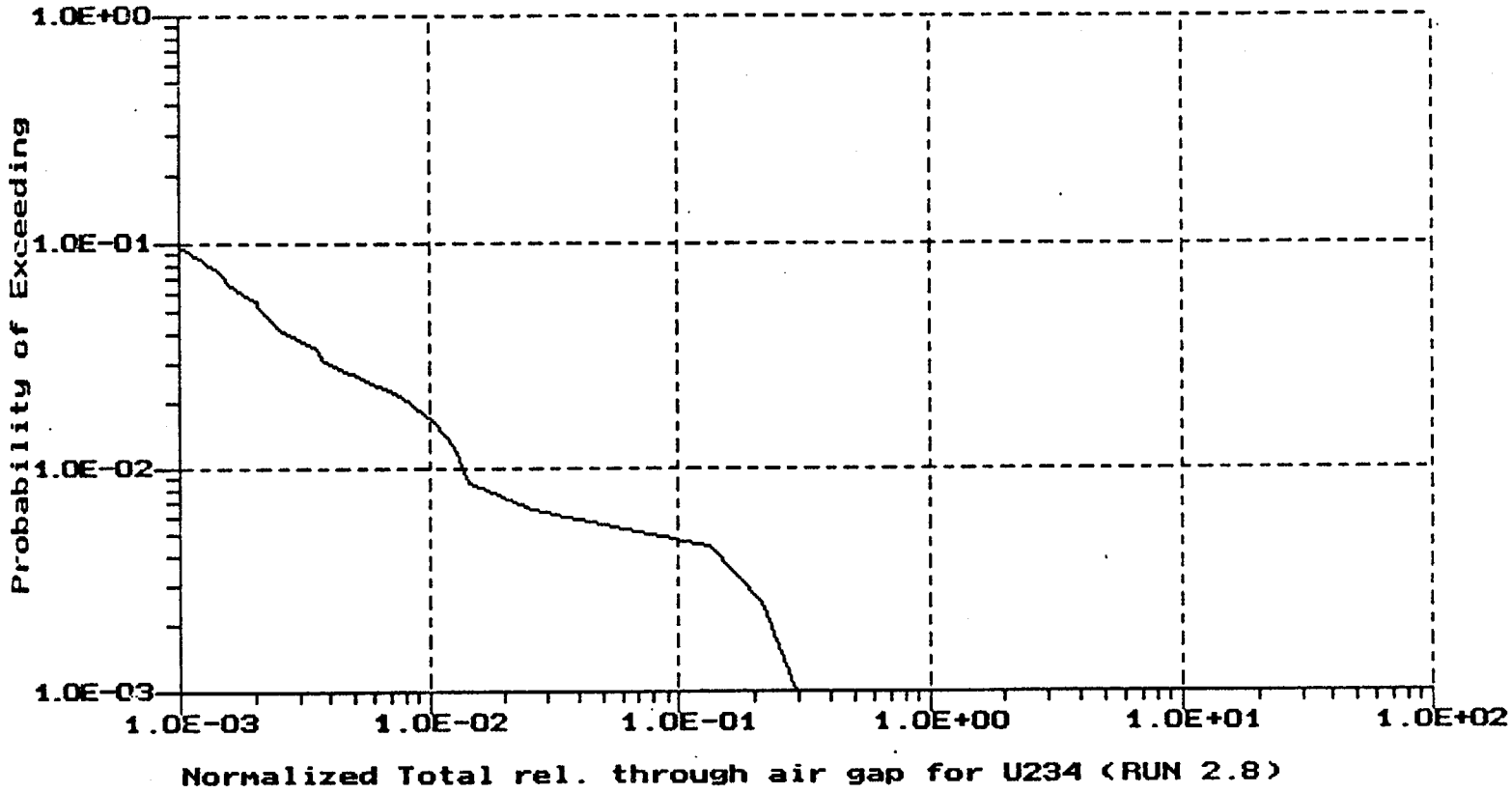

Distribution of Results

Mean= 1.681E-03

S.D.= 1.752E-02

Kurtosis= 2.829E+02

Skewness= 1.608E+01

Figure 2-25. ^{234}U Implemented with q_s with Air Gap - CCDF

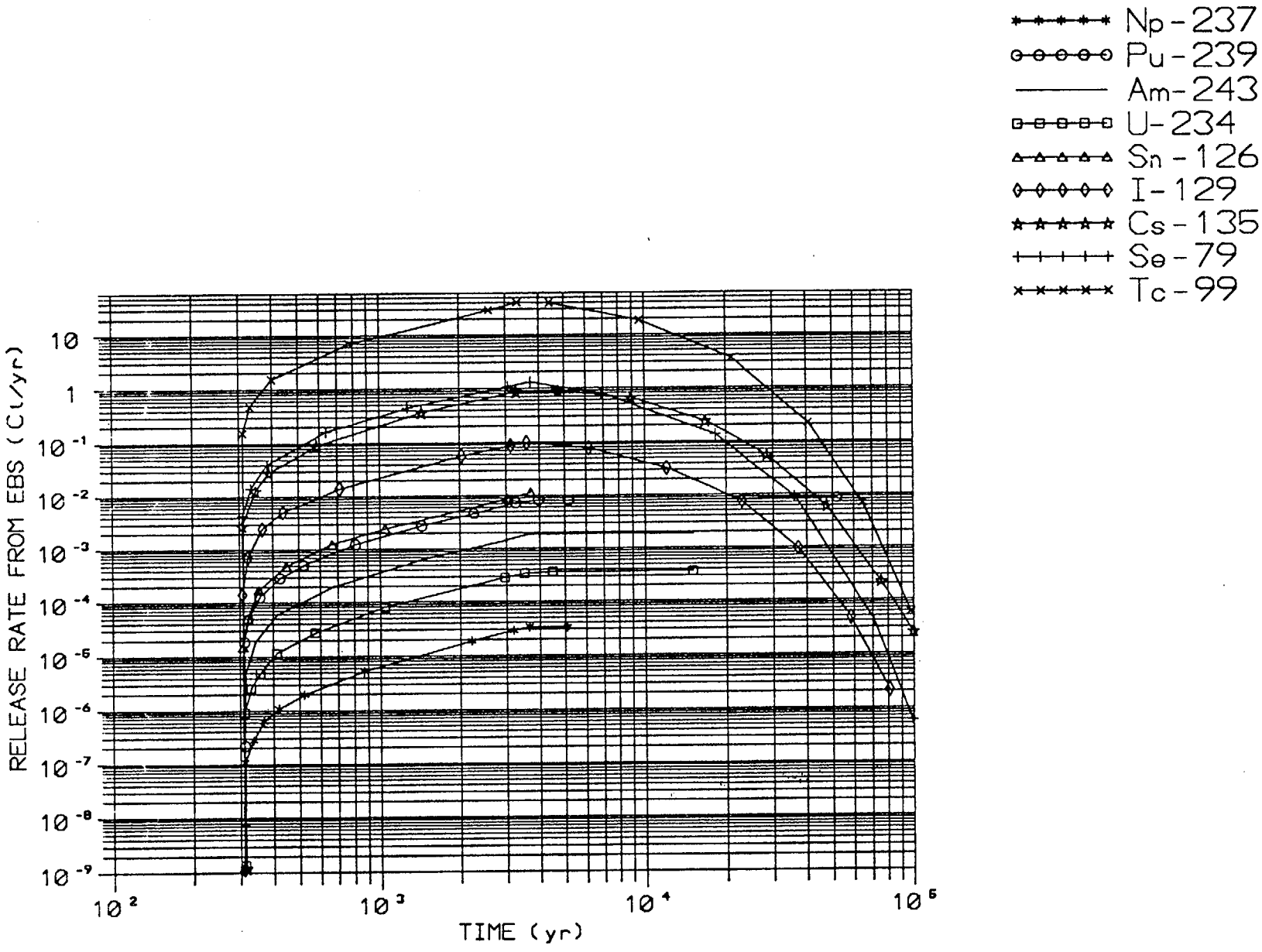

Figure 2-26. TSPA-1991 Individual Radionuclide Release Curves (non-normalized)

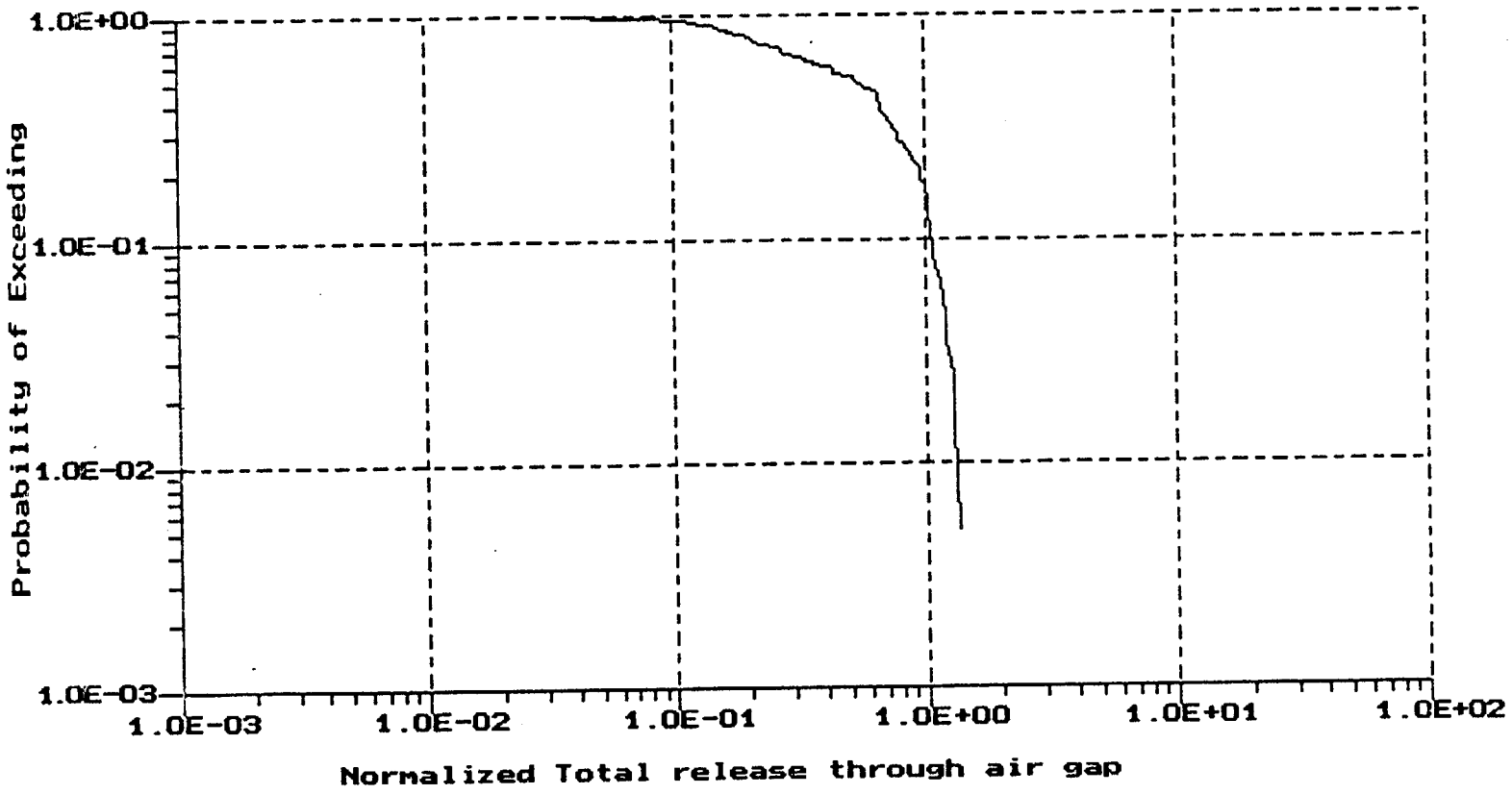

Distribution of Results

Mean= 5.701E-01

S.D.= 3.598E-01

Kurtosis= 1.906E+00

Skewness= 3.286E-01

Figure 2-27. Release Initiated at 300 Years - CCDF

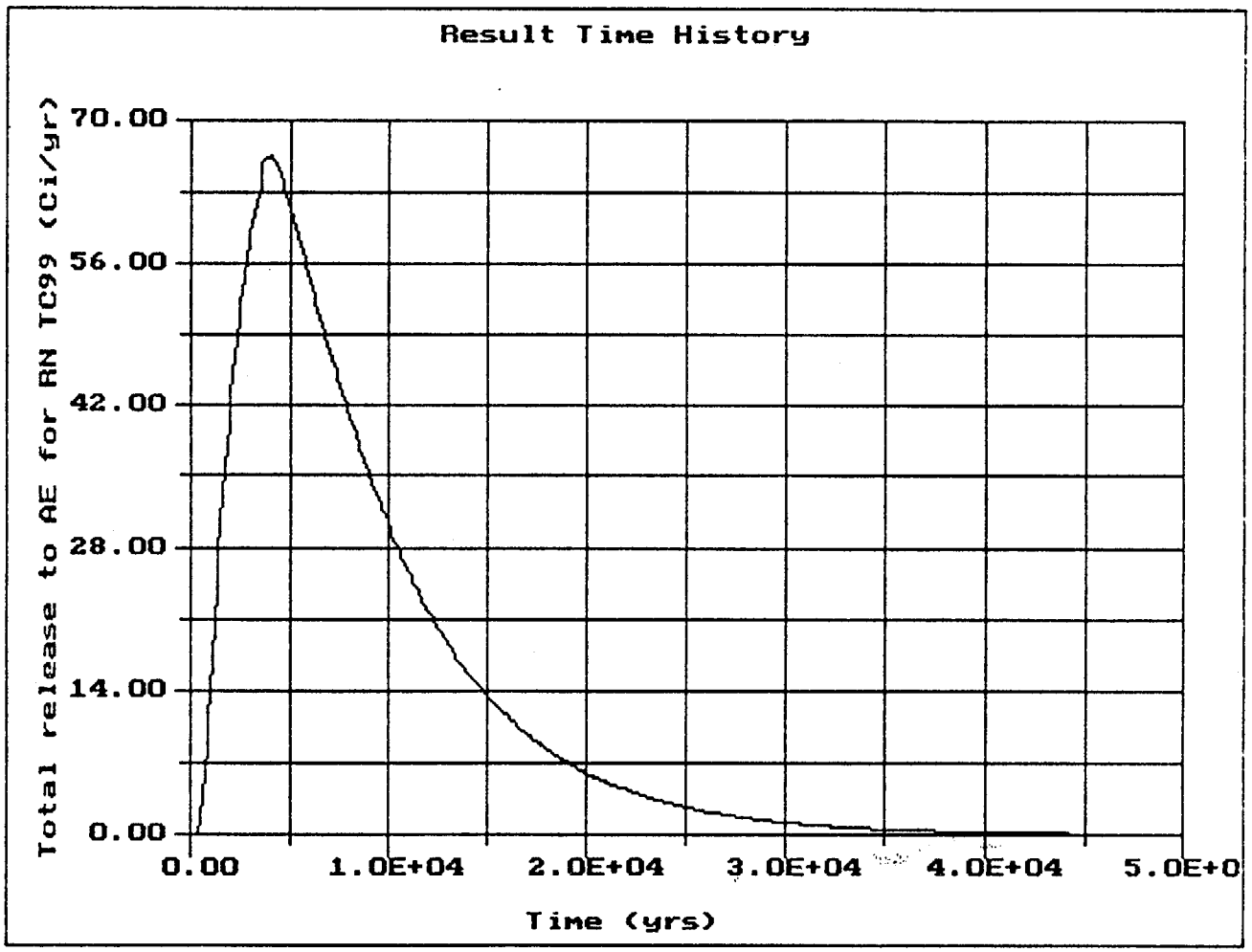

Figure 2-28. Individual Radionuclide Release Curve (^{99}Tc)

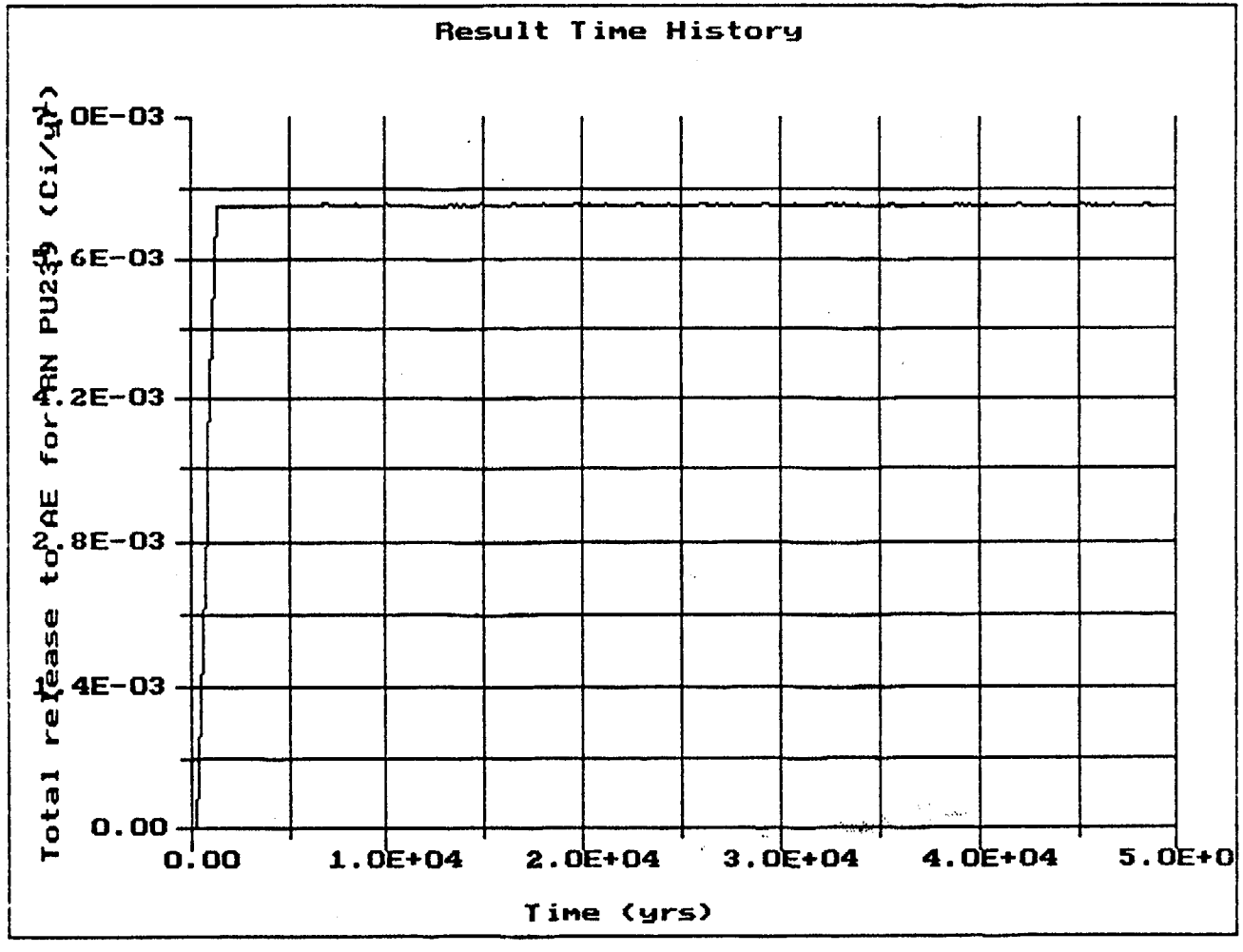

Figure 2-29. Individual Radionuclide Release Curve (^{239}Pu)

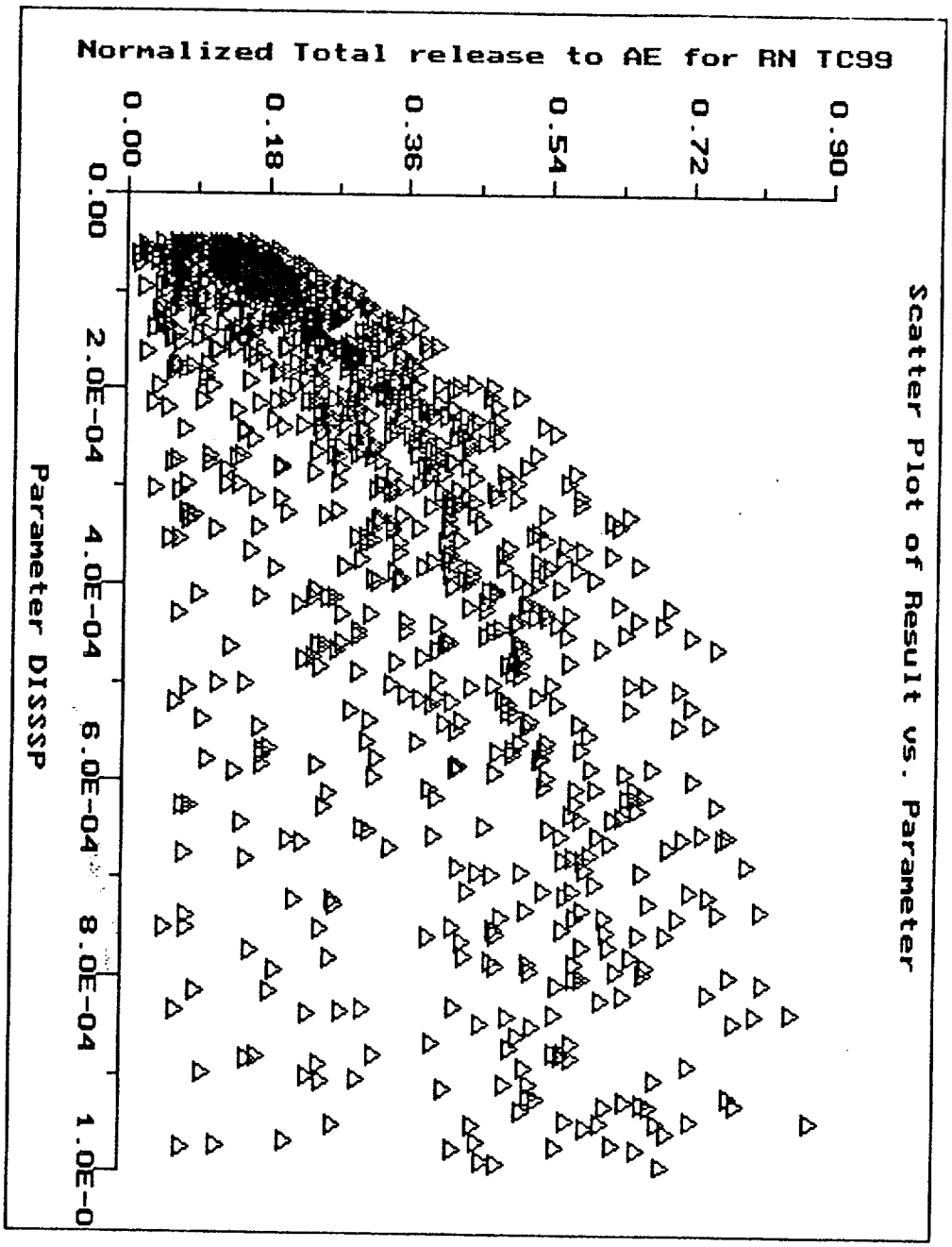

Figure 2-30. Sensitivity of ^{99}Tc Release to Matrix Dissolution Rate

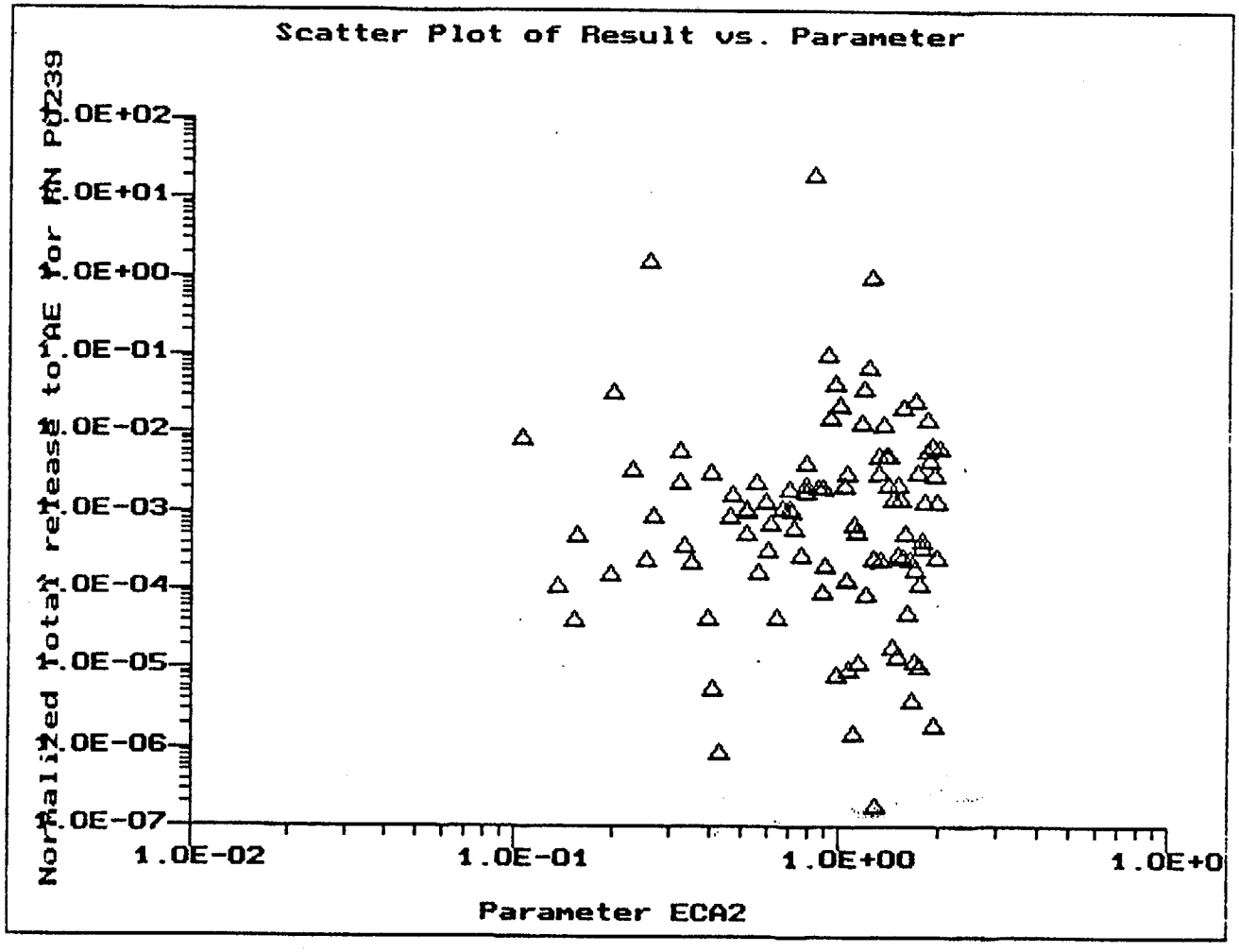

Figure 2-31. Sensitivity of ^{239}Pu Release to Effective Catchment Area

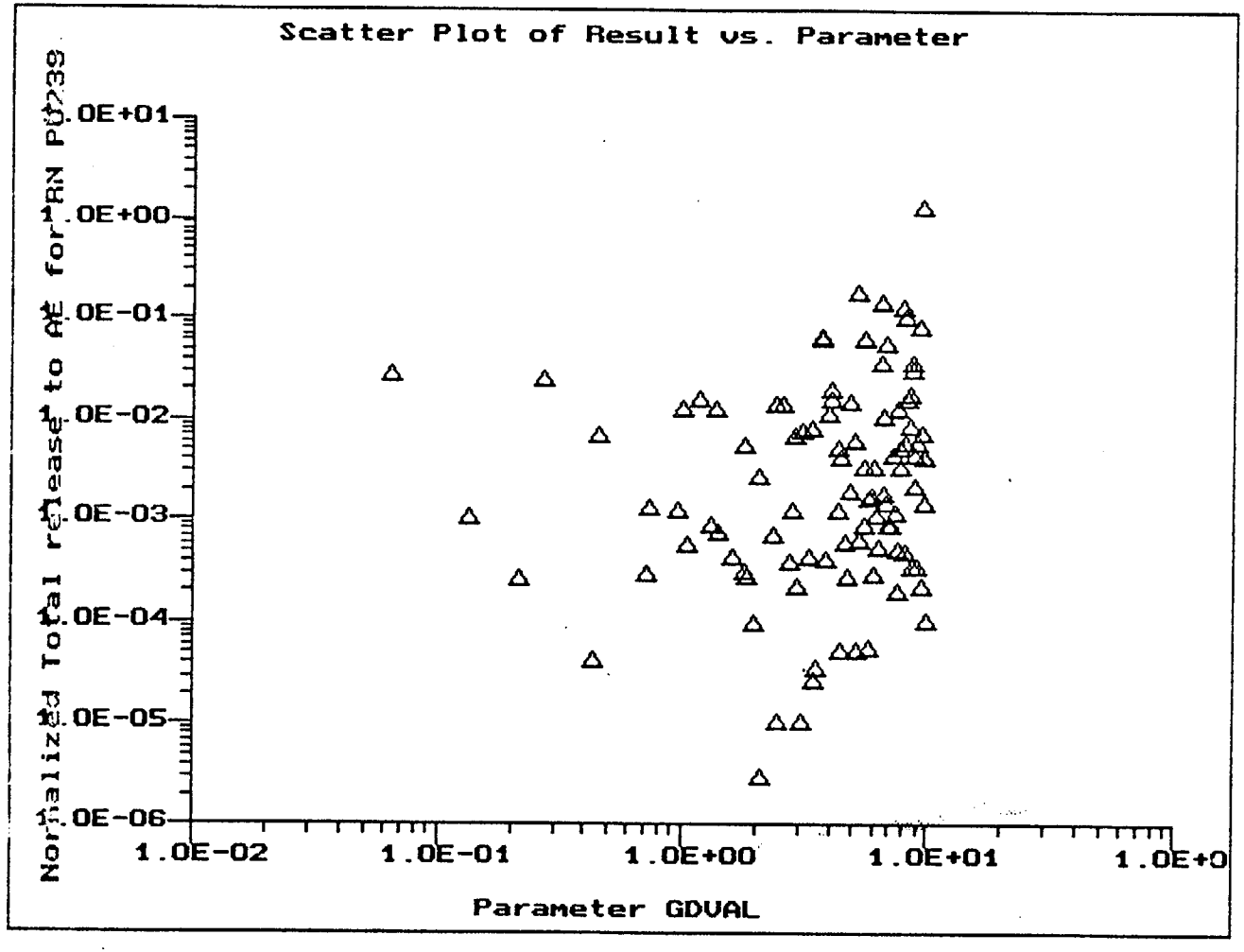

Figure 2-32. Sensitivity of ^{239}Pu Release to Geometric Diffusion Factor

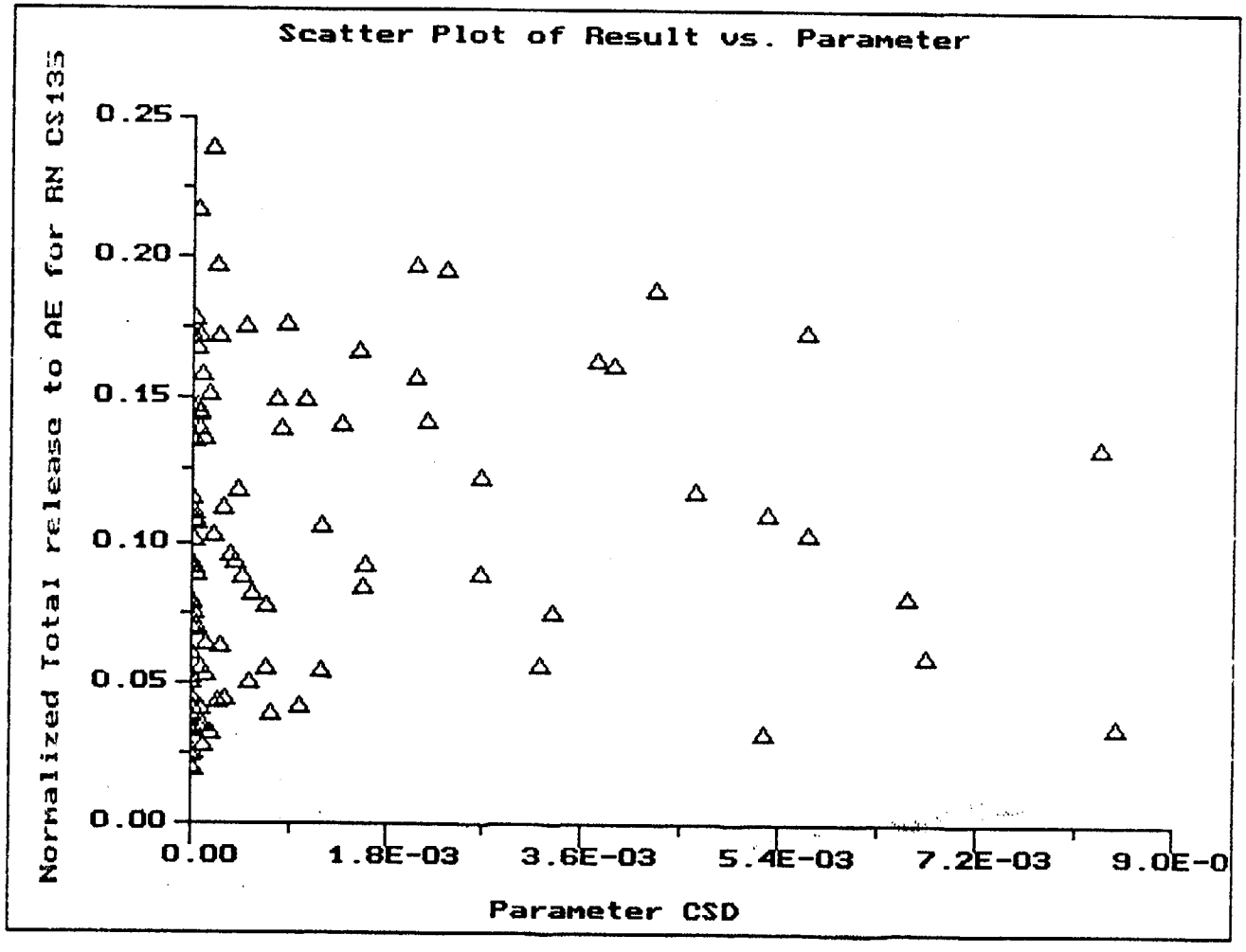

Figure 2-33. Sensitivity of ^{135}Cs to Diffusion Coefficient

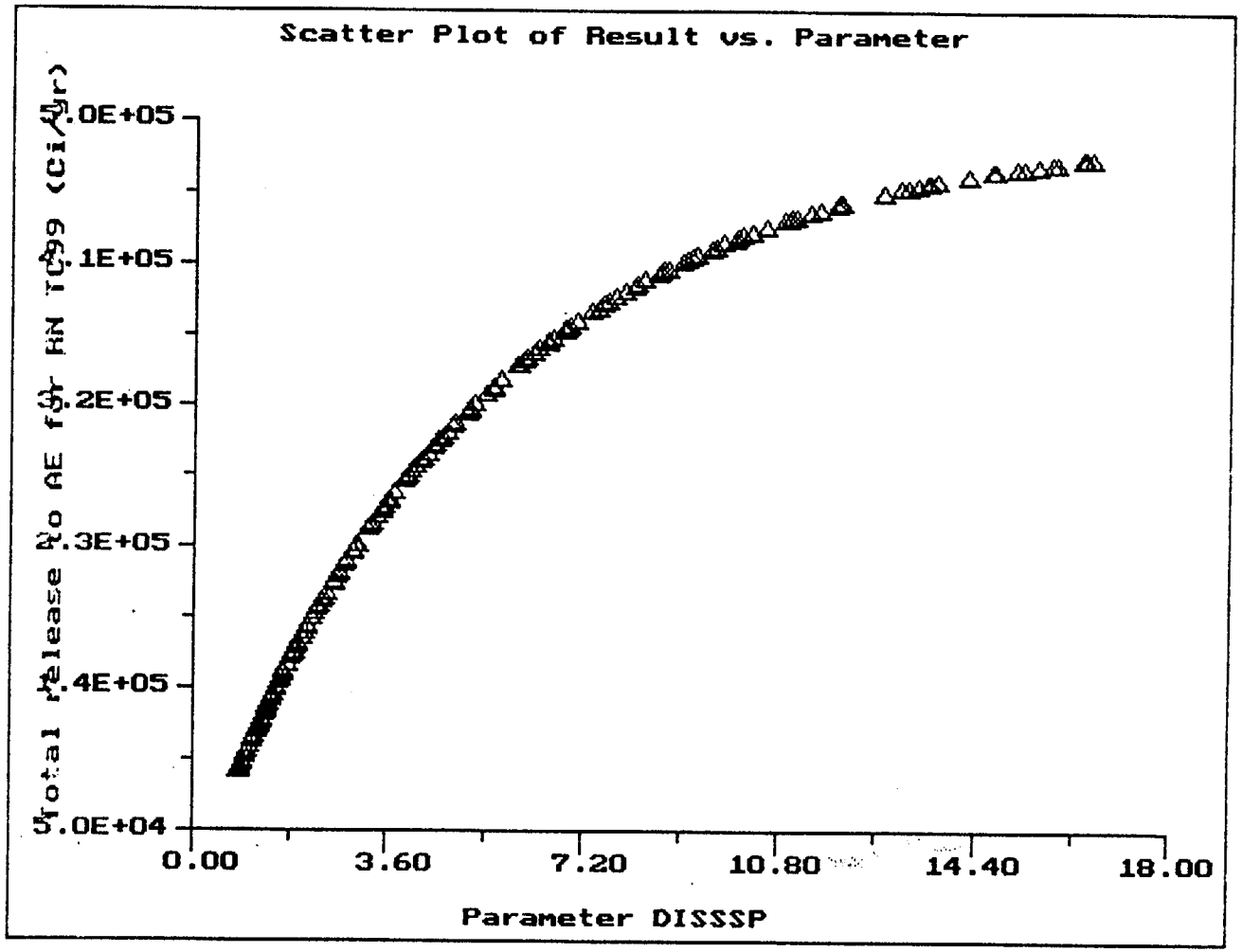

Figure 2-34. Sensitivity Curve of the Release of ^{99}Tc to the Accessible Environment as a Function of the Matrix Dissolution Rate

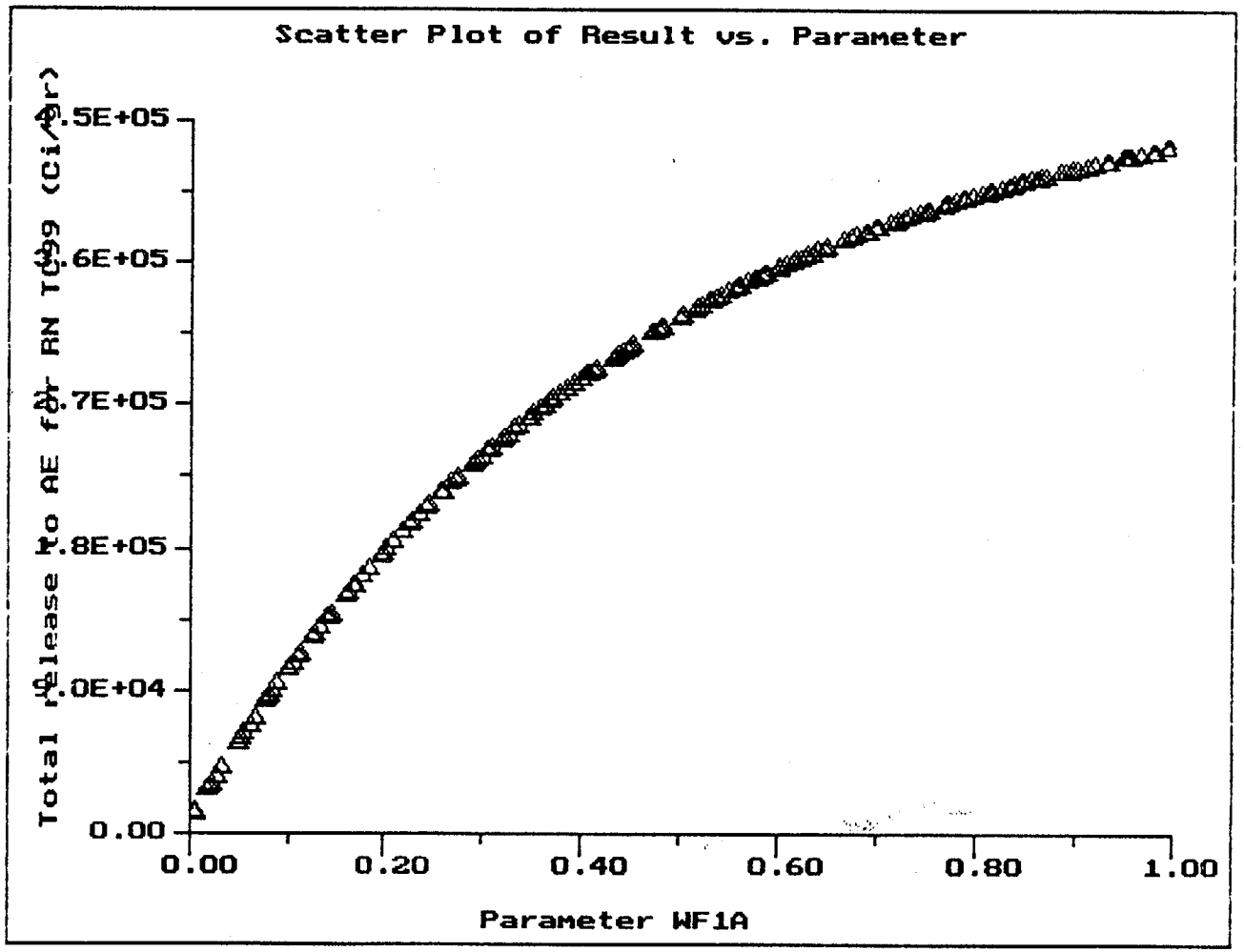

Figure 2-35. Sensitivity Curve of the Release of ^{99}Tc to the Accessible Environment as a Function of the Fraction of Waste Wetted

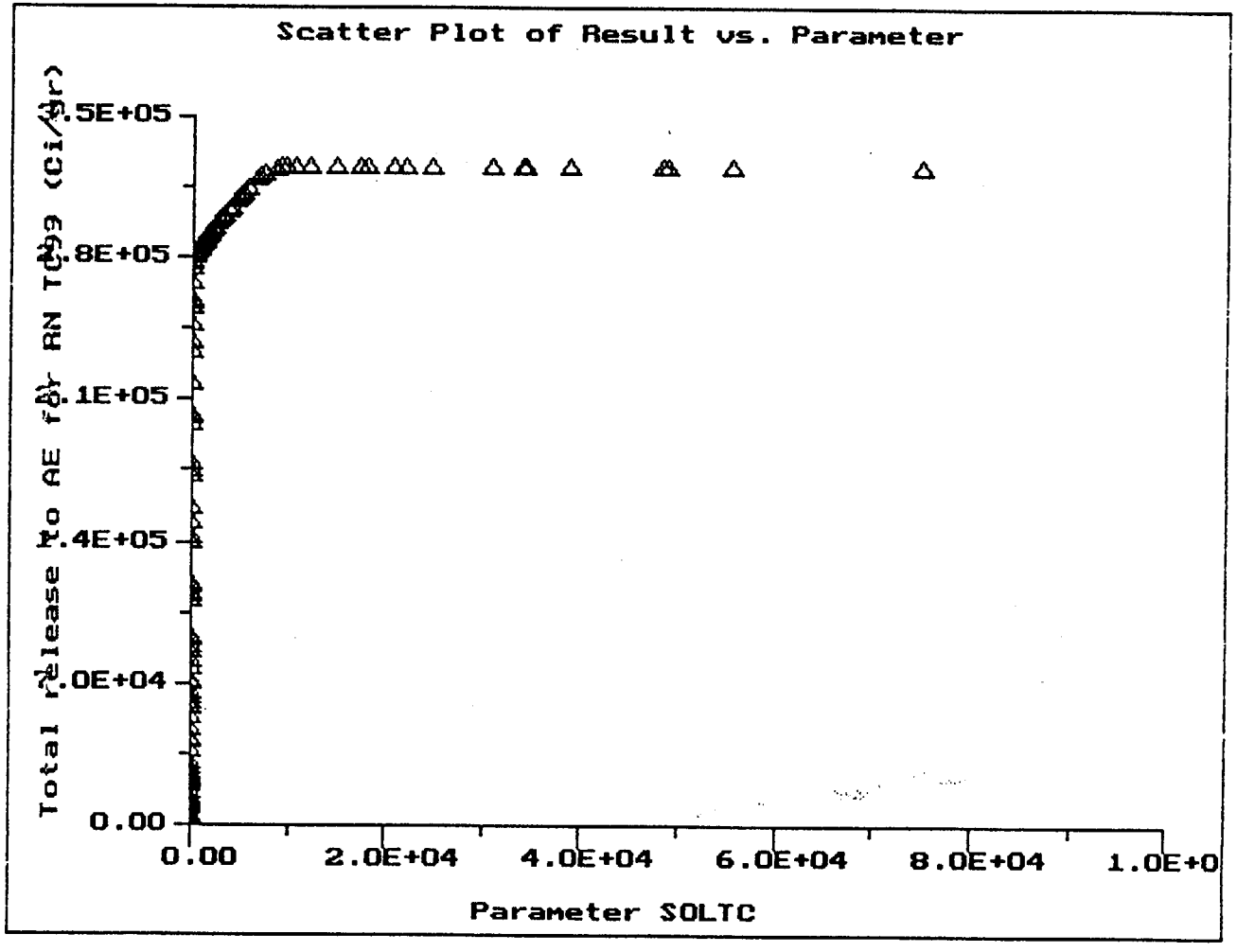

Figure 2-36. Sensitivity Curve of the Release of ^{99}Tc to the Accessible Environment as a Function of Technetium Solubility

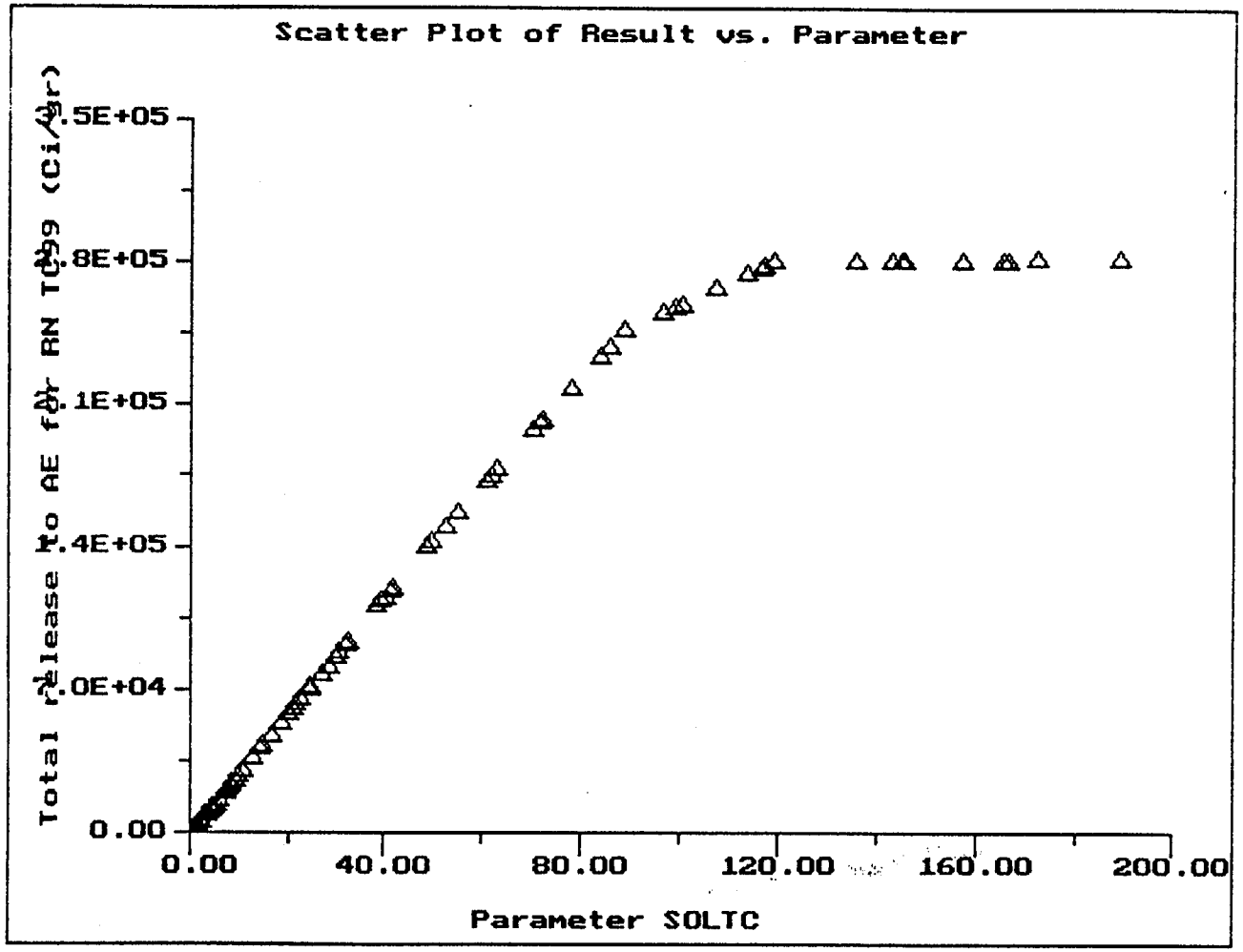

Figure 2-37. Sensitivity Curve of the Release of ^{99}Tc to the Accessible Environment as a Function of Technetium Solubility (low values of S_{Tc})

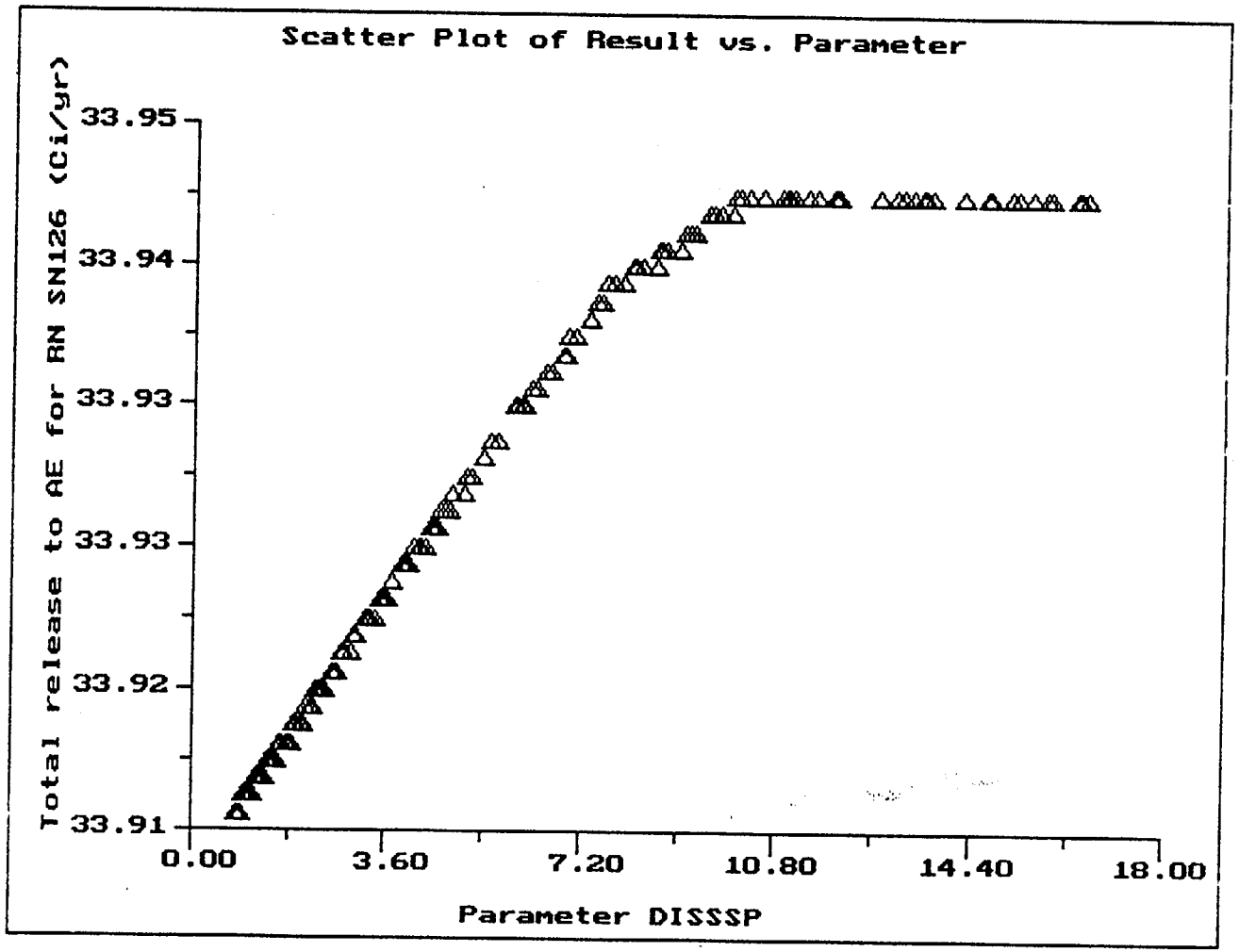

Figure 2-38. Sensitivity Curve of the Release of ^{126}Sn to the Accessible Environment as a Function of the Matrix Dissolution Rate

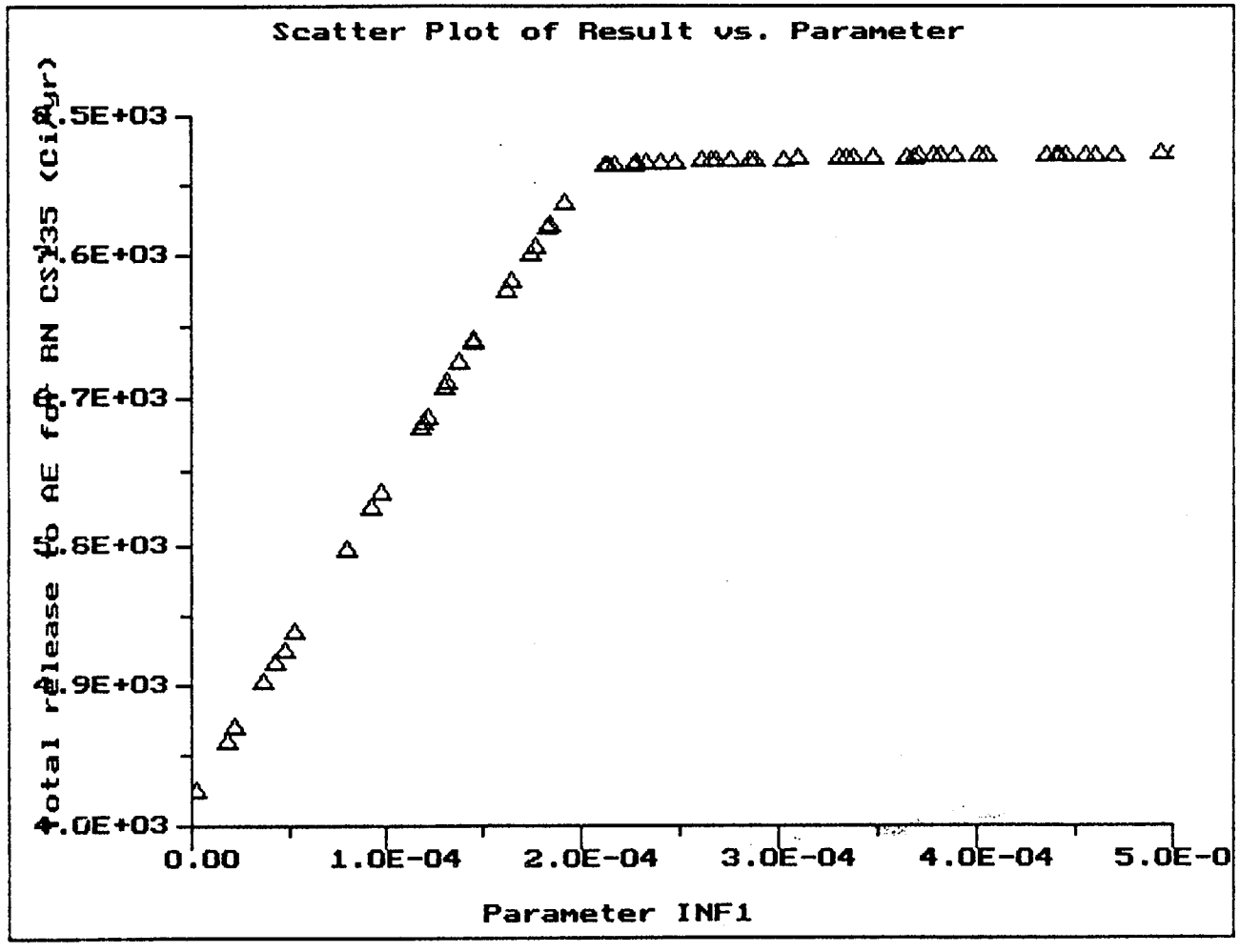

Figure 2-39. Sensitivity Curve of the Release of ^{135}Cs to the Accessible Environment as a Function of the Repository Infiltration Rate

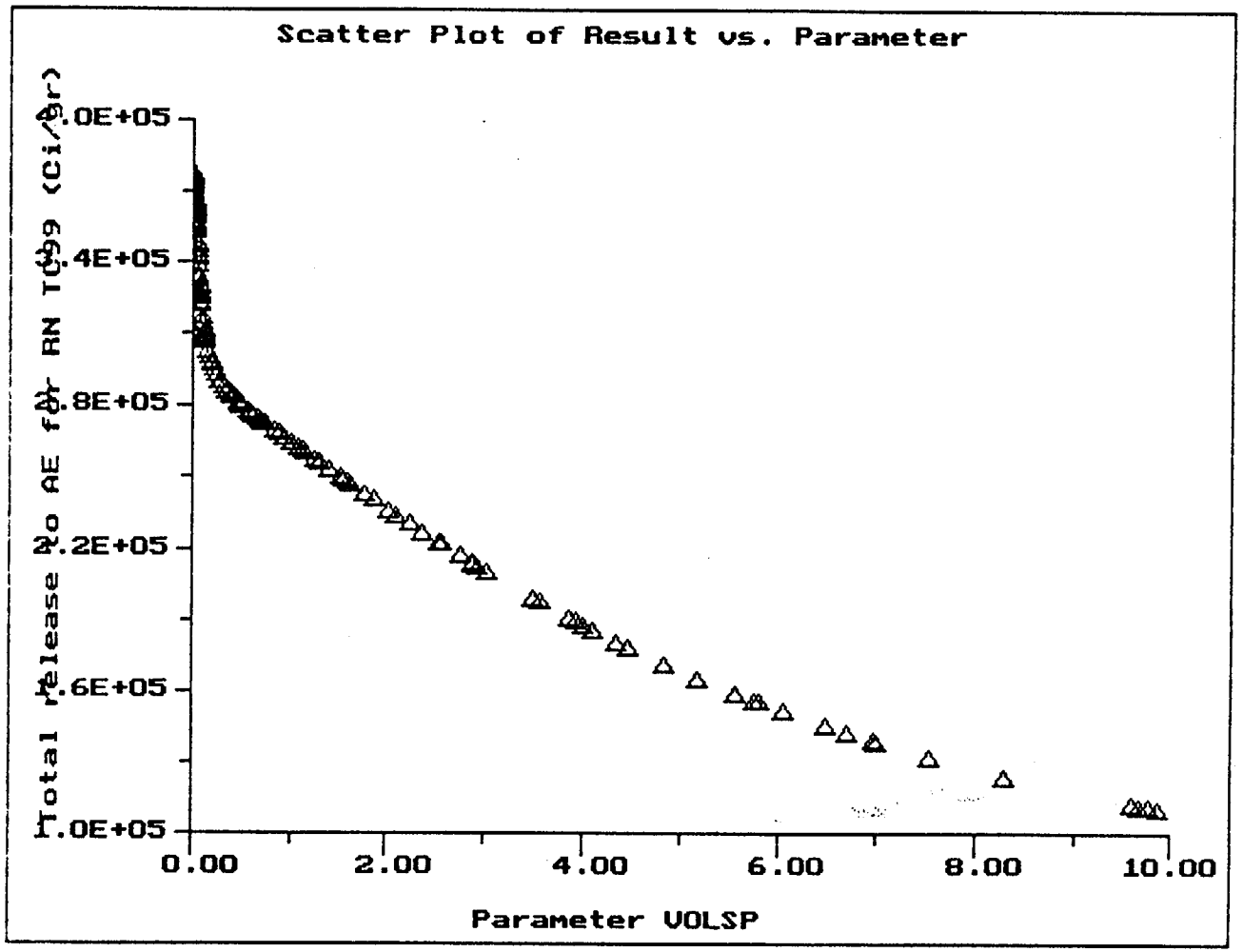

Figure 2-40. Sensitivity Curve of the Release of ^{99}Tc to the Accessible Environment as a Function of the Volume of Water Contacting the Matrix

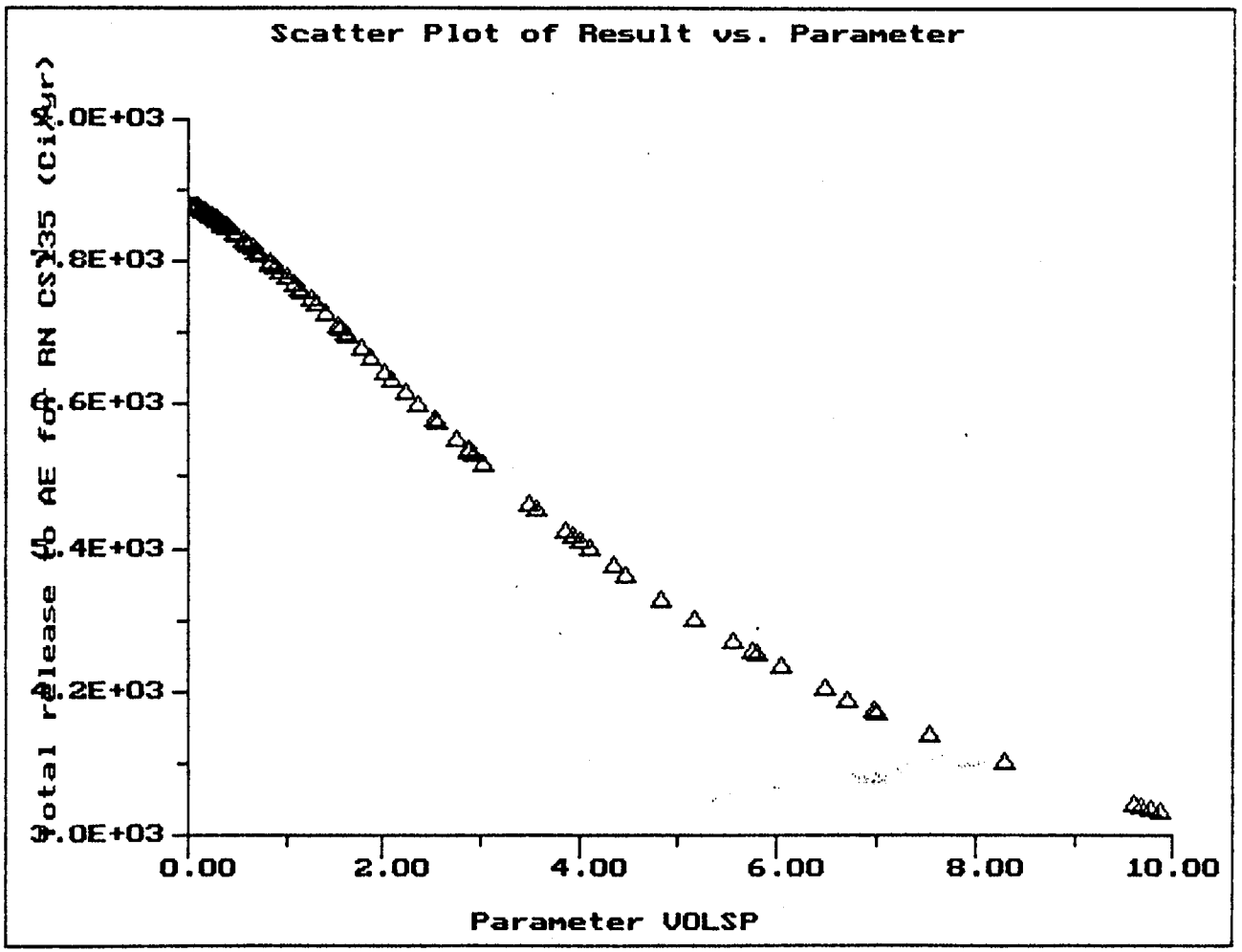

Figure 2-41. Sensitivity Curve of the Release of ^{135}Cs to the Accessible Environment as a Function of the Volume of Water Contacting the Matrix

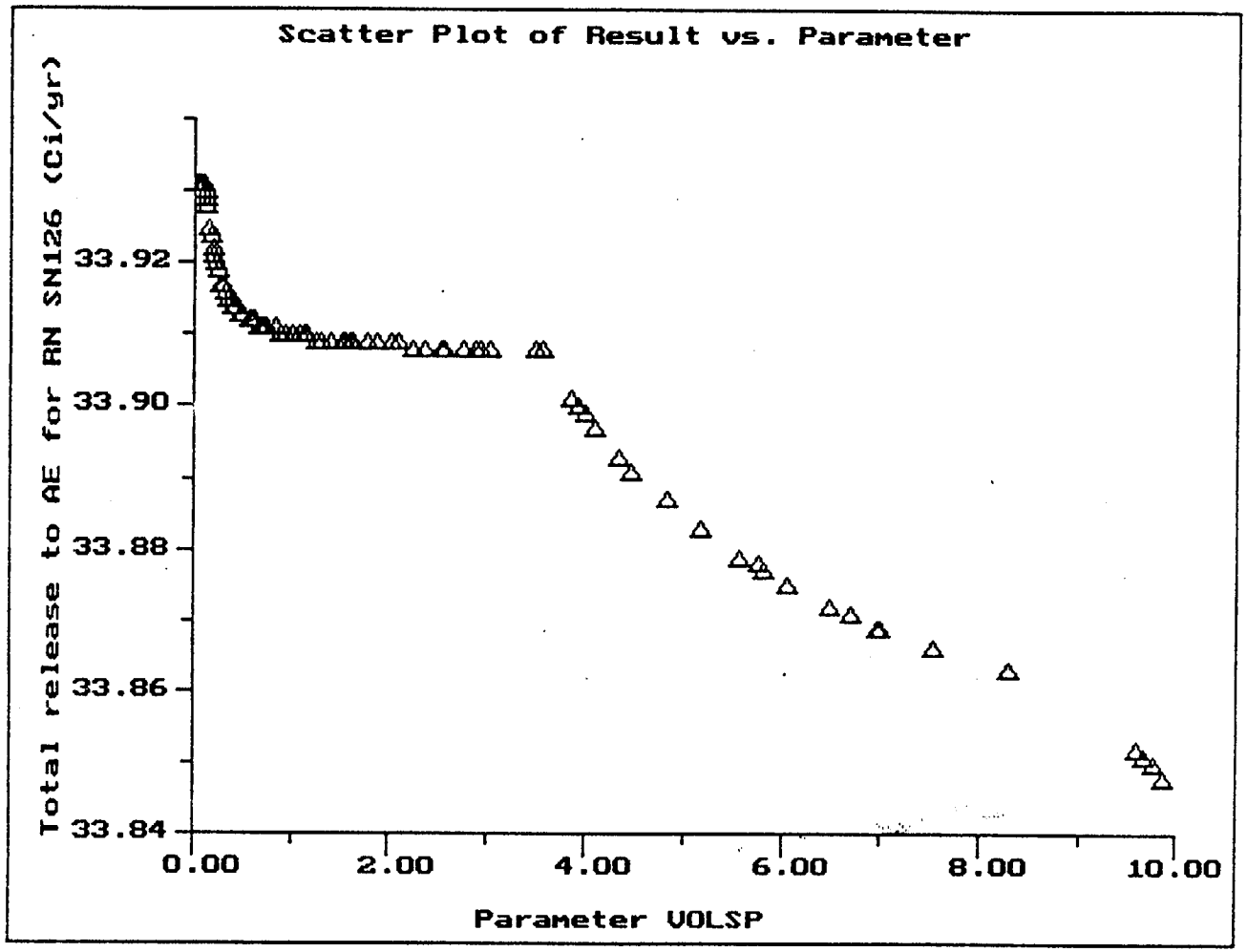

Figure 2-42. Sensitivity Curve of the Release of ^{126}Sn to the Accessible Environment as a Function of the Volume of Water Contacting the Matrix

Table 2-1. Inventory of Radionuclides for Various Analyses

Radionuclide	Aqueous Release Analyses (TSPA-1991 and RIP)	Aqueous Release Analyses Daughter Products (RIP Only)	Gaseous Release Analyses (TSPA-1991 and RIP)
^{243}Am	X		
^{135}Cs	X		
^{129}I	X		
^{237}Np	X		
^{239}Pu	X		
^{79}Se	X		
^{126}Sn	X		
^{99}Tc	X		
^{234}U	X		
^{231}Pa		X	
^{210}Pb		X	
^{226}Ra		X	
^{229}Th		X	
^{230}Th		X	
^{233}U		X	
^{235}U		X	
^{14}C			X

Table 2-2. Comparison of TSPA-1991 Container Parameters with RIP Parameters

TSPA-1991 Model Parameter	TSPA-1991 Base Case	TSPA-1991 Reference (page)	RIP Model Parameter	RIP Base Case
No. waste containers	33,300	4-29	No. packages	PWR - 19,980 BWR - 13,320
Waste burnup (MWd/MTHM)	PWR - 33,000 BWR - 27,500	4-14	Waste burnup (MWd/MTHM)	PWR - 33,000 BWR - 27,500
MTHM in repository	70,000	4-29	Mass waste/pkg = MTHM in repository/# of waste containers	2.1 MTHM/ container

Table 2-3. Comparison of TSPA-1991 Inventory Parameters with RIP Parameters

Inventory	TSPA-1991 Base Case (1) Ci/MTHM (2) Prompt release (3) Solubility (mol/l) (4) Activity (Ci/mol)	TSPA-1991 Reference (page)	RIP Base Case (1) Ci/container[1] (2) Gap fraction (3) Solubility (g/m^3) (4) Activity (Ci/g)
^{243}Am	(1) 1.54×10^{1} (2) 0 (3) LU: 1.2×10^{-11}, 3.8×10^{-9}, 6.6×10^{-10} (4) 4.84E1	4-13 4-13 4-29 4-13	(1) 32.34 (2) 0 (3) LU: 2.92×10^{-6}, 9.2×10^{-4}, 1.6×10^{-4} (4) 2×10^{-1}
^{135}Cs	(1) 3.51×10^{-1} (2) 0.02 (3) Infinite (4) 1.55×10^{-1}	4-13 4-13 Wilson, 1993 4-13	(1) 7.37×10^{-1} (2) 0.02 (3) Infinite (4) 1.15×10^{-3}
^{129}I	(1) 2.95×10^{-2} (2) 0.02 (3) Infinite (4) 2.28×10^{-2}	4-13 4-13 Wilson, 1993 4-13	(1) 6.19×10^{-2} (2) 0.02 (3) Infinite (4) 1.77×10^{-4}
^{237}Np	(1) 1.12 (2) 0 (3) LU: 5.9×10^{-11}, 1.9×10^{-8}, 3.3×10^{-9} (4) 1.67×10^{-1}	4-13 4-13 4-29 4-13	(2) 2.35 (2) 0 (3) LU: 1.4×10^{-5}, 4.5×10^{-3}, 7.82×10^{-4} (4) 7.06×10^{-4}
^{239}Pu	(1) 3.08×10^{-2} (2) 0 (3) LU: 1.6×10^{-10}, 5.1×10^{-8}, 8.8×10^{-9} (4) 1.49×10^{1}	4-13 4-13 4-29 4-13	(1) 6.47×10^{2} (2) 0 (3) LU: 3.82×10^{-5}, 1.22×10^{-2}, 2.1×10^{-3} (4) 6.22×10^{-2}
^{79}Se	(1) 3.81×10^{-1} (2) 0.02 (3) Infinite (4) 5.5	4-13 4-13 Wilson, 1993 4-13	(1) 8.0×10^{-1} (2) 0.02 (3) Infinite (4) 6.98×10^{-2}
^{126}Sn	(1) 7.15×10^{-1} (2) 0 (3) LU: 1.0×10^{09}, 3.2×10^{-7}, 5.5×10^{-8} (4) 3.58	4-13 4-13 4-29 4-13	(1) 1.50 (2) 0 (3) LU: 1.26×10^{-4}, 4.03×10^{-2}, 6.93×10^{-3} (4) 2.84E-2
^{99}Tc	(1) 1.23×10^{-1} (2) 0.02 (3) Infinite (4) 1.68	4-13 4-13 Wilson, 1993 4-13	(1) 2.58×10^{1} (2) 0.02 (3) Infinite (4) 1.7×10^{-2}
^{234}U	(1) 1.89 (2) 0 (3) LU: 7.1×10^{-11}, 2.3×10^{-8}. 4.0×10^{-9} (4) 1.46	4-13 4-13 4-29 4-13	(1) 3.97 (2) 0 (3) LU: 1.66×10^{-5}, 5.38×10^{-3}, 9.36×10^{-4} (4) 6.26E-3

LU = Log-Uniform: min, max, expected values

[1] Ci/container = Ci/MTHM · 2.1 mthm/container

Table 2-4. Comparison of TSPA-1991 WP Failure Parameters with RIP Parameters

TSPA-1991 Model Parameter	TSPA-1991 Base Case	TSPA-1991 Reference (page)	RIP Model Parameter	RIP Base Case
Beginning of resaturation period (yr)	300	4-29	Primary container failure definition: start at 800 years	Uniform: 800 - 1,800 years
Duration of resaturation period (yr)	1,000	4-29	Primary container failure definition: start at 800 years	Uniform: 800 - 1,800 years
Container lifetime when wet (yr)	LU: 500, 10,000, 3,170	4-29	Secondary container failure	1) Weibull: 1, 1650 2) LU: 500-10,000; gradual failure 3) LU: 500-10,000; all fail at once 4) LU: 500-10,000; sample maximum failure and fail gradually to that time

LU = Log-Uniform: min, max, expected value

Table 2-5. Comparison of TSPA-1991 Exposure Parameters with RIP Parameters

TSPA-1991 Model Parameter	TSPA-1991 Base Case	TSPA-1991 Reference (page)	RIP Model Parameter	RIP Base Case
Fraction of containers with rubble in air gap (f_r)	0.5	4-29	(1) Fraction of containers in water contact mode 3 - moist continuous (2) Fraction of waste wetted (3) Effective catchment area (ECA) (4) Effective diffusion coefficient (EDC)	0.25 0.5 0 SNL moist diff. coeff. (LU: 3.0×10^{-10} - 3.0×10^{-4})
Fraction of fuel wet with seepage (f_{ws})	0.5	4-29	(1) Fraction of containers in water contact mode 2 - wet drip (2) Fraction of waste wetted (3) ECA (4) EDC	0.25 0.5 1 0
Fraction of fuel wet and diffusing (f_{wd})	0.5	4-29	(1) Fraction of containers in water contact mode 1 - wet feet (2) Fraction of waste wetted (3) ECA (4) EDC	0.25 0.5 1 SNL wet diff. coeff. (LU: 9.0×10^{-4} - 9.0×10^{-3})
Nominal case - no release			(1) Fraction of containers in water contact mode 4 - nominal case	0.25
			Air alteration rate	0
Matrix alteration rate (a_m) (1/yr)	LU: 5.0×10^{-5}, 1.0×10^{-3}, 3.17×10^{-4}	4-29	Matrix dissolution rate ($g/m^2/yr$)	LU: 5.0×10^{-5}, 1.0×10^{-3}, 3.17×10^{-4}
			Surface area of matrix (m^2/g) (combined with matrix dissolution rate)	1
Prompt alteration rate (a_p) (1/yr)	0.5	4-29	N/A -- RNs put in gap fraction	
Spent fuel surface area per package (A) (m^2)	140	4-29	Included in water volume contacting matrix (m^3) (=surface area · water film thickness · fraction of fuel wet)	0.07
Water film thickness (d_{film}) (mm)	1	4-29	Included in water volume contacting matrix (m^3)	0.07

LU = Log-Uniform: min, max, expected value

Table 2-6. Comparison of TSPA-1991 Transport Parameters with RIP Parameters

TSPA-1991 Model Parameter	TSPA-1991 Base Case	TSPA-1991 Reference (page)	RIP Model Parameter	rip Base Case
Moist diffusion coefficient (m^2/yr)	LU: 3.0×10^{-6}, 3.0×10^{-4}, 6.45×10^{-5}	4-29	Effective diffusion coefficient (m^2/yr)	LU: 3.0×10^{-6}, 3.0×10^{-4}, 6.45×10^{-5}
Wet diffusion coefficient (m^2/yr)	LU: 9.0×10^{-4}, 9.0×10^{-3}, 3.52×10^{-3}	4-29	Effective diffusion coefficient (m^2/yr)	LU: 9.0×10^{-4}, 9.0×10^{-3}, 3.52×10^{-3}
Flux coefficient of variation	1.3	4-29	None	
Percolation rate (mm/yr)	Beta: 1.1, 0, 39	3-21	Repository infiltration rate (m/yr)	Beta: 1.0×10^{-3}, 9.0×10^{-4}, 0, 3.9×10^{-2} (only for contact modes 1,2)
Effective diffusion area (m^2)	0.172	4-29	Geometric factor for diffusion (m)	0.1 (only for contact modes 1,3)
Fraction of seepage through A_{cross} actually entering container	0.5	4-29	N/A (see effective catchment area)	
Water collection area (A_{cross}) (m^2)	2	4-29	Effective catchment area (m^2) = water collection area · fraction of seepage entering container	Contact 1 = 1 Contact 2 = 1 Contact 3 = 0 Contact 4 = 0
Rubble thickness (cm)	3	4-29	Delay pathway (only in moist continuous)	3 cm

LU = Log-Uniform: min, max, expected value

Table 2-7. Major Parameter Differences between RIP Simulations

Run	Log-Uniform WP Failure Distribution	Nine RNs	Hi-Solubility for ^{99}Tc, ^{135}Cs	Revised Failure Distri-bution	Implement f_s, f_r WP Distribution Calculations	Air Gap	Figure No.
2.1	N	N	N	N	N	N	2-13
2.2	Y	N	N	N	N	N	2-14
2.3	Y	Y	N	N	N	N	2-15
2.4	Y	Y	Y	N	N	N	2-16
2.5	Y*	Y	Y	Y	N	N	2-17
2.6	Y*	Y	Y	Y	Y	N	2-18
2.7	Y*	Y	Y	Y	Y	Y	2-19
2.8	Y*	Y	Y	Y	Y	Y	2-20

* Log-uniform distribution is implemented in the start time of the secondary container failure distribution.

Table 2-8. Comparison of Peak Values for Individual Radionuclide Release (Ci/yr)

Radionuclide	TSPA-1991	Run 2.8	Run 2.5	Run 2.4
SOLUBILITY-LIMITED				
^{237}Np	3.2×10^{-5}	2.6×10^{-5}	2.6×10^{-5}	2.6×10^{-5}
^{239}Pu	8.0×10^{-3}	6.1×10^{-3}	6.1×10^{-3}	6.1×10^{-3}
^{243}Am	1.9×10^{-3}	1.5×10^{-3}	1.5×10^{-3}	1.5×10^{-3}
^{234}U	3.4×10^{-4}	2.7×10^{-4}	2.7×10^{-4}	2.7×10^{-4}
^{126}Sn	1.2×10^{-2}	9.3×10^{-3}	9.3×10^{-3}	9.3×10^{-3}
ALTERATION-LIMITED				
^{129}I	0.10	0.17	0.18	0.11
^{135}Cs	0.88	2.0	2.1	1.3
^{79}Se	1.2	2.1	2.2	1.4
^{99}Tc	40	70	73	46

Table 2-9. High-Solubility Radionuclides (^{99}Tc) Waste Alteration Sensitivity Analyses

Parameter	Range	Expected Value	Sensitivity	Sensitivity Due To Modes
Matrix dissolution rate ($g/m^2/yr$)	0.84 - 16.8	5.33	Log-like: 440% increase	WF, WD, MC
Fraction of waste wetted	0.0 - 1.0	0.5	Log-like: 2900% increase	WF, WD, MD
Solubility (g/m^3)	0.035 - 990,000	12,540	Linear:(1) 0-90: $m_1 = 2,700$ 120 - 9,000: $m_2 = 5.2$ 9,000 - 9.9×10^{-5}: $m_3 = 0$	WF, WD, MC

(1) The sensitivity curve is a series of three line segments, decreasingly steep as the solubility increases. The transition from one line segment to the next is smooth, and it does not appear that there are discontinuities in slope.

Table 2-10. Low-Solubility Radionuclides (^{239}Pu) Waste Alteration Sensitivity Analyses

Parameter	Range	Expected Value	Sensitivity	Sensitivity Due To Modes
Matrix dissolution rate ($g/m^2/yr$)	0.84 - 16.8	5.33	None(1)	N/A(1)
Fraction of waste wetted	0.0 - 1.0	0.5	None(2)	N/A(2)
Solubility (g/m^3)	3.8×10^{-5} - 0.012	0.0021	Linear: m = 10,627	WF, WD, MC

(1) Of the low-solubility radionuclides, only ^{126}Sn exhibits any sensitivity to changes in the matrix dissolution rate. The release increases linearly (m=0.004) until it becomes constant at R_{dis}=10. Tin has a higher solubility than the other low-solubility radionuclides, and this accounts for its sensitivity. The *wet-feet* and *wet-drip* modes are the important mechanisms for this release.

(2) ^{239}Pu and ^{237}Np are not dependent on f_w, but the release of ^{234}U and ^{126}Sn increase and then becomes constant as f_w increases. However, the overall increases are relatively small (0.1% and 0.7%, respectively). The release is dependent on the WF, WD, and MC modes.

Table 2-11. High-Solubility Radionuclides (^{99}Tc) Release Parameter Sensitivity Analyses

Parameter	Range	Expected Value	Sensitivity	Sensitivity Due to Modes
Repository infiltration rate (m/yr)	0.0 - 0.039	0.001	0 - 0.00008: linear $m = 1.2 \times 10^9$ 0.0004 - 0.039: constant	WF, WD
Water volume contacting matrix	0.001 - 10	0.07	Monotonically decreasing: 244%	WF, SD, MC
MC diffusion coefficient (m^2/yr)	3×10^{-6} - 3×10^{-4}	6.45×10^{-5}	0 - 0.0006:(1) linear: $m = 1.5 \times 10^9$ 0.00006 - 0.0003: constant	MC
WF diffusion coefficient (m^2/yr)	9×10^{-4} - 9×10^{-3}	3.52×10^{-3}	None	N/A
Geometric factor for diffusion (m)	0.1 - 10.0	1.0	Left-most point(2)	MC
Effective catchment area (m^2)	0.1 - 10.0	1.0	None(3)	N/A(3)

(1) The sensitivity depends on the radionuclide and the range of values of the parameter of interest. The release of ^{135}Cs increases linearly over the entire range of interest. ^{99}Tc and ^{79}Se increase linearly before they become constant, and ^{129}I is constant.

(2) The sensitivity depends on the radionuclide. ^{135}Cs increases linearly from 0.1 to 3.2, with a slope m = 1270, then becomes constant at w = 3.2. ^{99}Tc seems to have a similar dependence, only it is shifted left so that almost all the linear rise is outside the range of interest. The sensitivity curves for ^{129}I and ^{79}Se are shifted over even more, so that the 0.1 - 10 window covers the constant region only; there is no dependence.

(3) As for the two comments above, the sensitivity to A_c depends on the radionuclide. ^{135}Cs release increases linearly, then becomes constant. The sensitivity arises from the *wet-drip* waste packages. ^{79}Se, ^{99}Tc, and ^{129}I are constant over the range of interest.

Table 2-12. Low-Solubility Radionuclides (^{239}Pu) Release Parameter Sensitivity Analyses

Parameter	Range	Expected Value	Sensitivity	Sensitivity Due to Modes
Repository infiltration rate (m/yr)	0.0 - 0.039	0.001	Linear: m = 19,000	WF, WD
Water volume contacting matrix	0.001 - 10	0.07	None(1)	N/A(1)
MC diffusion coefficient (m^2/yr)	3×10^{-6} - 3×10^{-4}	6.45×10^{-5}	Linear: m = 950	MC
WF diffusion coefficient (m^2/yr)	9×10^{-4} - 9×10^{-3}	3.52×10^{-3}	Linear: m = 953	WF
Geometric factor for diffusion (m)	0.1 - 10.0	1.0	Linear: m = 33.9	WF, MC
Effective catchment area (m^2)	0.1 - 10.0	1.0	Linear: m = 19.0	WF, WD

(1) The releases of ^{239}Pu and ^{237}Np are constant. For sufficiently large volumes, the releases of ^{234}U, ^{243}Am, and ^{126}Sn decrease as the volume increases. The dependence is due to the WF, WD, and MC water contact modes.

Table 2-13. Correlation Coefficients for RUN 2.9

RN	$D_{eff,mc}$	R_{dis}	f_w	S_{Tc}
^{243}Am	0.901	0.045	0.031	-0.00
^{237}Np	1.005	0.054	0.045	-0.00
^{239}Pu	1.013	0.055	0.046	-0.00
^{126}Sn	0.104	0.034	0.063	0.008
^{234}U	0.909	0.044	0.027	-0.00
^{135}Cs	0.120	0.710	0.618	-0.00
^{129}I	0.077	0.711	0.618	-0.00
^{79}Se	0.077	0.714	0.609	-0.00
^{99}Tc	0.115	0.378	0.336	0.226

Table 2-14. Correlation Coefficients for RUN 2.10

RN	$D_{eff,wf}$	$D_{eff,mc}$	A_c	w	q_{int}	S_{Pu}
^{234}Am	0.362	0.008	0.335	0.640	0.290	-0.03
^{237}Np	0.362	0.008	0.335	0.640	0.290	-0.03
^{239}Pu	0.149	-0.00	0.143	0.296	0.113	0.562
^{126}Sn	0.361	0.008	0.336	0.640	0.290	-0.03
^{234}U	0.362	0.008	0.335	0.640	0.290	-0.03
^{135}Cs	-0.00	0.504	0.176	0.501	0.297	0.014
^{129}I	-0.00	-0.00	-0.00	-0.00	-0.00	-0.00
^{79}Se	0.001	0.001	-0.00	0.000	0.000	0.000
^{99}Tc	-0.04	0.397	-0.02	0.394	0.058	0.029

3. AQUEOUS FLOW AND TRANSPORT TO THE ACCESSIBLE ENVIRONMENT

This section presents the analyses related to aqueous transport of radionuclides from the potential repository to the accessible environment, through the unsaturated and saturated flow zones. The approach adopted by Sandia National Laboratories for TSPA-1991 (Barnard et al., 1992) is described briefly, along with their choice of the different hydrogeological and geochemical parameters. The present approach to these analyses with RIP uses different models which involve different conceptualizations of the flow and transport regimes. These conceptualizations are also described here, together with the parameters used for these analyses.

The present analyses use the same definitions of the problem domain and stratigraphy used in TSPA-1991. Most of the hydrogeologic and geochemical parameters are common to the previous analysis of Barnard et al. (1992). The RIP analysis seeks to use the same values for such parameters. However, RIP imposes restrictions on the parameter distributions which are different from those in TSPA-1991 (Barnard et al., 1992). The present analyses incorporate such required modifications in the distributions of those parameters.

This section also presents the results of the RIP simulations and compares them with those of the TSPA-1991 (Barnard et al., 1992) analyses.

3.1 PROBLEM DOMAIN

The details related to the definition of the problem domain and the stratigraphy are presented here. These are taken directly from TSPA-1991 (Barnard et al., 1992).

The flow and transport problem domain sampled the volume directly beneath the potential repository to the water table and, in the saturated zone, out to the accessible environment. Figure 3.1 shows the boundary of the potential repository. A 2-D cross-section across the potential repository block was chosen in TSPA-1991 to represent unsaturated-zone hydrologic conditions throughout the potential repository block (Figures 3-1 and 3-2). The potential repository was divided into six equal subregions. Each subregion is represented by a vertical column for simulating unsaturated flow. The subregions and the location of the columns are shown in Figure 3-1.

The saturated zone parameters used in TSPA-1991 were based on flow models by Czarnecki and Waddell (1984) and Czarnecki (1985).

A five-layer model was used in TSPA-1991 to define the unsaturated zone (Figure 3-3). The layers represent different types of ash-flow tuff observed at Yucca Mountain. From the top of the domain to the bottom, the layers are given in Table 3-1. The elevations of each layer are summarized in Table 3-2.

The percolation rate was modeled in TSPA-1991 by a beta distribution with a total range from 0.0 to 39 mm/year with a mean of 1.0 mm/yr.

3.2 CONCEPTUALIZATION AND MATHEMATICAL MODEL (TSPA-1991)

Two different conceptual models of flow in the unsaturated zone are studied in TSPA-1991: (1) the composite-porosity model that combines matrix and fractures into a single composite porosity medium for analysis; this model permits unrestricted water movement between fractures and matrix; and (2) the weeps model, a model that depicts essentially all of the percolating water traveling down fractures. The potential repository thermal effects are ignored. Radionuclide retardation during transport is modeled by a simple distribution coefficient (K_d).

In the TSPA-1991 analyses using the composite porosity model, the characteristic curves, i.e., the relative permeability versus the capillary pressure and saturation curves used to describe the hydrologic properties of the matrix and fractures, determine the distribution of flow between matrix and fractures. These curves for the matrix and fractures are dissimilar, and as a result flow tends to reside primarily in the matrix until the flux exceeds the saturated conductivity of the matrix, at which point the excess flow would be diverted into the fractures.

Models that allow the matrix and fractures to be completely decoupled (e.g., the weeps model) result in markedly different steady-state flow solutions. The results of such models are not comparable to the analyses presented herein, which assume a composite-porosity formulation. The details of such models, pursued in TSPA-1991, are not presented here.

Figure 3-3 shows the six columns used for the composite-porosity model in TSPA-1991 and this study. The top of each column is 10 m above the repository horizon. Elevations for each of the units within each column, and at each drill hole, are presented in Table 3-3.

For the TSPA-1991 calculations, the saturated zone was simplified to a one-dimensional flow tube 5000 m in length. For every calculation, radionuclides released from the repository were provided as a point-source to the flow tube underlying the potential repository.

The transport model in the TRANS module of TOSPAC is a one-dimensional dual-porosity model of solute transport, containing two generalized advection-dispersion differential equations. The equation models retardation and the transfer between matrix and fracture due to advection and diffusion mechanisms. The model is used for transport both in saturated and unsaturated zones.

The parameter distributions used by the TSPA-1991 analyses are given in Tables 3-4 through 3-9. Most of the distributions are taken to be described by beta distributions. In addition, these tables also provide the distributions as used in the present analyses using the RIP code.

The Yucca Mountain tuffs were represented by three rock types for purposes of defining the sorption-coefficient distributions: devitrified, zeolitic, and vitric. The relationship between those rock types and the stratigraphy defined earlier is shown in Table 3-9. The distributions of K_d values for the different nuclides in the different rock types are shown in Table 3-10.

3.3 RIP MODEL: FLOW AND TRANSPORT SIMULATION CAPABILITY

In the RIP model, the physical domain of flow and transport is represented as a network of one-dimensional legs, designated as *pathways*. Each leg may have flow in one mode or in several modes. When there are multiple modes in a leg, each mode relates to one flow velocity. A leg with one mode may represent a homogeneous medium. In a leg with two modes, for example, mode 1 can correspond to flow in a fracture, while mode 2 can correspond to flow in the matrix. For purposes of the present application, a maximum of two modes is used. In each mode (fracture and matrix), the flow velocity is considered uniform (constant) for a given leg. The degree of interaction between the modes is governed by the choice of a Poisson transition rate parameter.

In reality, the RIP model cannot simulate flow conditions. It demands an input of flow velocity (interstitial), either directly or indirectly. It requires input of flow parameters such as flow rate (Q), the cross-sectional area of the leg (A), and porosity (ϕ), and computes the interstitial velocity (v), by:

$$v = \frac{Q}{A \cdot \phi} \tag{3-1}$$

The user may input interstitial velocity for each mode directly, which then overrides the above computed value. When there are two modes, the user also needs to input the flow fraction for the fracture mode. The input parameters may be given as numerical values, or as algebraic or logical functions of other input parameters. The model does not distinguish between saturated and unsaturated flow conditions.

The transport simulation within RIP consists of two stages. The principle behind the actual algorithm may be explained as follows:

- Computing a breakthrough curve and deducing an impulse source response function
- Convolution of the source rate with the impulse source response to give the nuclide release rate.

For legs with a single flow mode, the analytical solution for the one-dimensional advection-dispersion transport equation is used to generate the breakthrough curve. For this purpose, the dispersivity of the medium needs to be input.

For legs with multiple modes, a Markov process algorithm is used to generate the breakthrough curve. In RIP, a simplified version of the Markov process is implemented. In the Markov process, a particle is released into the flow system and may enter mode 1 or mode 2. The probability of the particle entering any mode is proportional to the flow fraction for that mode. The particle travels a random length in that mode, and then tranfers into the other mode (in a system with only two modes, as in the present application). In a true Markov process, the process of traveling a random length in a given mode and transitioning to the next mode may occur a number of times before the particle exits the leg. In the simplified version implemented in RIP, the particle travels only one random length in the given medium, with the remaining

length of the leg traveled at the temporal mean velocity of the two modes. An analytical expression for the cumulative distribution function of the travel times for this simplified Markov process is available and is used to represent the breakthrough curve. (For a true Markov process, random simulation of travel times is required to obtain the CDF, which constitutes the breakthrough curve.) Breakthrough curves are derived separately for each radionuclide, considering their retardation factors. The impulse source response can be constructed by a procedure of numerical differentiation.

For numerical implementation of the above scheme, discretization in the time domain is done as follows. Discrete time points are defined by:

$$0,\ \Delta t,\ f\Delta t,\ f^2\Delta t,\ f^3\Delta t,\ f^4\Delta t,\ \text{etc.}$$

where Δt is a user-specified time step and f is a time-stepping factor, set at f = 2 in the current version of RIP. For example, if Δt = 100 years, the time points would be:

$$0,\ 100,\ 200,\ 400,\ 800,\ 1600,\ \text{etc.}$$

Consider, for example, the time window from 800 years to 1600 years. The mass of nuclides released during this time window is the difference between the ordinates of the breakthrough curve at 1600 years and 800 years. This mass is released at the end of the leg, at a uniform rate, starting from 800 years to 1600 years. (This corresponds to a piece-wise linear approximation of the breakthrough curve.) Further, nuclide decay will also be accounted for during this time period. This numerical algorithm produces an earlier breakthrough than the true case (see Appendix B). The error of the earlier breakthrough time reduces if f is chosen closer to one, but this dramatically increases the run time.

The parameters governing the nuclide release rates, which are essential inputs, are:

- Length of the leg
- Flow proportions of each mode
- Flow velocity in each mode (v)
- Retardation factors (R)
- Poisson transition rate (λ).

The *Poisson Transition Rate* parameter, λ, is a parameter defining the exponential distribution, which is assumed for random travel length in a mode. The reciprocal of λ gives the particle's mean length of travel in the mode. The standard deviation for this distribution equals the mean value.

3.4 CONCEPTUALIZATION OF FLOW AND TRANSPORT IN RIP

The problem domain, stratigraphy, and the six one-dimensional vertical columns used for unsaturated flow in the composite-porosity model of TSPA-1991 have been used with our RIP analyses without modifications. Also, the horizontal leg for the saturated flow is used in exactly the same way as in the TSPA-1991 analysis. The differences that arise due to the code features are described below.

The six vertical columns shown in Figure 3-3 and defined in Table 3-3 are used for simulating the unsaturated flow. Each stratigraphic unit is treated as one leg (or pathway) per column. Thus, columns 1 through 4 have five legs each, while columns 5 and 6 have four legs each, giving a total of 28 legs for unsaturated flow.

As mentioned earlier, the RIP code does not distinguish between saturated and unsaturated flow. However, the special input capabilities of the code have been exploited to mimic the physics of unsaturated flow. In this analysis, the legs simulating unsaturated flow have been assigned two modes, corresponding to the fracture and the matrix. The logic presented below describes the apportionment of the infiltration rate between the matrix and the fracture. This logic is designed to mimic the physics of the composite-porosity model of TSPA-1991.

It is known that the matrix can carry the infiltration at a maximum rate equal to the saturated hydraulic conductivity of the matrix (under a unit hydraulic gradient). Thus, if the infiltration rate is less than the saturated hydraulic conductivity of the matrix, the entire infiltration would pass through the matrix, with no flow in the fractures. If, however, the infiltration rate is higher, the matrix carries the flow rate equal to its saturated hydraulic conductivity, and the balance will be carried by the fractures. This conceptualization is illustrated in Figure 3-4. The composite-porosity flow model, which can simulate the physics of unsaturated flow, with complete interaction between fractures and the matrix, results in a similar apportionment of flow between matrix and fractures. It may be noted that the RIP model does not use soil characteristic parameters that define the water-retention properties of the matrix and fractures. (These are used by the composite-porosity model of TSPA-1991.) For the determination of the interstitial pore velocity, the matrix is assumed to be fully saturated. The degree of saturation in fractures is assumed to be 10% (see Appendix C).

The geometry of the one-dimensional leg used for the simulation of saturated flow is the same as in the TSPA-1991 analysis. All the input parameters used (velocity, porosity, retardation parameters) are also the same as in the TSPA-1991 analysis. In RIP, this leg is used with one mode which corresponds to a homogeneous porous medium.

The transport parameters used in the RIP analysis, such as retardation parameters for the unsaturated and saturated zones, and dispersivity for saturated zones, remain the same as those used in TSPA-1991. A new transport parameter, the Poisson transition rate, λ, is required as input to RIP. Although this parameter has limited physical significance, it is an important model input for the two-mode (fracture and matrix) transport in the unsaturated zone. The sensitivity of the results (e.g., EPA sum at the accessible environment) are investigated for a range of values of λ (10^{-8}, 10^{-3}, 10^{-2}, 10^{-1}, 10^{0}, 10^{1}, 10^{8} m^{-1}) by repeating the stochastic simulations of 1,000 realizations for each value of λ chosen.

The parameters used for the RIP model, and their distributions, are essentially the same as used in the TSPA-1991 analysis. It has already been noted that the RIP model does not use the soil characteristic parameters characterizing the water-retention properties of the matrix and fractures. For this analysis, the Poisson transition rate λ value has been kept as constant and is not defined by a distribution. Most of the probability density functions are defined by beta distributions. The RIP model imposes some restrictions on the beta distributions. For example, the coefficient of variation (C_v) should be less than one for RIP, while many of the beta distributions in

TSPA-1991 have a C_v of unity. Similarly, the range between the maximum and minimum should be less than 40 times the standard deviation in the RIP model. Thus, the beta distributions input to the RIP model are different from those in TSPA-1991. However, those differences are insignificant and are not considered to have any effect on the results.

Tables 3-4 through 3-9, which show the distributions for the different parameters used in TSPA-1991, also show the corresponding values used for the RIP model.

3.5 RESULTS OF RIP SIMULATIONS

Several simulations have been performed for the flow and transport through the unsaturated and saturated zones. The results from the RIP model are compared with those from the TSPA-1991 analysis. For purposes of presentation, these results are separated into three categories:

- Verification tests for RIP (see Appendixes B and C)
- CCDFs for nuclide release
- Sensitivity analyses.

3.5.1 Distribution of Nuclide Releases

Using the RIP model, 1,000 realizations of the stochastic input parameters are generated and the nuclide releases at the end of a 10,000-year period for each realization are computed. The 10,000-year release has been computed -

- At the edge of the EBS
- At the end of the unsaturated flow zone, i.e., at the water table
- At the accessible environment.

Figure 3-5 presents conditional CCDFs for aqueous releases from the EBS, from the unsaturated zone, and to the accessible environment, as calculated by RIP for the particular case of $\lambda = 0.1$ m^{-1} (RUN 3.1). The plot shows the probability of exceeding a given release in terms of the EPA sum.

The cross-hatched area in Figure 3-5 indicates regions where the EPA limit is exceeded; however, it applies only to releases to the accessible environment (the normalized releases from the EBS and from the unsaturated zone are not actually EPA sums because they do not represent releases to the accessible environment). Also, note that the EPA sums shown in Figure 3-5 are really *partial* EPA sums because they include only aqueous releases and not releases by other mechanisms, such as gaseous releases or other scenarios.

The figure indicates that the calculated aqueous releases to the accessible environment are approximately two orders of magnitude below the EPA limit. The releases to the water table are well below those from the EBS, indicating that the unsaturated zone provides an important barrier to the release of radionuclides. As indicated on the plot, however, the saturated zone adds little additional impediment to the radionuclides. Although matrix diffusion and radionuclide retardation are just as operable in the saturated zone, the ground-water travel time for the present

saturated-zone model is only about 1200 years and the unretarded radionuclides are transported relatively quickly through the saturated zone to the accessible environment.

Figure 3-6 shows the releases to the accessible environment, normalizing the EPA limits as contributed by ^{99}Tc and ^{129}I and the total release for the case $\lambda = 0.1\ m^{-1}$. It may be noted that these nuclides are unretarded through the saturated and unsaturated zones and provide the bulk of the cumulative release over the 10,000-year time period of interest.

It may be recalled that, in the present application of RIP, the important transport parameter, the Poisson transition rate, λ, has been kept constant across all the 1000 realizations generated for deriving the CCDF. The CCDF result presented earlier corresponds to the case of $\lambda = 0.1\ m^{-1}$, which happens to be the closest to the TSPA-1991 analysis. To determine the sensitivity of the results to this parameter, CCDF computations have been repeated for several other values of λ: 10^{-8}, 10^{-3}, 10^{-2}, 10^{-1}, 1, 10 m^{-1}. Figure 3-7 shows the results for two values of λ, 0.01 and 0.1 m^{-1}, which bound the CCDF from the TSPA-1991 analysis. It can be seen that the $\lambda = 0.1\ m^{-1}$ case is closer to the CCDF derived by the TSPA-1991 analysis. Figure 3-8 presents CCDFs for the EPA sum for all the λ values cited above and the CCDF for the TSPA-1991 analysis. The releases increase with decreasing λ, as expected and in agreement with the definition of λ. It may be recalled that λ is a measure of the interaction between the matrix and the fracture, with smaller λs denoting less interaction. Thus, smaller λs generate more fracture transport leading to higher releases. It is interesting to note that, for all λ less than $10^{-3}\ m^{-1}$, the CCDFs are insensitive to the λ chosen.

Although the above results indicate that it is possible to reproduce the TSPA-1991 results with a properly chosen matrix-fracture transition rate (λ) in RIP, there is little physical basis for how one should choose an appropriate value of λ. In order to test the importance of λ in comparison to the simulated numerical results generated with TOSPAC, we conducted a number of single column "tests." These results (presented in Appendix C) indicate that using the two-mode approximation of fracture-matrix flow and transport in RIP overpredicts the mass breakthrough in comparison to TOSPAC (or TRACR3D). While fracture-matrix flow is important in layers 1, 2, and 4, layers 3 and 5 are predominantly matrix flow for virtually all realizations. As a result, we conducted additional "tests" treating these matrix-dominated flow layers as one-mode flow and transport media in RIP. This produced much better breakthrough curves (in comparison to the dispersion-dominated breakthrough predicted in the numerical models; see Appendix C). In order to test the significance of this on the CCDF, we conducted a simulation with layers 3 and 5 treated as equivalent porous media for all six unsaturated zone columns. (Note: layer 5 does not exist in columns 5 and 6.) The results of this simulation are presented in Figure 3-9. These results match the TSPA-1991 results very well.

While it is possible to compare CCDFs to determine qualitatively how well RIP is able to reproduce the results presented in TSPA-1991 (Barnard et al., 1992), it is also useful to compare other measures of performance. Figures 3-10a through 3-10e display time history plots of radionuclide releases to the accessible environment for ^{99}Tc, ^{120}I, ^{237}Np, ^{234}U, and ^{79}Se, respectively. For the case $\lambda = 0.1\ m^{-1}$, these plots can be compared with Figure 4-45 of Barnard et al. (1992), reproduced here as Figure 3-11. While our plots are linear-linear rather than the log-log plots presented in TSPA-1991, it is apparent that, in general, the RIP peaks occur a little

earlier than those in TSPA-1991, and are either slightly higher or slightly lower than the maximum release rate determined in TSPA-1991.

3.5.2 Sensitivity Studies

The RIP model has been used to perform sensitivity studies. For this purpose, all the parameters are kept at their expected values, except for the parameter whose sensitivity is studied. For that parameter, the stochastic description using its probability density function is retained. Two hundred realizations of the sensitivity parameter are generated and simulated. Since only one parameter varies across the realizations, a scatter-plot of the 10,000-year EPA sum and the chosen parameter provides an understanding of the sensitivity.

The chosen parameters of sensitivity are:

- Infiltration rate
- Matrix hydraulic conductivity in layer 3
- Poisson transition rate (λ).

Figure 3-12 shows the scatter plot of infiltration flux versus cumulative release. The EPA sum is directly related to the infiltration rate. The EPA sum would increase continuously with infiltration. For comparison, Figure 3-13 illustrates the sensitivity of cumulative release to the infiltration flux when all parameters are sampled. There is clearly a very high correlation between infiltration and release in both cases.

Figure 3.14 shows the sensitivity of the release to the matrix hydraulic conductivity in layer 3. If the matrix hydraulic conductivity is greater than the infiltration rate, no flow occurs in the fractures. Since the expected infiltration rate is 1 mm/year, matrix hydraulic conductivities equal to or greater than 1 mm/year cause the fractures to be dry. In these cases, the total release depends on the travel time through the matrix and does not change for values of hydraulic conductivity greater than 1 mm/year (all other parameters constant). This aspect becomes evident in the scatter plot, shown in Figure 3-14. Furthermore, when the matrix conductivity is lower than 1 mm/year, the infiltration goes partly through fractures, and thus greater releases are seen at the accessible environment. A greater proportion of the infiltrating water goes into fractures as the matrix conductivity is reduced progressively below 1 mm/year, resulting in larger releases at the accessible environment.

Figure 3-15 presents the scatter plot of the EPA sum versus the Poisson transition rate. The range of λ is from 0.01 to 0.1, the limits between which the CCDF of the TSPA-1991 analysis remains bounded. As expected, the EPA sum decreases for increasing λ. If λ was chosen over a wider range, it would have shown that, for values of λ smaller than a particular value, λ_{min}, the EPA sum would remain constant. Similarly, when λ is increased beyond a particular value λ_{max}, the nuclide releases would reach a small value and would then remain invariant with a further increase in λ.

3.5.3 Additional Sensitivity to Infiltration Flux

The net flux at the potential repository is one of many uncertain parameters. A range of values has been developed, generally with 1 mm/yr as the expected value. Additional simulations were conducted to determine the effect of using different infiltration distributions. The four distributions used in these additional simulations are listed in Table 3.11.

The infiltration distributions are presented graphically in Figures 3-16a to 3-16e. Figure 3-16d shows the distribution when sampled 1000 times, rather than the theoretical results. These distributions were applied to the case $\lambda = 0.1\ m^{-1}$.

When evaluated at the edge of the waste package domain, the different infiltration distributions had no discernible effect on release. This reflects the fact that the high solubility, alteration-limited radionuclides, ^{99}Tc and ^{129}I, control the release from the EBS. However, at the accessible environment, the differences are quite pronounced. The results for the four simulations using different infiltration distributions are presented in Figures 3-17a to 3-17d. Note that the results for the beta distribution (RUN 3.1) are presented in Figure 3-5.

When compared with the CCDF for the release (Figure 3-5) corresponding to the beta distribution for infiltration (RUN 3.1), run 3.2 produces greater release; RUN 3.3 produces even greater release; RUN 3.4 produces greater release than RUN 3.1 but less than RUN 3.2; and RUN 3.5 produces the greatest release. These differences can be explained by reviewing the infiltration distributions. The uniform infiltration distribution has a higher probability for exceeding higher infiltration values than does the log-uniform distribution. The log normal infiltration distribution has a greater probability for low infiltration values and a lower probability for high infiltration values than the beta distribution and the log-uniform distribution. The distribution for RUN 3.5 is higher than the other distributions, with 64 percent probability that the values will be greater than or equal to 5.0 mm/yr. The sensitivity to the infiltration flux distribution shape and range is as expected, given the high correlation between flux and release exhibited in the sensitivity analyses (Figures 3-12 and 3-13).

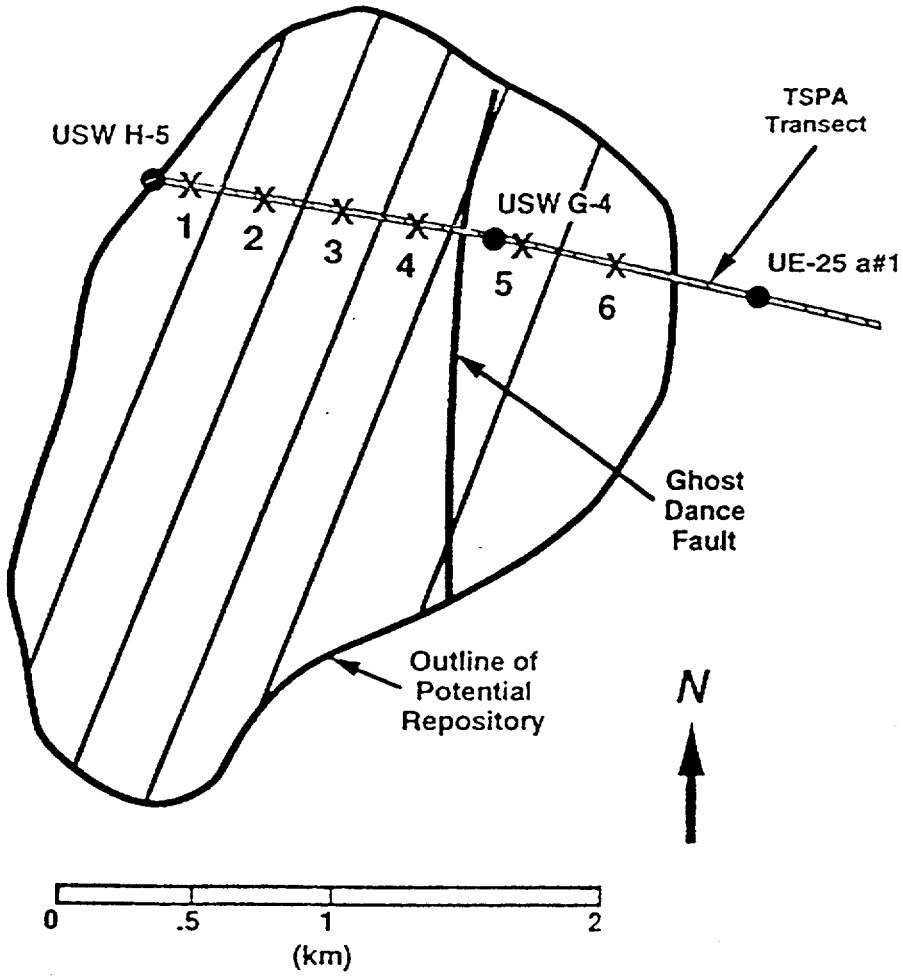

Figure 3-1. Map of the Boundary of Potential Repository at Yucca Mountain (taken from Barnard et al., 1992)

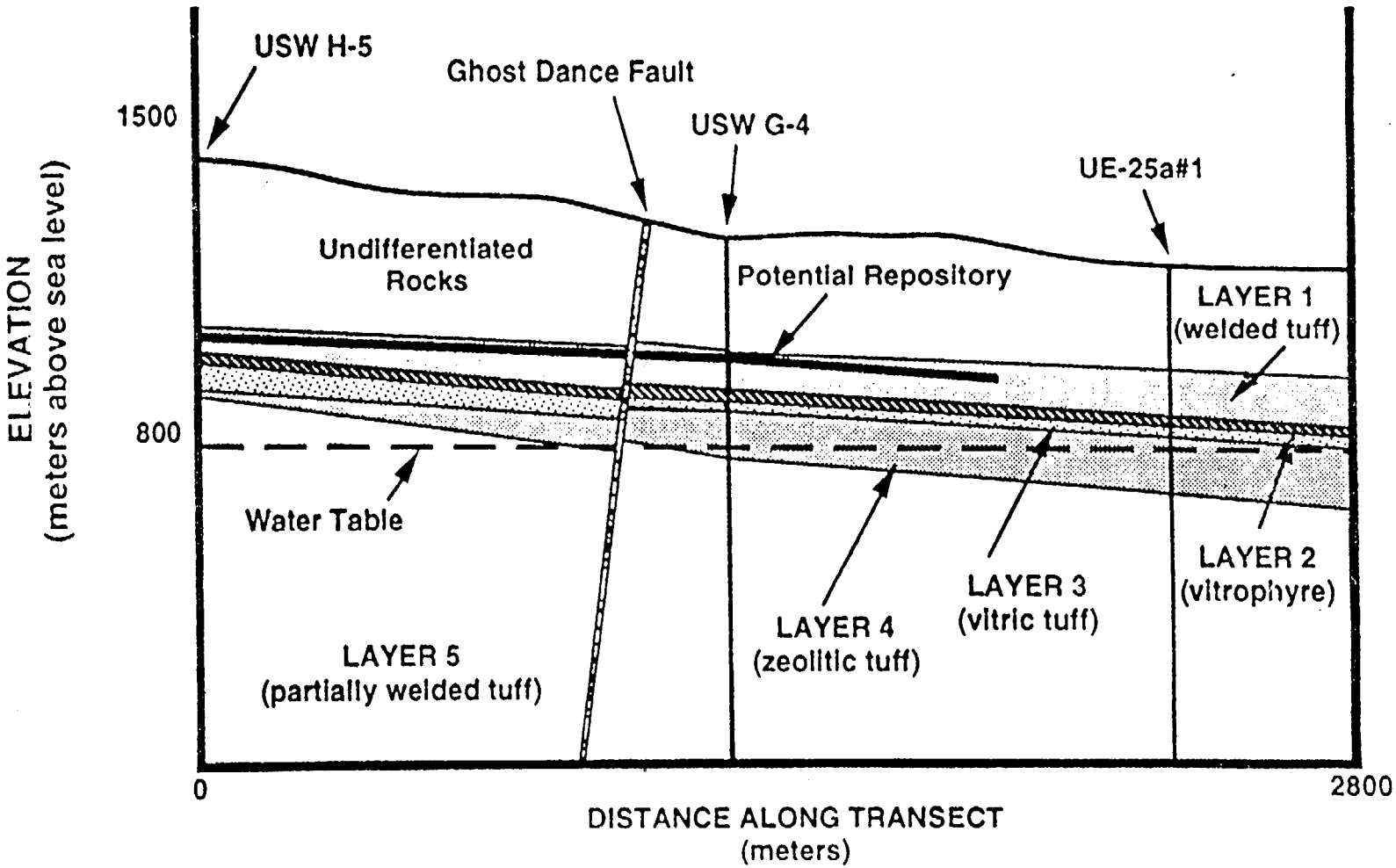

Figure 3-2. Schematic Cross-Section of Unsaturated-Zone Stratigraphy (taken from Barnard et al., 1992)

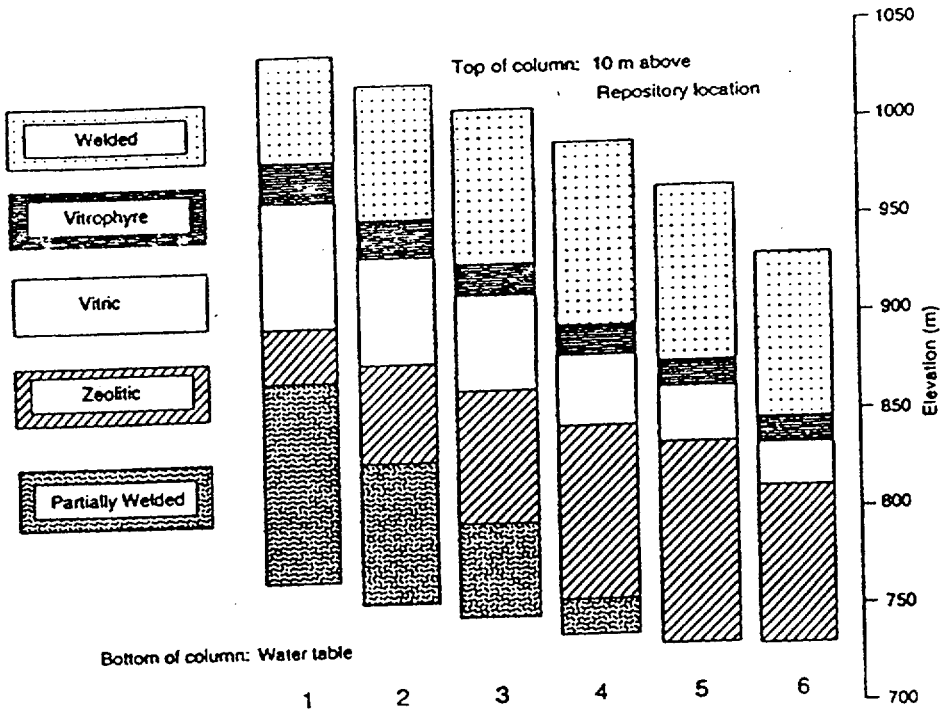

Figure 3-3. Stratigraphies of the Six Vertical Columns Used for the Simulation of Unsaturated Flow (taken from Barnard et al., 1992)

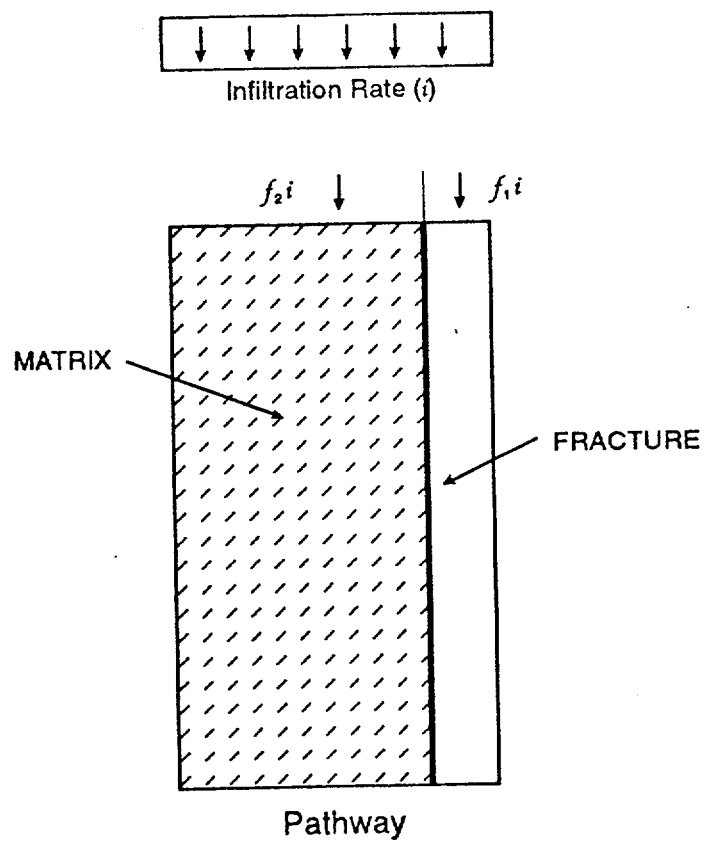

$$f_1 = \text{Max}\left(0, \frac{i - K_m}{i}\right)$$

$$f_2 = 1 - f_1$$

K_m = Saturated Hydraulic Conductivity of Matrix

Figure 3-4. Apportionment of a Flow Rate to Matrix and Fractures: A Conceptualization

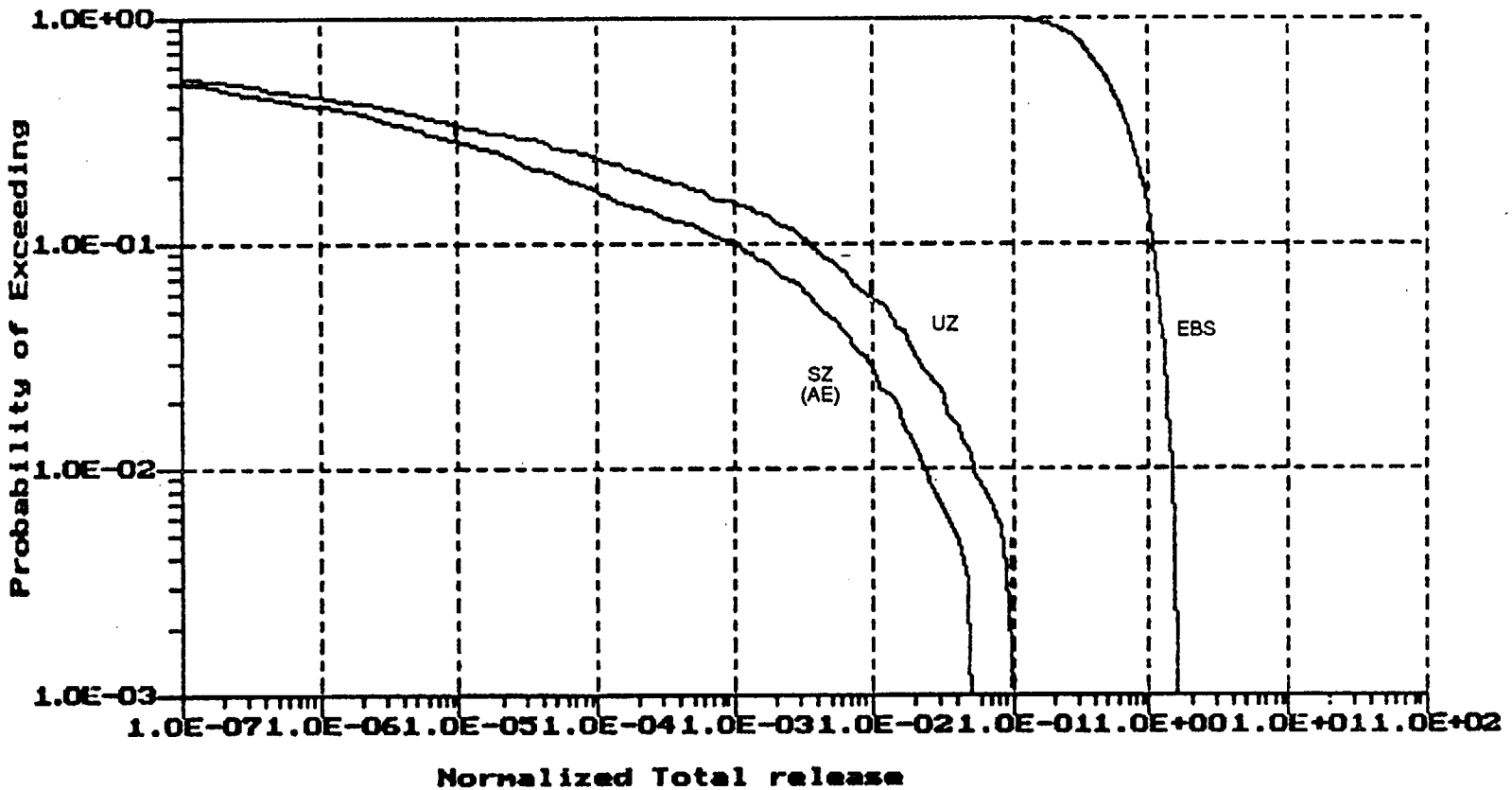

Figure 3-5. CCDFs for Nuclide Releases (EPA Sum) for the Case $\lambda = 0.1m^{-1}$

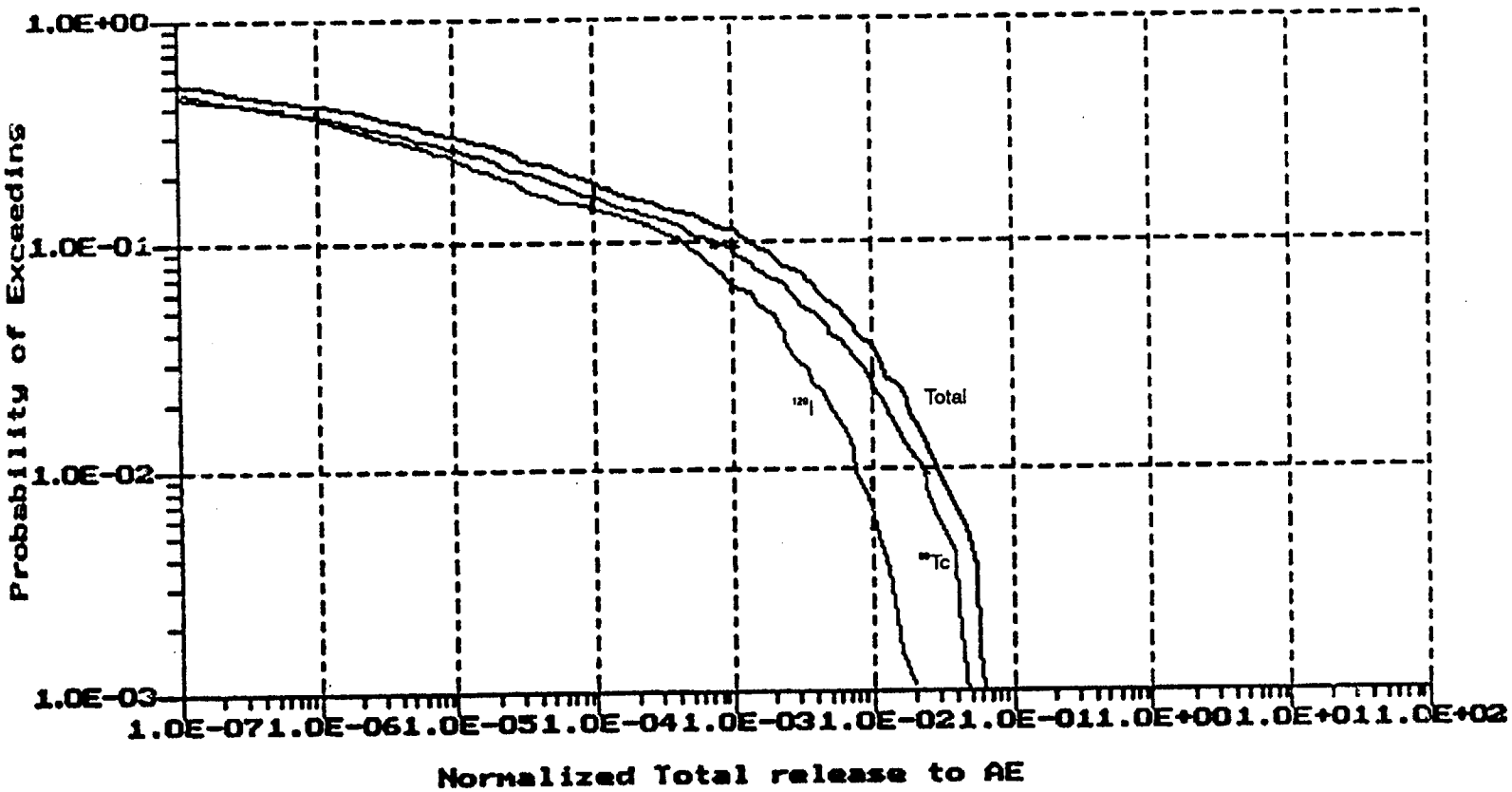

Figure 3-6. CCDFs for EPA Sum and Ratios for ^{99}Tc and ^{129}I for the Case $\lambda = 0.1\ m^{-1}$

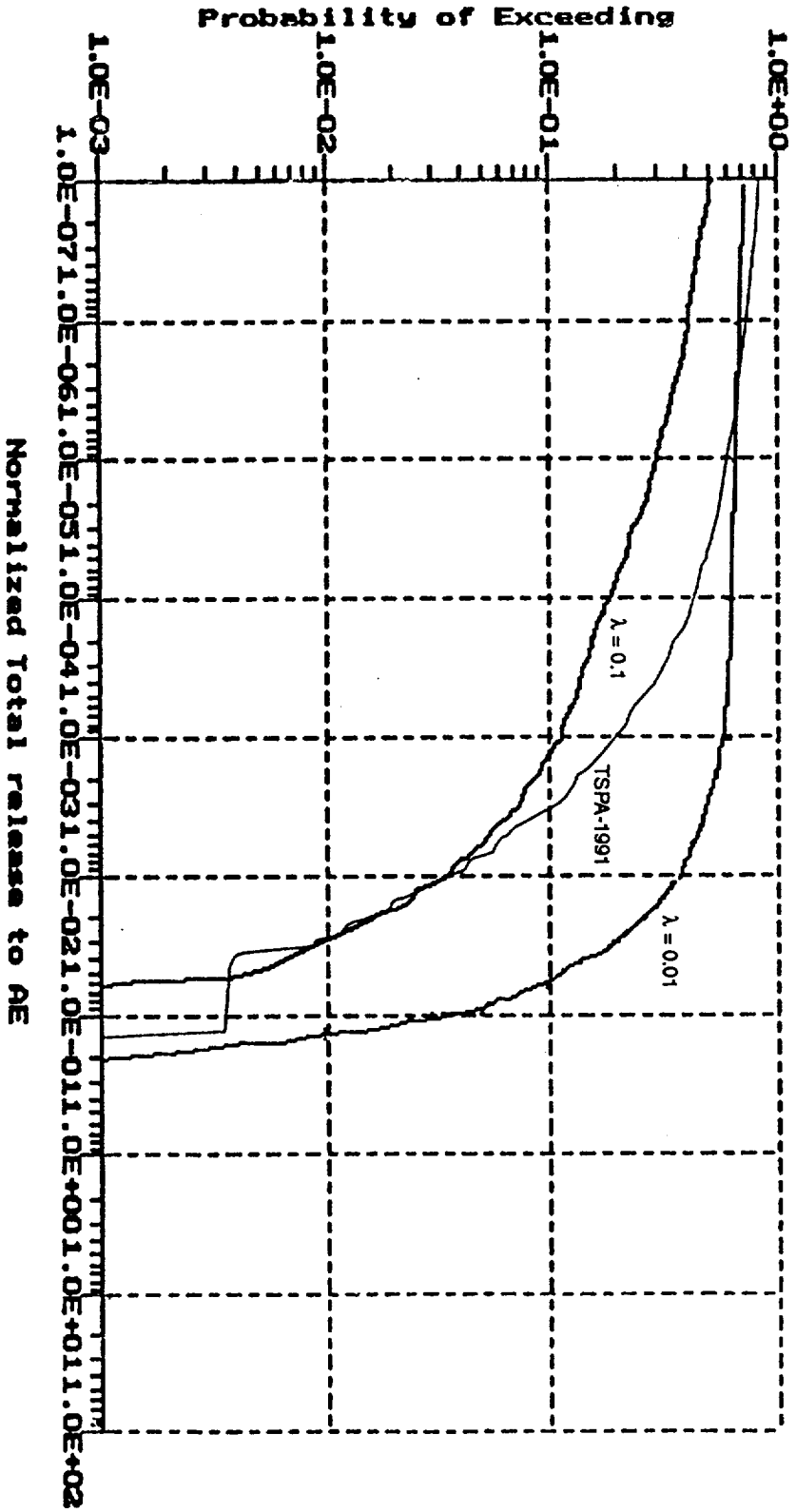

Figure 3-7. CCDFs for EPA Sum for λ = 0.1, 0.01 m^{-1}, and from TSPA-1991

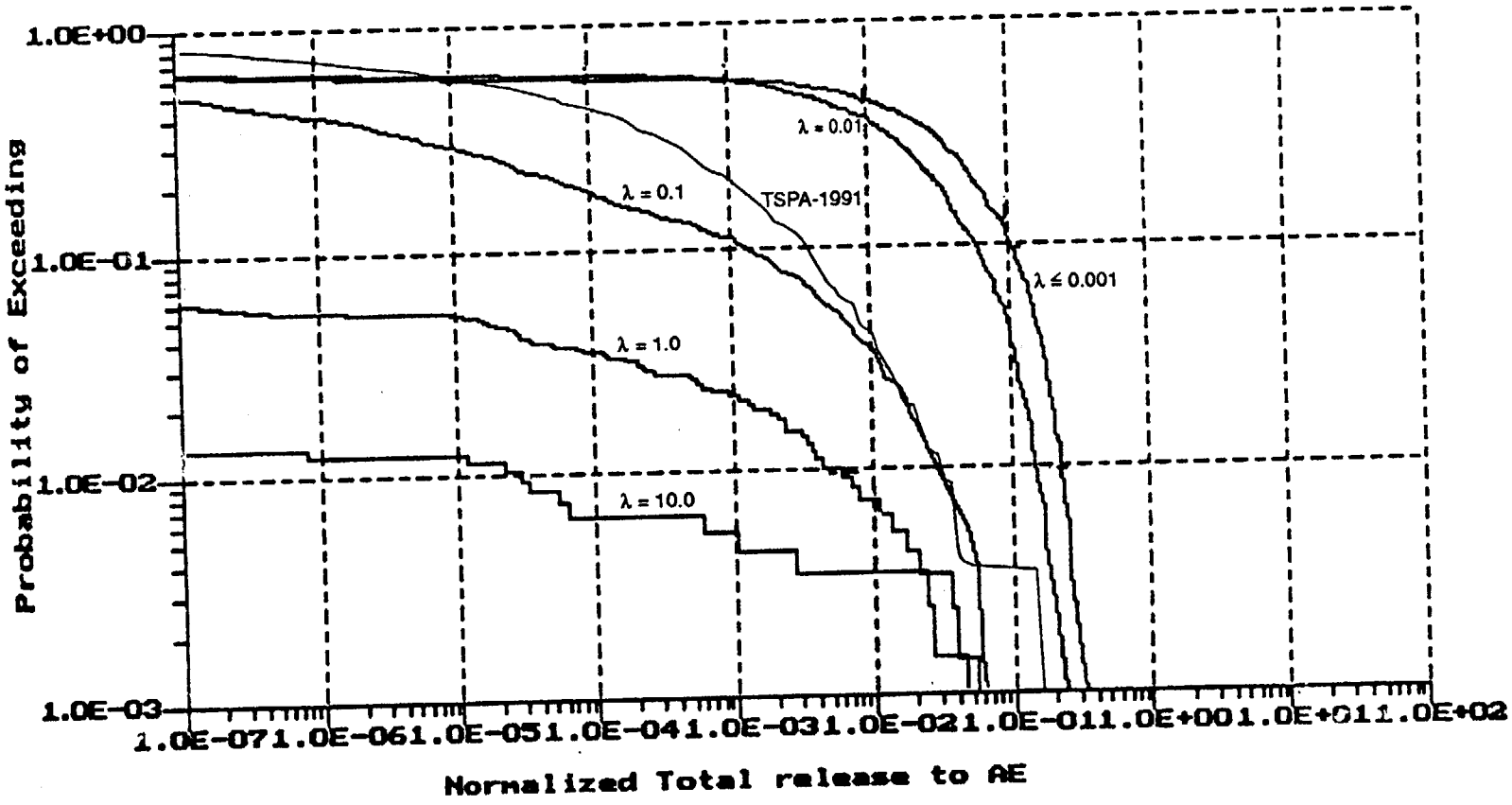

Figure 3-8. Sensitivity of CCDFs for EPA Sum to Poisson Transition Rate

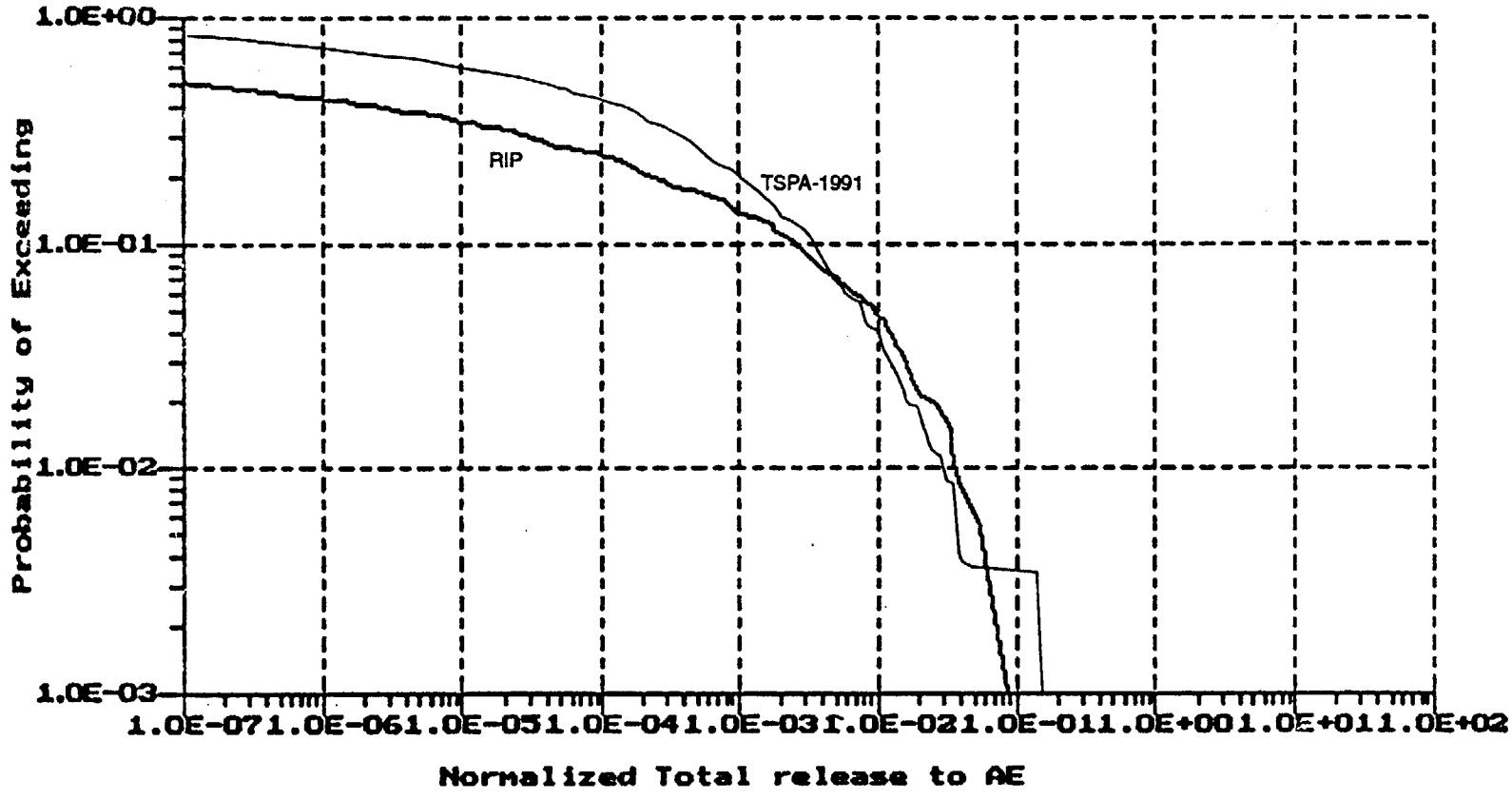

Figure 3-9. CCDFs for the EPA Sum: Layers 3 and 5 Treated as Single Mode Media in RIP (λ = 0.1 m^{-1} for other layers)

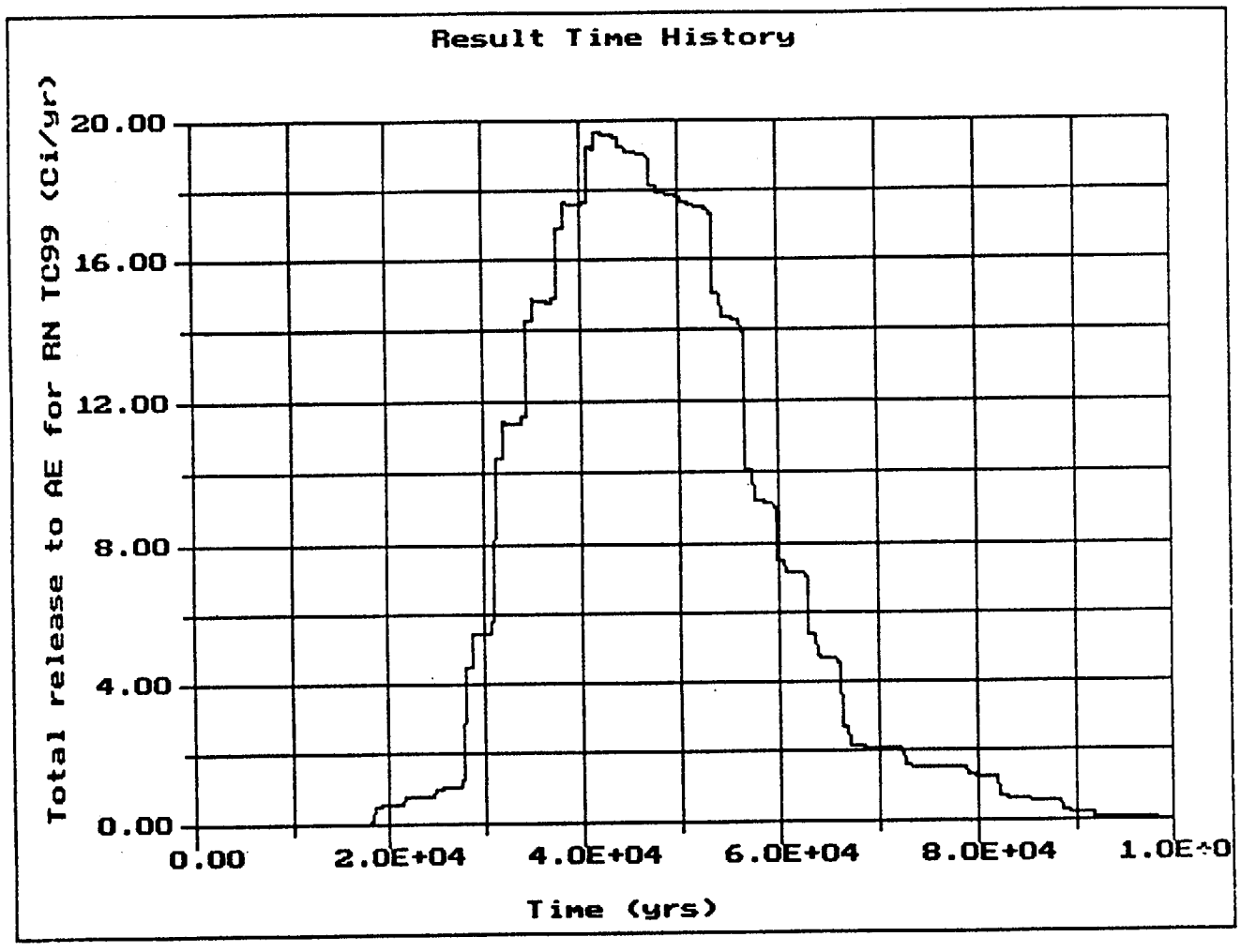

Figure 3-10a. Time History of Release Rate to Accessible Environment for ^{99}Tc

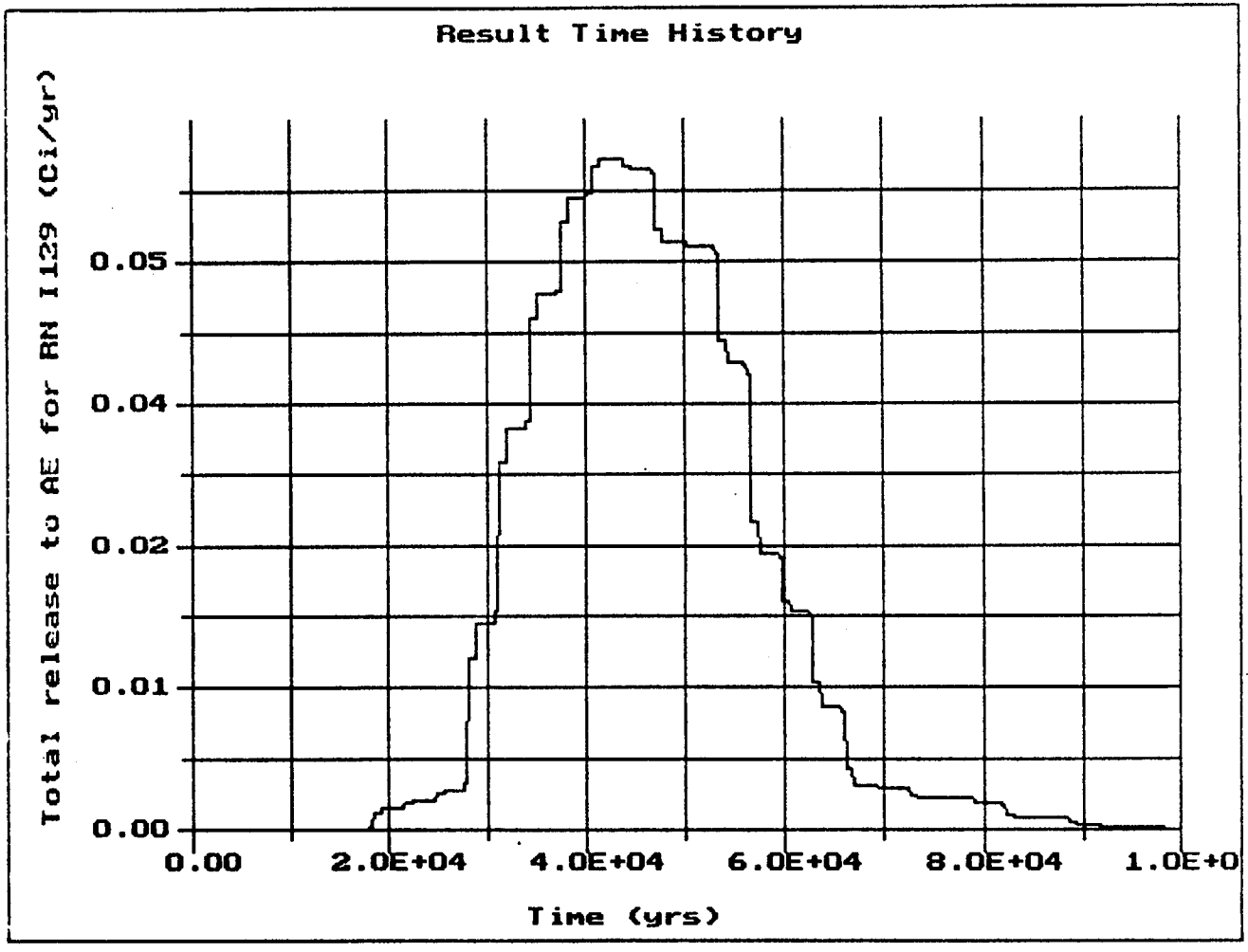

Figure 3-10b. Time History of Release Rate to Accessible Environment for ^{129}I

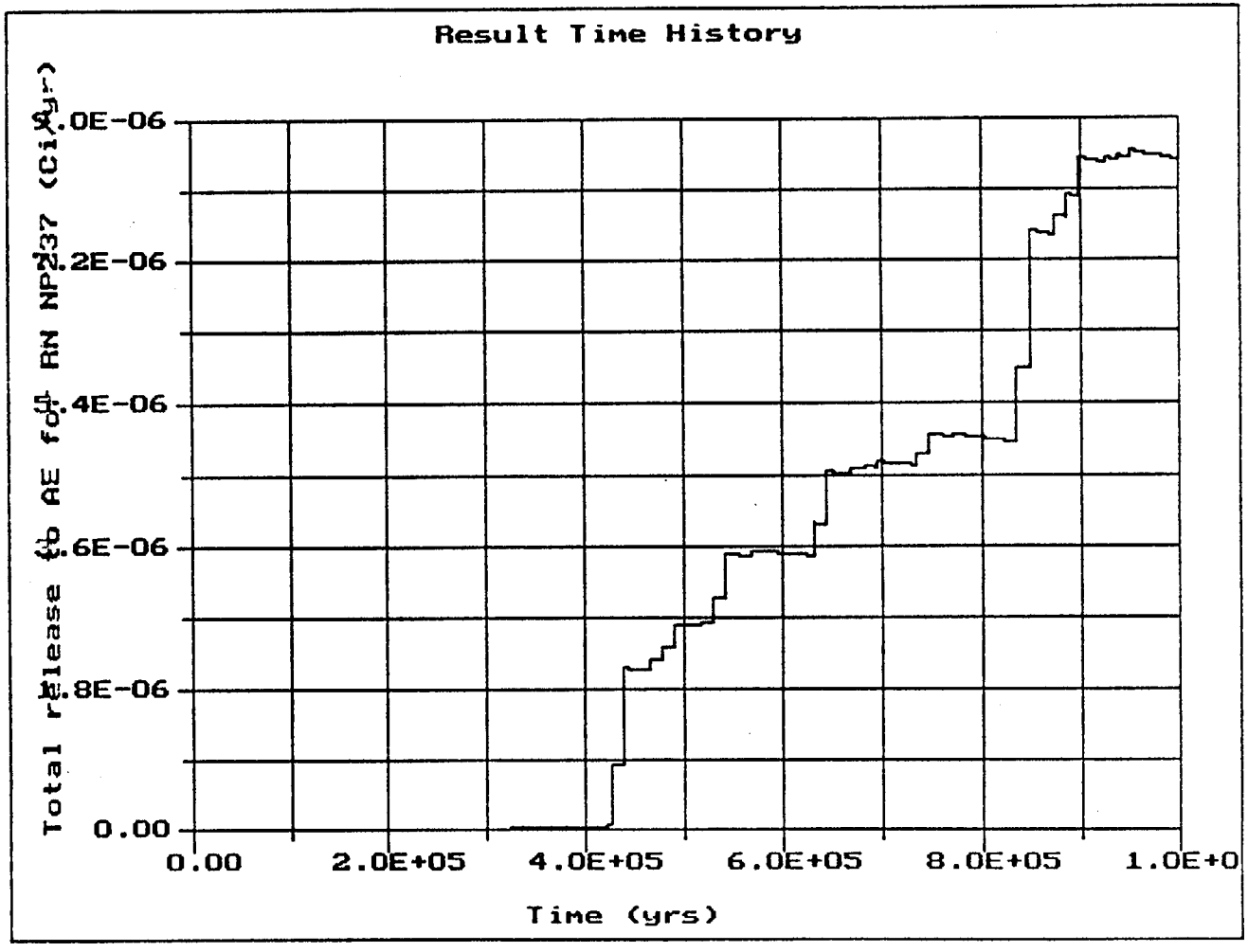

Figure 3-10c. Time History of Release Rate to Accessible Environment for ^{237}Np

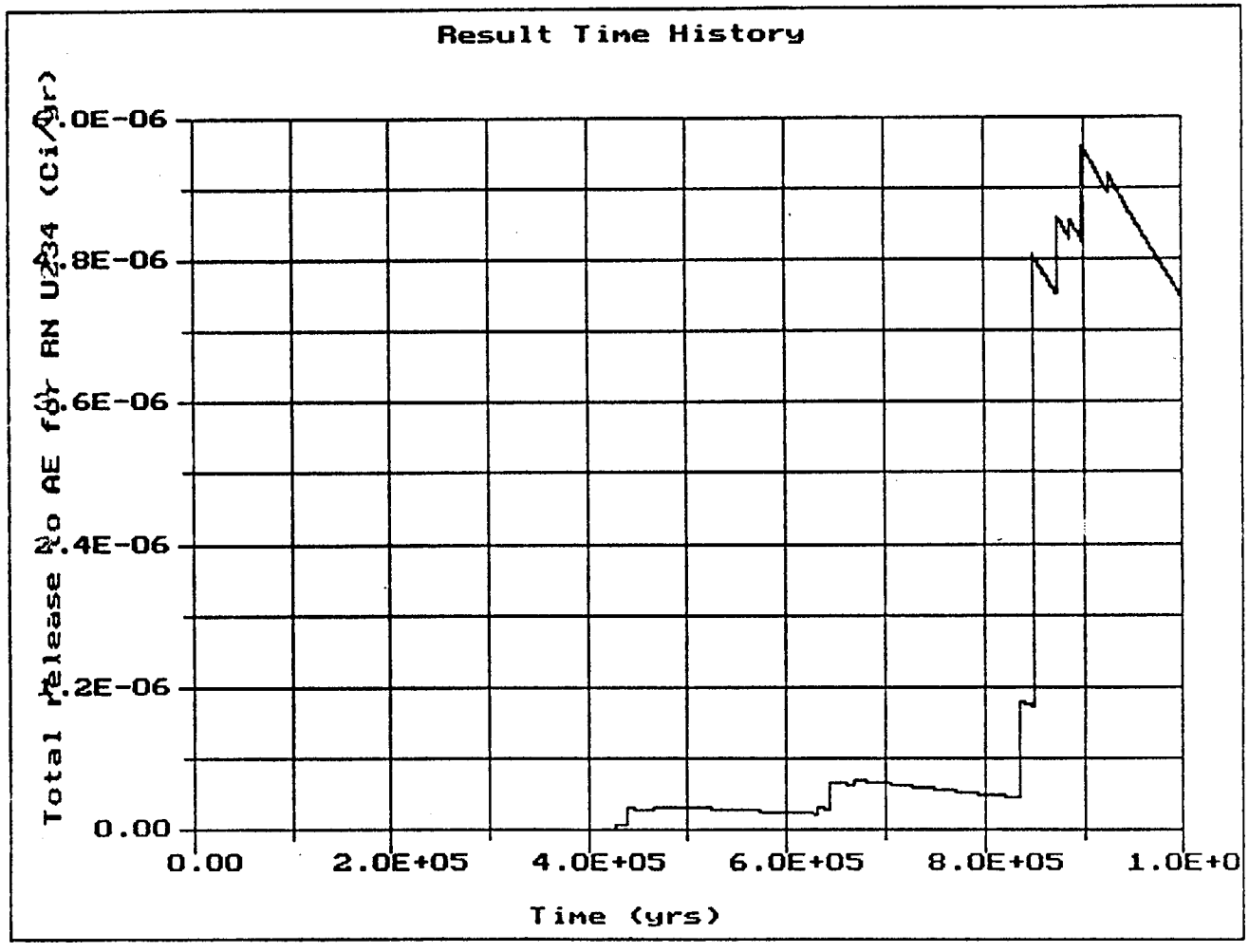

Figure 3-10d. Time History of Release Rate to Accessible Environment for ^{234}U

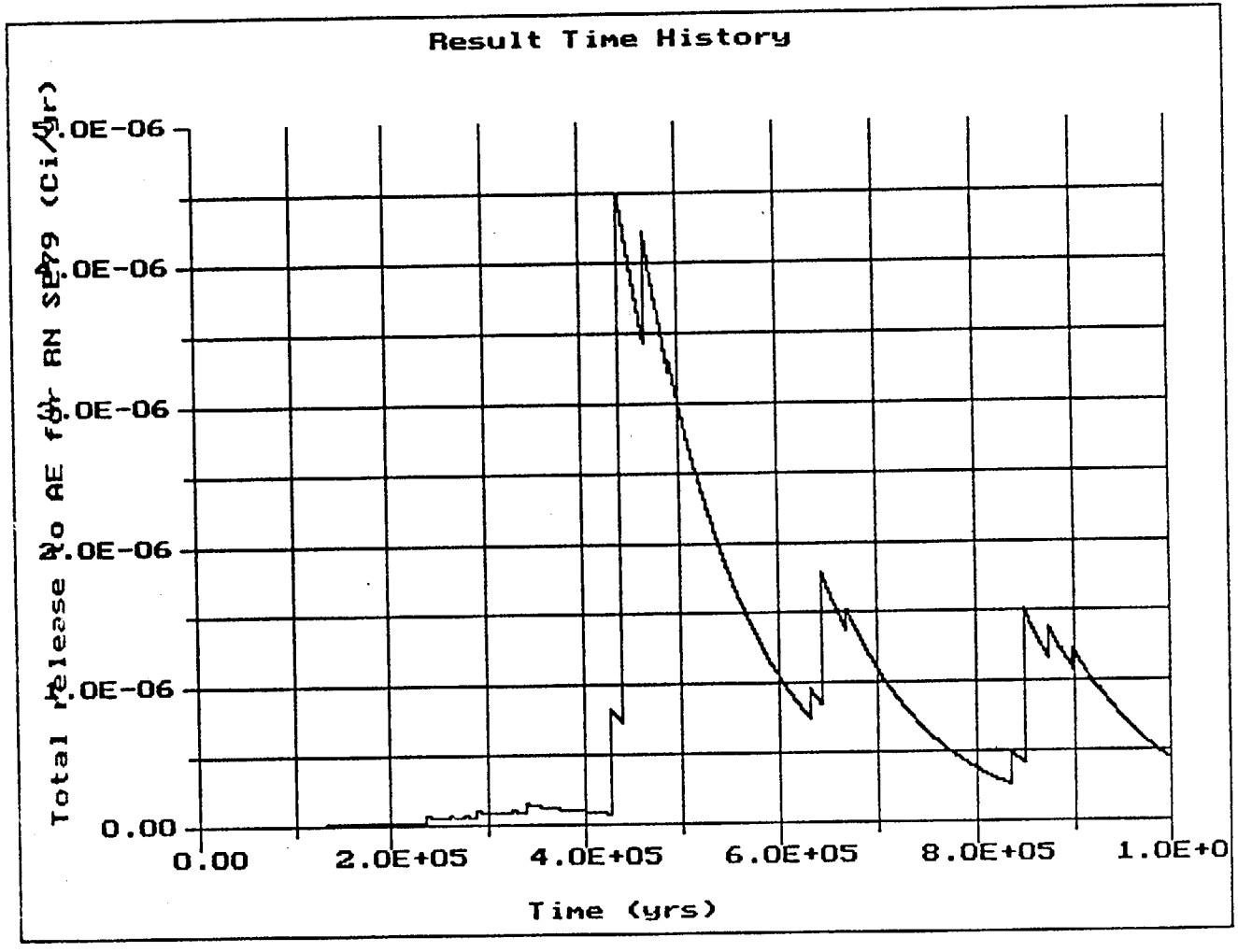

Figure 3-10e. Time History of Release Rate to Accessible Environment for ^{79}Se

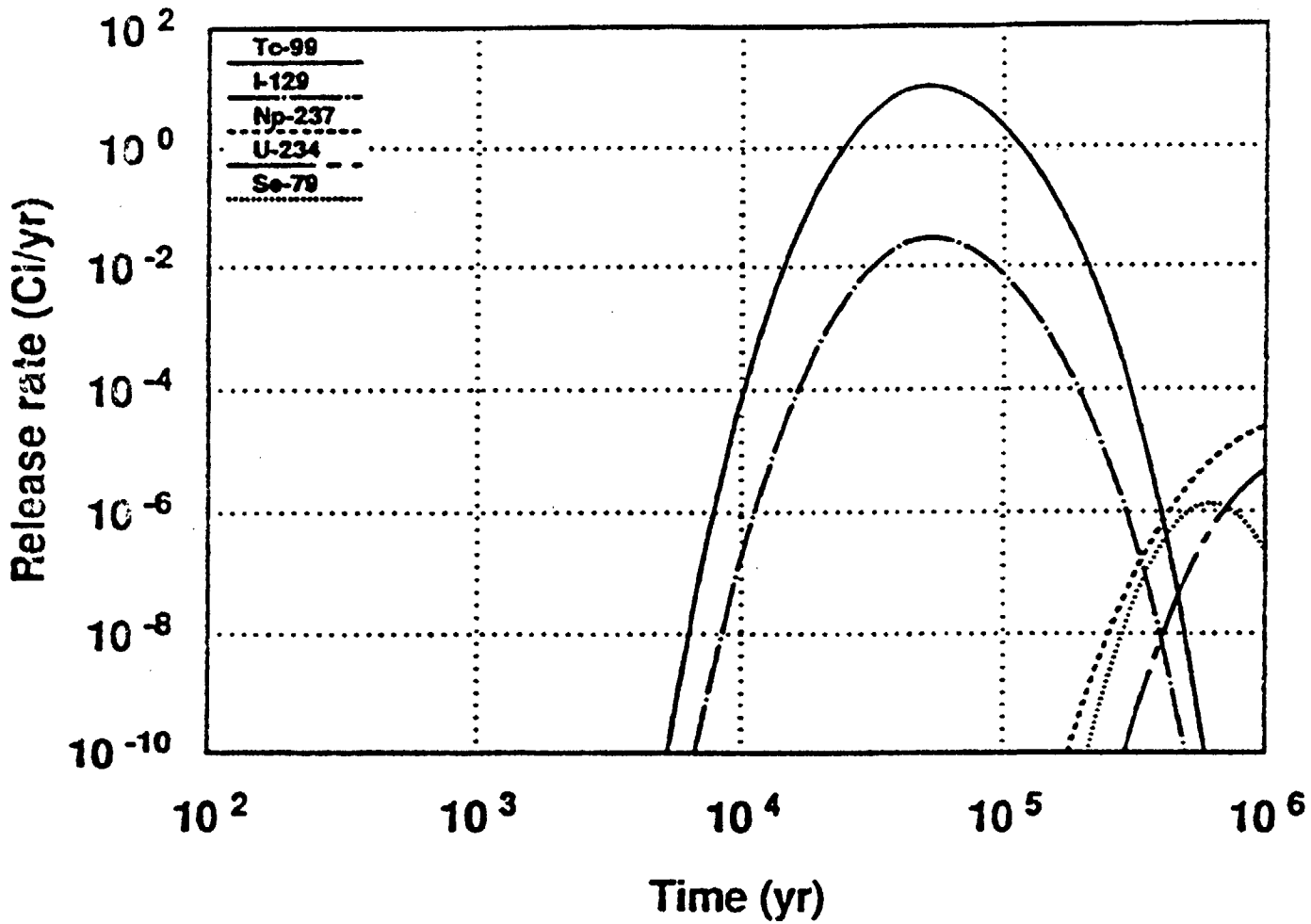

Figure 3-11. Release Rates to Accessible Environment for Radionuclides Released Using Composite Porosity Flow Model (taken from Barnard et al., 1992)

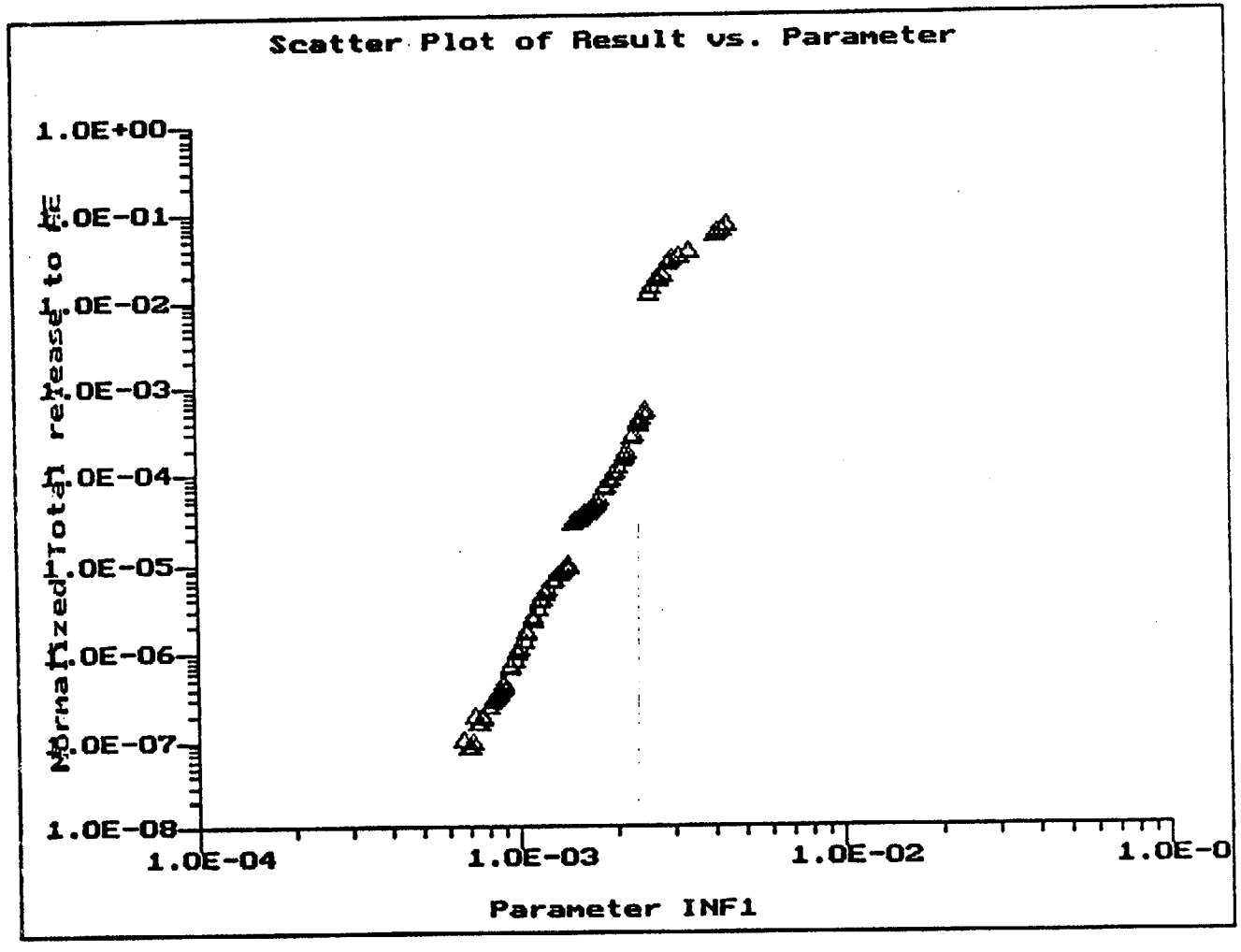

Figure 3-12. Scatter Plot of EPA Sum versus Infiltration Rate (all other parameters at mean value)

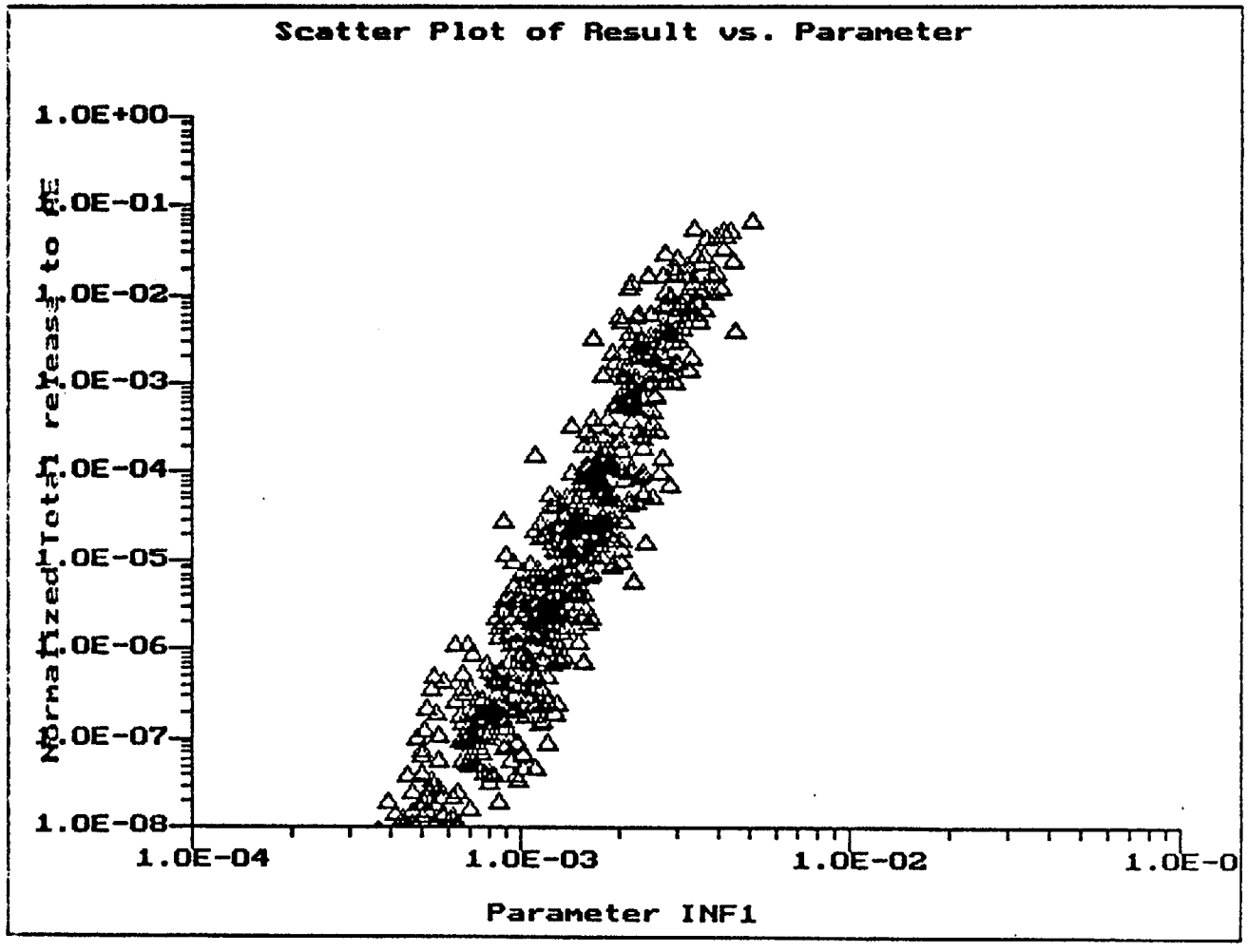

Figure 3-13. Scatter Plot of EPA Sum versus Infiltration Rate (all parameters are sampled)

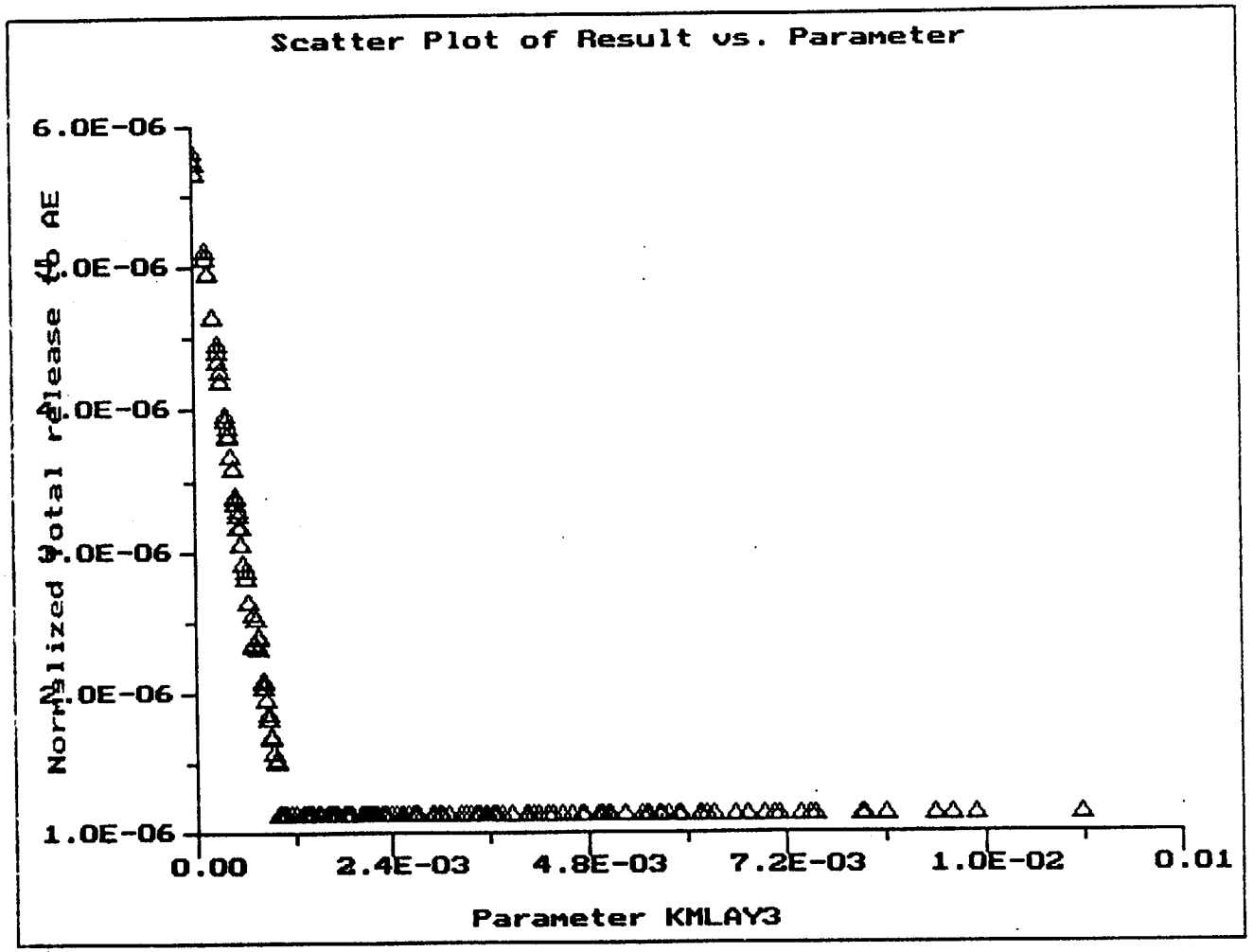

Figure 3-14. Scatter Plot of EPA Sum versus Matrix Hydraulic Conductivity of Layer 3

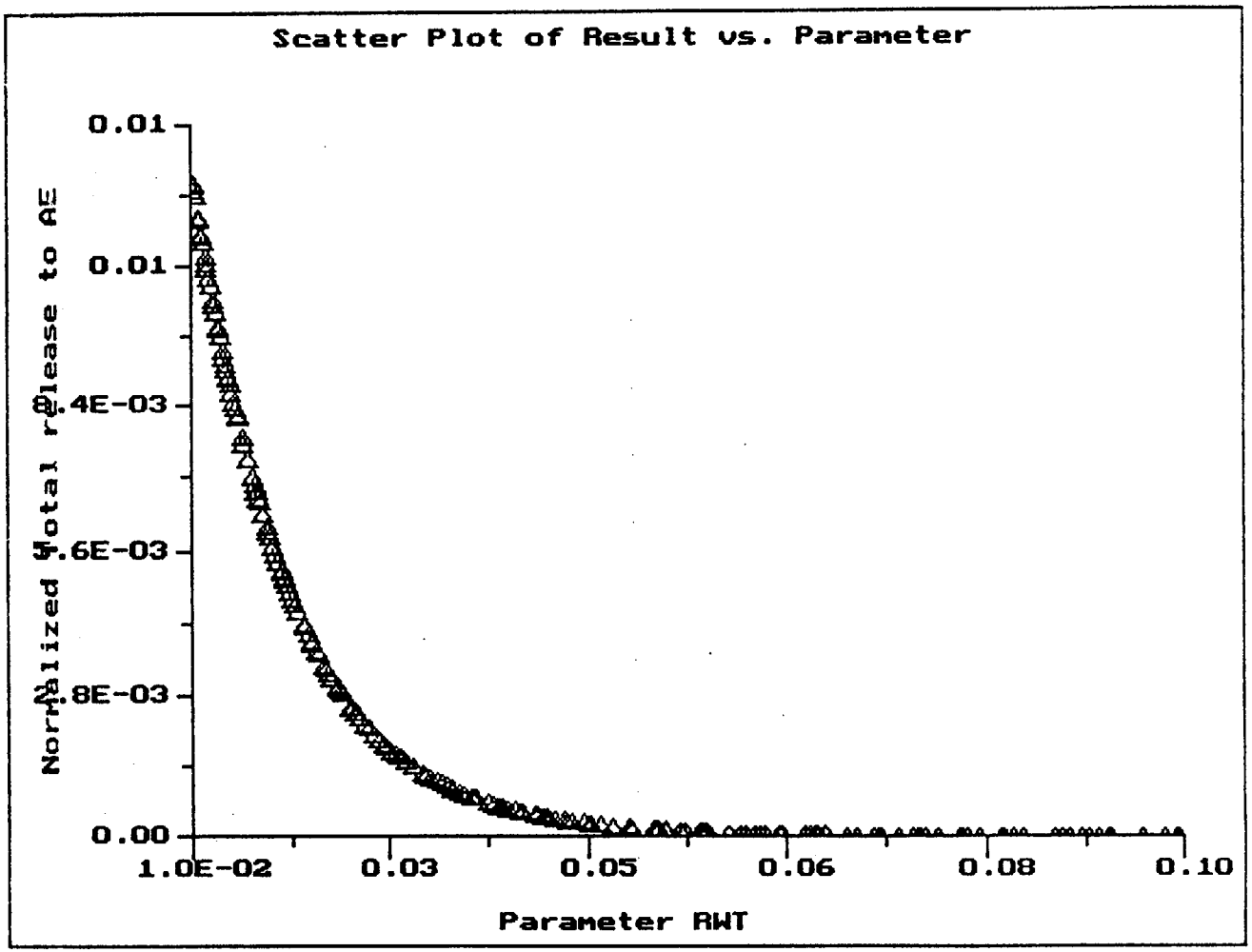

Figure 3-15. Scatter Plot of EPA Sum versus Poisson Transition Rate

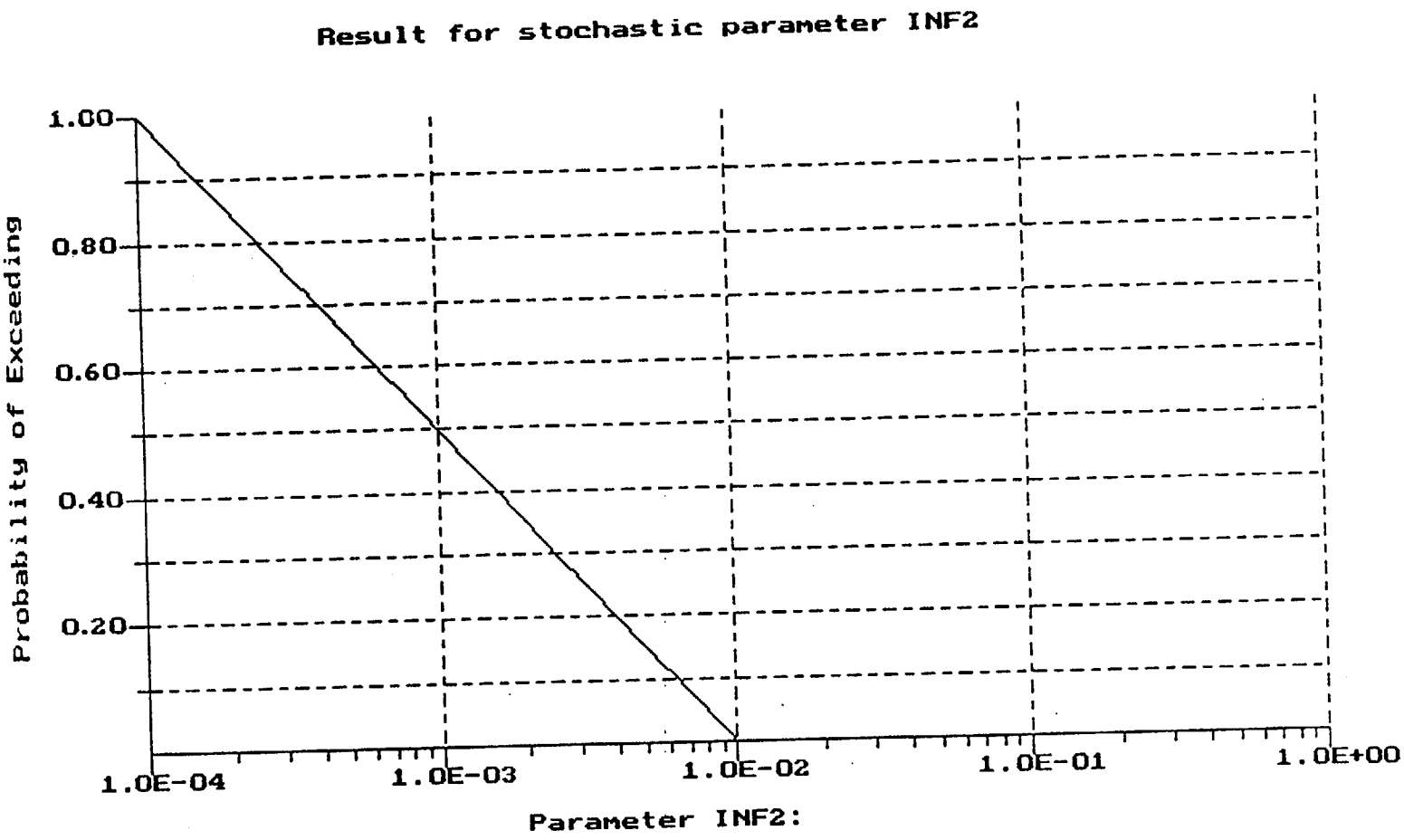

Log-Uniform Distribution

Min= 1.000E-04

Max= 1.000E-02

Figure 3-16a. CCDF for Infiltration — Run 3.2

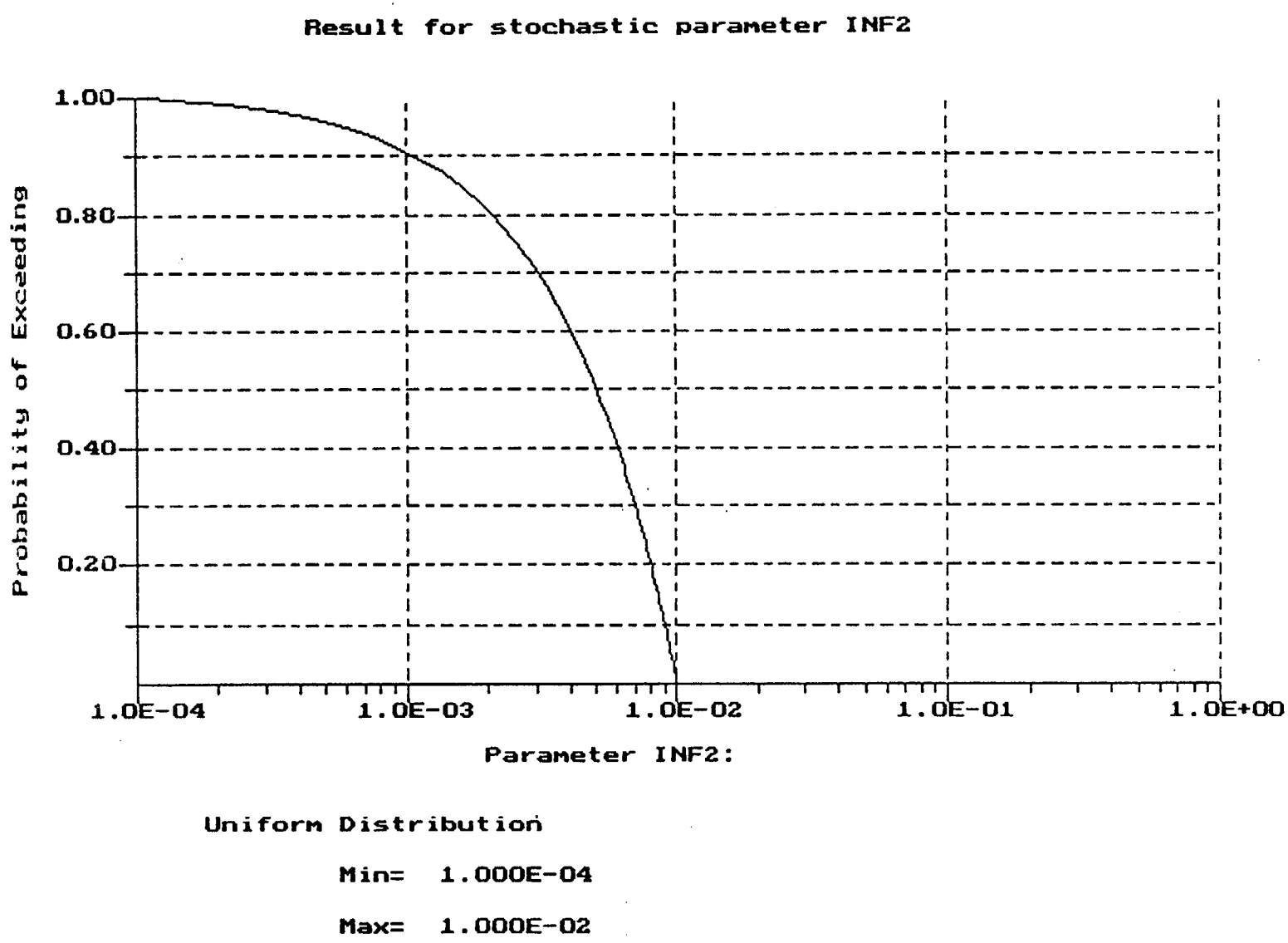

Figure 3-16b. CCDF for Infiltration — Run 3.3

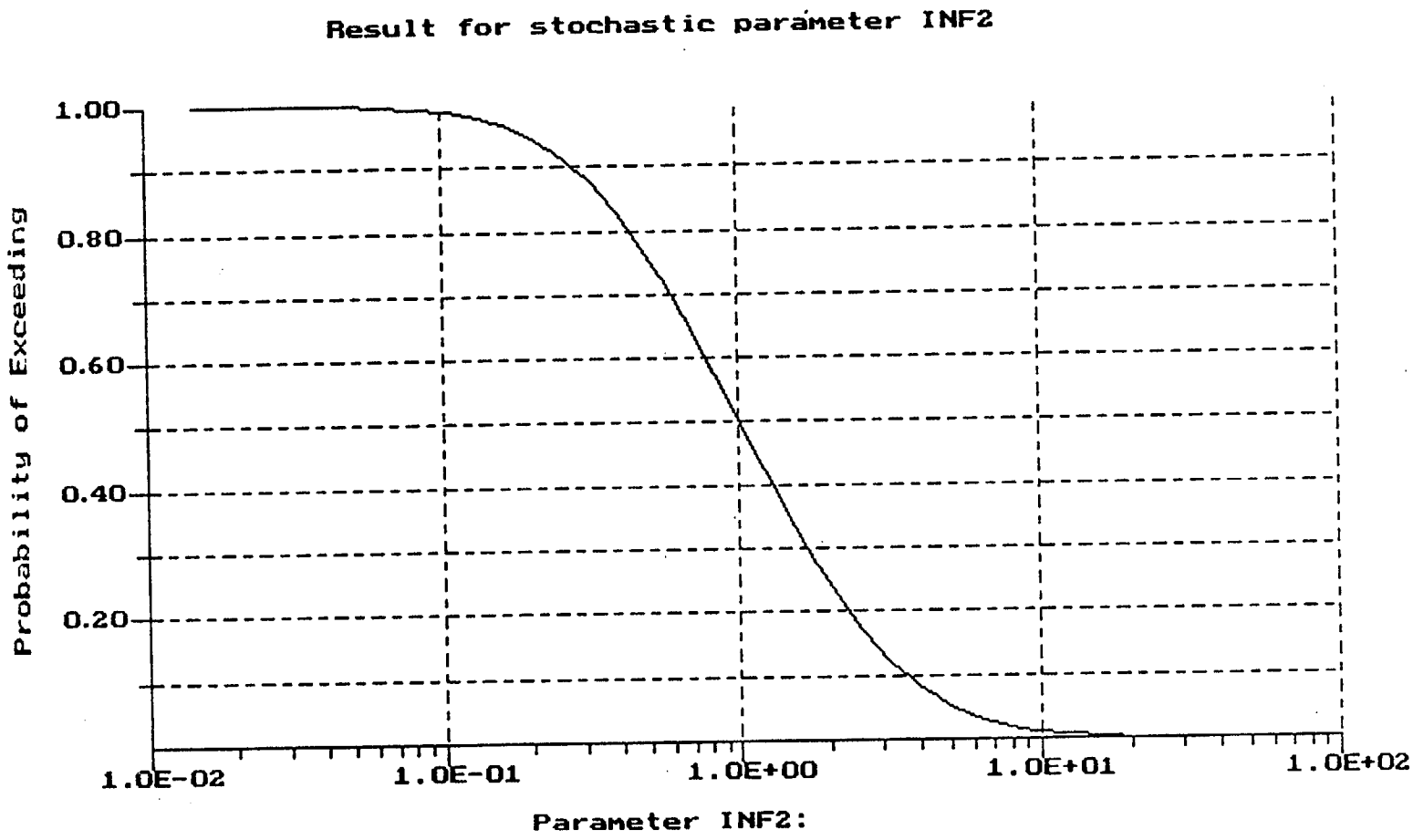

Log-Normal Distribution

Mean= 1.000E+00

S.D.= 4.300E-01

Figure 3-16c. CCDF for Infiltration — Run 3.4

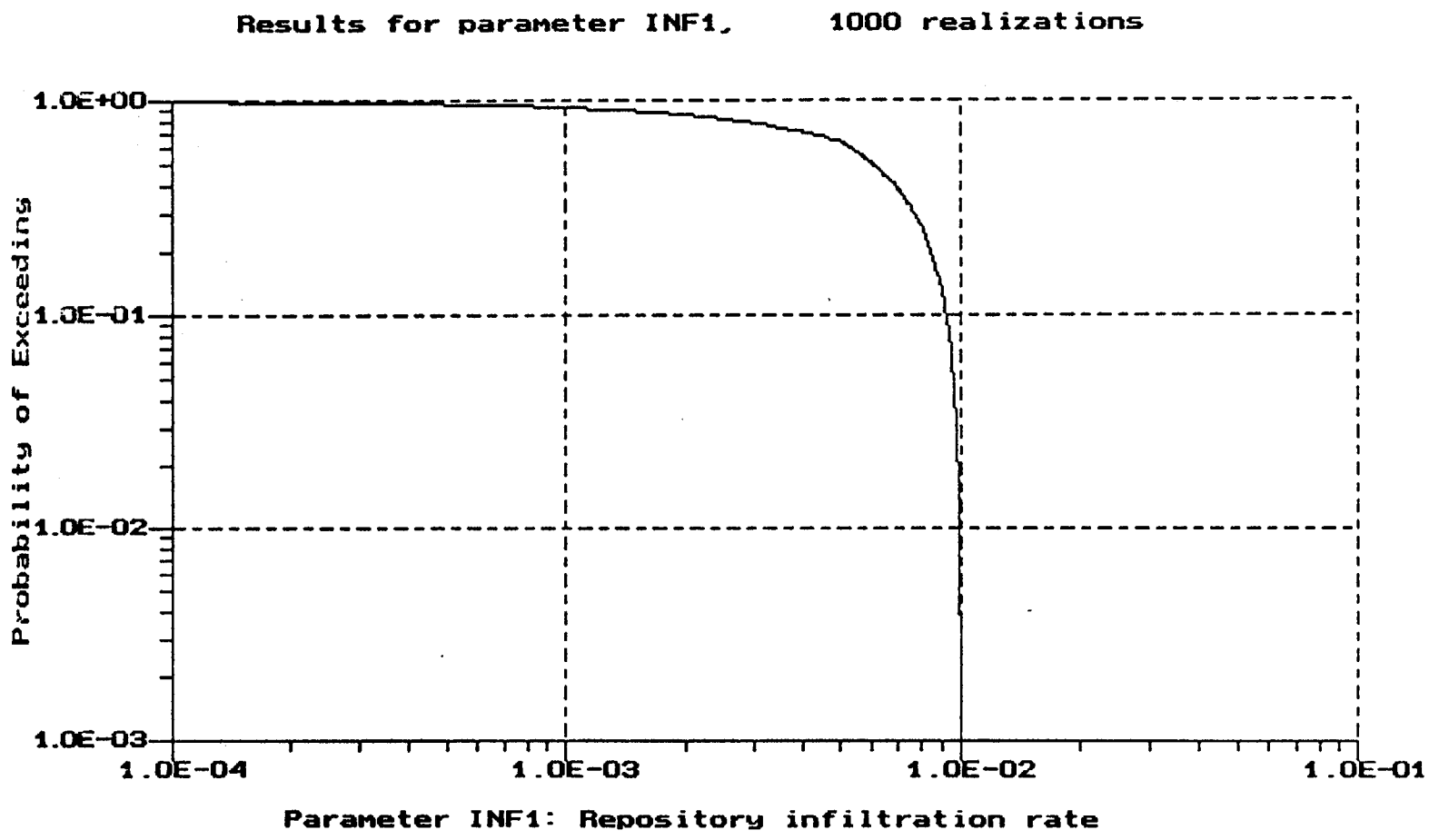

Distribution of Results

Mean= 5.701E-03

S.D.= 2.803E-03

Kurtosis= 2.021E+00

Skewness= -3.669E-01

Figure 3-16d. CCDF for Infiltration — Run 3.5

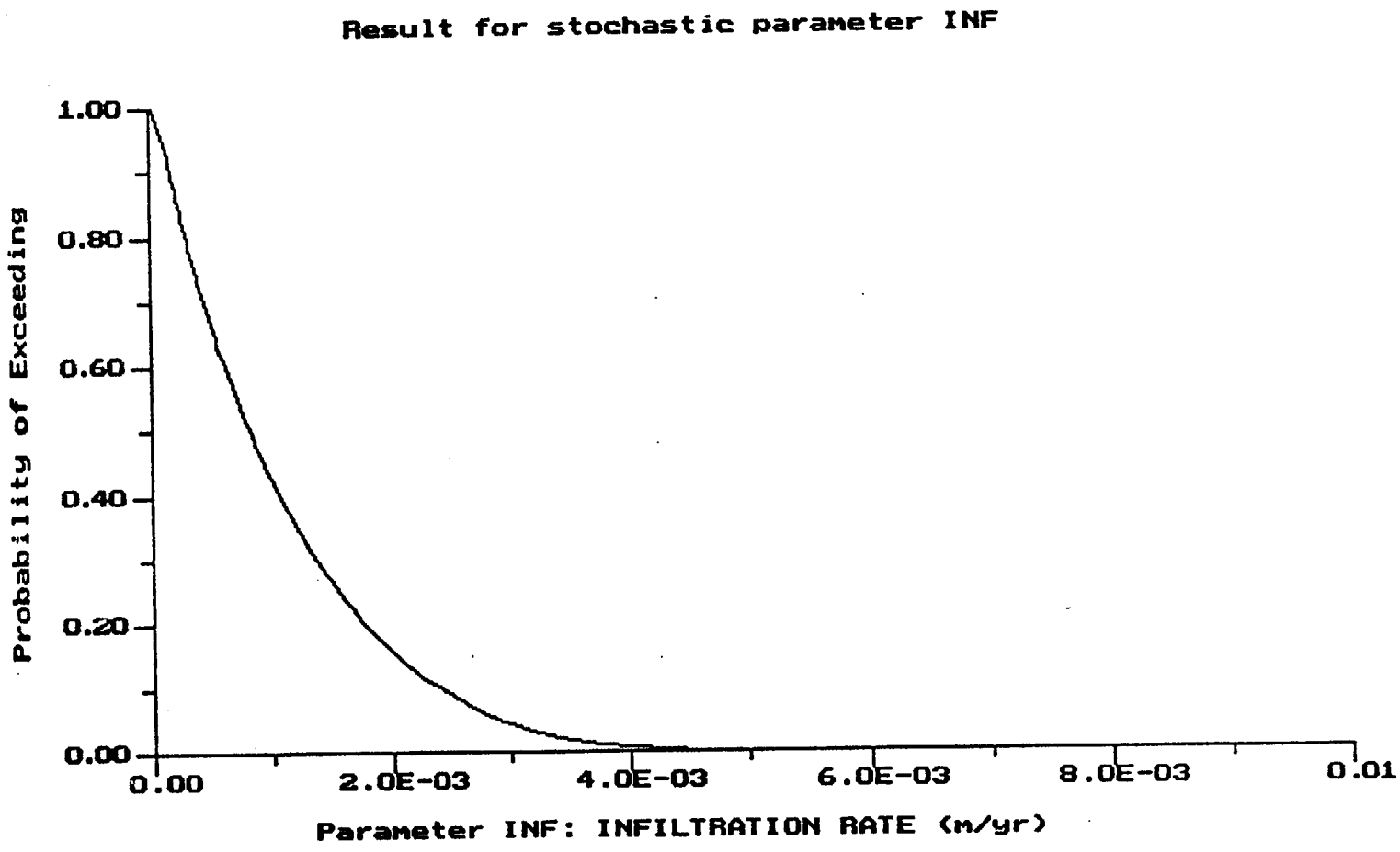

Beta Distribution

Mean= 1.000E-03

S.D.= 9.000E-04

Figure 16e. CCDF for Infiltration — Run 3.1

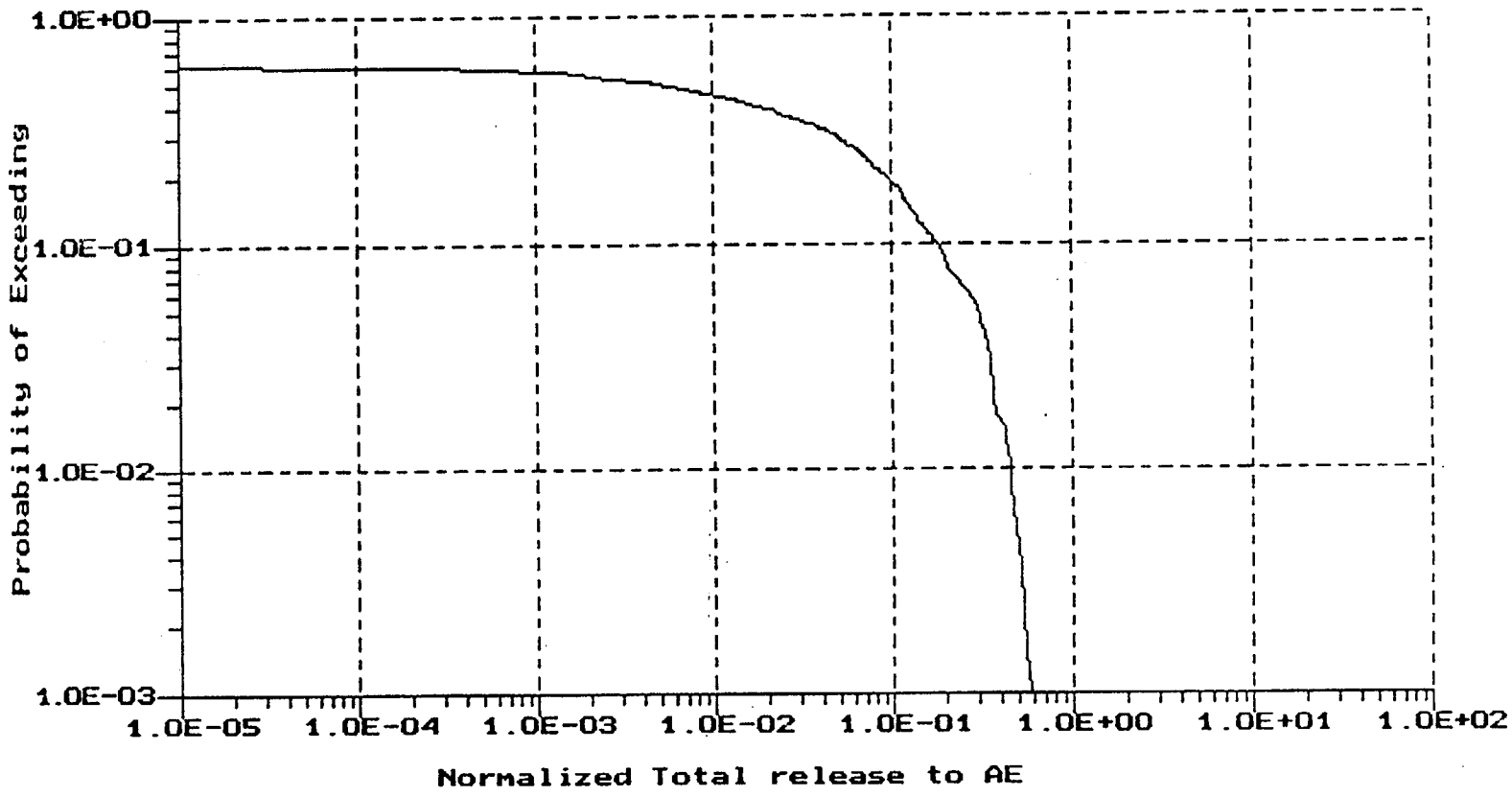

Distribution of Results

Mean= 5.484E-02

S.D.= 9.855E-02

Kurtosis= 9.324E+00

Skewness= 2.474E+00

Figure 3-17a. CCDF for EPA Sum — Run 3.2

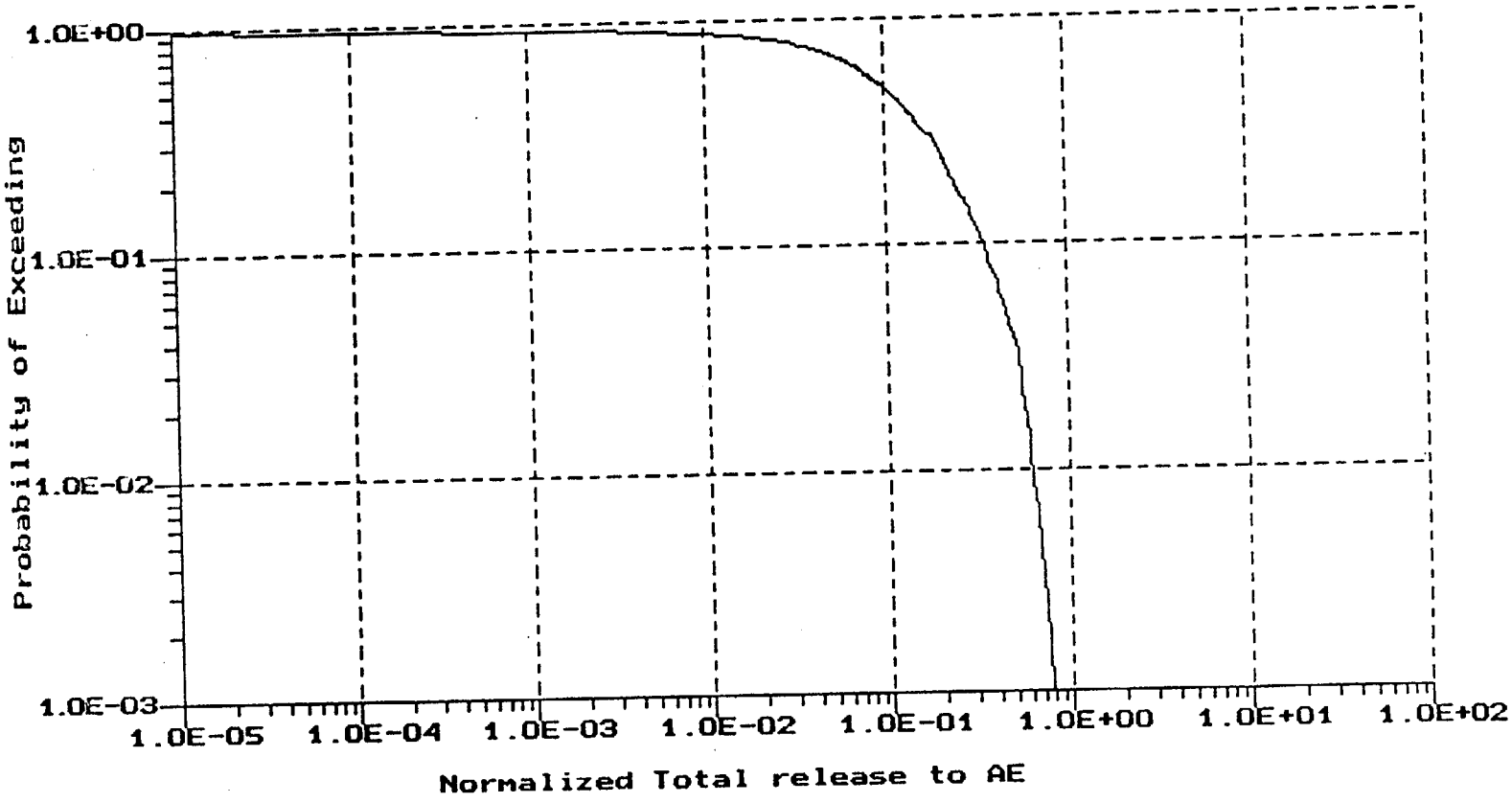

Distribution of Results

Mean= 1.423E-01

S.D.= 1.436E-01

Kurtosis= 5.452E+00

Skewness= 1.571E+00

Figure 3-17b. CCDF for EPA Sum — Run 3.3

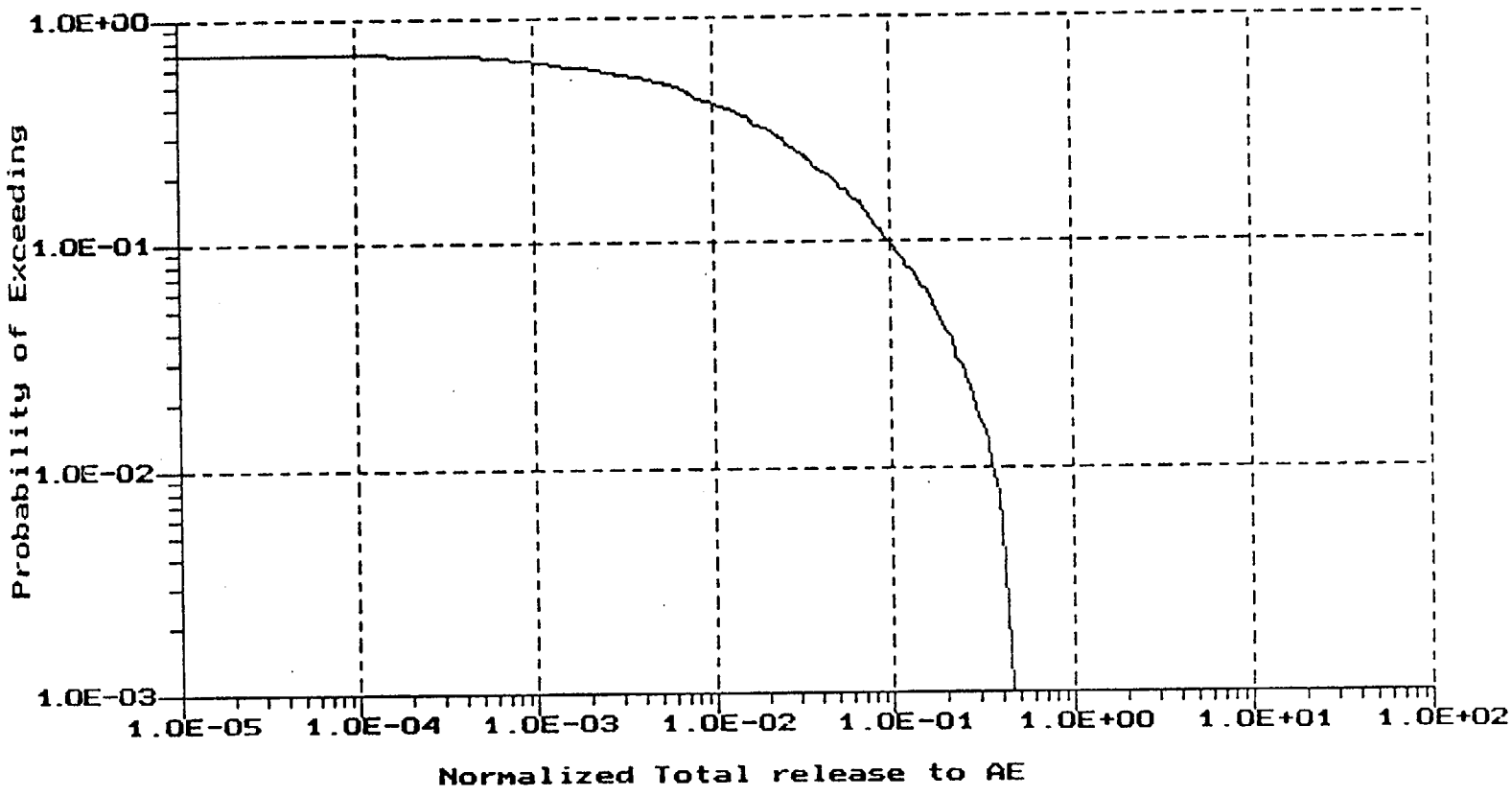

Distribution of Results

Mean= 3.333E-02

S.D.= 6.818E-02

Kurtosis= 1.518E+01

Skewness= 3.304E+00

Figure 3-17c. CCDF for EPA Sum — Run 3.4

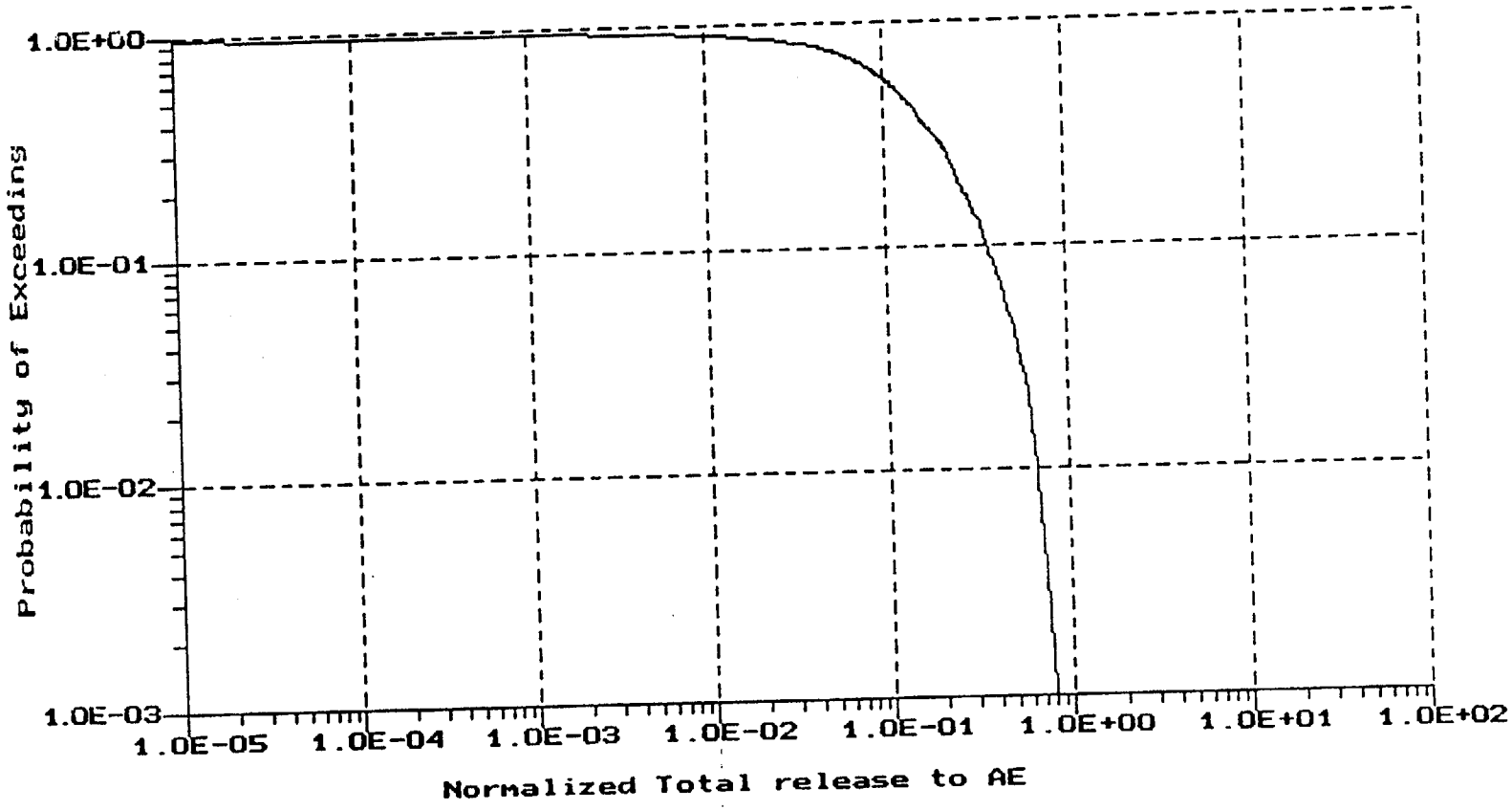

Distribution of Results

Mean= 1.613E-01

S.D.= 1.497E-01

Kurtosis= 5.022E+00

Skewness= 1.438E+00

Figure 3-17d. CCDF for EPA Sum — Run 3.5

Table 3-1. Hydrostratigraphy Used for Unsaturated-Zone Aqueous Problems (after Barnard et al., 1992)

Layer	Dominant Lithology
1	Moderately welded
2	Vitrophyre
3	Vitric, non- to partially welded
4	Zeolitic, non- to partially welded
5	Partially to moderately welded

Table 3-2. Elevations of Layers at Selected Locations in Geohydrologic Problem Domain (after Barnard et al., 1992)

Layer No. or Feature	Lithology	USW H-5 (m)*	West Boundary of Ghost Dance Fault (m)*	USW G-4 (m)*	UE-25 a#1 (m)*	500 m East of UE-25 a#1 (m)*
Surface		1478	1309	1270	1199	1175
Repository		1030	966	956	(870)	(831)
1	Welded tuff	996	875	869	811	781
2	Vitrophyre	974	863	860	798	771
3	Vitric tuff	905	832	836	784	759
4	Zeolitic tuff	885	734	723	637	596
5	Partially welded tuff/ water table boundary	770	731	731	729	730

* Elevation above sea level of the feature, or in the case of an individual layer, to the base of that layer. (Values in parentheses are projections.)

Table 3-3. Elevations[1] Used for the Composite-Porosity Model of the UZ (after Barnard et al., 1992)

Location	Elevation at Top of Layer						
	1	Re.[2]	2	3	4	5	Water Table
USW H-5	1478[3]	1035	996	974	905	885	770
120 m E (Col. 1)	1038[4]	1028	983	962	897	869	766
420 m E (Col. 2)	1021[4]	1011	950	932	877	827	755
660 m E (Col. 3)	1007[4]	997	923	907	861	794	747
940 m E (Col. 4)	990[4]	980	893	879	843	756	737
1099 m E Ghost Dance	1309[3]	971	875	863	832	734	731
1280 m E Ghost Dance	1309[3]	971	889	877	846	748	731
1280 m E (Col. 5)	966[4]	956	877	864	836	--[5]	731
1313 m E USW G-4[6]	1270[3]	961	869	860	836	--[5]	731
1700 m E (Col. 6)	930[4]	920	848	835	813	--[5]	730
UE-25a #1	1199[3]	(875)	811	798	784	--[5]	729

1 In meters

2 The repository is modeled as a 5-meter-thick layer

3 Ground surface

4 Top of simulated column

5 Below the water table

6 Not used in the linear interpolation

Table 3-4. Matrix Hydraulic Conductivity Distributions Used in TSPA-1991 and RIP (after Barnard et al., 1992)

Layer	Matrix Hydraulic Conductivity (m/yr): Beta Distribution			
	Mean	**Standard Deviation**	**Minimum**	**Maximum**
1	6.30×10^{-4}	6.10×10^{-4} (6.30×10^{-4})	0	2.50×10^{-2}
2	9.49×10^{-5}	6.00×10^{-5} (9.49×10^{-5})	9.40×10^{-6} (0)	4.00×10^{-3}
3	2.50×10^{-3}	2.30×10^{-3} (2.50×10^{-3})	0	9.78×10^{-2}
4	9.49×10^{-5}	6.00×10^{-5} (9.49×10^{-5})	9.40×10^{-6} (0)	4.00×10^{-3}
5	4.40×10^{-1}	4.30×10^{-1} (4.40×10^{-1})	0	1.71×10^{1}

( ) TSPA-1991 values

Table 3-5. Matrix Porosity Distributions Used in TSPA-1991 and RIP (after Barnard et al., 1992)

Layer	Matrix Porosities: Beta Distribution			
	Mean	**Standard Deviation**	**Minimum**	**Maximum**
1	0.11	0.022	0.044	0.197
2	0.09	0.018	0.037	0.161
3	0.209	0.042	0.001	1.0
4	0.41	0.082	0.001	1.0
5	0.24	0.048	0.001	1.0

Table 3-6. Fracture Porosity Distributions Used in TSPA-1991 and RIP

Layer	Fracture Porosity: Beta Distribution			
	Mean	**Standard Deviation**	**Minimum**	**Maximum**
1	5.94×10^{-3}	5.20×10^{-3} (5.94×10^{-3})	5.00×10^{-4} (0)	0.22 (0.42)
2	7.48×10^{-3}	7.20×10^{-3} (7.48×10^{-3})	1.00×10^{-4} (0)	0.3 (0.528)
3	4.20×10^{-4}	3.90×10^{-4} (4.20×10^{-4})	1.00×10^{-5} (0)	0.019 (0.0298)
4	3.36×10^{-4}	2.90×10^{-6} (3.36×10^{-4})	0 (0)	0.013 (0.024)
5	9.24×10^{-5}	8.00×10^{-5} (9.24×10^{-5})	1.00×10^{-4} (0)	0.038 (0.065)

( ) TSPA-1991 values

Table 3-7. Infiltration Rate Distribution Used in TSPA-1991 and RIP

Infiltration Rate (m/yr): Beta Distribution			
Mean	**Standard Deviation**	**Minimum**	**Maximum**
0.001	0.0009 (0.001)	0	0.039

( ) TSPA-1991 values

Table 3-8. Parameters Used to Model the Saturated Zone in TSPA-1991 and RIP (after Barnard et al., 1992)

Model Parameter	Distribution	Distribution Parameters[1]	Mean Value
Ground-water velocity, v (m/yr)	Beta	3.2, 5.9, 0.84, 2.87	4.07
Bulk porosity, ϕ_b	Beta	0.09, 0.29, 0.738, 1.37	0.175

[1] Parameters for the distribution are min, max, α, and β.

Table 3-9. Geohydrologic Units for Geochemistry in TSPA-1991 and RIP (after Barnard et al., 1992)

Geohydrologic Unit	Rock Type for K_d Definition
Welded	Devitrified
Vitrophyre	Vitric
Vitric	Vitric
Zeolitic	Zeolitic
Partially welded	Devitrified
Tuff saturated zone	Devitrified

Table 3-10. K_d Probability Density Distributions Used in TSPA-1991 and RIP (after Barnard et al., 1992)

Parameter	E[x]	C_v[x]	Min[x]	Max[x]	α	β
Beta Distributions						
K_d*, Cs Devitrified, or Vitric Tuff	50	0.20	20	100	4.25	7.75
K_d, Cs Zeolitic Tuff	2000	0.25	0	6000	9.33	19.67
K_d, Np Devitrified Tuff	2	1.00	0	50	-0.08	21.08
K_d, Np Vitric Tuff	0.5	1.00	0	12.5	-0.08	21.08
K_d, Np Zeolitic Tuff	4	1.00	0	100	-0.08	21.08
K_d, U (or Se) Devitrified Tuff	2.5	0.577	0	5	0.0	0.0
K_d, U (or Se) Vitric Tuff	2	0.577	0	4	0.0	0.0
K_d, U (or Se) Zeolitic Tuff	10	0.30	5	21	0.59722	2.51389
Constant Values						
K_d, C (all rocks)	0					
K_d, Tc (all rocks)	0					
K_d, Sn (all rocks)	100					
K_d, I (all rocks)	0					
K_d, Pu (all rocks)	100					
K_d, Am (all rocks)	100					

K_ds for all entries in table are in ml/g.

α, β are exponents in the Beta probability density function given below

E[x] = expected value

C_v[x] = coefficient of variation

f(x) = $C \cdot (x - a)^{\alpha} (b - x)^{\beta}$ = probability density

C = normalizing constant

a = Min[x]

b = Max[x]

Table 3-11. Additional Infiltration Distributions

Simulation	Type of Distribution	Infiltration (m/yr)	Figure	Reference
Run 3.2	Log-uniform	Range: 0.0001 to 0.01	3016a	--
Run 3.3	Uniform	Range: 0.0001 to 0.01	3-16b	--
Run 3.4	Log-normal	Mean = 0.001 s.d. = 0.00043	3-16c	--
Run 3.5	Discrete	36% probability LU: 0 - 0.005 3-16d 64% probability LU: 0.005 - 0.010	3-16d	NRC-DOE Technical Exchange, December 14, 1992
Run 3.1	Beta	Beta: min: 0.0 max: 0.039 mean: 0.001	3-16e	Barnard et al. (1992)

4. UNSATURATED GASEOUS TRANSPORT

4.1 DESCRIPTION OF TSPA-1991

Gaseous release from the waste package/EBS and transport to the accessible environment was investigated in TSPA-1991 (Barnard et al., 1992). This section summarizes the data, methodology and results, utilized in TSPA-1991 (Barnard et al., 1992). All information in this section was obtained from TSPA-1991, which considered the gaseous release from the waste packages and transport through the unsaturated zone to the atmosphere or accessible environment. The only gaseous radionuclide considered in TSPA-1991 was ^{14}C in the form of $^{14}CO_2$. The source term configuration is similar to that of the aqueous flow and transport section, with the exception of the addition of ^{14}C.

As mentioned in Section 3.2, TSPA-1991 considered both composite-porosity and "weeps" flow models. The source inventories, waste-package failure models, and far field velocity regimes are identical for the two transport models, with the only difference being the percentage of waste packages assumed to fail (i.e., to be intersected by "weeps"). This section will discuss only the gaseous flow and transport based on the composite-porosity model. The only radionuclide included in the gaseous release and transport source term is ^{14}C. The ^{14}C inventory presented in TSPA-1991 is summarized in Table 4-1.

The waste package conceptual model used in TSPA-1991 considers that the majority of the ^{14}C release will come from an initial release event. This initial release event is comprised of the releases (1) due to an oxidation layer on the surface of the fuel-rod cladding (quick release), and (2) from the inventory in the gap between the cladding and the fuel pellets (gap/grain boundary). The quick-release and gap-grain boundary inventories were combined into the initial release event due to limitations in the TSPA-1991 source model (Barnard et al., 1992). This problem neglects all of the assembly hardware inventory and almost all of the cladding inventory except for the portion included in the initial release fraction. The quick-release portion was considered to be 0.5 to 5 percent of the total inventory of 1.54 Ci/MTHM (Barnard, et al., 1992). The gap-grain boundary inventory was considered to be 2.0 percent of the fuel-matrix inventory of 0.58 Ci/MTHM, as in the aqueous releases. In TSPA-1991, the quick-release portion and the gap-grain boundary inventory were lumped to obtain a "prompt" inventory fraction. This fraction includes 0.0077 to 0.077 Ci/MTHM for the quick-release and 0.012 Ci/MTHM for the gap-grain boundary, yielding a total "prompt" release inventory that varies from 0.019 to 0.089 Ci/mthm. When the quick-release portion is added to the fuel-matrix inventory (0.58 Ci/MTHM), the entire modeled inventory varies from 0.58 to 0.65 Ci/MTHM. The gap-grain boundary inventory is used in calculating the percentage of the entire modeled inventory released in the prompt fraction, but is not considered in the calculation of the entire modeled inventory since it is already a certain percentage of the fuel-matrix inventory. Therefore, the percent of the entire modeled inventory released in the prompt fraction varies between 3 to 14 percent. Uniform distributions with means of 0.615 Ci/MTHM and 0.085 Ci/MTHM were used to describe the entire modeled inventory and prompt fraction, respectively.

The gas-flow model used in TSPA-1991 was based on the results of gas-flow modeling of Yucca Mountain incorporating the potential repository conducted by Ross et al., (1992). Using the two-dimensional, steady-state gas-flow model TGIF, Ross et al. generated gas-flow pathlines for Yucca Mountain under ambient conditions and with a heated repository. Figure 4-1 is a cross-sectional view of Yucca Mountain, with Solitario Canyon as the western boundary, the atmosphere as the upper boundary, the base of the welded Topopah Springs (TSw) unit as the lower boundary, and the eastern boundary placed beyond influence. From data based on naturally occurring ^{14}C studies and permeability tests, the non-welded Paintbrush tuff layer (PTn) was assumed to have a permeability on the order of 10^{-2} of the value for welded tuffs (TSw and TCw). Ross et al. conducted simulations under ambient conditions (300 K) and for a repository under heated conditions of 315, 330, and 360 K. Figures 4-2 and 4-3 present the results for the 300 and 330 K simulations. The non-welded tuff with a lower permeability displays a significant effect on the overall transport of gas through Yucca Mountain.

Travel-time distributions were determined for each of the four Ross et al. simulations (Figure 4-4). These distributions were incorporated directly into the TSPA-1991 calculations. As the age of the post-closure repository increases, the overall temperature in and around the repository will decrease from an initial post-closure maximum temperature. This temperature transient is incorporated into the TSPA-1991 calculations by shifting the ^{14}C release between travel-time distributions as the post-closure time increases. The times at which the shifts in travel-time distributions occur are presented in Table 4-2. However, the fraction of ^{14}C released from the waste package/EBS to the far field pathway in each time segment, is transported at that particular travel-time distribution and does not change with the shifting of temperature ranges. This will lead to a higher calculated release due to the transport velocity remaining constant and not lowering with time and distance away from the repository (which would occur due to the movement into cooler regions).

Ross et al. incorporated attenuation of the ^{14}C by retardation into the travel-time distribution calculations. Due to uncertainties in the actual value of the retardation parameters and the permeability of the different geological layers, TSPA-1991 incorporated a retardation/permeability factor to modify the gaseous advective velocities and travel times presented in Ross et al. (1992). This factor is multiplied by the travel time to account for variations from the base case parameter selections. The retardation/permeability factor is represented by a log-uniform distribution from 0.5 to 10.

Using the Ross et al. travel-time distributions, the modeled ^{14}C inventory, and the retardation/permeability factor, 1,000 realizations were conducted to obtain a conditional CCDF for gaseous release from the waste package and to the accessible environment for a 10,000-year period.

4.2 RIP ANALYSIS

The integrated performance assessment code RIP was used to determine the cumulative release of ^{14}C to the accessible environment due to gaseous (^{14}C) releases from the waste packages. The overall approach used in the RIP analyses was identical to the TSPA-1991 approach (Barnard et al., 1992). Table 4-3 presents the parameter comparison between the RIP and TSPA-1991 data

sets. The main difference in the two data sets is that in RIP, the travel-time distributions were converted into unit-velocity distributions for the transport calculations (see below).

The waste package inventory used by RIP is the same as in TSPA-1991. The main waste package and inventory specifics used in the RIP analysis are therefore described in Section 4.1. The only variations were the inclusion of the ^{14}C inventory and the prompt release fraction. The ^{14}C inventory was entered as a uniform distribution from 0.58 to 0.65 Ci/MTHM. The prompt fraction was entered as a uniform distribution from 0.03 to 0.14. Since the primary container failure in RIP is used to simulate the rewetting period, the secondary container failure mode corresponds to the failure of the waste package container itself.

Upon failure of the waste package, the ^{14}C is discharged to a certain pathway based on two factors. The first being the time at which the release occurred. This is considered to be due to the change in the repository temperature with time. (The temperature variations were not explicitly modeled in TSPA-1991, so time is used as a surrogate parameter to describe the variation of travel times.) A group of pathways, each representing a different travel time distribution, is specified for each operating temperature. The second factor is that for each of the four operating temperatures, the ^{14}C releases were proportioned out in relation to a unit-velocity distribution. The unit-velocity distributions were generated from each travel-time distribution (Figure 4-4) by taking the inverse of the travel time distributions. The unit-velocity distributions for each of the four travel-time distributions are presented in Figures 4-5 through 4-8, and are taken as the velocity of ^{14}C over a path length of one meter from the waste package to the accessible environment. The velocity distributions were then divided into four or five steps that best described the curve.

Once the ^{14}C is discharged from the waste package, it is then apportioned according to these steps, with different percentages of the release inventory traveling at different, but constant, velocities. This stair-stepping procedure was necessary since the velocity in each specified pathway must remain constant for each realizations. Each pathway was assumed to discharge to the accessible environment. Figure 4-9 presents a flow chart of the RIP pathway setup.

Each of the 18 pathways have a specified base velocity as denoted in Figure 4-9. However, the actual pathway velocity will be different for each realization due to the incorporation of the retardation/permeability factor. A single value for the retardation/permeability factor is obtained per realization, and this value is divided into each of the base pathway velocities to obtain the actual simulated velocities.

In the RIP analysis, as in the TSPA-1991 analysis, 1,000 realizations were conducted to obtain the gaseous (^{14}C) releases to the accessible environment over a 10,000 year period. The probability of releases from the waste package and to the accessible environment are plotted and compared to the TSPA-1991 results in the next section.

4.3 RESULTS

In the RIP analysis, 1,000 realizations of 10,000 years in length were conducted to determine the cumulative release of gaseous radionuclides (^{14}C) to the accessible environment through the

unsaturated zone at Yucca Mountain. The results which will be used for the comparison of the TSPA-1991 and RIP simulations are cumulative probability versus the normalized release of ^{14}C from the waste package and to the accessible environment.

The TSPA-1991 simulation results are presented in Figure 4-10. The RIP results are presented in Figure 4-11. The RIP results are very similar to the TSPA-1991 results, as would be expected, but they do yield slightly higher releases from the waste package and to the accessible environment. This is due to the Weibull distribution used for the container failure distributions (see Section 2.3.1). Scatter plots have been generated that show the relative effect of the variation in ^{14}C inventory (Figure 4-12), prompt fraction (Figure 4-13), and retardation/permeability factor (Figure 4-14) on the release of ^{14}C to the accessible environment. These plots show that the factor that is included to represent the uncertainty in the retardation and permeability values has the dominant effect on the release of ^{14}C to the accessible environment.

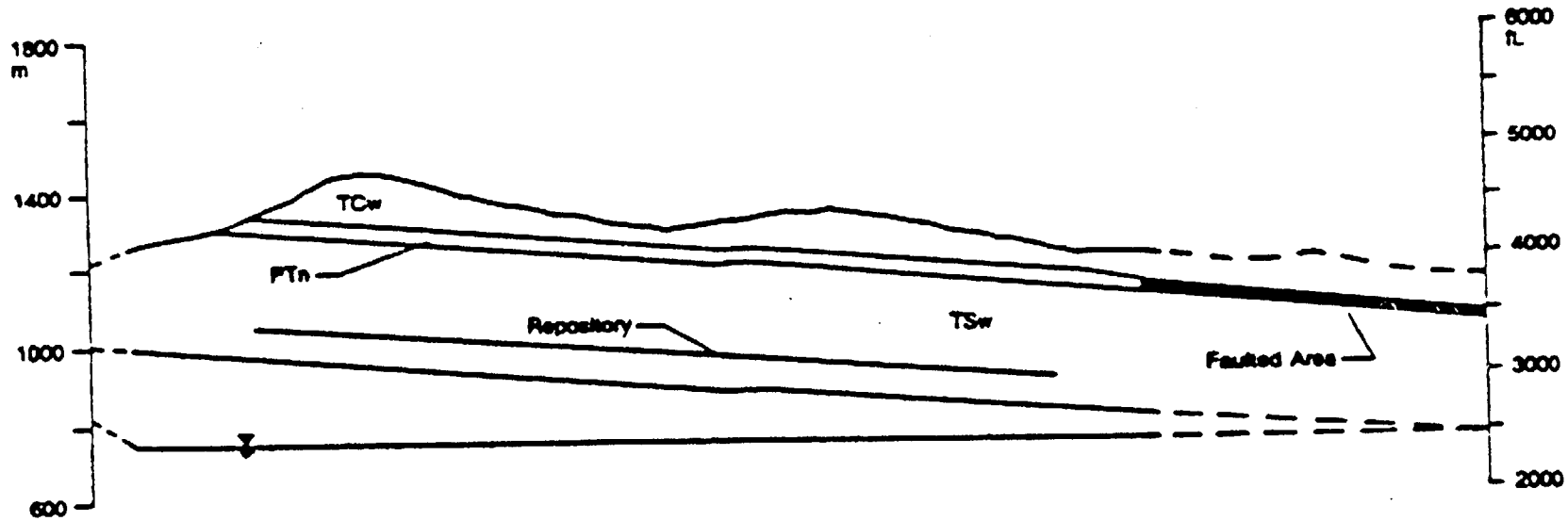

Figure 4-1. Cross-Section Through Yucca Mountain (taken from Barnard et al., 1992)

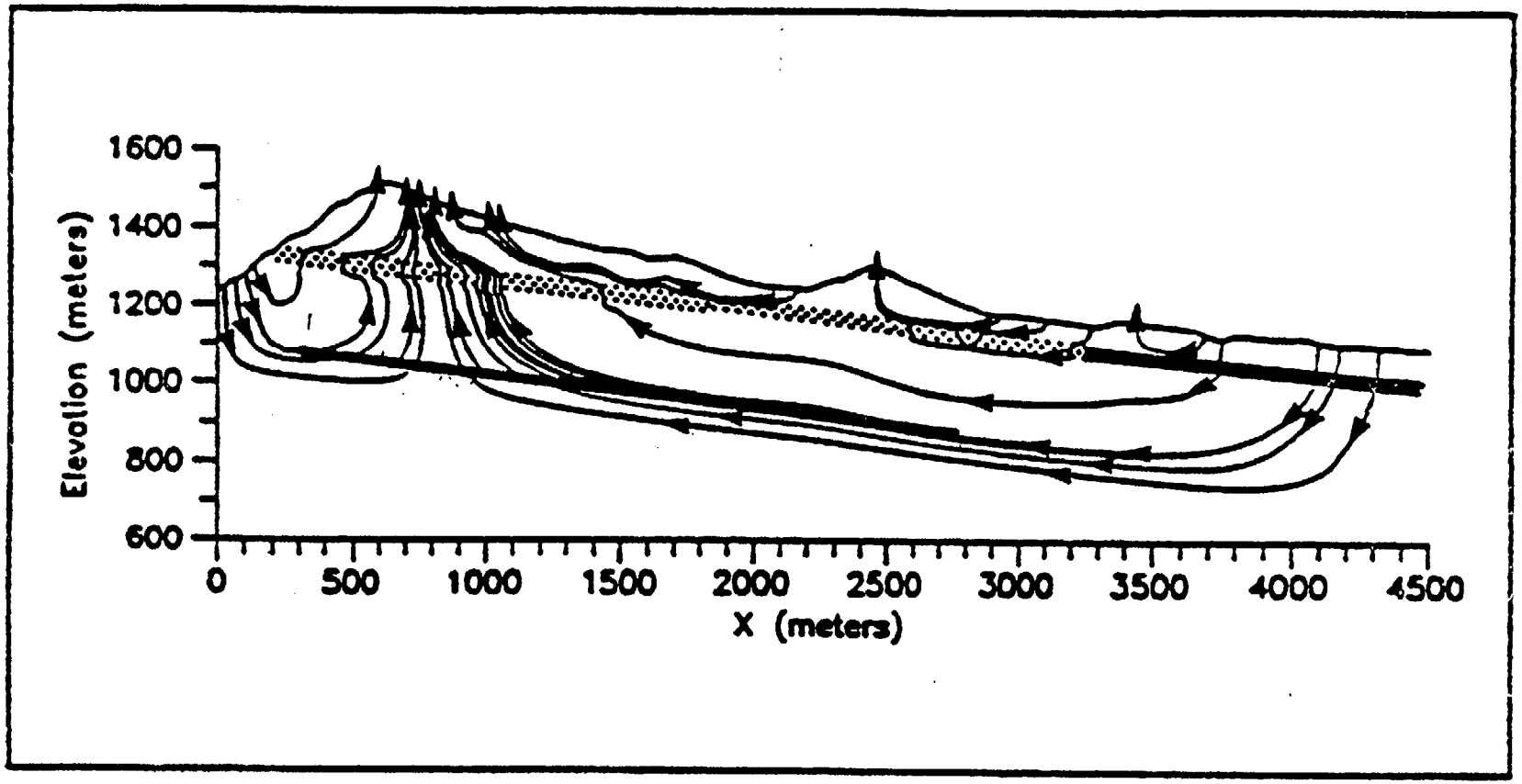

Figure 4-2. Gas-Flow Path Lines within Yucca Mountain with the Repository at Ambient Temperature Conditions (300 K) (taken from Barnard et al., 1992)

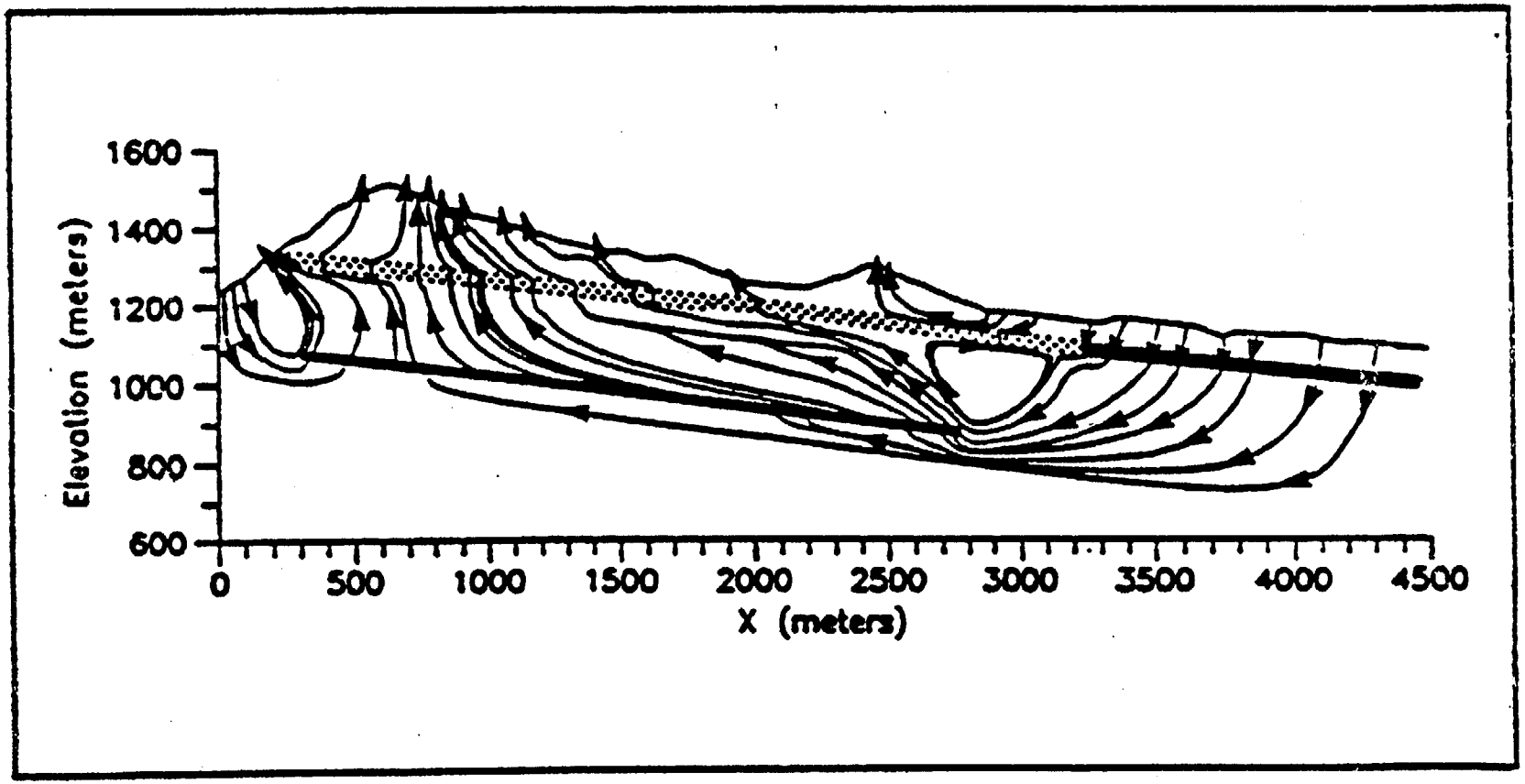

Figure 4-3. Gas-Flow Path Lines within Yucca Mountain with the Repository at a Temperature of 330 K (taken from Barnard et al., 1992)

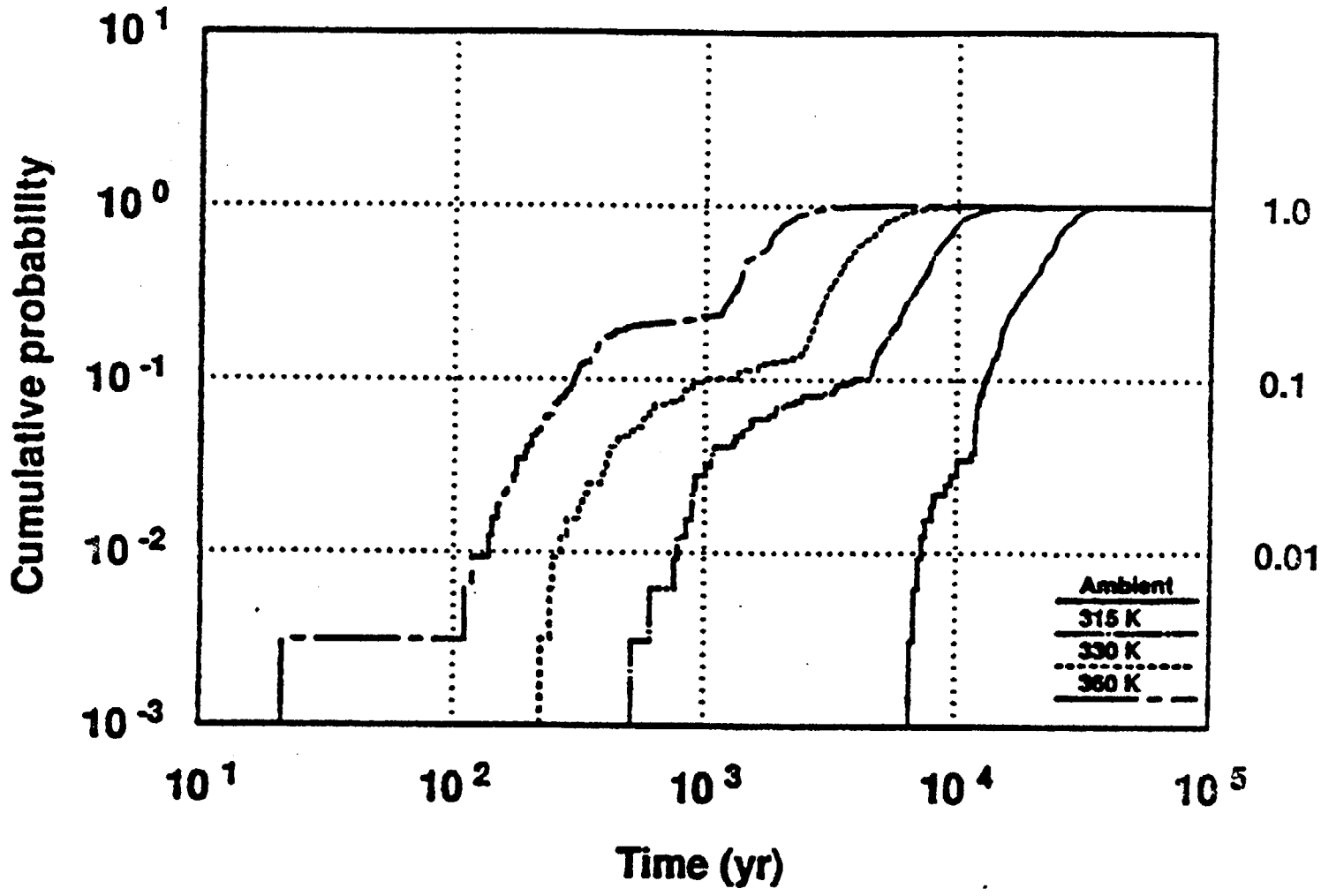

Figure 4-4. Travel-Time Distributions for ^{14}C Transport (taken from Barnard et al., 1992)

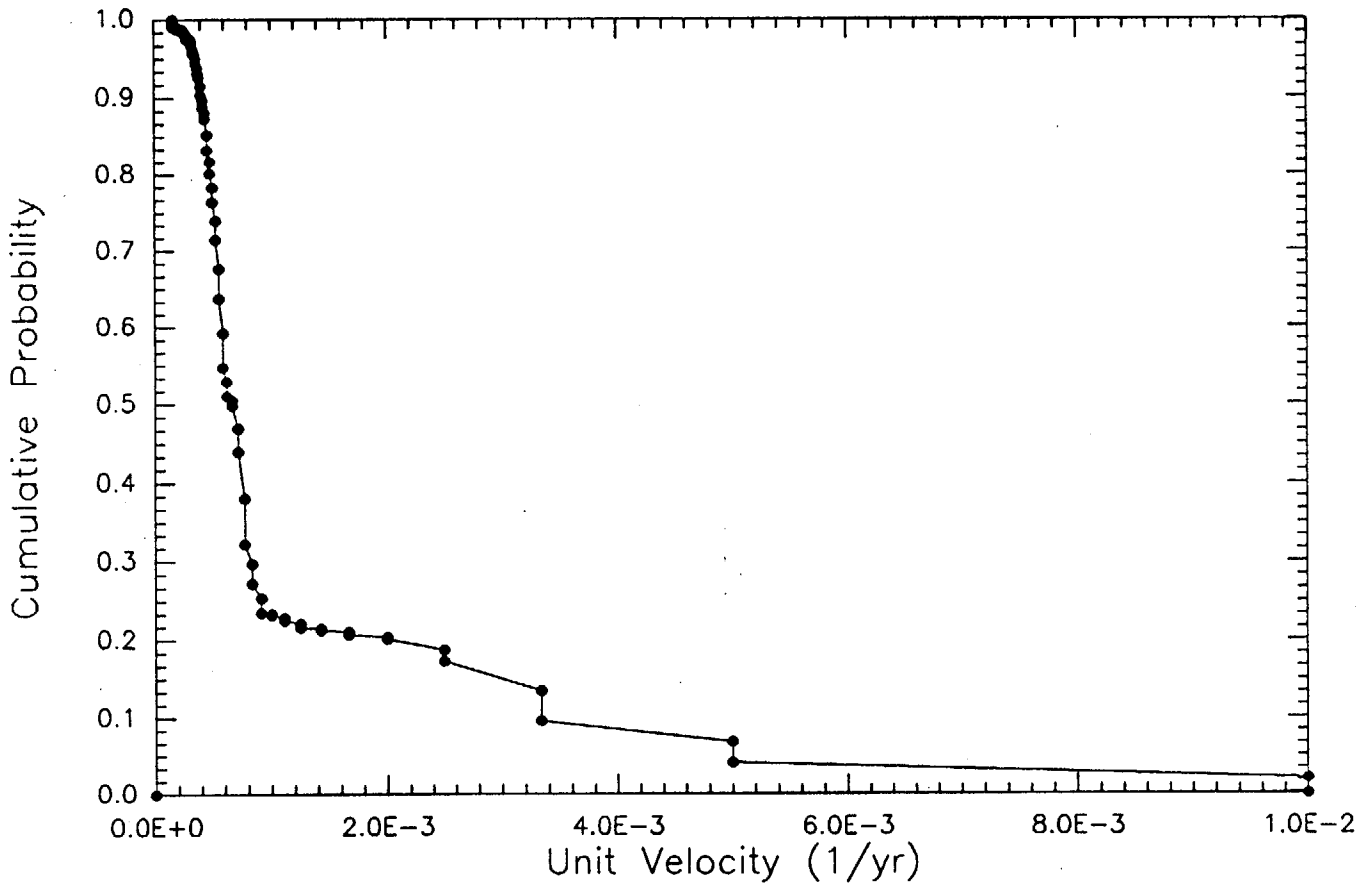

Figure 4-5. ^{14}C Unit-Velocity Distribution for a Repository Temperature of 360K

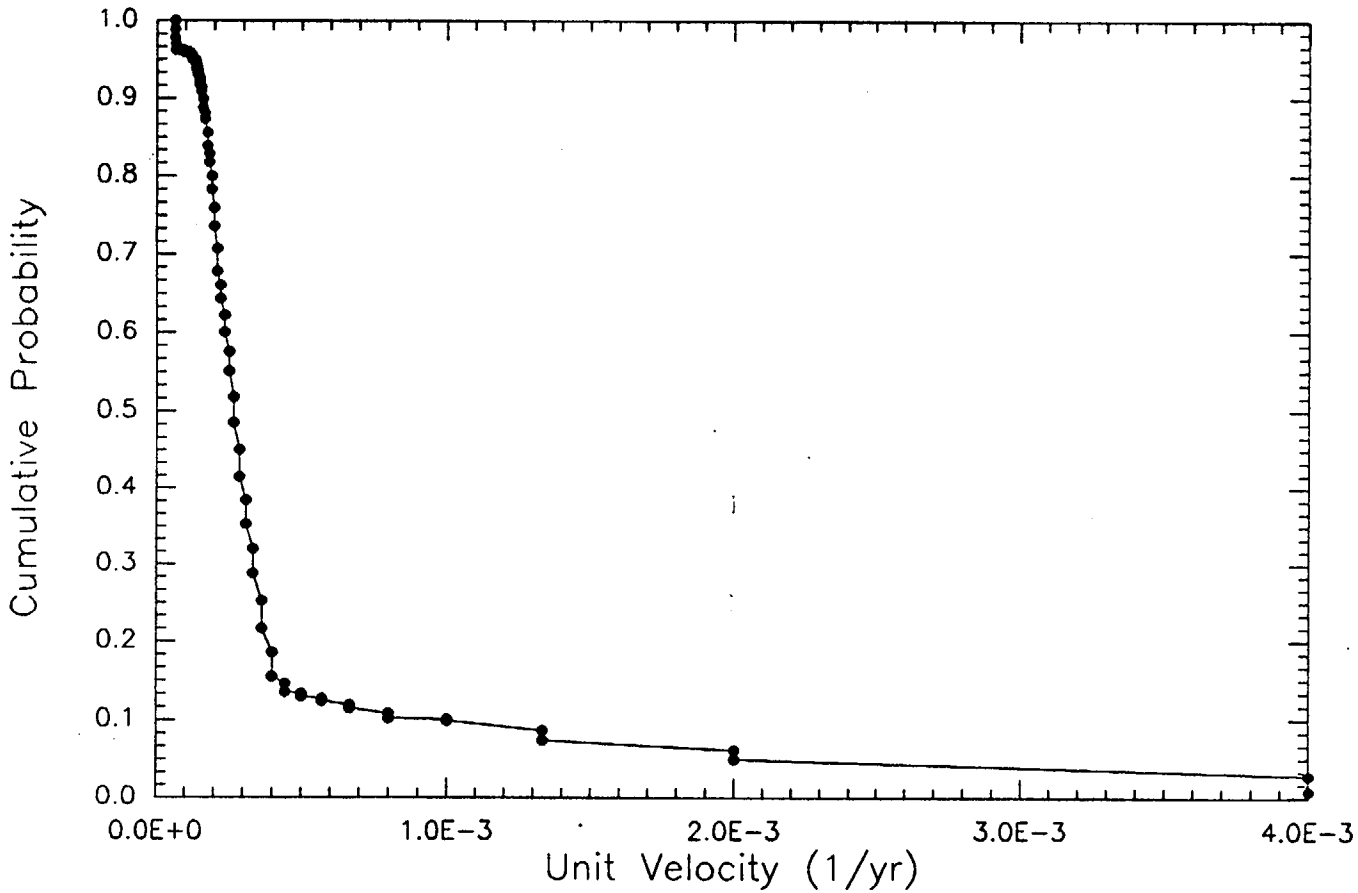

Figure 4-6. ^{14}C Unit-Velocity Distribution for a Repository Temperature of 330 K

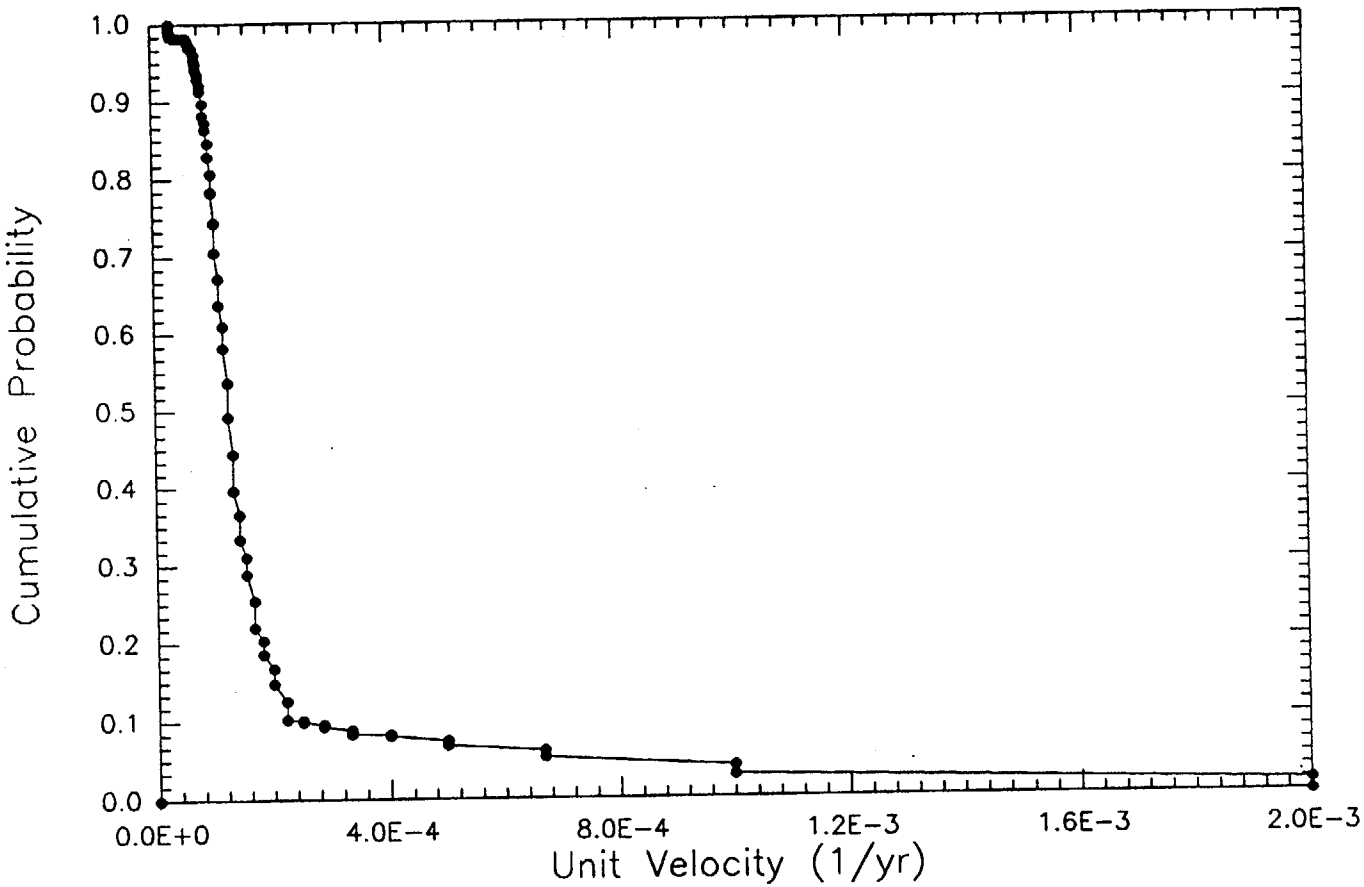

Figure 4-7. ^{14}C Unit-Velocity Distribution for a Repository Temperature of 315 K

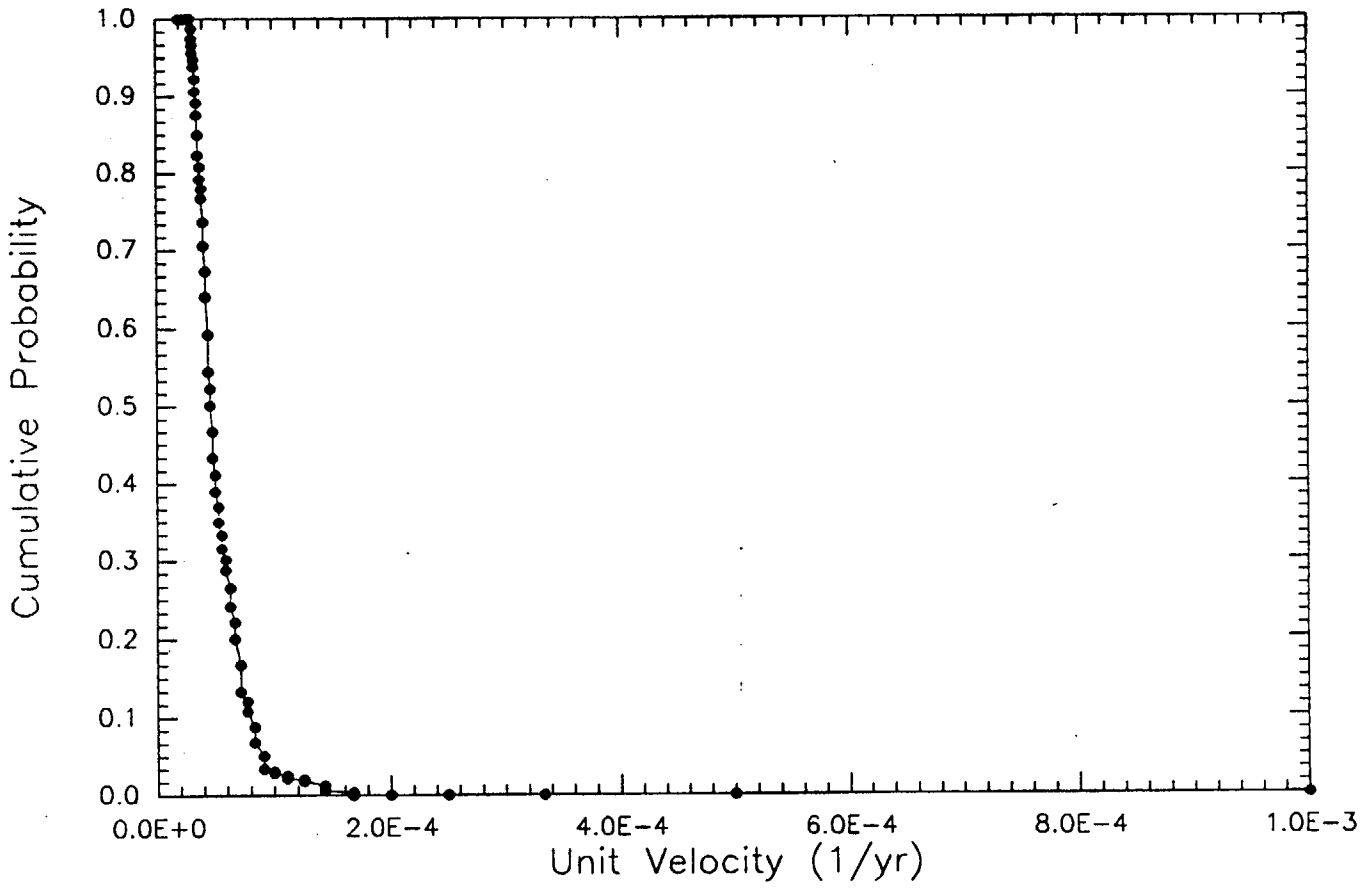

Figure 4-8. ^{14}C Unit-Velocity Distribution for a Repository Temperature of 300 K

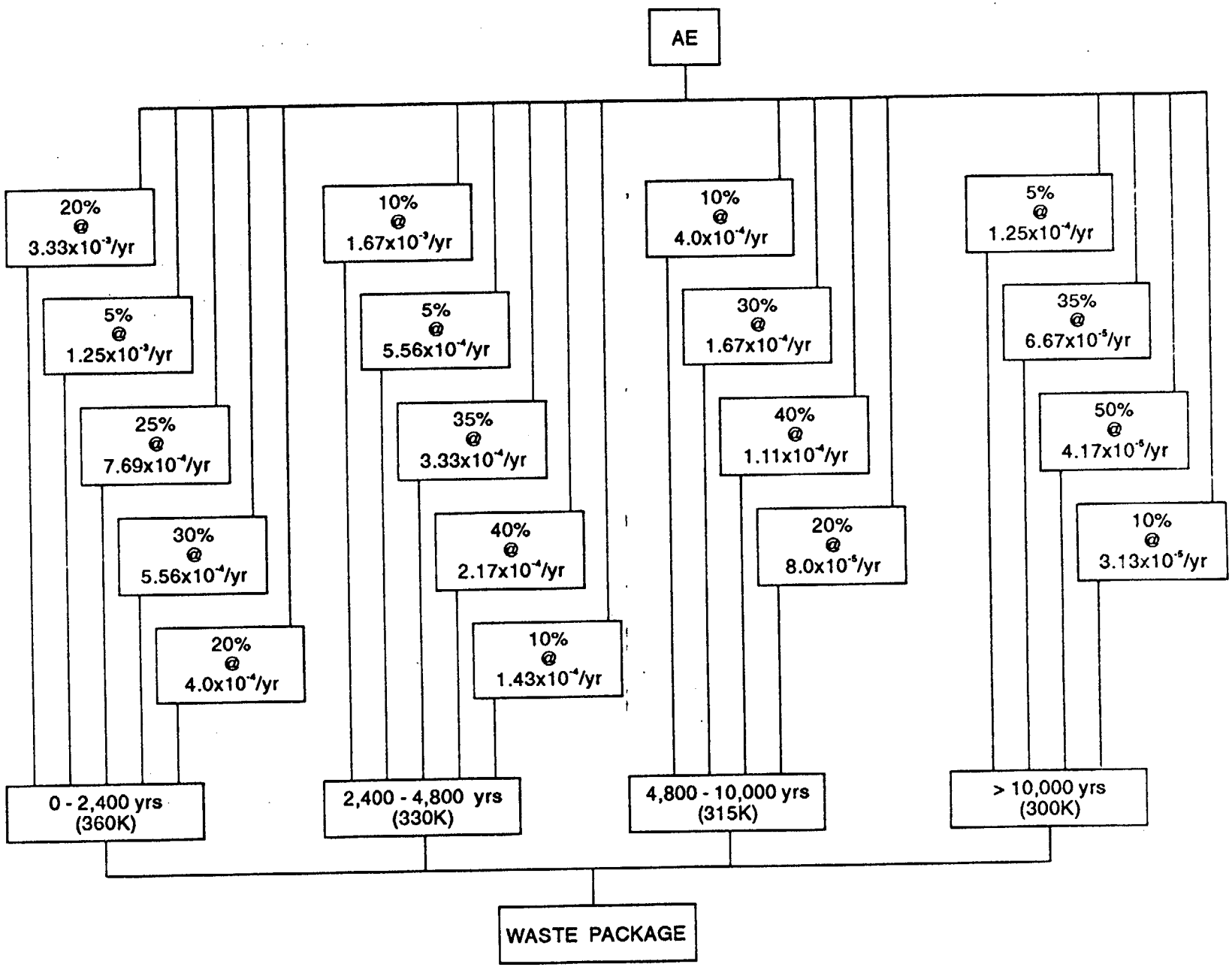

Figure 4-9. ^{14}C Mass and Velocity Distributions per RIP Pathway

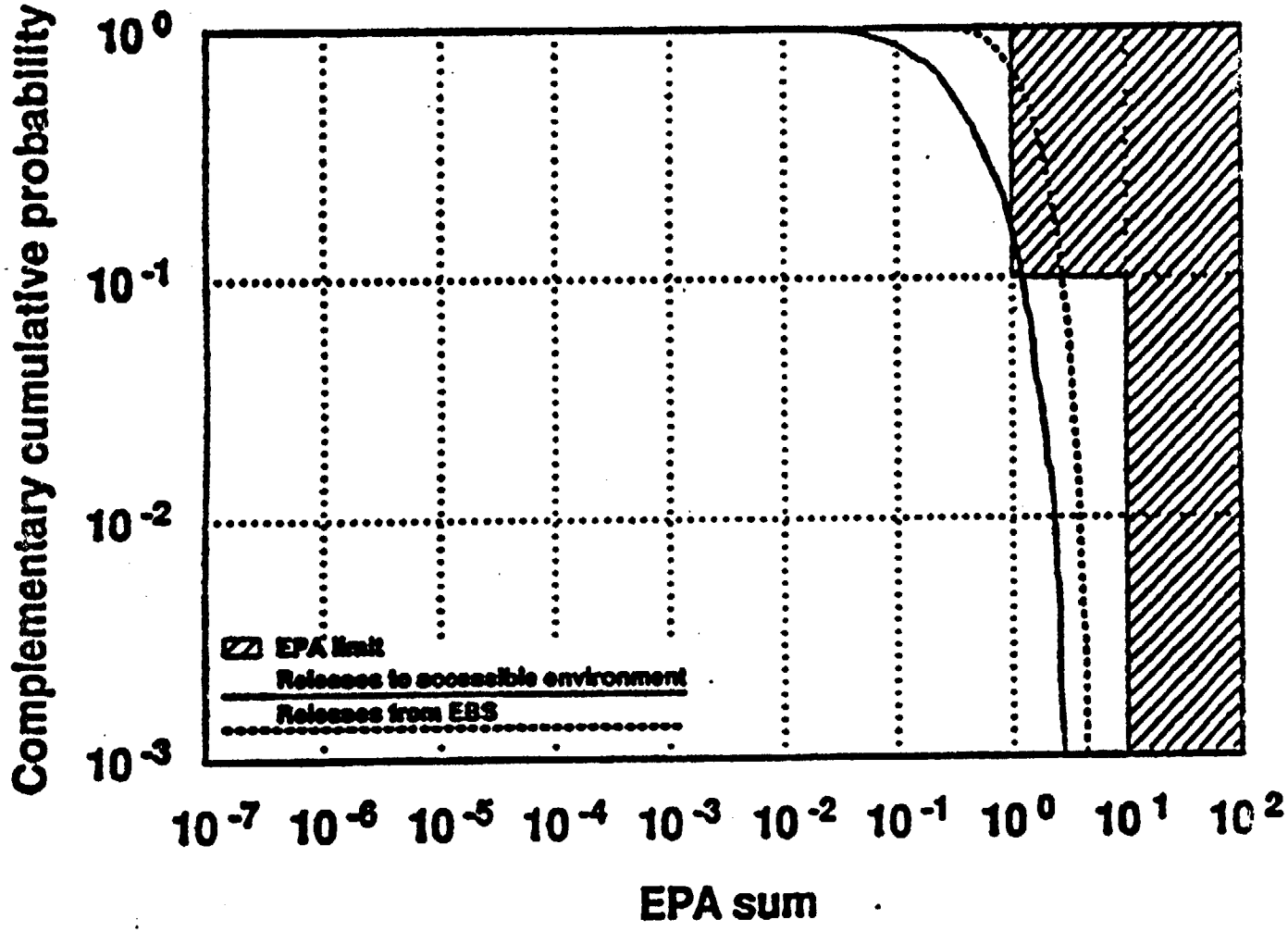

Figure 4-10. Conditional CCDF for Gaseous Releases (taken from Barnard et al., 1992)

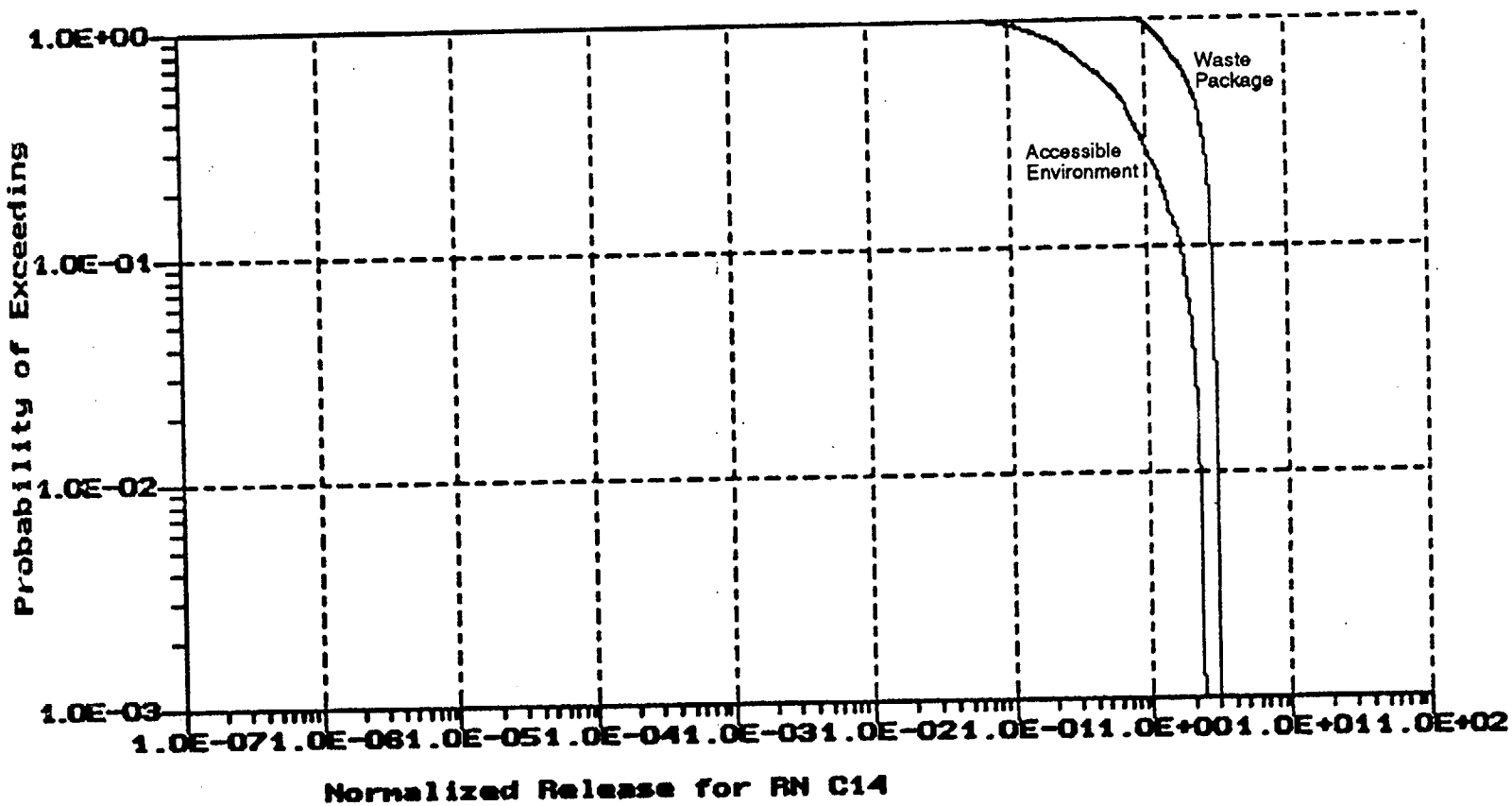

Figure 4-11. Conditional CCDF for Gaseous Releases from RIP

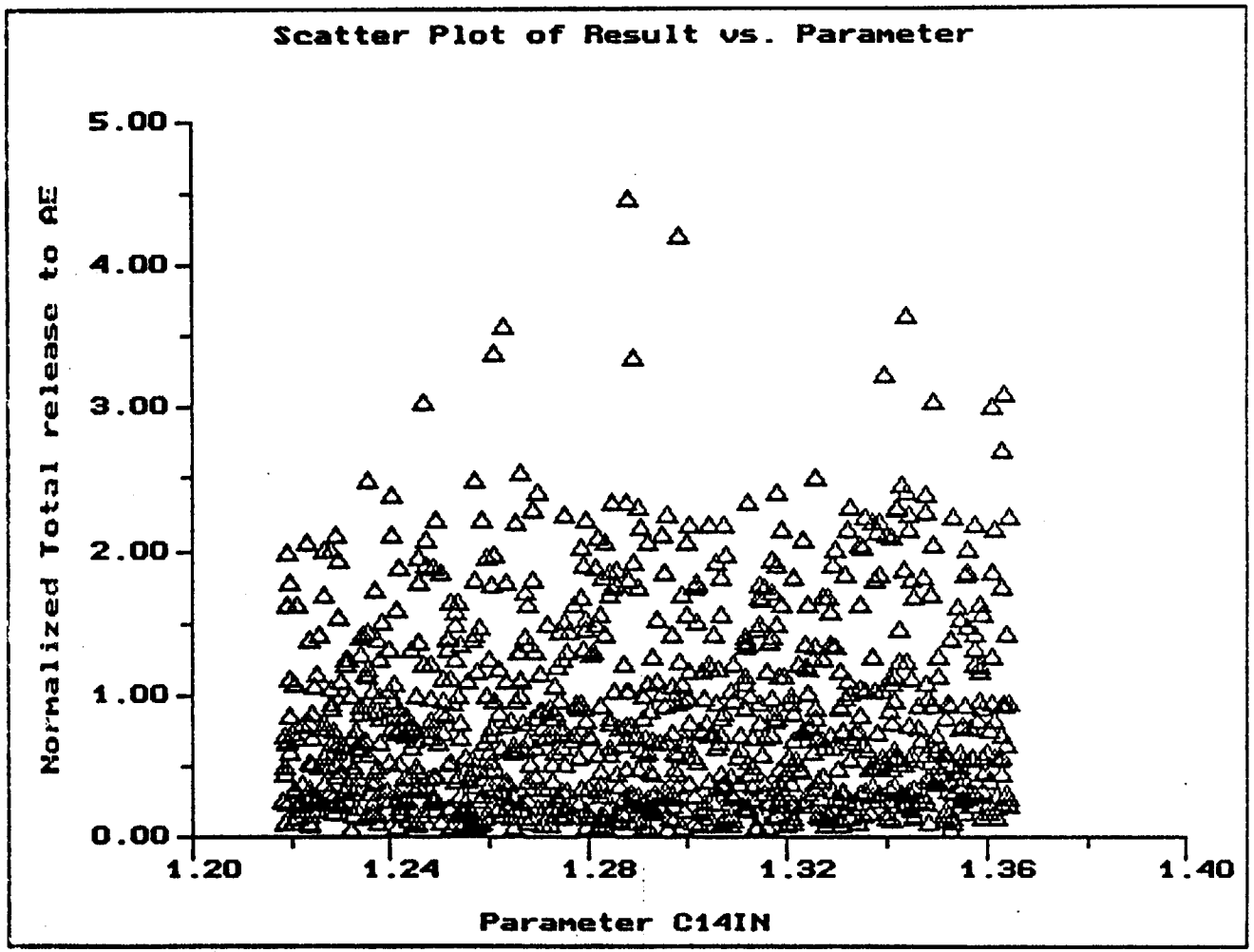

Figure 4-12. Scatter Plot of Modeled ^{14}C Inventory versus Total Normalized Release to the Accessible Environment

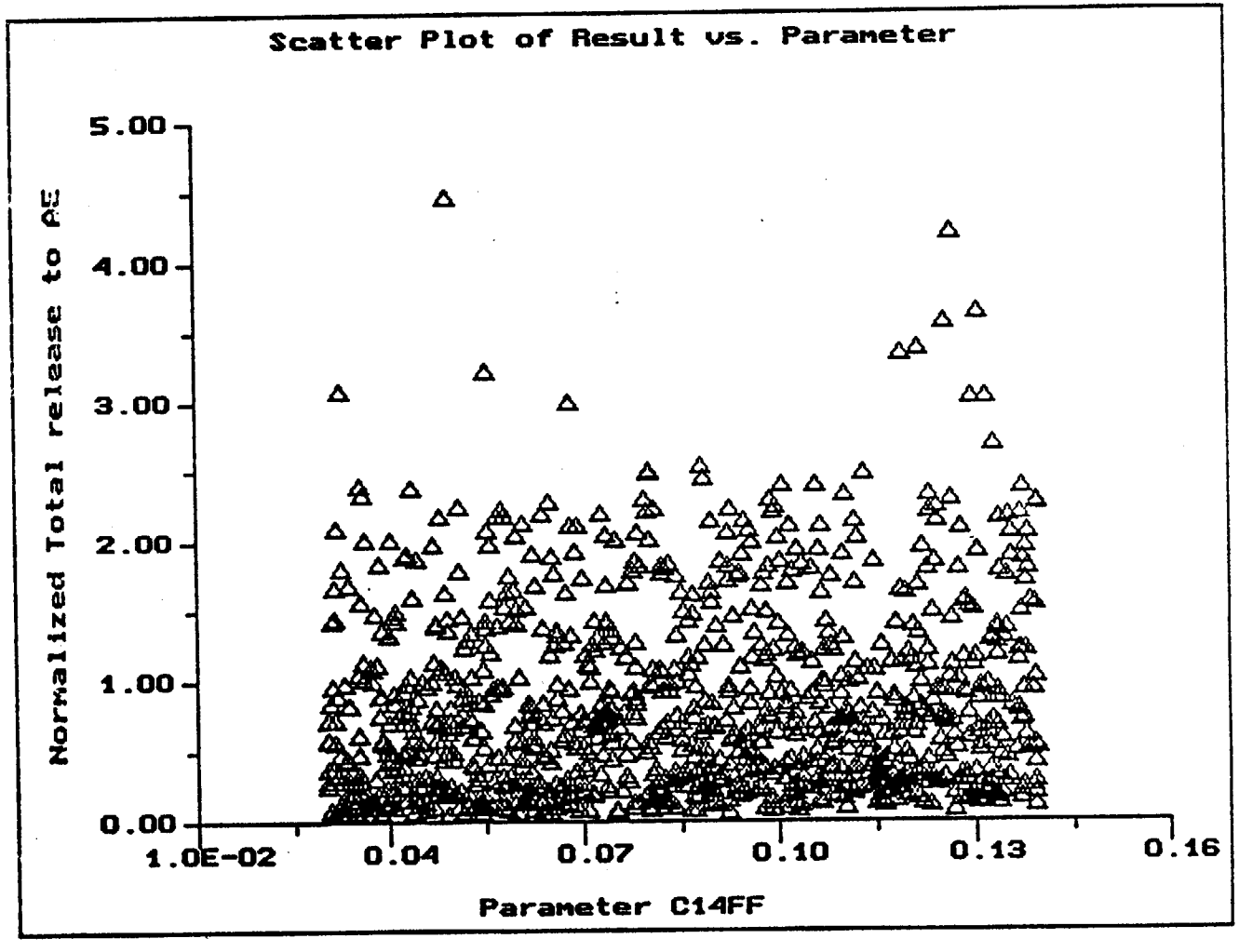

Figure 4-13. Scatter Plot of ^{14}C Prompt Fraction versus Total Normalized Release to the Accessible Environment

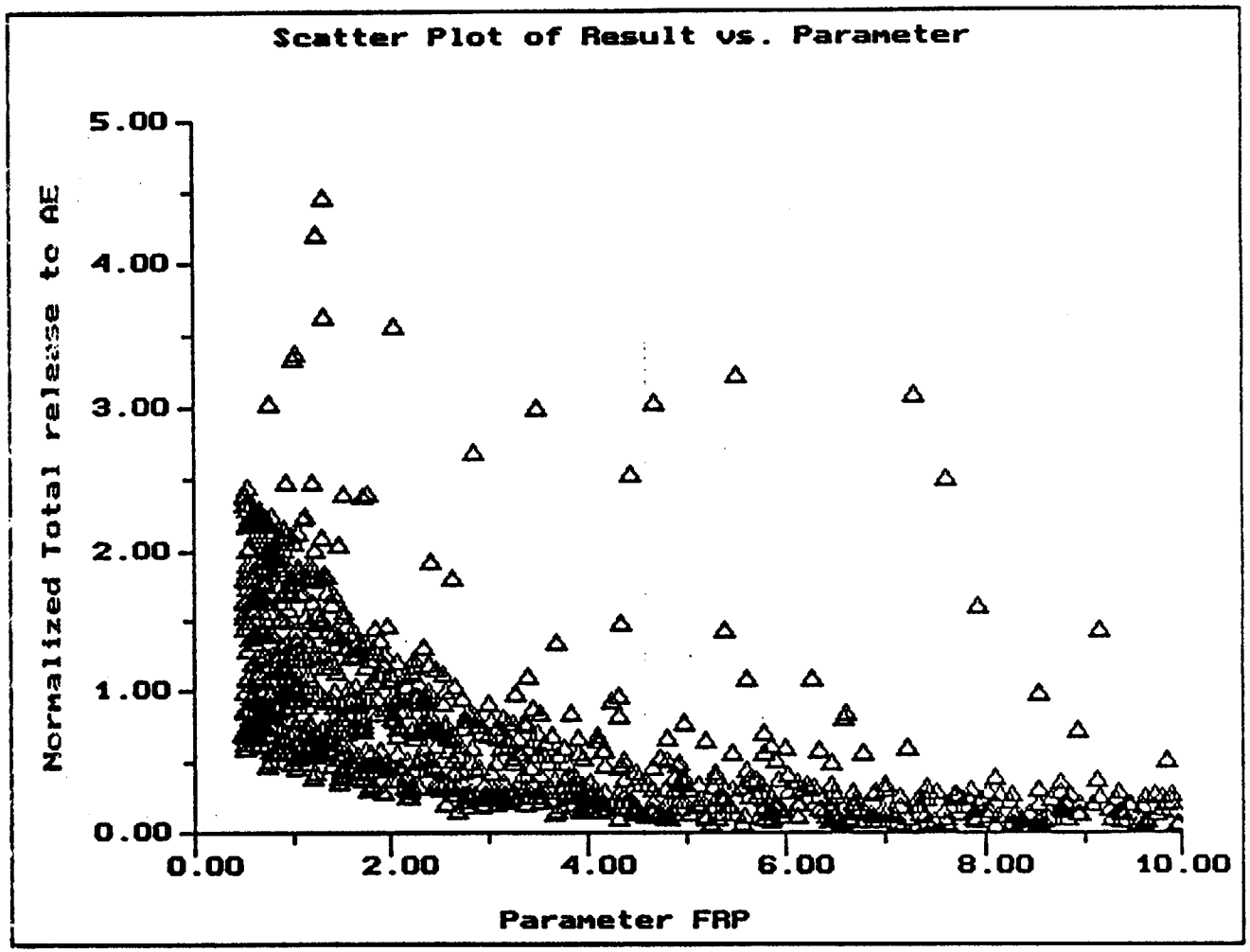

Figure 4-14. Scatter Plot of the Retardation/Permeability Factor versus Total Normalized Release to the Accessible Environment

Table 4-1. TSPA-1991 ^{14}C Source Term Data (after Barnard et al., 1992)

Parameter	Value
^{14}C Inventory (Ci/MTHM):	
Total	1.54
Fuel matrix	0.58
Cladding	0.51
Assembly hardware	0.45
Half-life (yr):	5729
Activity (Ci/mol):	62.4
EPA Limit (Ci/MTHM):	0.1

Table 4-2. TSPA-1991 ^{14}C Travel Time Specifications (after Barnard et al., 1992)

Time Range (years)	Travel-Time Distribution
0 to 2400	360 K
2400 to 4800	330 K
4800 to 10,000	315 K
greater than 10,000	300 K

Table 4-3. Comparison of TSPA-1991 and RIP Simulation Parameters

Parameter	TSPA-1991 Distribution	TSPA-1991 Distribution Parameters (min, max)	RIP Distribution	RIP Distribution Parameters
^{14}C Inventory (Ci/MTHM)	Uniform	0.58, 0.65	Uniform	0.58, 0.65
Prompt Fraction	Uniform	0.03, 0.14	Uniform	0.03, 0.14
Retardation/ Permeability Factor	Log-Uniform	0.5, 10	Log-Uniform	0.5, 10

5. EXTERNAL EVENTS AND PROCESSES

5.1 VOLCANIC INTRUSION SCENARIO

5.1.1 Description of TSPA-1991

TSPA-1991 (Barnard et al., 1992) investigated the potential effects that a future volcanic event might have on the release of radionuclides to the surface. The movement of the radionuclides was assumed to be by entrainment in a moving magma body (or dike) that flows onto the surface. Once on the surface, the radionuclides are considered released to the accessible environment. This section summarizes the TSPA-1991 data and methodology. All information in this section was obtained from the TSPA-1991 report (Barnard et al., 1992).

The possible effects of volcanic activity were simulated by conducting 1000 realizations with each realization simulated for 10,000 years after closure. The source term consisted of over 40 radionuclides as specified in Table 6-4 of the TSPA-1991 report (Barnard et al., 1992). Radioactive decay was allowed to occur within the waste packages but the waste packages were not allowed to fail. Therefore, if a volcanic event did not occur, there would be no release to the accessible environment.

The probability of volcanic activity occurring within the region of the potential repository at Yucca Mountain was determined from the known history frequency of volcanic events in the Yucca Mountain region. TSPA-1991 used a probability of 2.4×10^{-4} per 10,000 years as the actual probability of occurrence (Barnard et al., 1992). Due to the very low probability of occurrence, the TSPA-1991 analysis allowed a volcanic event to occur in each realization (although the time of occurrence was assumed to be random) and the results were then multiplied by the probability of occurrence to determine the probability of cumulative releases to the accessible environment.

Two methods for the entrainment and movement of waste to the surface were investigated. Each method assumed that a dike passed through the potential repository and the amount of waste entrained in the magma was proportional to the overall size of the dike (Figure 5-1). Both methods assumed that the entire waste inventory was evenly distributed throughout the potential repository, and the fraction of the potential repository moved to the surface corresponded to the fraction of the waste moved to the accessible environment. Also, fracturing of the host rock and backfilled repository was assumed prior to the arrival of a dike, resulting in a void within the potential repository that the dike filled. Therefore, the volume of the potential repository entrained within the dike was not equal to the volume of the dike within the repository.

Method 1 uses the geometric shape of the dike to determine the amount of waste entrained. The parameters used to define the geometry of the dike are the dike length, dike width, dike orientation, and erosion depth. The dike length was assumed to be uniformly distributed between 0 to 5 km initiating from a random starting point outside the repository (see below). The dike width is the width of the dike within the potential repository and was assumed to range from 0.0 to 4.5 m, following a beta distribution with a mean of 1.5 m (Figure 5-2). The dike orientation is the trend of the dike through the potential repository and is assumed to range from

-10 to 90° east of north, following a beta distribution with a mean value of 15°. The erosion depth is the depth into the host rock that is eroded as the magma passes through the potential repository. The erosion depth was assumed to follow a beta distribution over a range from 4.0×10^{-3} to 2.0×10^{-1} m, with a mean of 5.0×10^{-2} m (Figure 5-3).

To determine the volume of the potential repository that is entrained in the dike, the orientation and periphery of the dike must be determined. Using an imaginary line drawn east-west below the southern boundary of the potential repository, a dike of random length with a random orientation was drawn from this imaginary line (Figure 5-4). The length of the dike that actually intersected the potential repository was then used, along with the dike width, to calculate the periphery of the dike $2(l + w)$. The periphery of the dike was then multiplied by the sampled erosion depth and the assumed repository height (5.0 m) to obtain the volume of the potential repository that was entrained in the dike. This entrained volume was then converted into a fractional volume of the entire potential repository. The fractional value was then multiplied by the radionuclide inventory existent at the time the event occurred to obtain the total release to the accessible environment.

Method 2 uses observed xenolith occurrence data obtained from surface flow observations in the Yucca Mountain region to estimate the amount of waste entrainment. In order to determine this, the total volume of a volcanic eruptive event must be known along with the fraction of that eruptive volume that would be derived from the potential repository horizon. The total eruptive volume was determined to range from 3.4×10^5 to 1.0×10^8 m^3, following a beta distribution with a mean of 2.7×10^7 m^3. The volumetric fraction derived from the potential repository horizon is calculated by multiplying the total eruptive volume by $W \cdot R \cdot F$, where W is the wall-rock fraction, R is the fraction of the xenoliths originating from the potential repository horizon, and F is the portion of the dike that contributes to the waste entrainment within the potential repository. Table 5-1 presents the assumed distributions for these parameters. The distribution for wall-rock fraction is presented in Figure 5-5. Once the fraction of the eruptive volume that originated from the potential repository is calculated, the fraction of the potential repository moved to the accessible environment is known. This fraction is then multiplied by each of the radionuclide inventories to obtain the total release to the accessible environment.

5.1.2 RIP Analysis

The integrated performance assessment code RIP was used to simulate volcanic intrusions for comparison to the results reported in the TSPA-1991 report (Barnard et al., 1992). RIP allows for the input of one or more user-definable event scenarios that can disrupt waste packages and move them as a whole or fraction to anywhere in the system, including the accessible environment. For comparison to the TSPA-1991 volcanic event scenarios, two different types of volcanic events were specified (corresponding to methods 1 and 2 of TSPA-1991) with annual probabilities and the declaration that a number of waste packages would be moved to the accessible environment once an event was realized.

The RIP analysis used the data and method setup described in the TSPA-1991 report with two exceptions. First, the actual probability of a volcanic event disrupting the potential repository was included as part of the RIP simulation instead of as a post-processing step. The annual probability used was 2.4×10^{-8} which corresponds to a 10,000 year probability of 2.4×10^{-4}.

This annual occurrence allows approximately 0.2 events to occur for 1,000 realizations over 10,000 years. Therefore, it is unlikely that any event would occur in 10,000 years if only 1000 realizations are used, and a larger number of realizations, resulting in greater computer usage time, would be required. To eliminate this problem, the importance sampling or pruning option in RIP that allows for the increased sampling of a low probability event was implemented as described below.

The importance sampling option allows for the number of event realizations simulated to be greater than the expected number of events, based strictly on the actual probability of occurrence. The event scenario is allowed to occur at a higher frequency than expected, with the event consequences adjusted to represent releases due to the actual probability of occurrence. Therefore, the consequences of a low probability event can be better defined without having to conduct simulations that require a very large number of realizations (Miller et al., 1993).

The second item that is different from the TSPA-1991 methodology is the calculation of the dike length in method 1. In RIP, the dike length uniform distribution was set to range from 0.0 to 3.5 km. The upper limit of 3.5 km was taken to be the maximum width of the repository as measured approximately north to south from Figure 5-5. The dike orientation was not incorporated into the RIP problem structure. The method of determining the dike length within the repository based on dike orientation, as was done in the TSPA-1991 report, could not be incorporated into RIP. However, since the mean of the dike orientation follows nearly the long axis of the potential repository, the modified dike length distribution should correctly represent the possible variance in the dike length.

Figure 5-6 presents the RIP input distribution for the dike width used in method 1. Figure 5-7 presents the RIP input distribution for the wall-rock fraction used in method 2.

The event scenarios set up in the RIP data sets followed the TSPA-1991 parameters except for the mentioned differences. The event specification in RIP allows the user to define functions that can sample the stochastic parameters and determine the volume of the potential repository and thus the radionuclide inventory that is moved to the surface per realization. This inventory volume is then converted to determine the total number, either whole or fractional, of waste packages moved directly to the accessible environment. The simulation time at which the event occurs is determined by the annual probability of occurrence of 2.4×10^{-8}.

5.1.3 Results

In the TSPA-1991 and RIP analysis, 1,000 realizations of 10,000 years in length were conducted to determine the probability of total normalized release to the accessible environment at Yucca Mountain due a to volcanic intrusion event. The performance measure that will be used for the comparison of TSPA-1991 and RIP simulations is the cumulative probability versus the total normalized release to the accessible environment.

The TSPA-1991 results for the normalized total release to the accessible environment due to method 1 and method 2 are presented in Figure 5-8. These results were then multiplied by the actual probability of occurrence of 2.4×10^{-4} per 10,000 years to obtain Figure 5-9. Figure 5-8 shows that even without the inclusion of the probability of occurrence, the conditional normalized

total release to the accessible environment from this event does not exceed the maximum EPA limits.

The RIP results for both methods are presented in Figure 5-10. The RIP results match well with TSPA-1991 except at a cumulative probability below 5 x 10^{-6}. This is a result of several RIP realizations having an event that occurred at 100 years (the first time step), resulting in higher releases due to the large inventory of very short-lived radionuclides (^{244}Cm, ^{238}Pu, and ^{137}Cs) that still exist at this early time. If a minimum event occurrence time limit of slightly greater than 100 years could be simulated with RIP, the results would follow those presented in TSPA-1991 more closely.

The effect of several parameters on the release of radionuclides to the accessible environment were examined by the use of scatter plots. For method 1, Figures 5-11 and 5-12 present the effect on the total normalized release to the accessible environment for the dike length and the erosion depth, respectively. Figure 5-11 shows that as the dike length increased, the overall release increased. This trend is as expected. The majority of the releases are at a normalized value of zero. These are the realizations in which an event did not occur. Figure 5-12 presents the ranges of release for a change in the erosion depth and it is also trending as expected.

For method 2, the values of the eruptive volume, wall-rock fraction, and fraction of dike in the potential repository were compared against the determined release value for each realization in Figures 5-13, 5-14, and 5-15, respectively. From these figures it is shown, as expected, that as the volume of an eruptive event increases, the fraction of the wall rock included in the volume increases, or the percentage of the potential repository intruded by the dike increases, the amount of waste transported to the surface also increases.

5.2 HUMAN INTRUSION SCENARIO

5.2.1 Description of TSPA-1991

TSPA 1991 (Barnard et al., 1992) included an analysis of the potential effects that human intrusion might have on the release of radionuclides from a potential repository. The human intrusion scenario to be discussed in this section consisted of the disturbance of a waste package due to exploratory drilling. Once a waste package was disturbed, the contents were instantly moved to one of two saturated aquifers underneath the potential repository and then transported to the accessible environment through the aquifer. While TSPA-1991 also simulated the release of radionuclides to the surface from a human intrusion (drilling) scenario, this was not conducted with RIP, as it would not greatly enhance the comparison of RIP with TSPA-1991. This section summarizes the TSPA-1991 data and methodology used in describing the human intrusion scenario. All information in this section was obtained from the TSPA-1991 report.

As in the volcanic intrusion scenario, the probability of an event actually occurring was determined in TSPA-1991. Based on the pattern and methodology of modern-day exploratory drilling, it was assumed that approximately 17 boreholes would be drilled within the potential repository boundaries over a 10,000-year period. The probability that one of the 17 boreholes would actually intersect a vertically emplaced waste package was determined to be 0.113, based on the ratio of the area of the waste package relative to the area of the repository (Barnard et al., 1992).

TSPA-1991 considered the release to the accessible environment through the aquifers based on a waste package being disturbed in each of 1000 realizations. The actual probability of a release was then calculated by multiplying these results by the probability of occurrence (0.113). The TSPA-1991 simulations allowed one waste package to be disturbed at some random time throughout a 10,000 year simulation and moved to the saturated aquifer.

The radionuclide inventories used in the human intrusion scenario are listed in Tables 4-1 and 6-4 of the TSPA-1991 report. The radionuclides selected were the only nuclides assumed to have any potential of release to the accessible environment. Other radionuclides were not considered due to either their short half-life, high sorption, and/or low inventory.

The two aquifers beneath the potential repository are a tuff aquifer and a lower carbonate aquifer (see Section 3.1.1). The release of radionuclides to the two aquifers were handled in two different sets of simulations, due to the differing flow and transport properties of the aquifers. Once a waste package was moved to the aquifer, the radionuclides were transported 5000 m to the accessible environment. The main attenuation factor the aquifer provides to the transport of the nuclides is sorption onto the surface of the medium. To approximate this mechanism, the distribution coefficient (K_d) ranges for each of the nuclides were determined for both aquifers. Tables 5-2 and 5-3 present the K_d distributions based on the two different aquifer types. The nuclides were divided into five or six different groups based on their similar distribution characteristics.

The flow and transport simulations for the human intrusion scenarios were performed using the one-dimensional, time-dependent groundwater flow and solute transport code TOSPAC. Table 5-4 presents the constant values and the mean values from stochastic distributions of the parameters used in the flow and transport simulations.

The human intrusion scenario consisted of the movement of a waste package to the saturated zone at a random time. The nuclides were then placed in the ground-water flow field and transported down gradient to the accessible environment 5000 m away. The distribution of releases to the accessible environment for 1000 realizations were then normalized to the EPA limits for total releases and for individual radionuclide releases, and multiplied by the probability of occurrence (0.113) to obtain the final probability distribution of cumulative releases to the accessible environment over a 10,000-year period.

5.2.2 RIP Analysis

The integrated performance assessment code RIP was used to simulate the human intrusion scenarios for comparison to the results reported in TSPA-1991 (Barnard et al., 1992). RIP allows for the input of one or more user-definable event scenarios that can disrupt waste packages and move them to anywhere in the system. For comparison to the TSPA-1991 human intrusion scenarios, two different events were specified with annual probabilities and the declaration that a single waste package would be moved to the saturated zone once an event was realized.

An event parameter in RIP was designated for the movement of a waste package to the saturated zone. The event parameter specification in RIP allows for the actual annual probability of occurrence to be input, therefore no post-processing of the results needs to be performed to obtain the actual distribution of cumulative releases. An annual probability of 1.13×10^{-5}, which

corresponds to a probability of 0.113 per 10,000 years, was input for the human intrusion scenarios. As in the TSPA-1991 simulations, 1,000 realizations were used to define the CCDF. For 1,000 realizations and the assumed annual probability, approximately 113 events would occur. Using the importance sampling feature in RIP (Section 5.1.2), a pruning factor of 10 was applied to the non-event samples. This resulted in a CCDF that represented approximately 800 events and a total number of 10,000 realizations.

A comparison of the TSPA-1991 and RIP parameters are listed in Tables 5-5 and 5-6, respectively. The saturated zone configuration in RIP consisted of declaring a pathway with a specified flow area, length, flow rate, porosity, longitudinal dispersivity and retardation. The following paragraphs present plots of several parameter distributions used in the RIP analysis which were taken directly from TSPA-1991 (Barnard et al., 1992).

For the tuff aquifer specification, the flow rate was entered as a function based on the stochastic groundwater velocity distribution (Figure 5-16). The porosity and dispersivity values were entered directly as stochastic distributions and are presented in Figures 5-17 and 5-18, respectively. The retardation values for each nuclide were declared as functions based on stochastic distributions of K_d, porosity, and bulk density. Plots of the K_d for uranium and neptunium are presented in Figures 5-19 and 5-20, respectively.

For the carbonate aquifer, the flow rate was also entered as a function based on the stochastic ground-water velocity distribution (Figure 5-21). The porosity and dispersivity values, presented in Figures 5-22 and 5-23, respectively, were entered directly as stochastic distributions. The retardation values for each radionuclide were declared in RIP as functions based on stochastic distributions of K_d, porosity, and bulk density. Plots of the K_d for plutonium, uranium, and neptunium are presented in Figures 5-24 through 5-26.

5.2.3 Results

In the TSPA-1991 and RIP analyses, 1,000 realizations of 10,000 years in length were conducted for the determination of the probability of normalized cumulative release to the accessible environment due to human intrusion. The performance measure that will be used for the comparison of the TSPA-1991 and RIP simulations is the cumulative probability versus the total normalized release to the accessible environment.

The TSPA-1991 results for the total normalized and the individual radionuclide releases to the accessible environment through the tuff aquifer are presented in Figure 5-27. These results still need to be multiplied by the actual probability of occurrence of 0.113 per 10,000 years to obtain the actual distribution. Figure 5-27 shows that even without the inclusion of the probability of occurrence, the conditional normalized total release to the accessible environment does not exceed the maximum EPA limits for this scenario.

Figure 5-28 presents the RIP results for the human intrusion scenario into the tuff aquifer. The actual probability of occurrence is incorporated in these results, yielding a maximum probability of occurrence equal to 0.113. As with the TSPA-1991 results, the maximum releases to the accessible environment do not exceed the EPA limits, either with or without the actual annual probability incorporated. The effect of certain parameters on the magnitude of the total release

to the accessible environment has been examined. Figures 5-29 and 5-30 present scatter plots of normalized total release to the accessible environment versus the ground-water velocity and the longitudinal dispersivity, respectively. These figures show no credible correlation between the magnitude of release to either the ground-water velocity or the longitudinal dispersivity. Figures 5-31 and 5-32 present scatter plots of normalized total release to the accessible environment versus the distribution coefficient for uranium and neptunium, respectively. These figures show that there is a correlation between the magnitude of release to the lower distribution coefficient, and therefore retardation, values for uranium and neptunium.

The TSPA-1991 results for the total normalized and the individual radionuclide releases to the accessible environment through the carbonate aquifer are presented in Figure 5-33. These results also need to be multiplied by the actual probability of occurrence of 0.113 per 10,000 years to obtain the actual distribution.

The RIP results for the human intrusion scenario into the carbonate aquifer are presented in Figure 5-34. These results have the actual probability of occurrence incorporated, yielding a maximum probability of occurrence equal to 0.113. As with the TSPA-1991 results, the maximum releases to the accessible environment do not exceed the EPA limits, either with or without the actual annual probability incorporated.

In the results from the human intrusion scenario in the tuff aquifer, six out of a possible twelve radionuclides were released to the accessible environment. However, for the flow and transport in the carbonate aquifer, all twelve of the radionuclides were released to the accessible environment. This can be attributed mainly to the lower porosity and higher velocity in the carbonate aquifer.

The effect of the total releases to the accessible environment from the carbonate aquifer based on several of the input parameter distributions was investigated. Figures 5-35 and 5-36 present scatter plots of the total normalized release to the accessible environment versus realized velocity and dispersivity values. Figures 5-37 through 5-39 present scatter plots of the realized K_d values for plutonium, uranium, and neptunium, respectively. These scatter plots show that the release to the accessible environment through the carbonate aquifer is most sensitive to the K_d values selected.

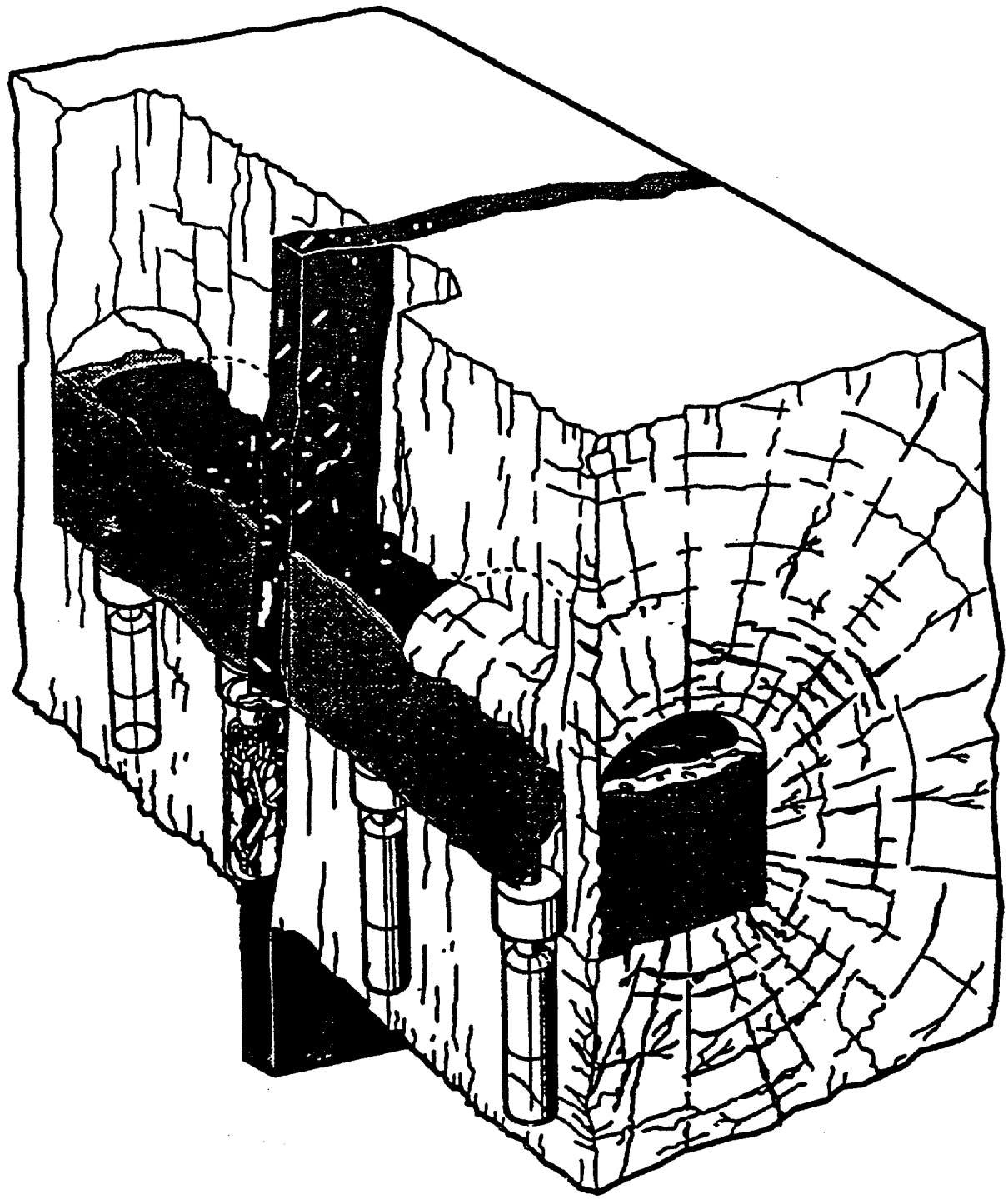

Figure 5-1. Conceptualization of Volcanic Intrusion Interaction with the Repository (taken from Barnard et al., 1992)

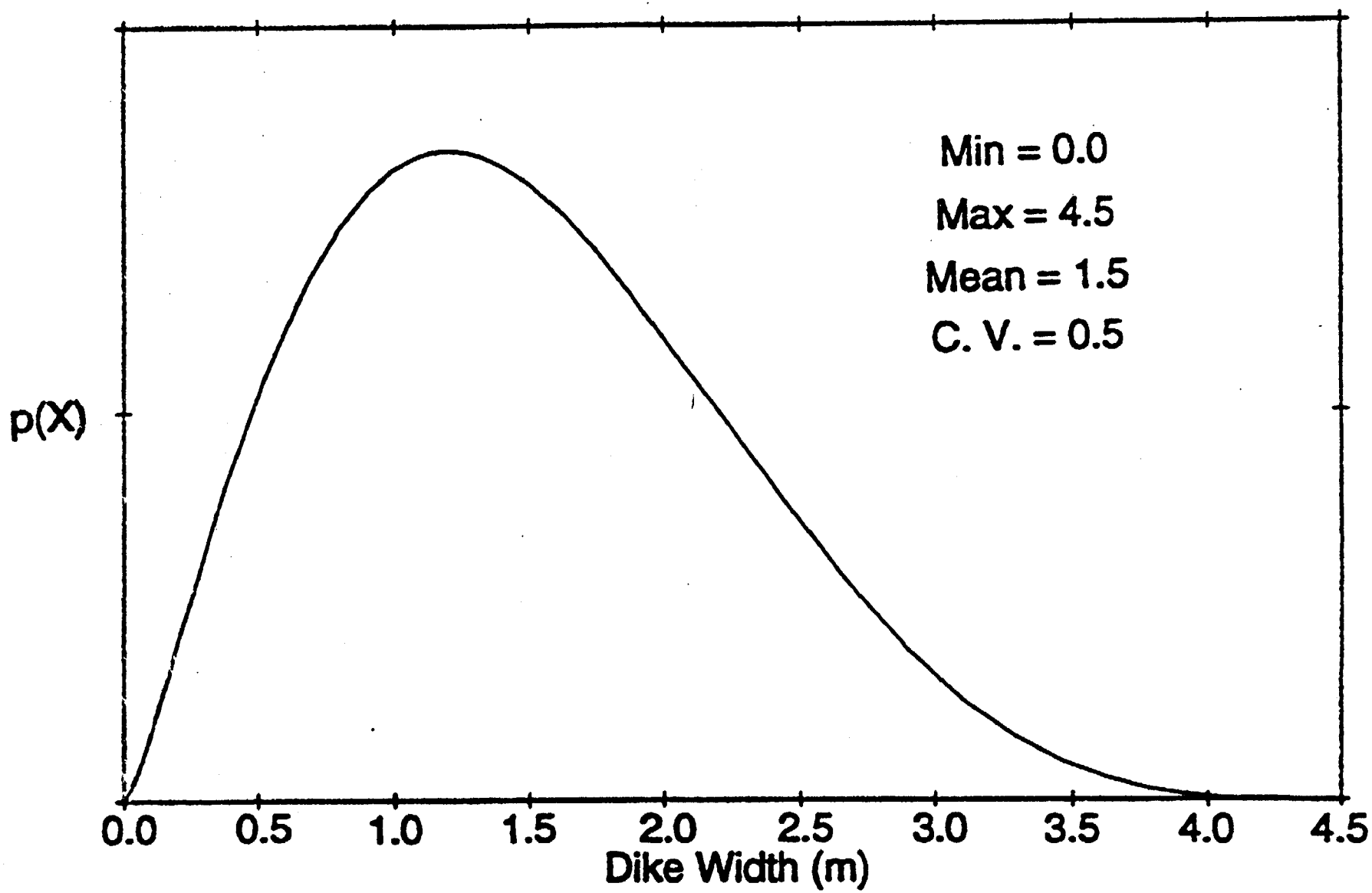

Figure 5-2. Probability Density Function of the Dike Width (taken from Barnard et al., 1992)

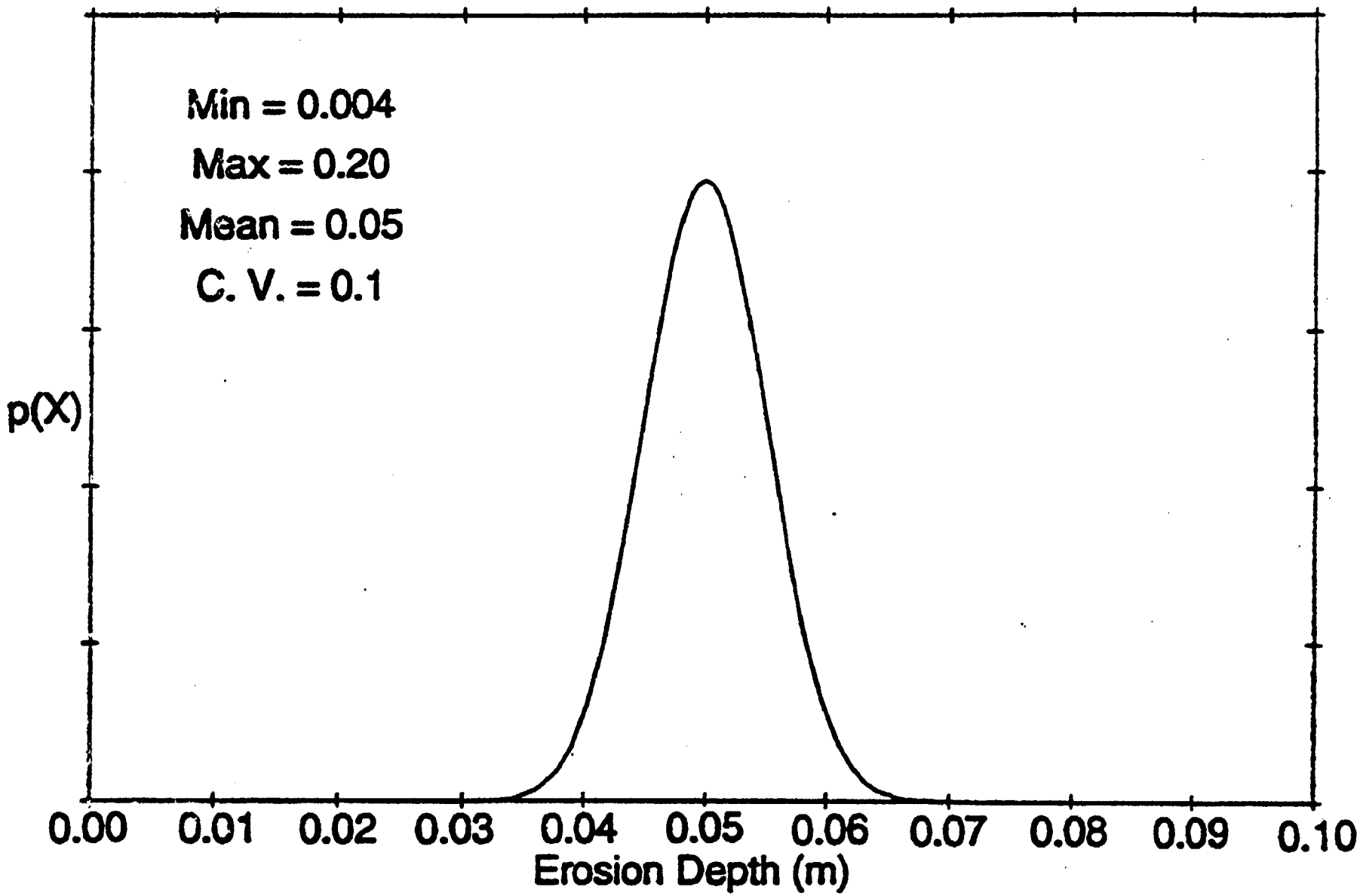

Figure 5-3. Probability Density Function of the Erosion Depth (taken from Barnard et al., 1992)

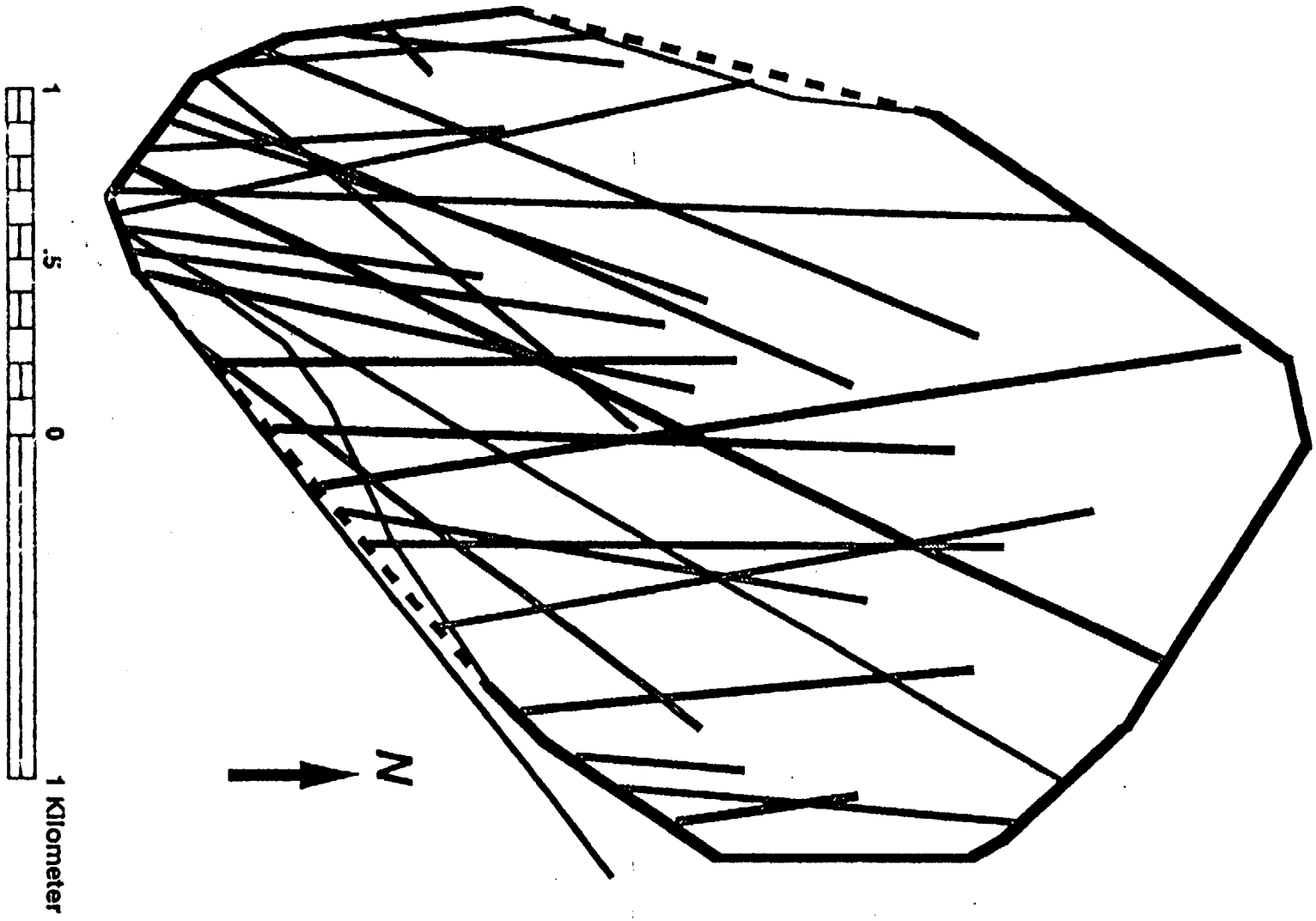

Figure 5-4. Dike Orientation and Length within the Repository for a Selected Number of Realizations (taken from Barnard et al., 1992)

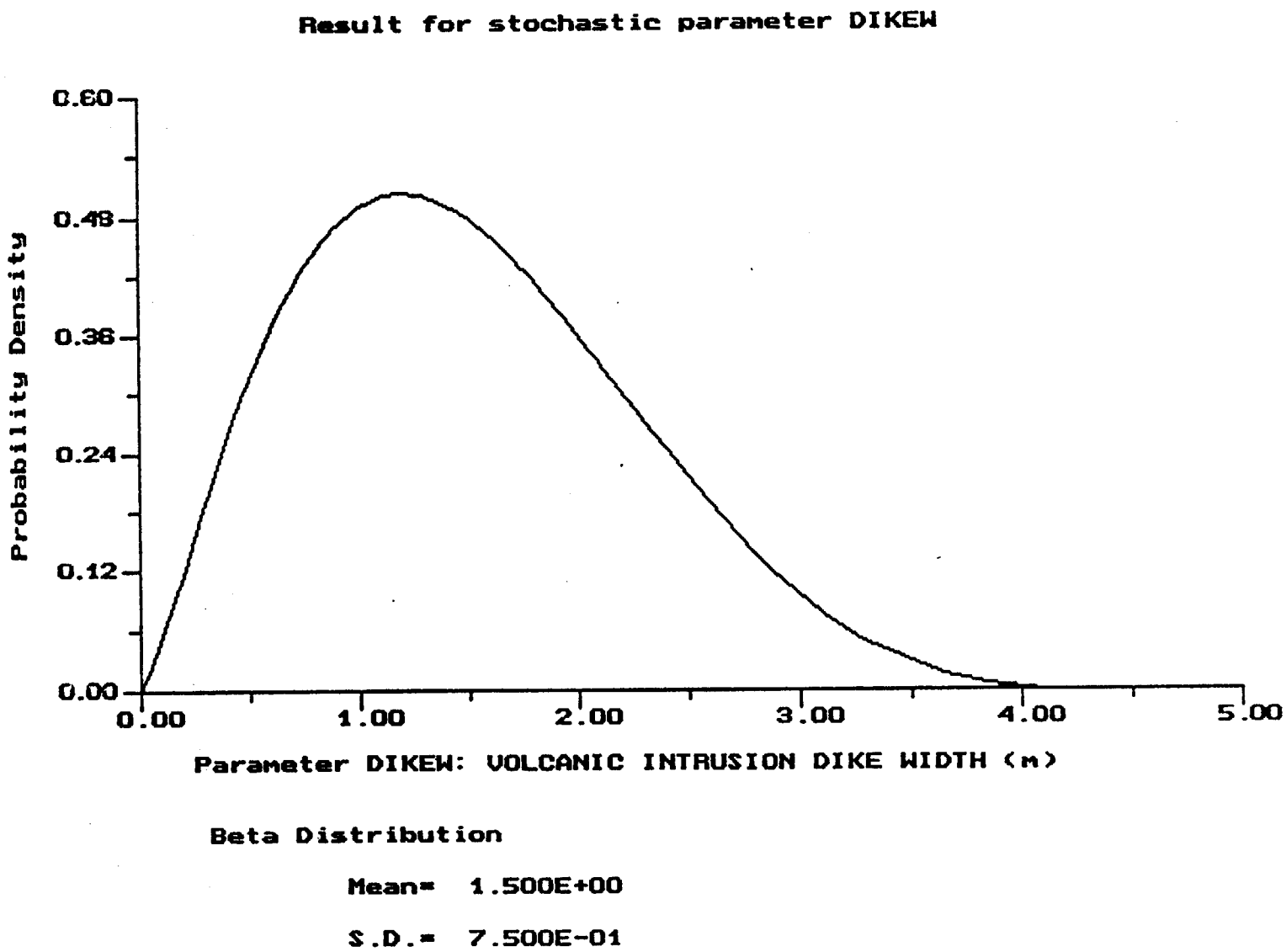

Figure 5-5. Probability Density Function of the Dike Width

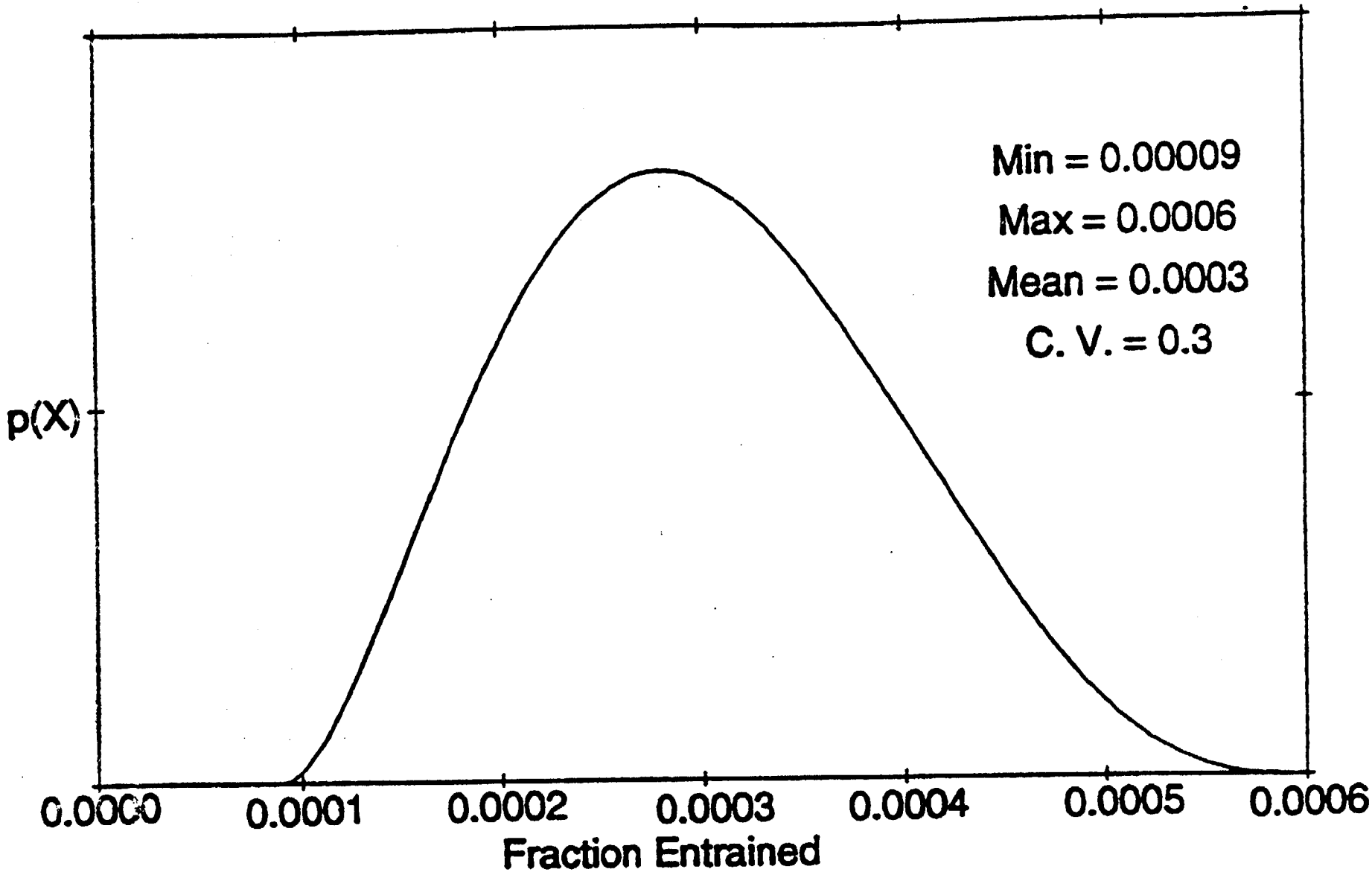

Figure 5-6. Probability Density Function of the Fraction Entrained (taken from Barnard et al., 1992)

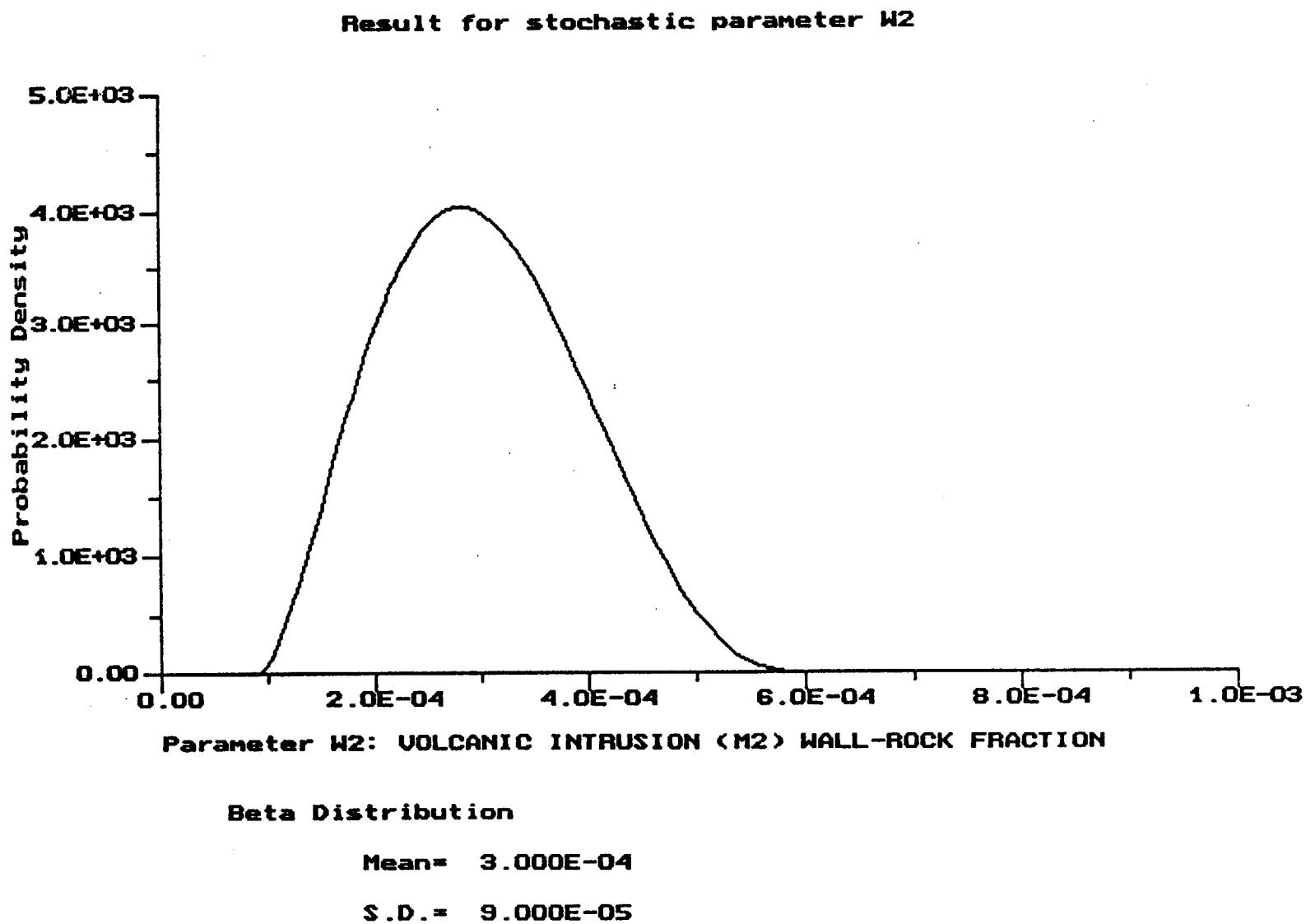

Figure 5-7. Probability Density Function of the Wall-Rock Fraction

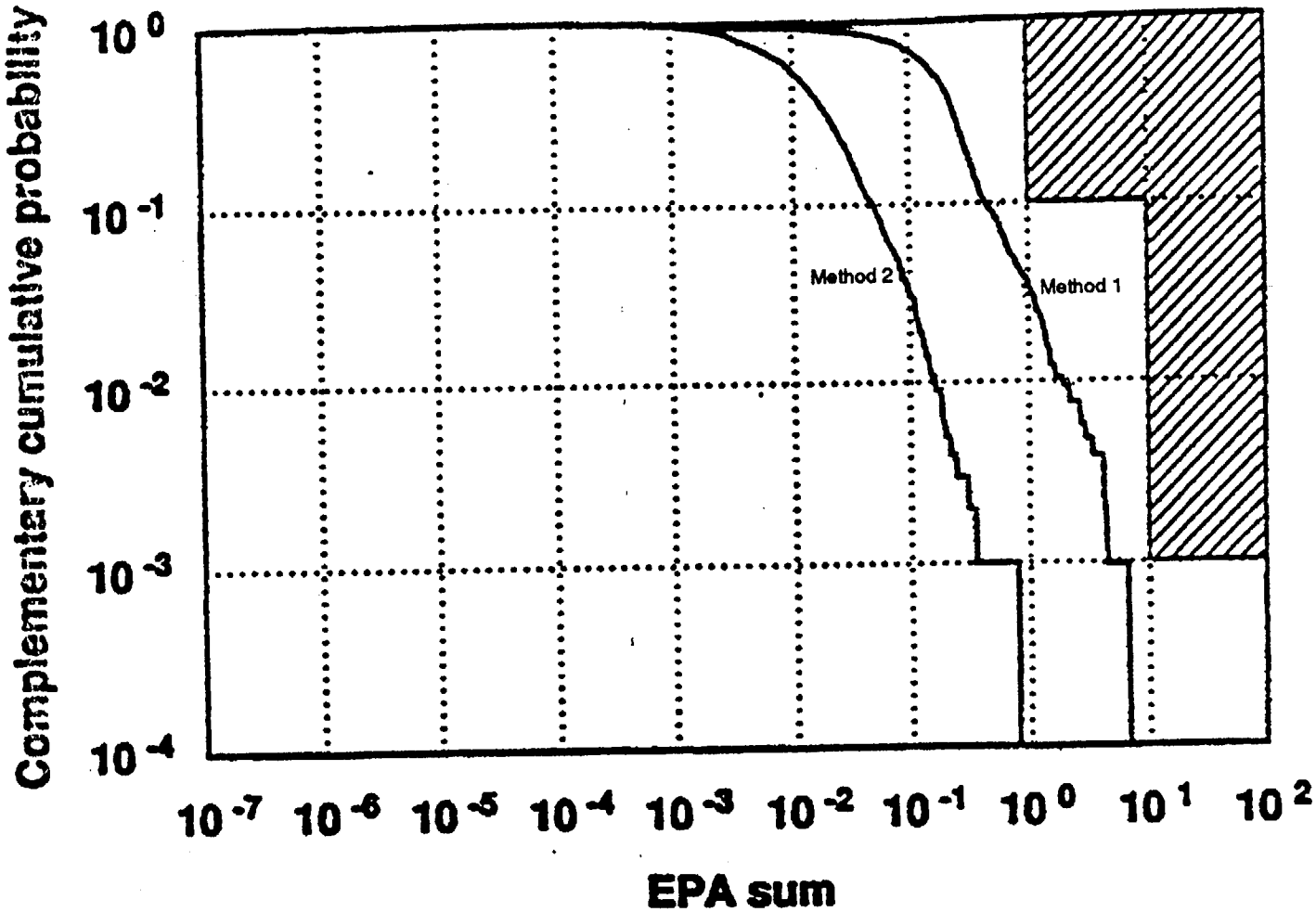

Figure 5-8. Conditional CCDF for Normalized Total Release to the Accessible Environment for Volcanic Intrusion Methods One and Two, Not Including the Probability of Occurrence (taken from Barnard et al., 1992)

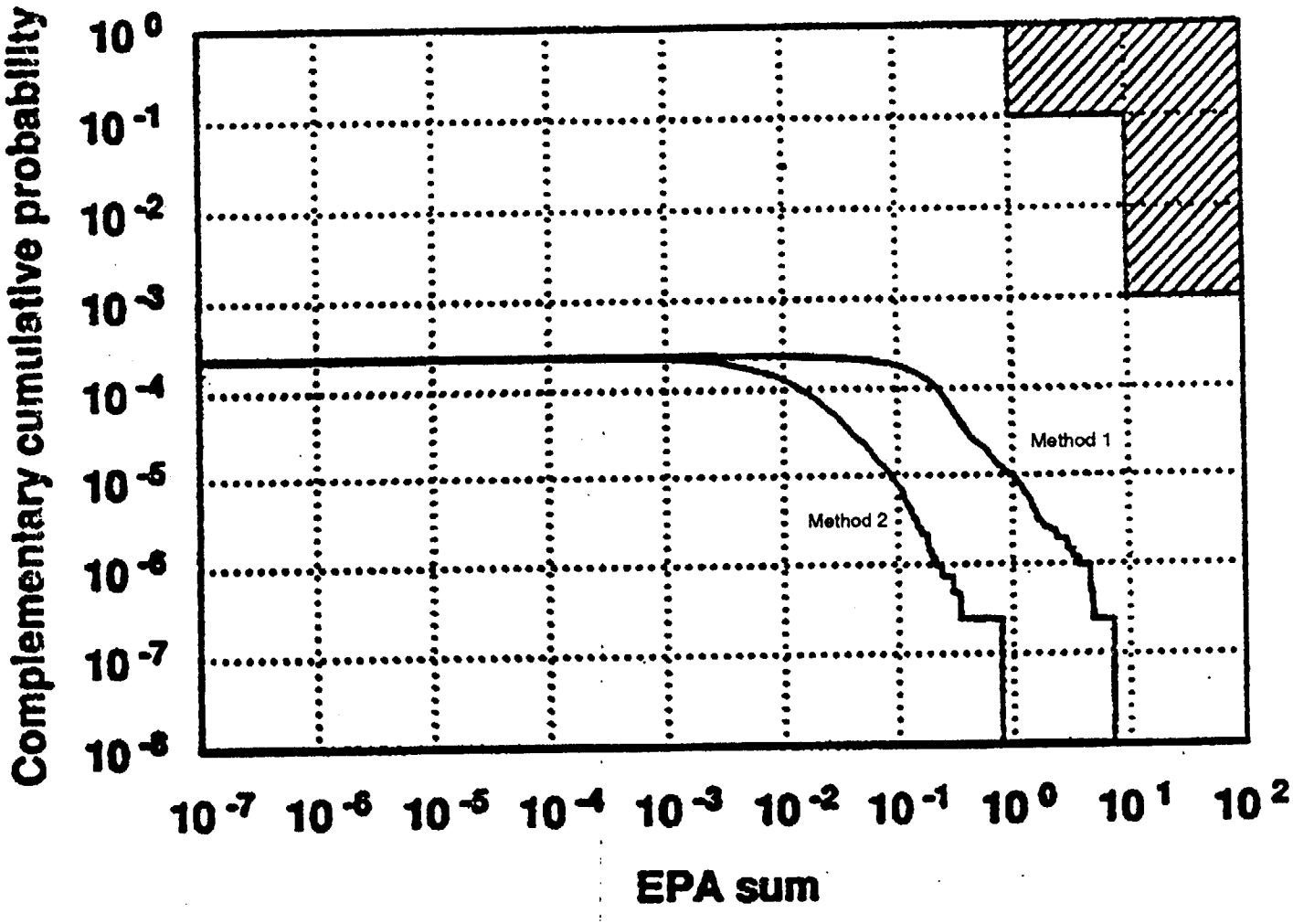

Figure 5-9. Conditional CCDF for Normalized Total Release to the Accessible Environment for Volcanic Intrusion Methods One and Two, Including the Probability of Occurrence (taken from Barnard et al., 1992)

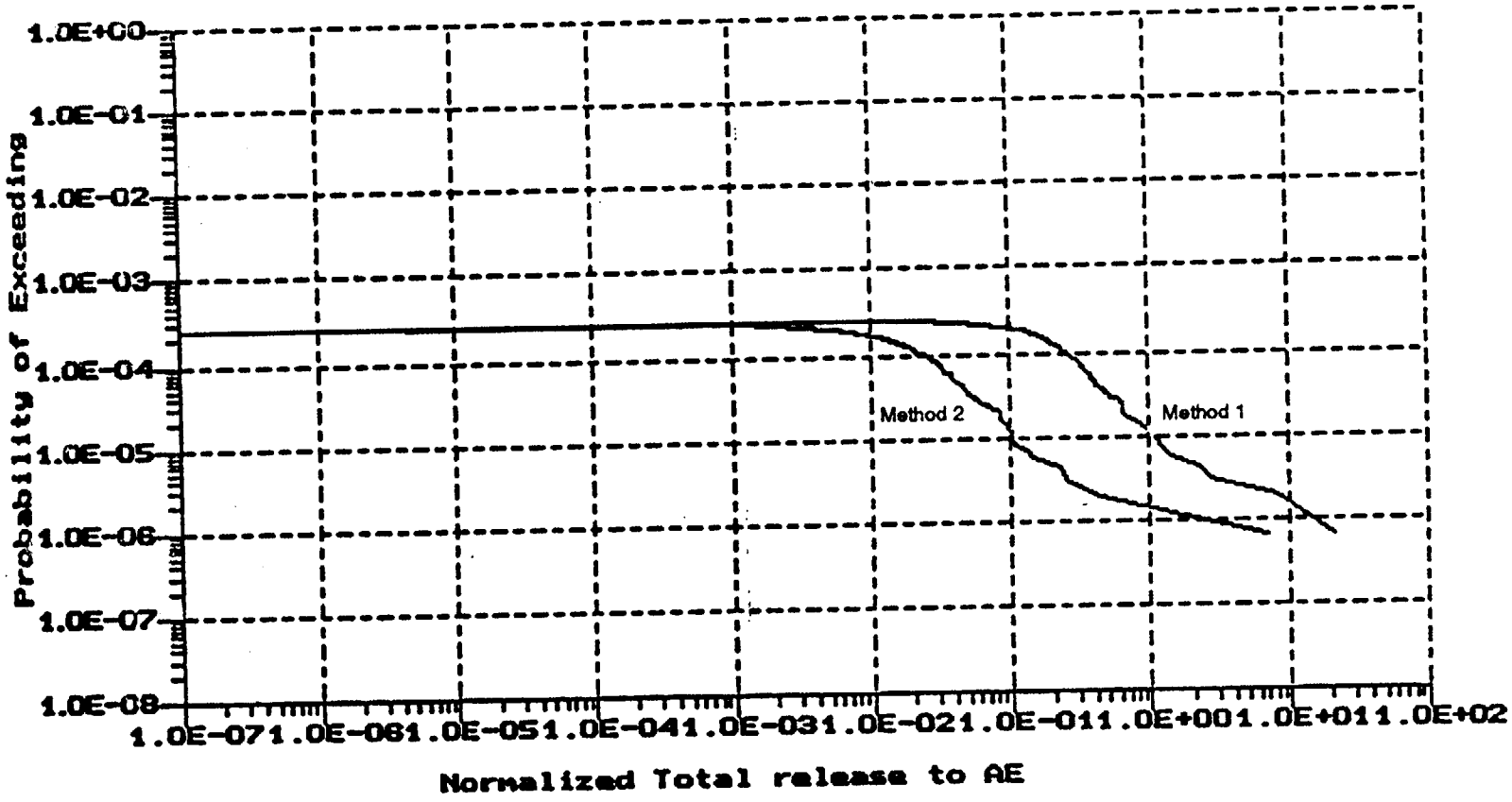

Figure 5-10. RIP Conditional CCDF for Normalized Total Release to the Accessible Environment for Volcanic Intrusion Methods One and Two, Including the Probability of Occurrence

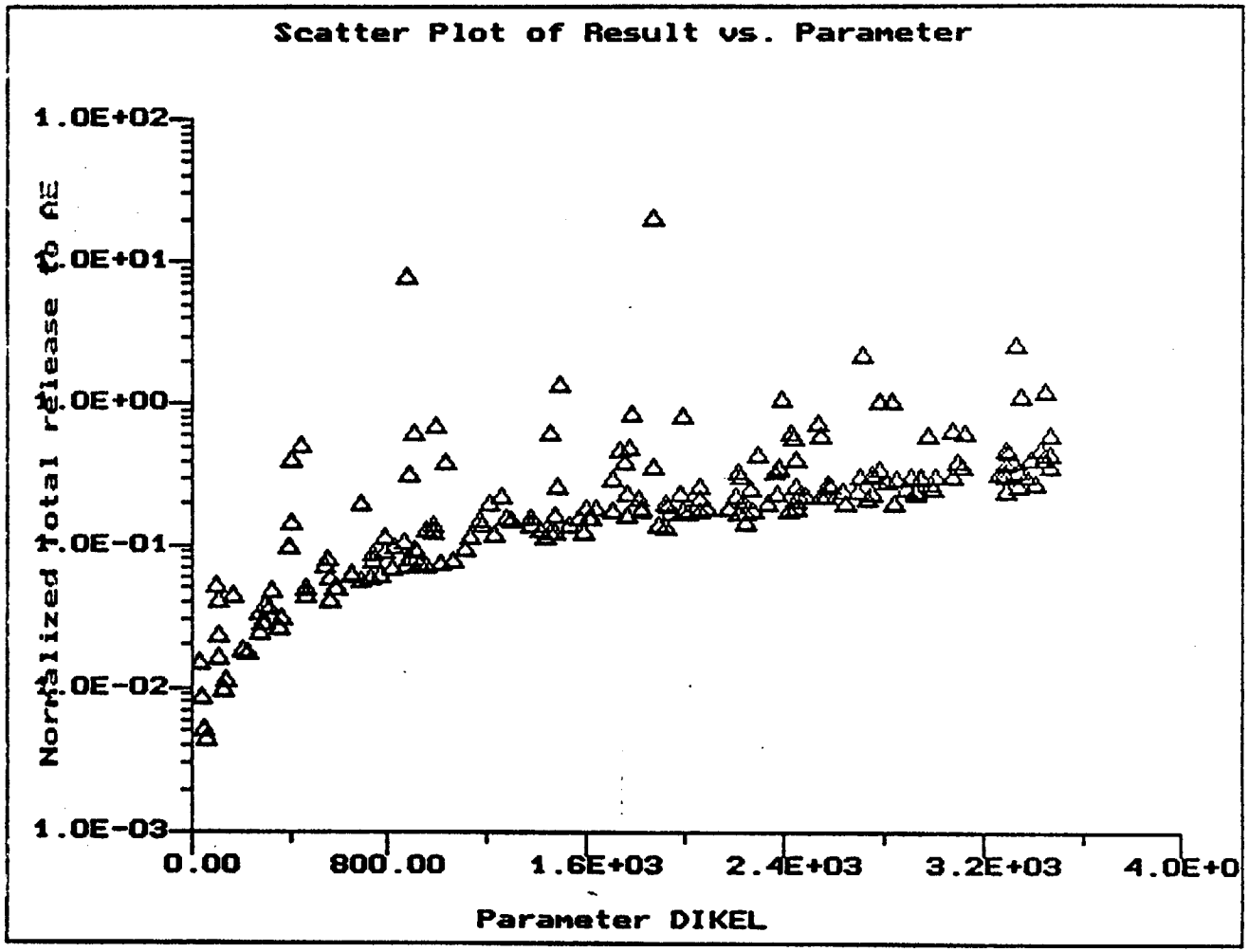

Figure 5-11. Scatter Plot of Dike Length versus Total Normalized Release to the Accessible Environment for Method One

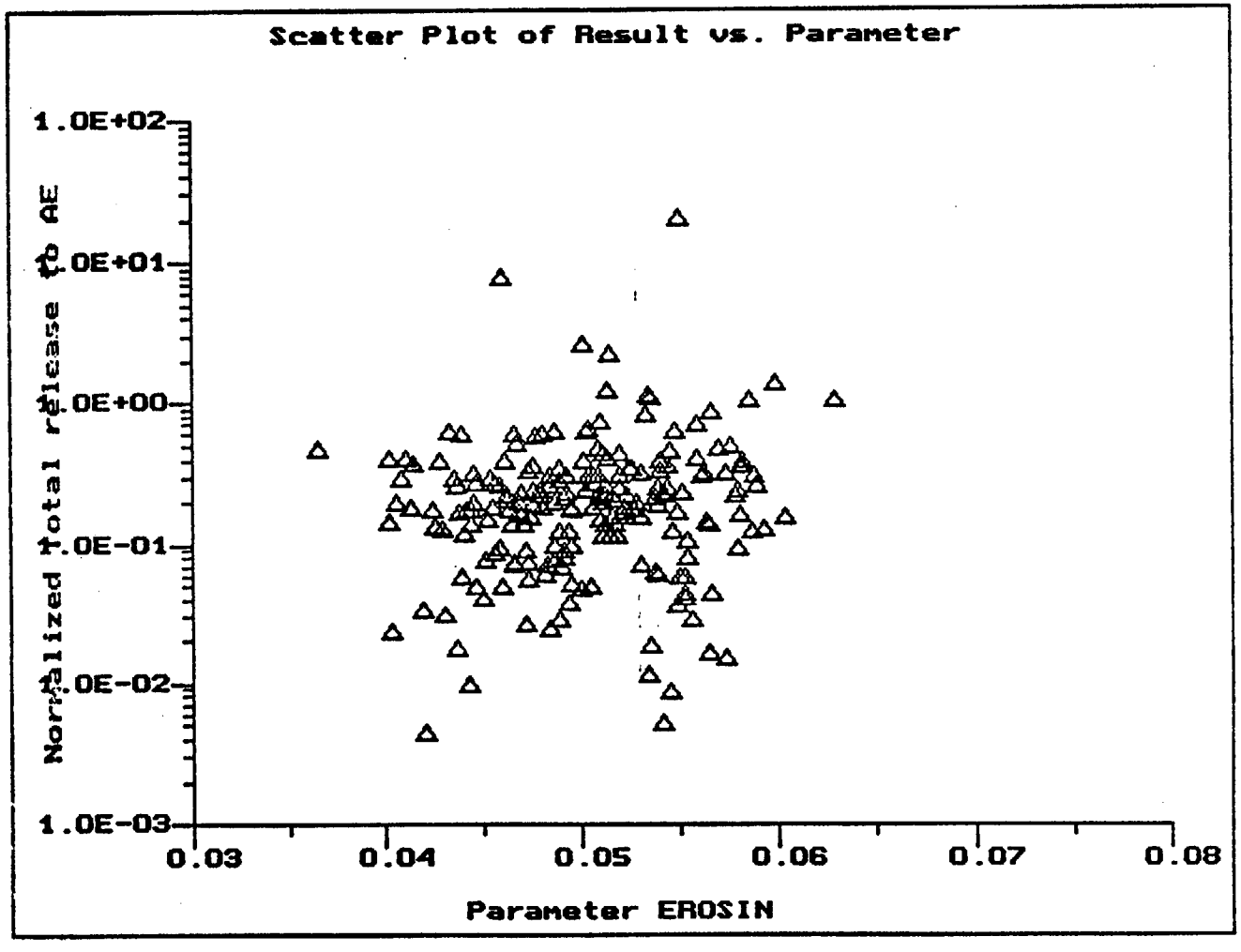

Figure 5-12. Scatter Plot of Erosion Depth versus Total Normalized Release to the Accessible Environment for Method One

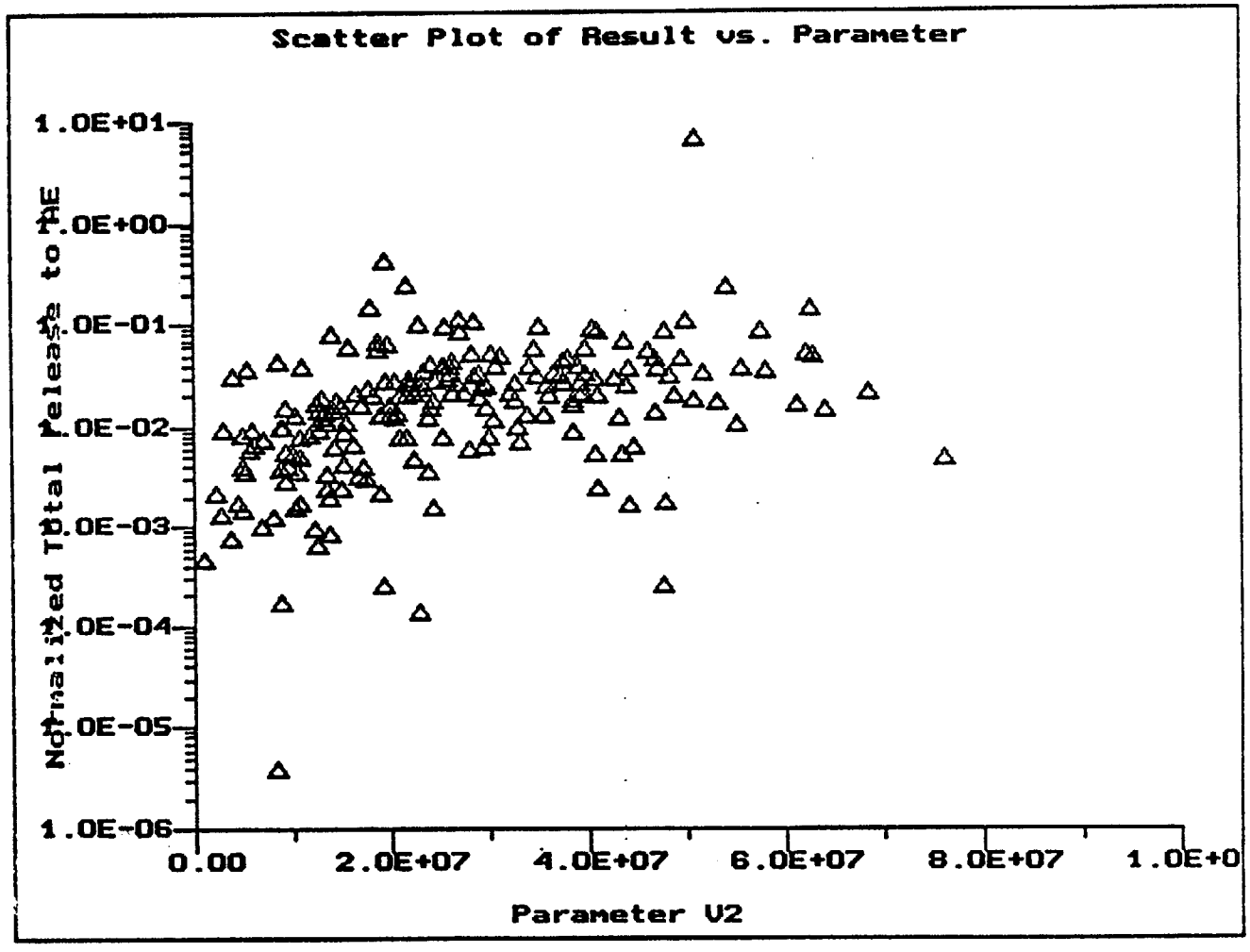

Figure 5-13. Scatter Plot of Eruptive Volume versus Total Normalized Release to the Accessible Environment for Method Two

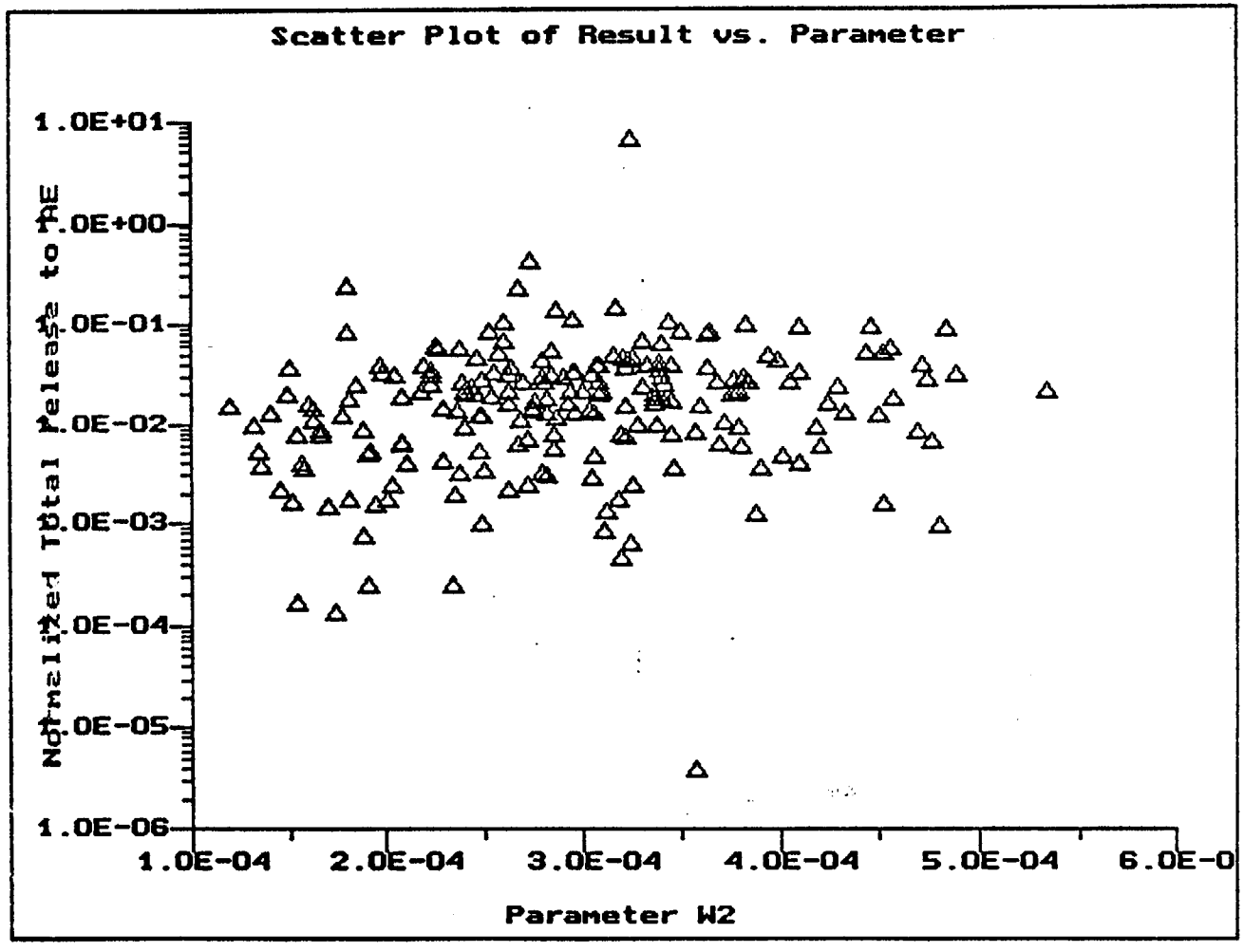

Figure 5-14. Scatter Plot of Wall-Rock Fraction versus Total Normalized Release to the Accessible Environment for Method Two

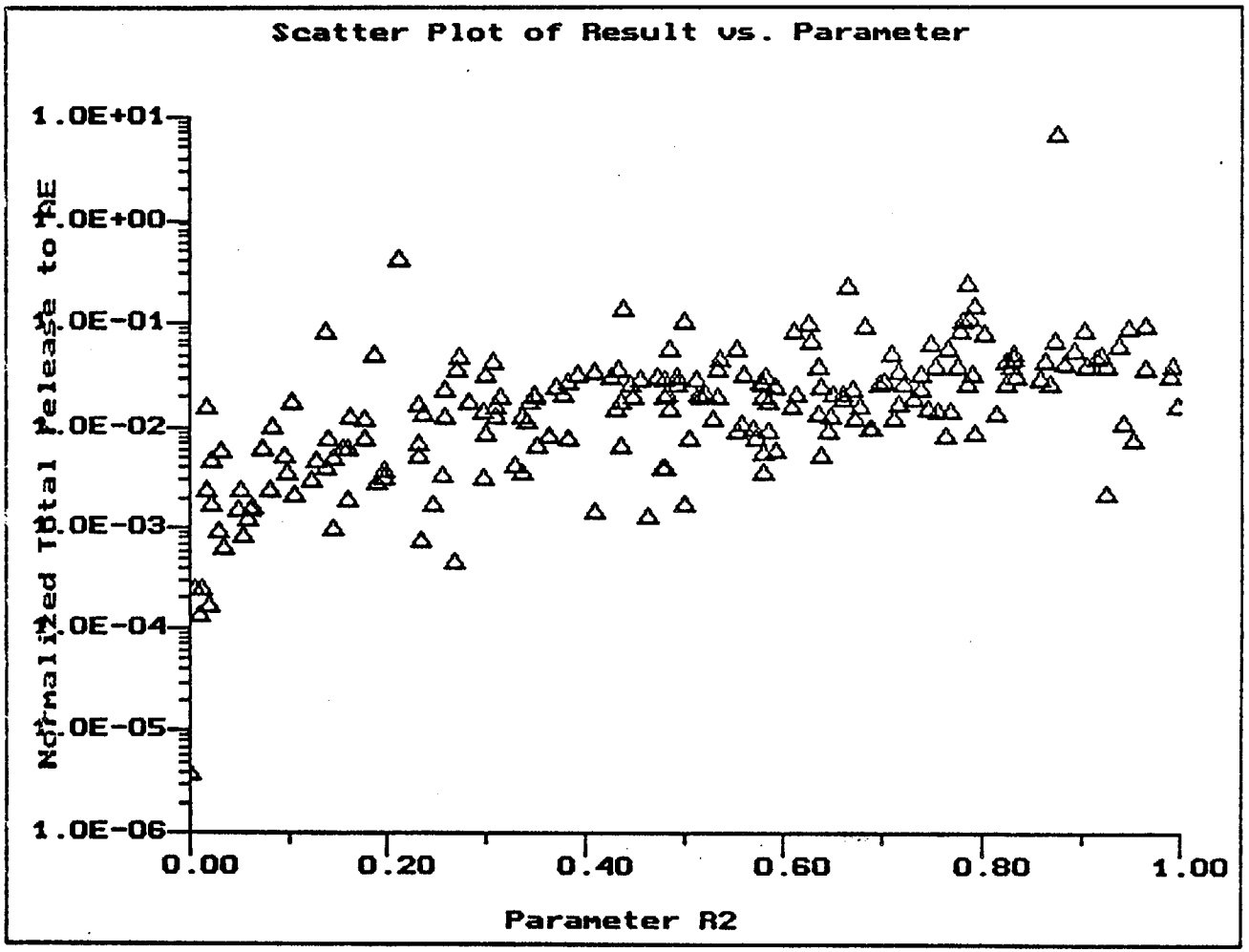

Figure 5-15. Scatter Plot of Fraction of Dike within Repository versus Total Normalized Release to the Accessible Environment for Method Two

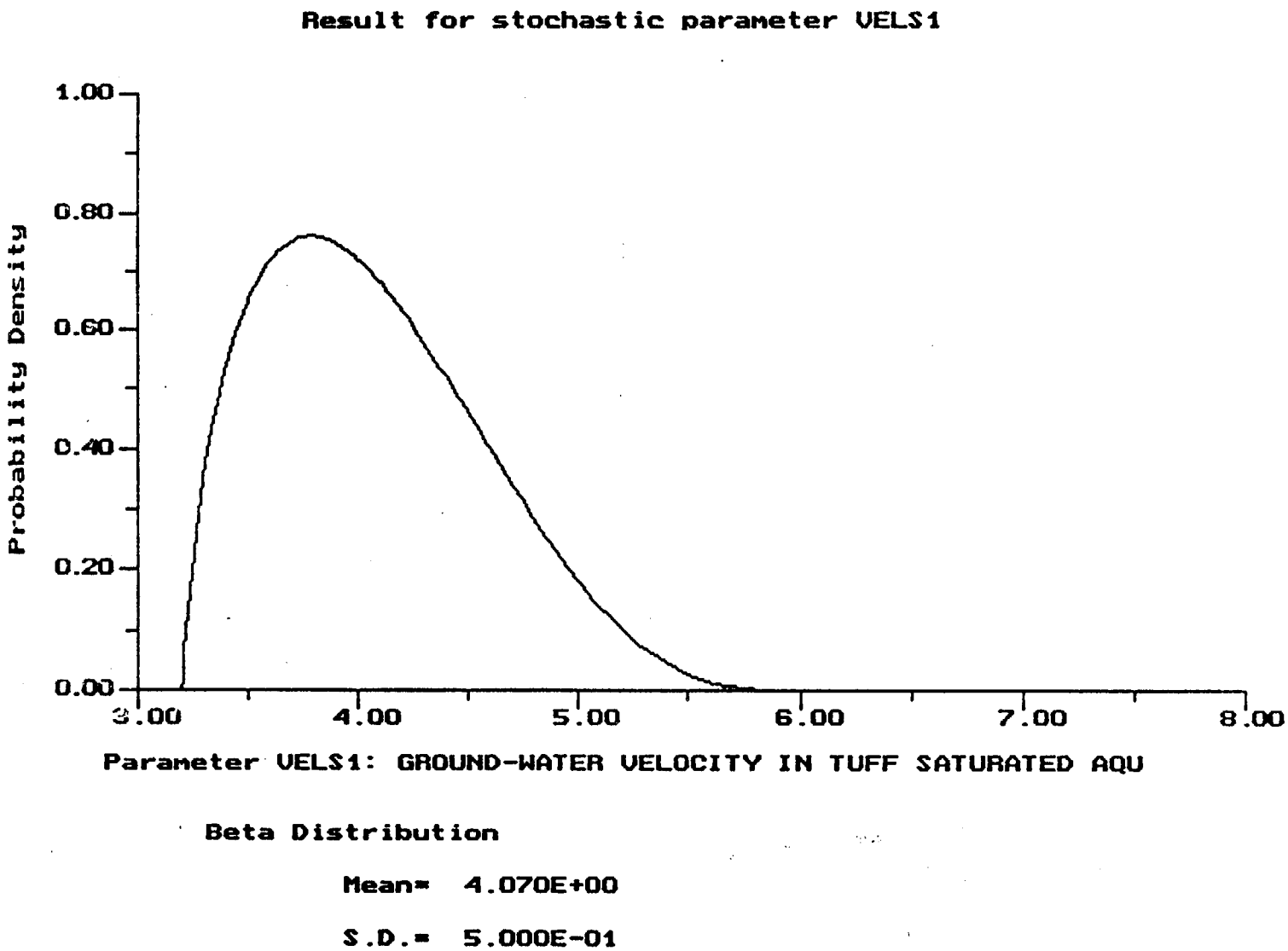

Figure 5-16. Probability Density Function of the Saturated Tuff Ground-Water Velocity

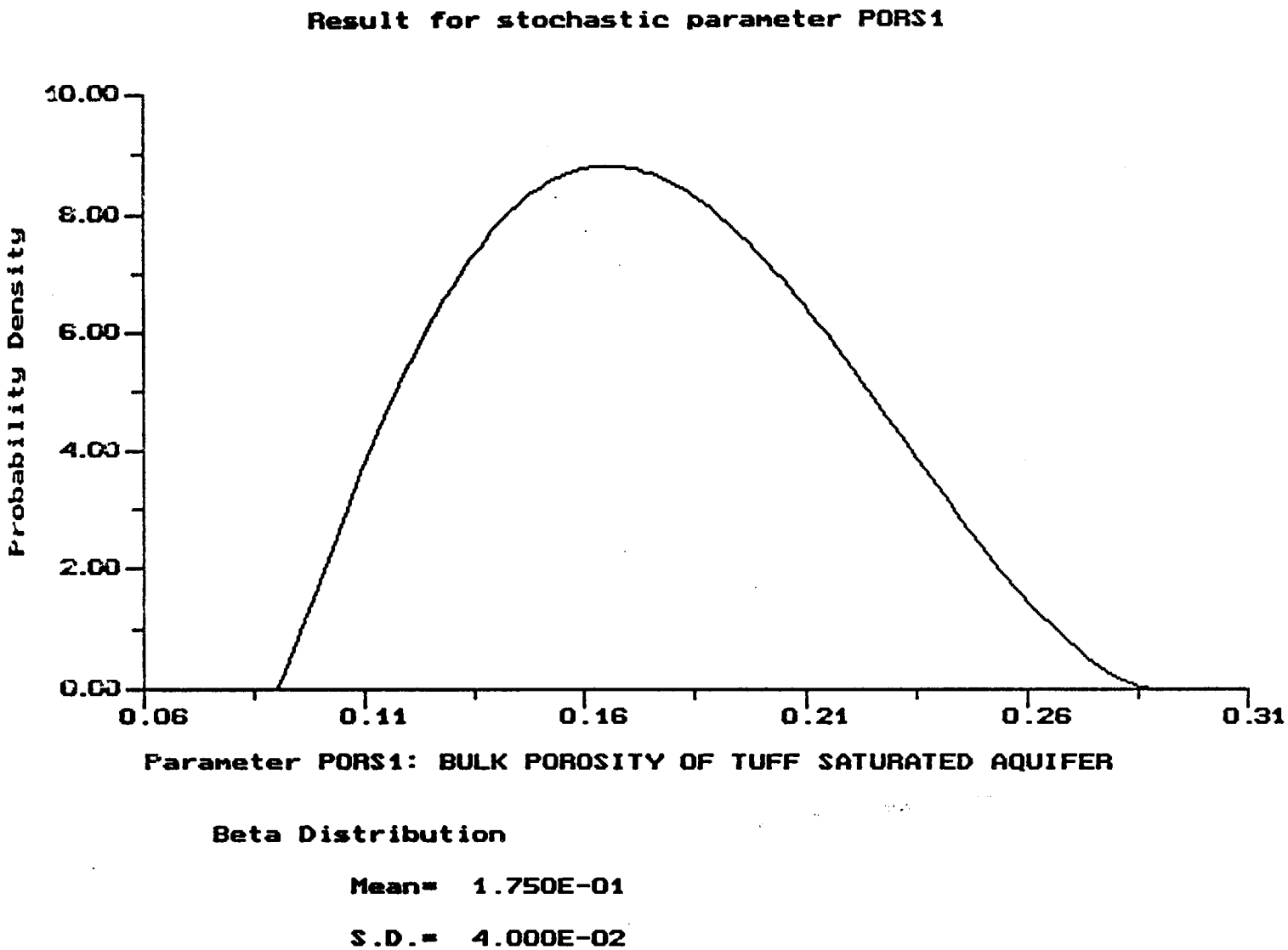

Figure 5-17. Probability Density Function of the Saturated Tuff Bulk Porosity

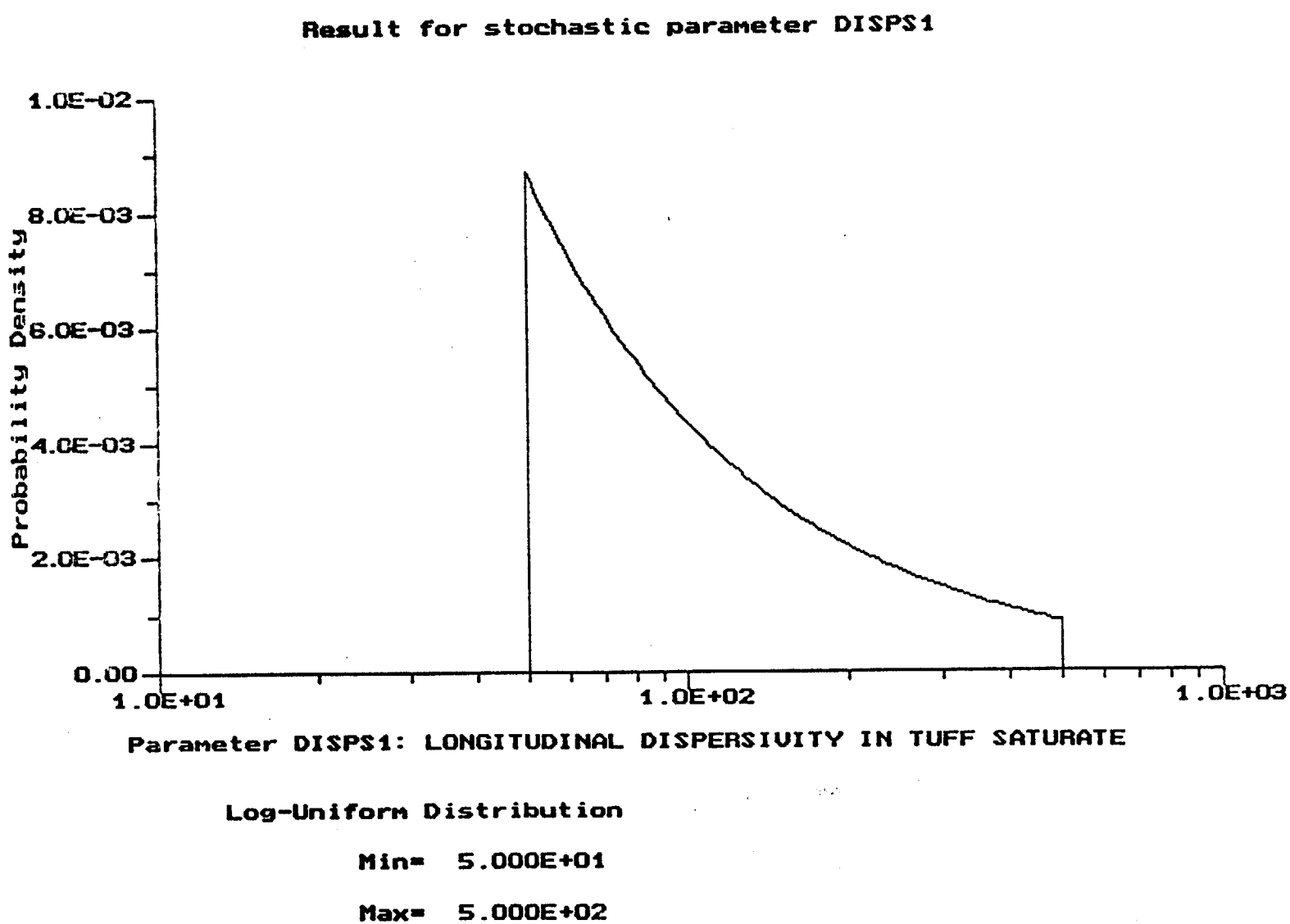

Figure 5-18. Probability Density Function of the Saturated Tuff Longitudinal Dispersivity

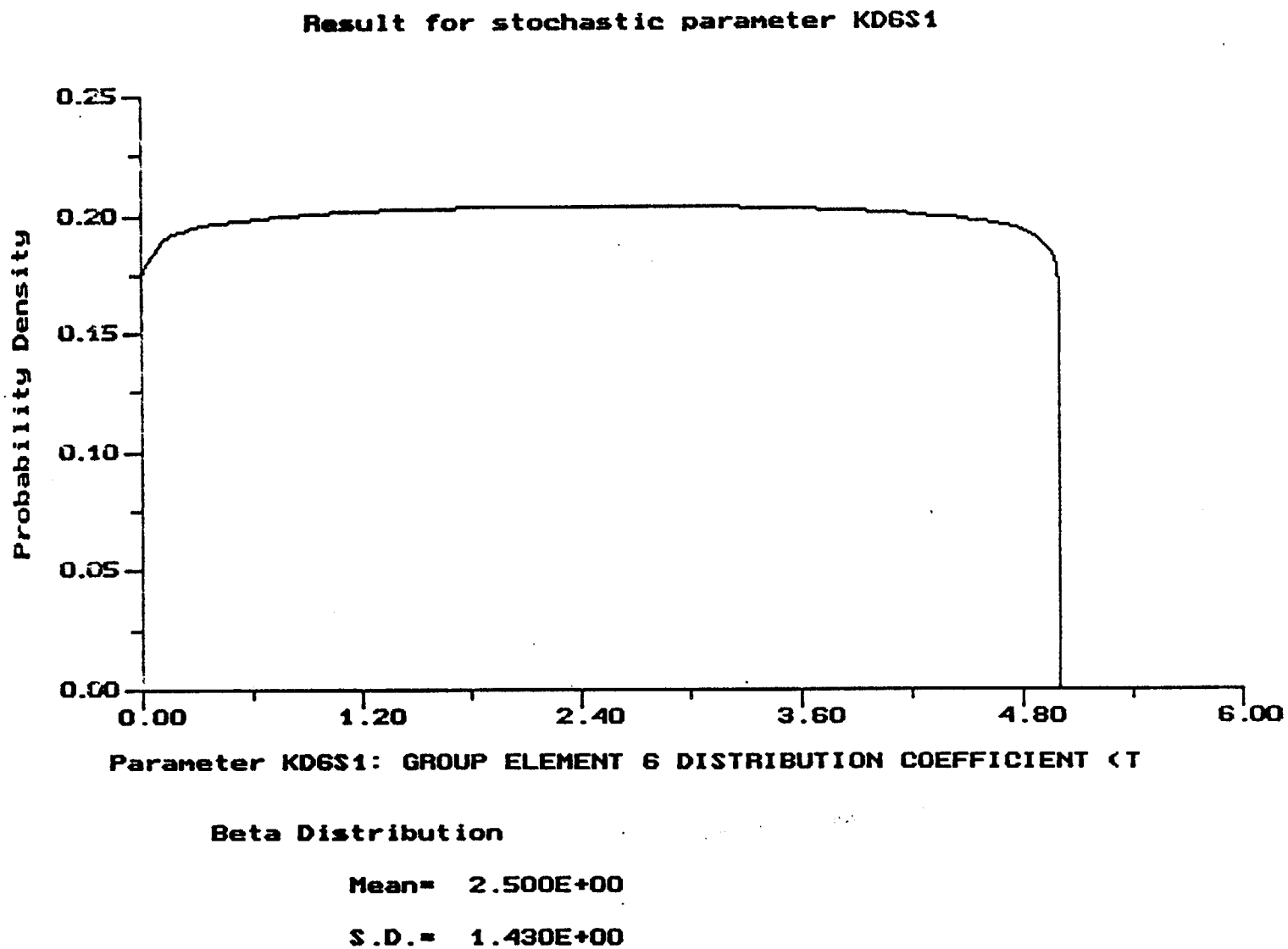

Figure 5-19. Probability Density Function of the Saturated Tuff Uranium Distribution Coefficient

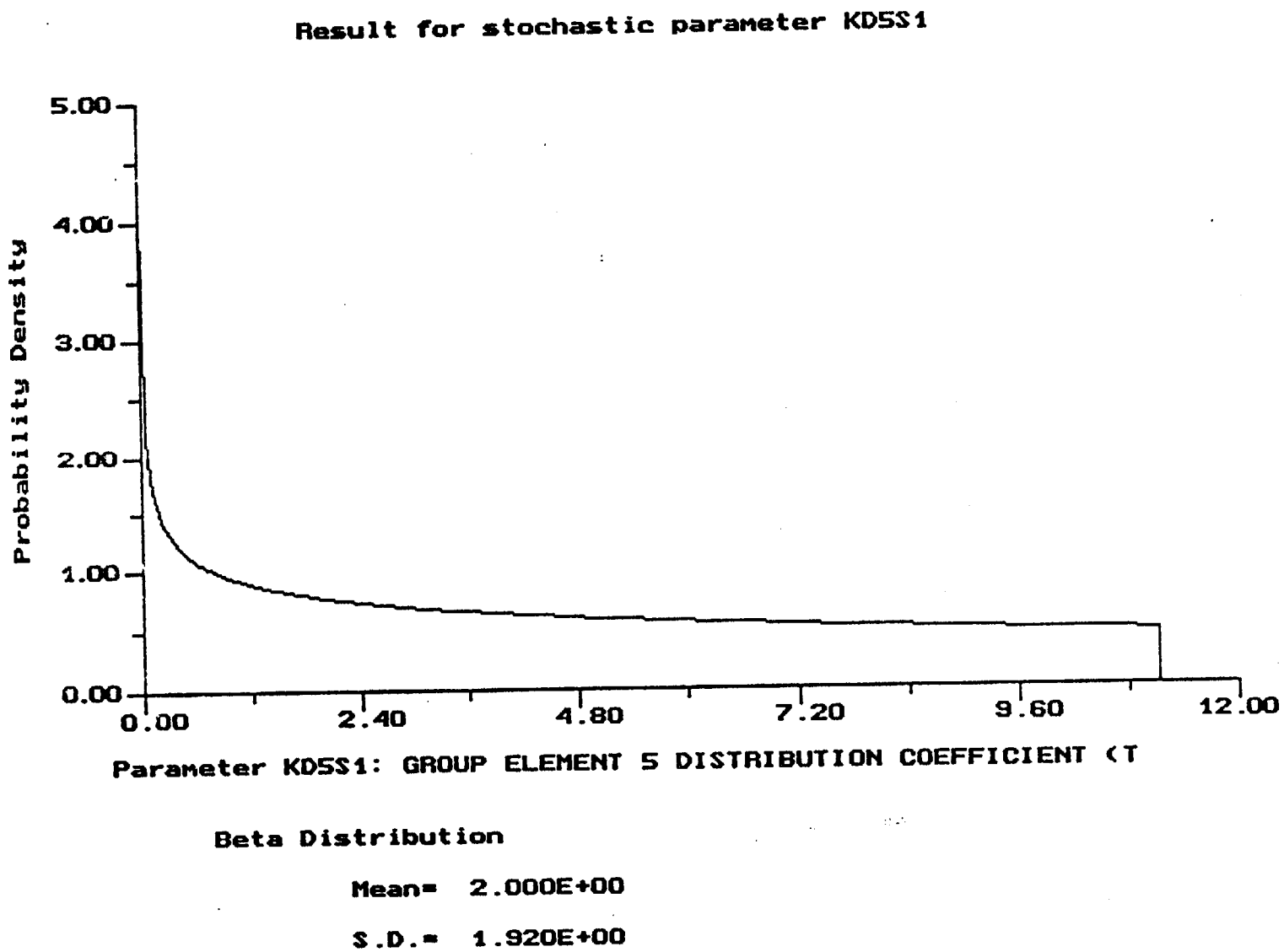

Figure 5-20. Probability Density Function of the Saturated Tuff Neptunium Distribution Coefficient

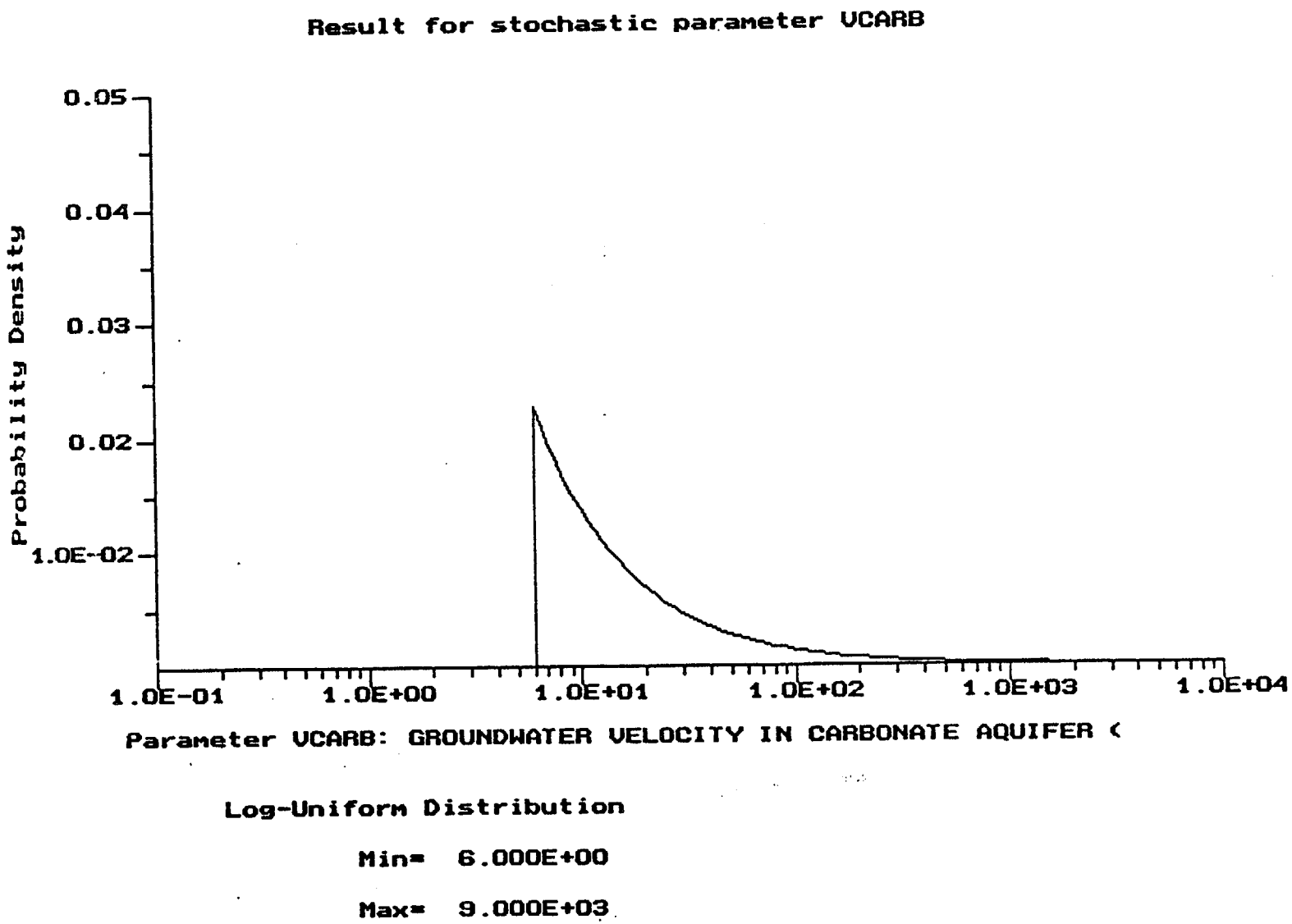

Figure 5-21. Probability Density Function of the Carbonate Aquifer Ground-Water Velocity

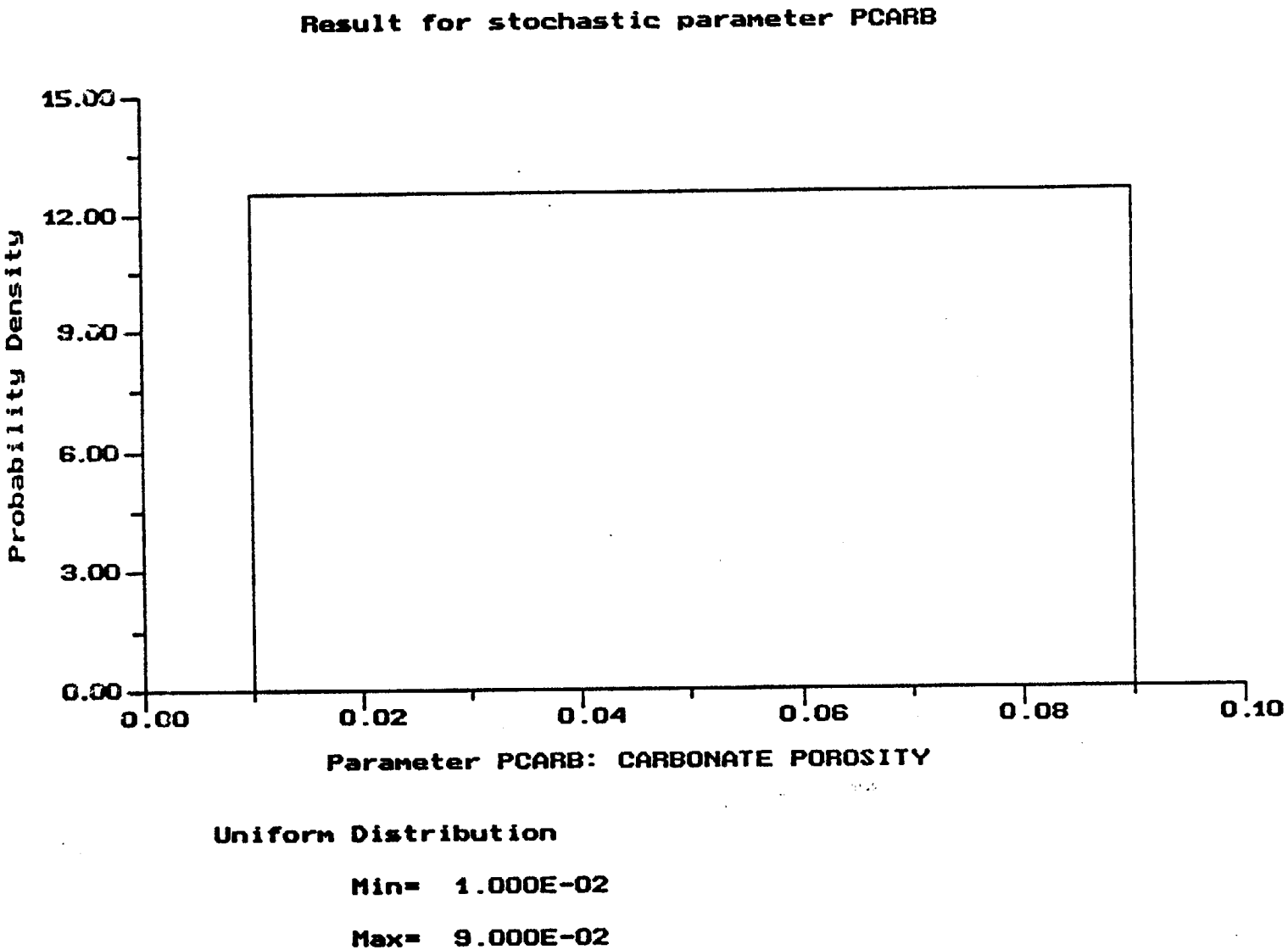

Figure 5-22. Probability Density Function of the Carbonate Aquifer Bulk Porosity

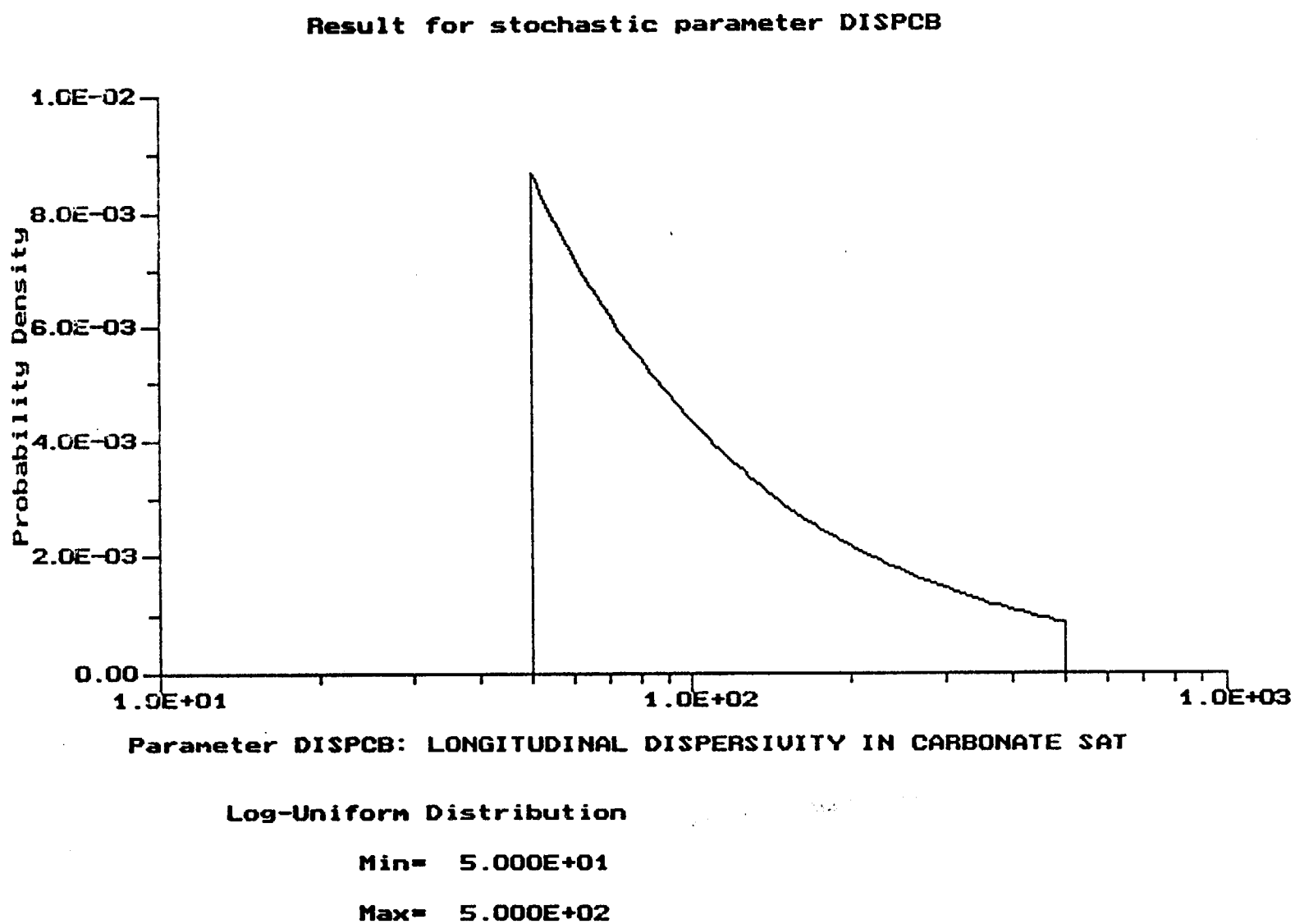

Figure 5-23. Probability Density Function of the Carbonate Aquifer Longitudinal Dispersivity

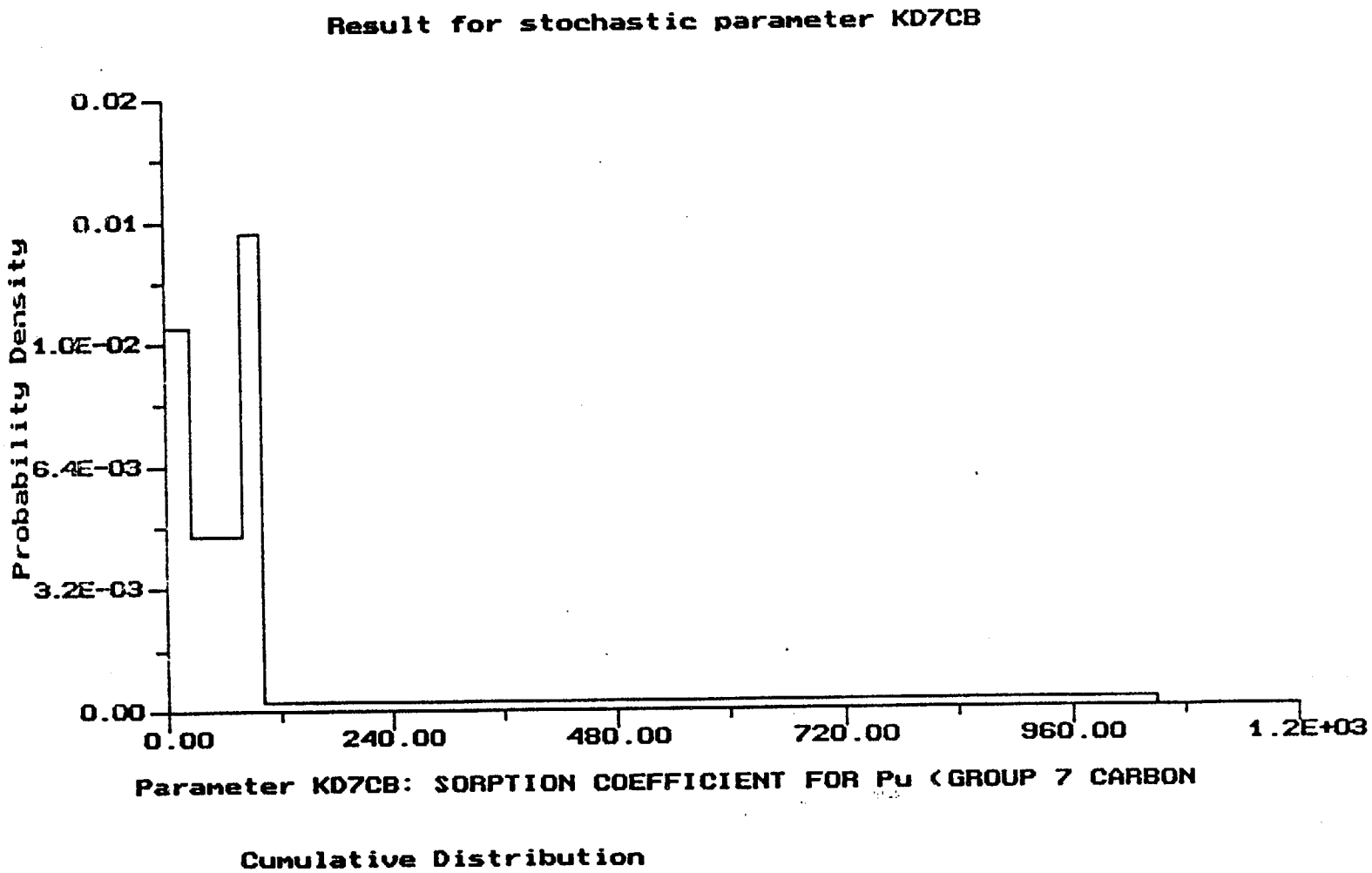

Figure 5-24. Probability Density Function of the Carbonate Aquifer Plutonium Distribution Coefficient

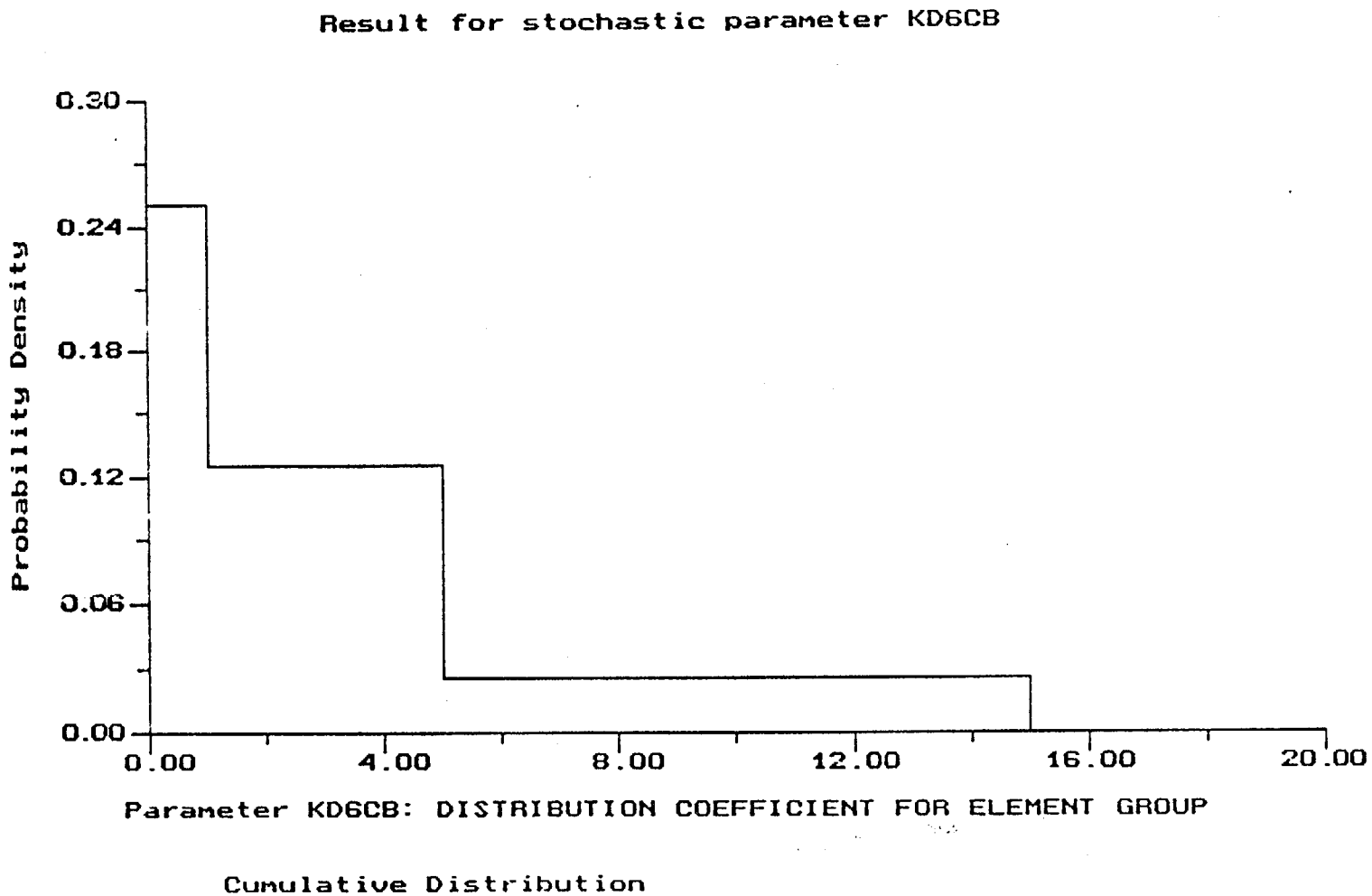

Figure 5-25. Probability Density Function of the Carbonate Aquifer Uranium Distribution Coefficient

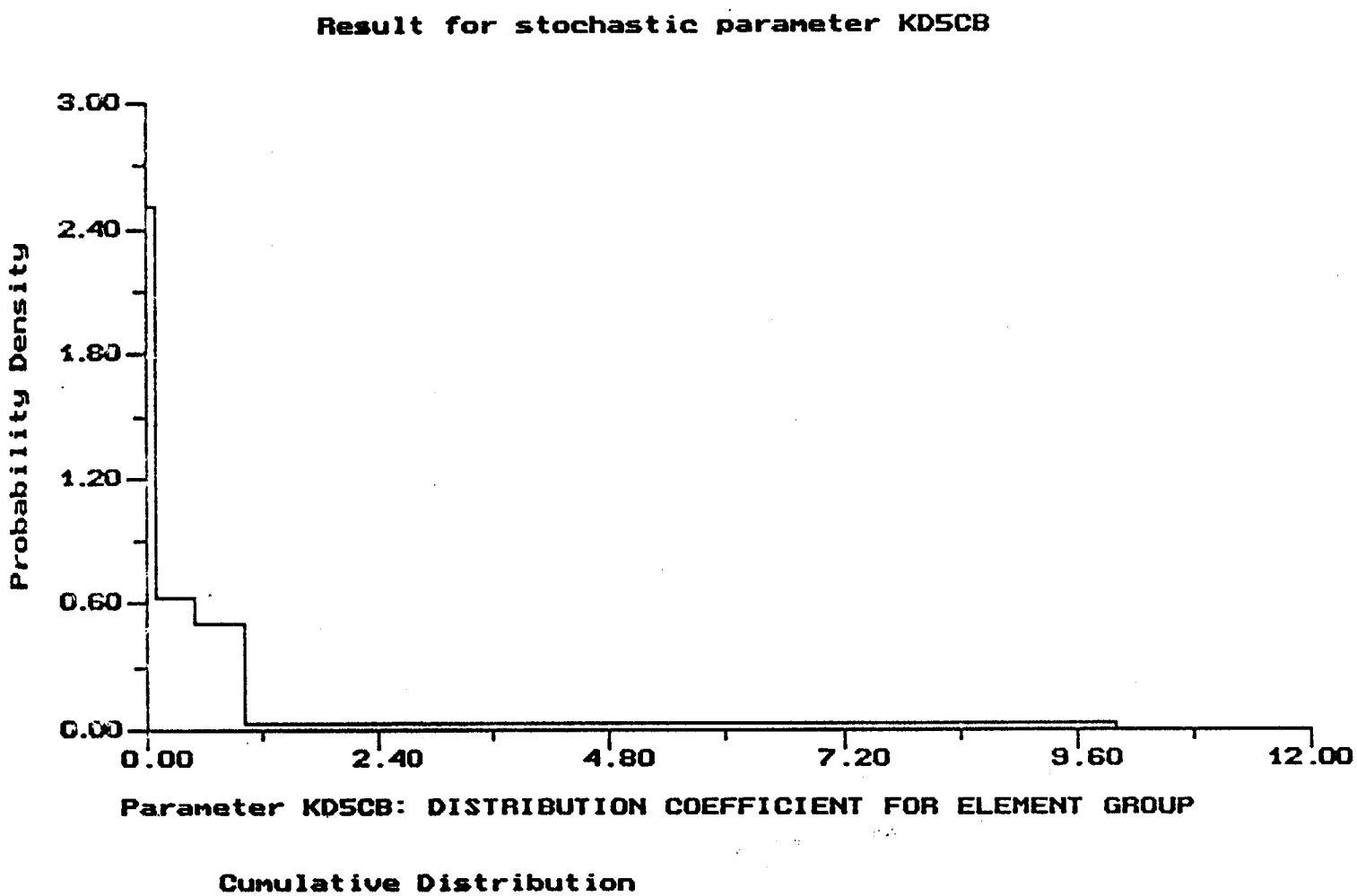

Figure 5-26. Probability Density Function of the Carbonate Aquifer Neptunium Distribution Coefficient

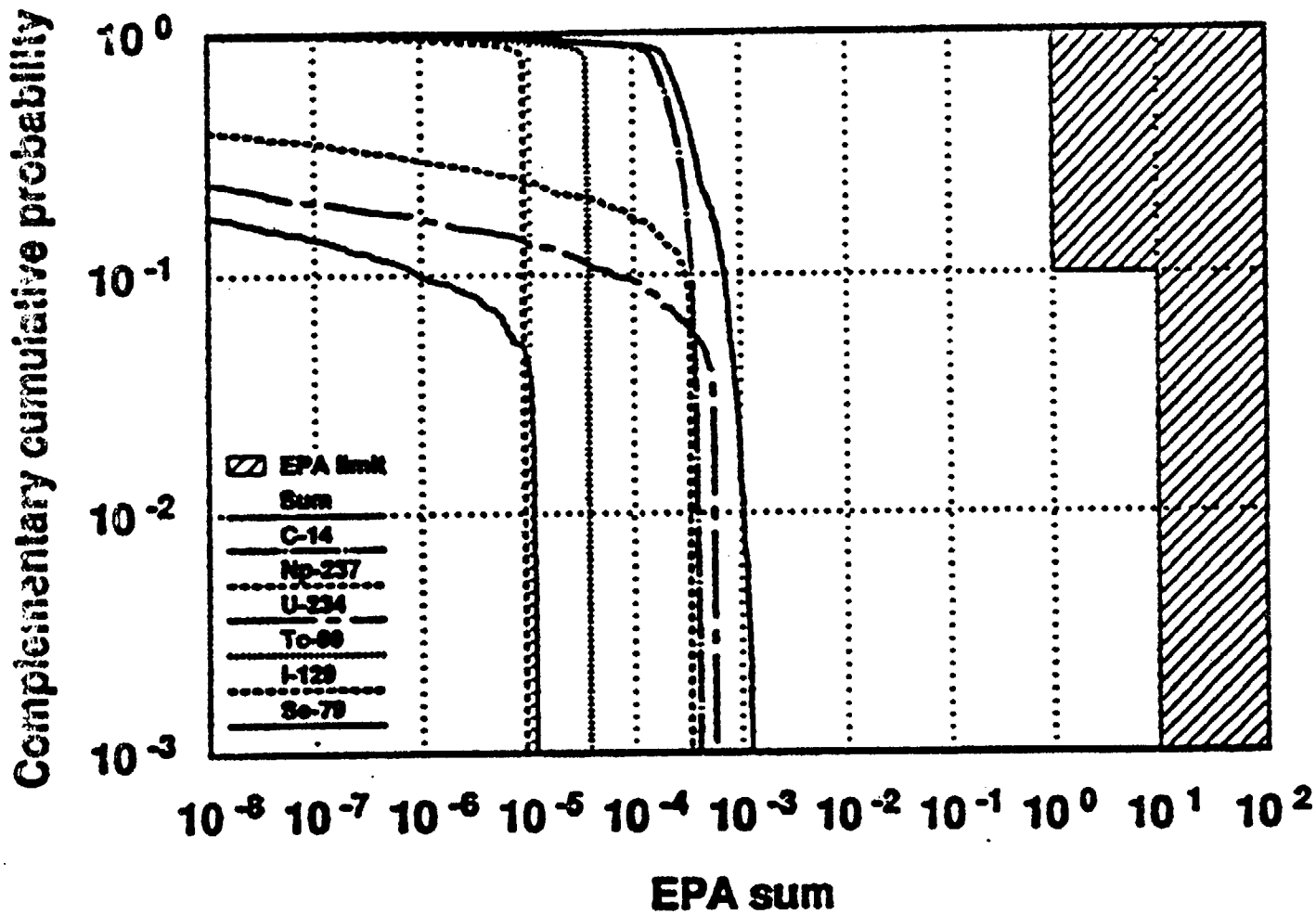

Figure 5-27. Conditional CCDF for Normalized Total Release to the Accessible Environment for the Human Intrusion into the Tuff Aquifer, Not Including the Probability of Occurrence (taken from Barnard et al., 1992)

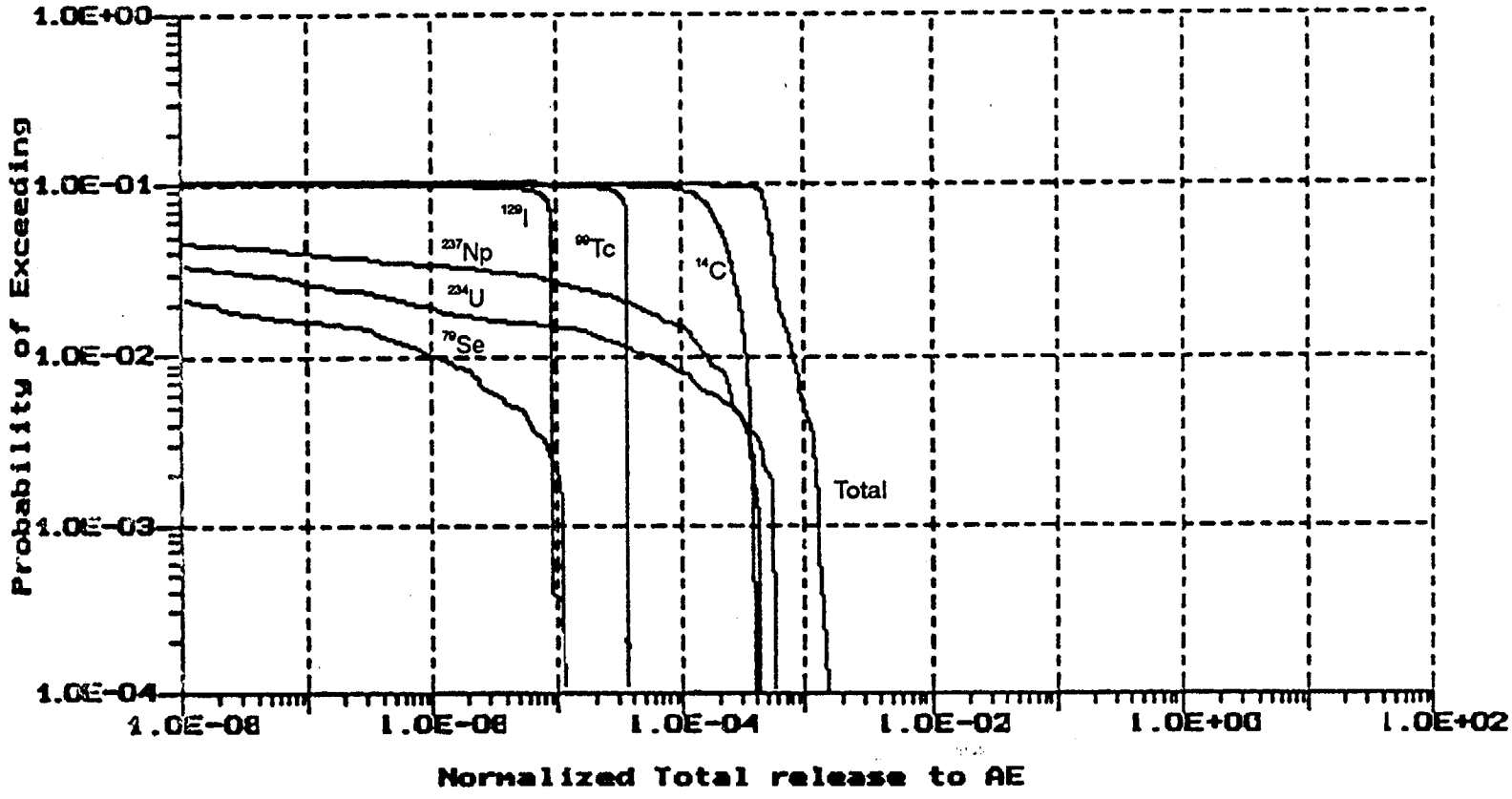

Figure 5-28. RIP Conditional CCDF for Normalized Total Release to the Accessible Environment for Human Intrusion into the Tuff Aquifer, Including the Probability of Occurrence

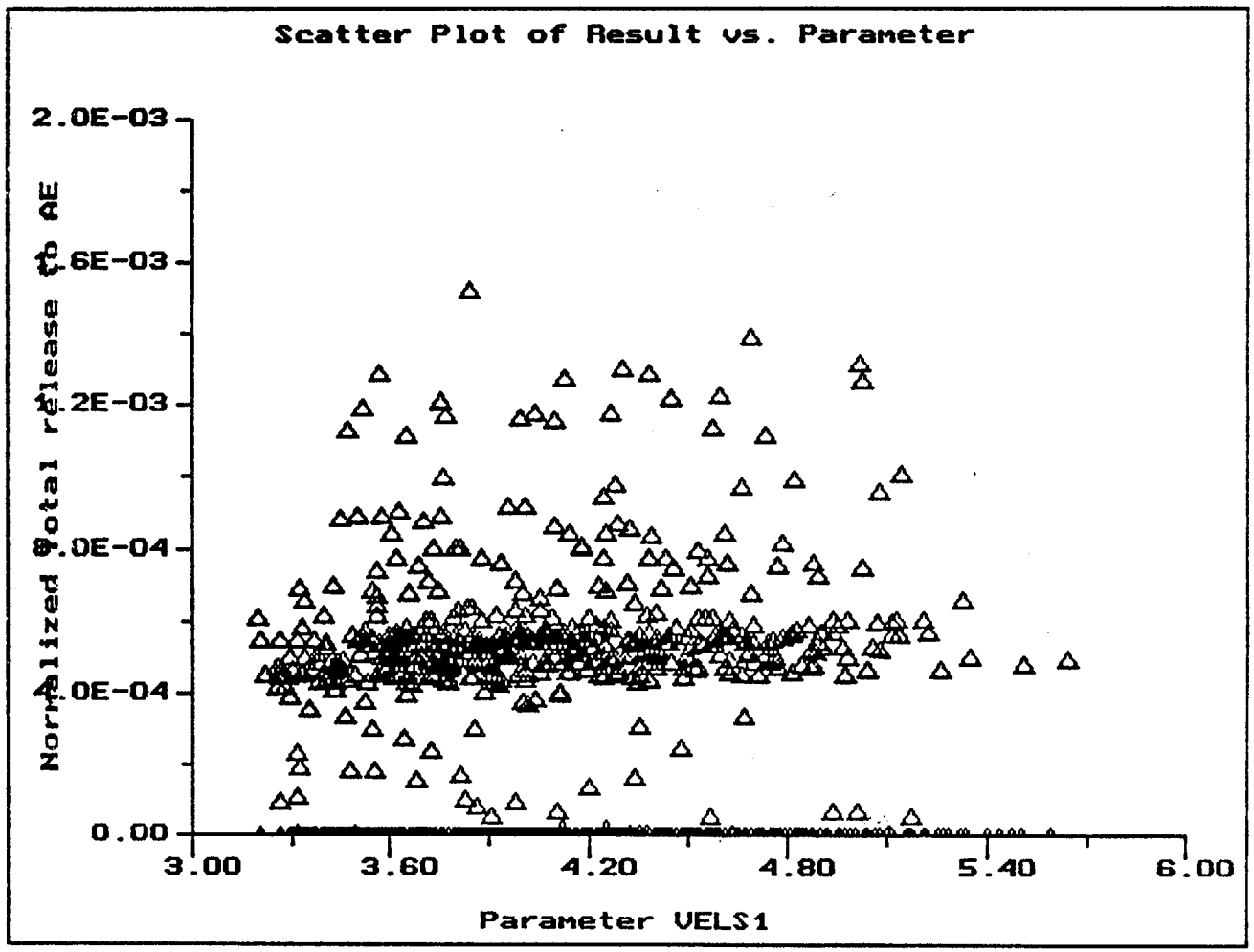

Figure 5-29. Scatter Plot of Ground-Water Velocity versus Total Normalized Release to the Accessible Environment for the Human Intrusion into the Tuff Aquifer

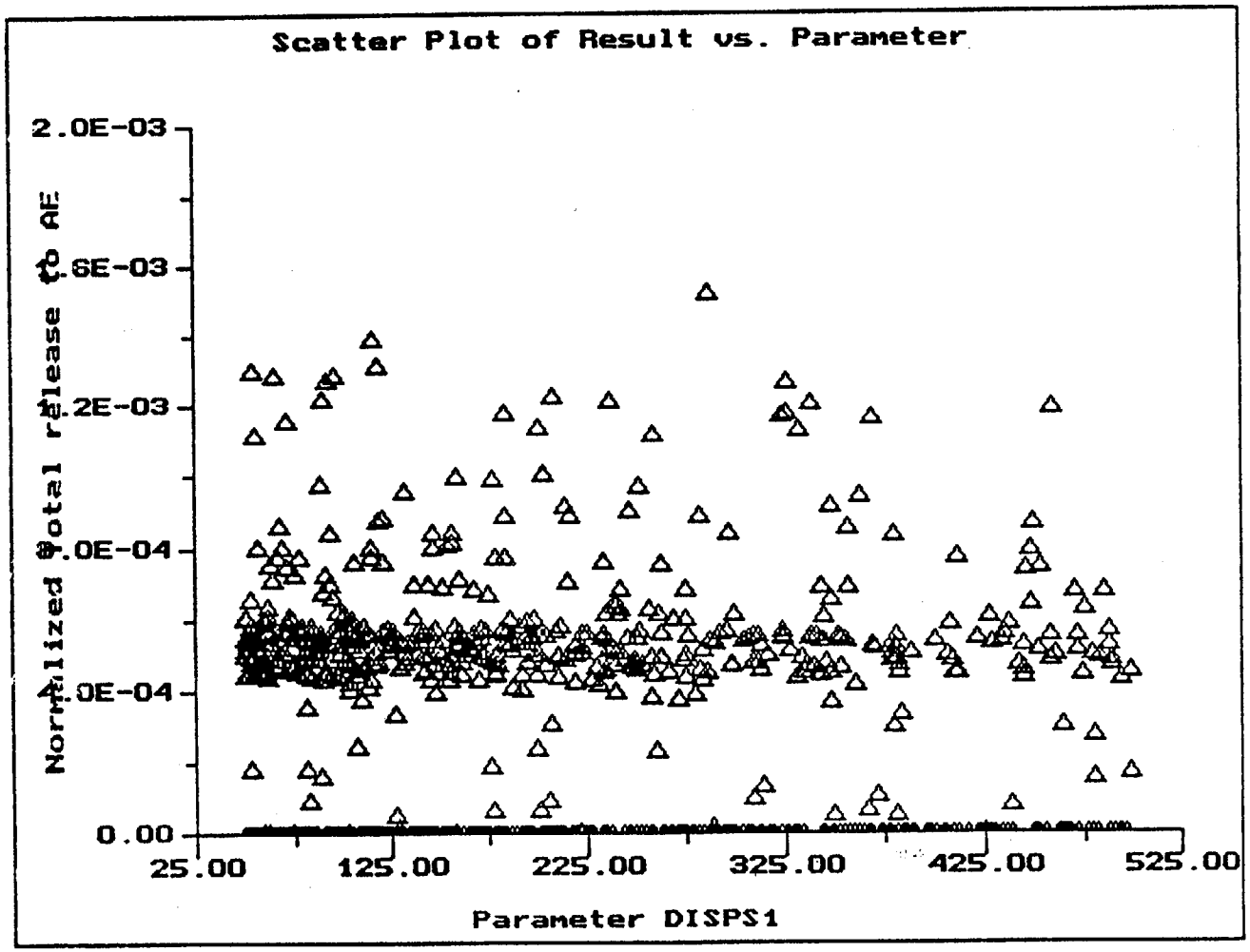

Figure 5-30. Scatter Plot of Longitudinal Dispersivity versus Total Normalized Release to the Accessible Environment for the Human Intrusion into the Tuff Aquifer

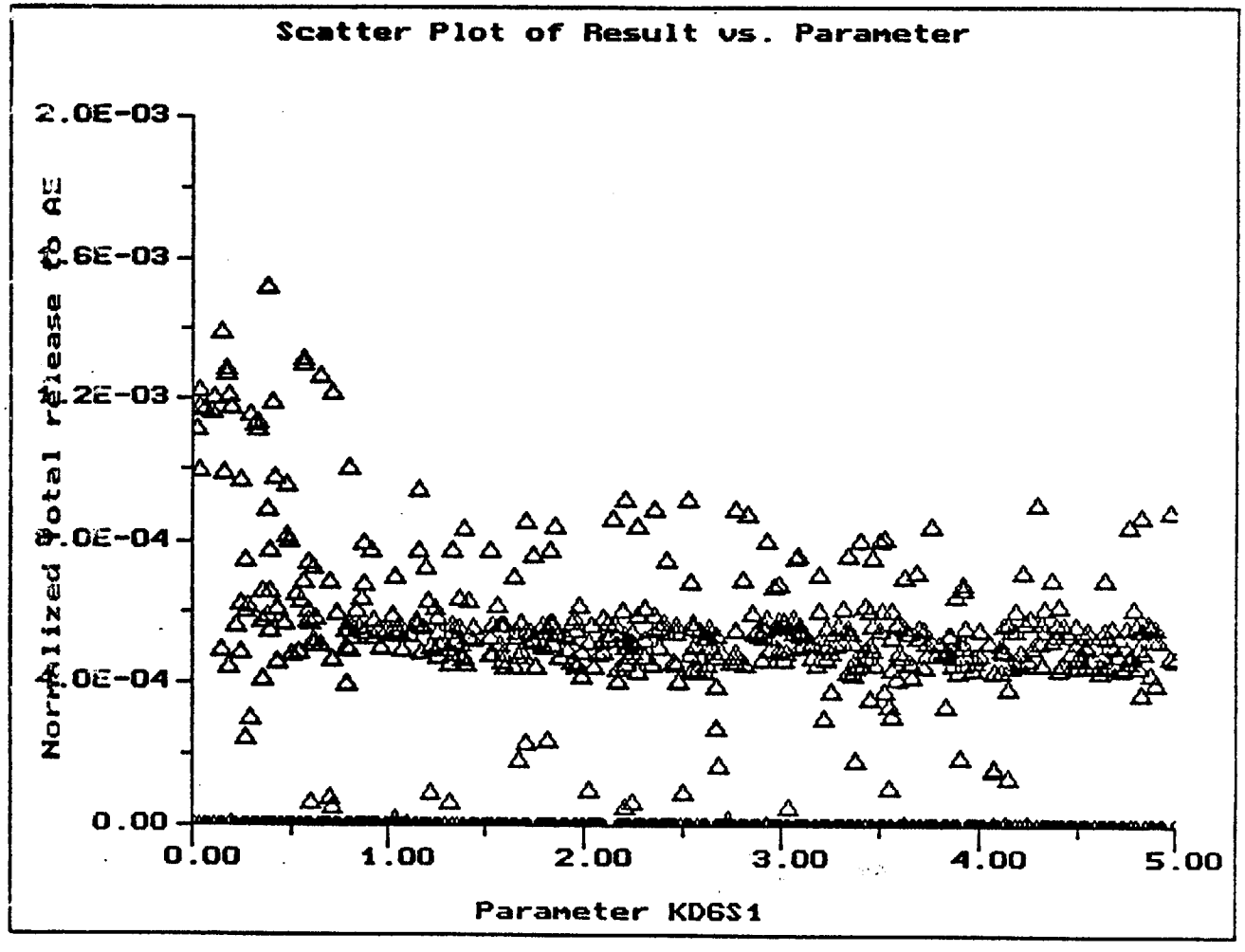

Figure 5-31. Scatter Plot of the Distribution Coefficient for Uranium versus Total Normalized Release to the Accessible Environment for the Human Intrusion into the Tuff Aquifer

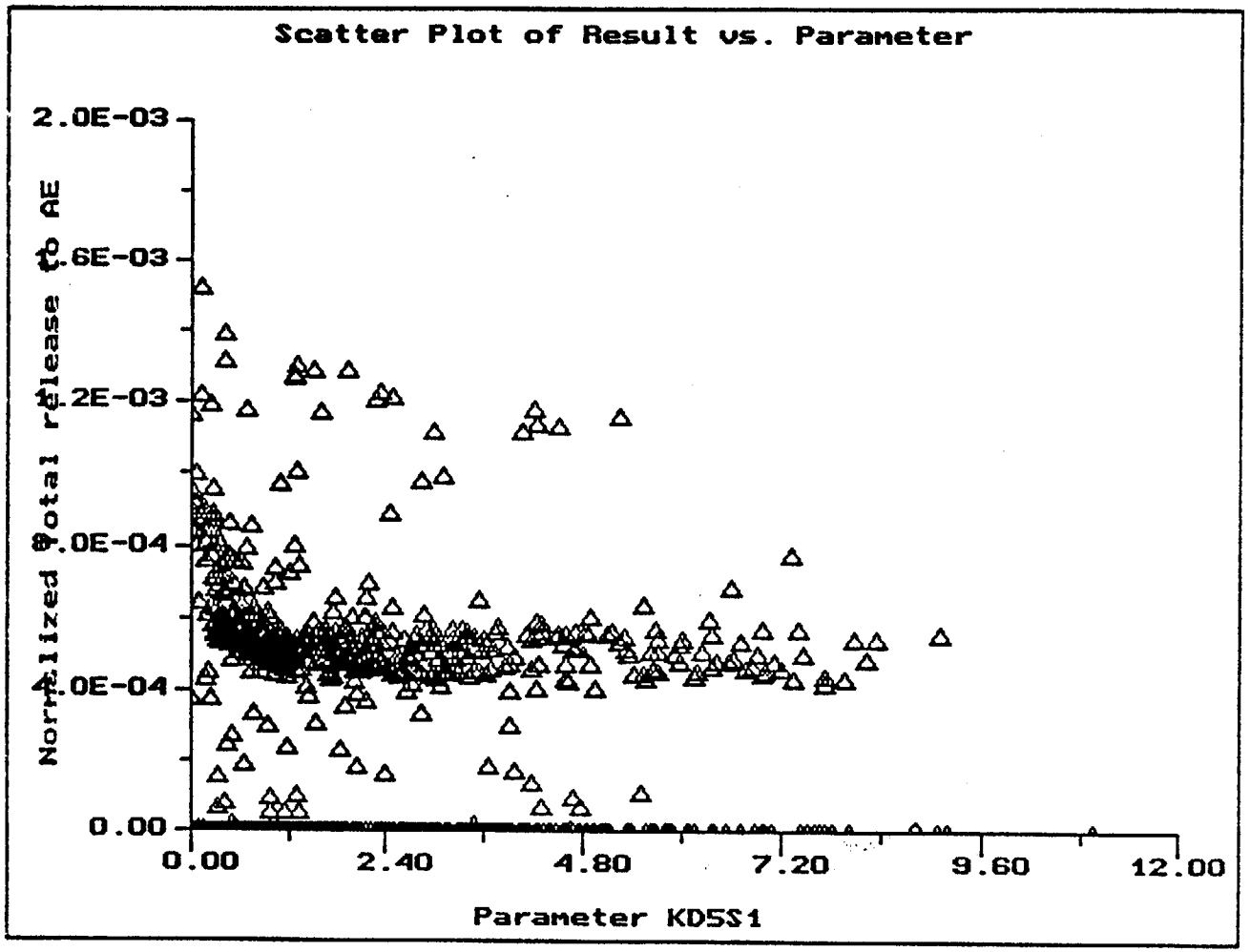

Figure 5-32. Scatter Plot of the Distribution Coefficient for Neptunium versus Total Normalized Release to the Accessible Environment for the Human Intrusion into the Tuff Aquifer

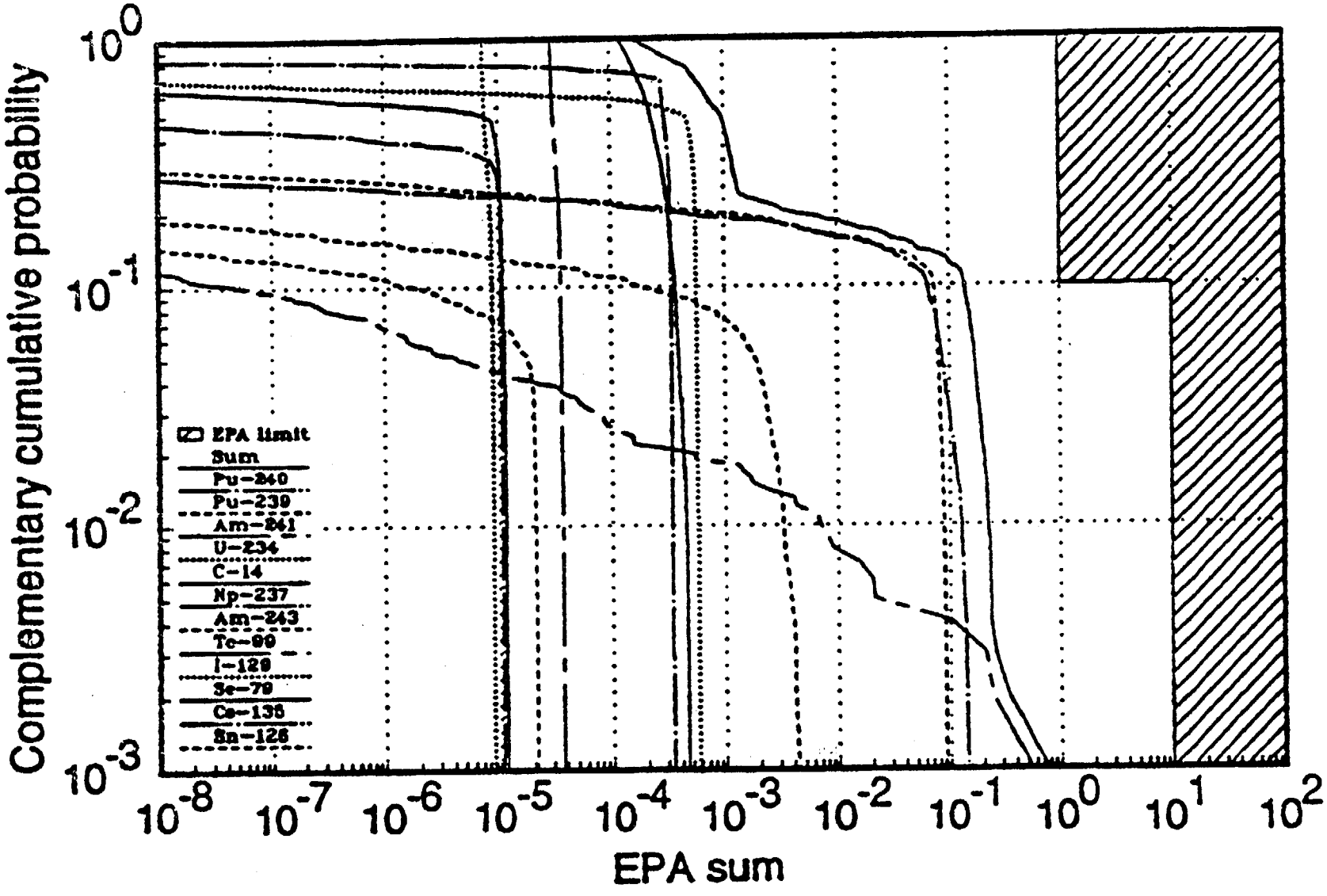

Figure 5-33. Conditional CCDF for Normalized Total Release to Accessible Environment for the Human Intrusion into the Carbonate Aquifer, Not Including the Probability of Occurrence (taken from Barnard et al., 1992)

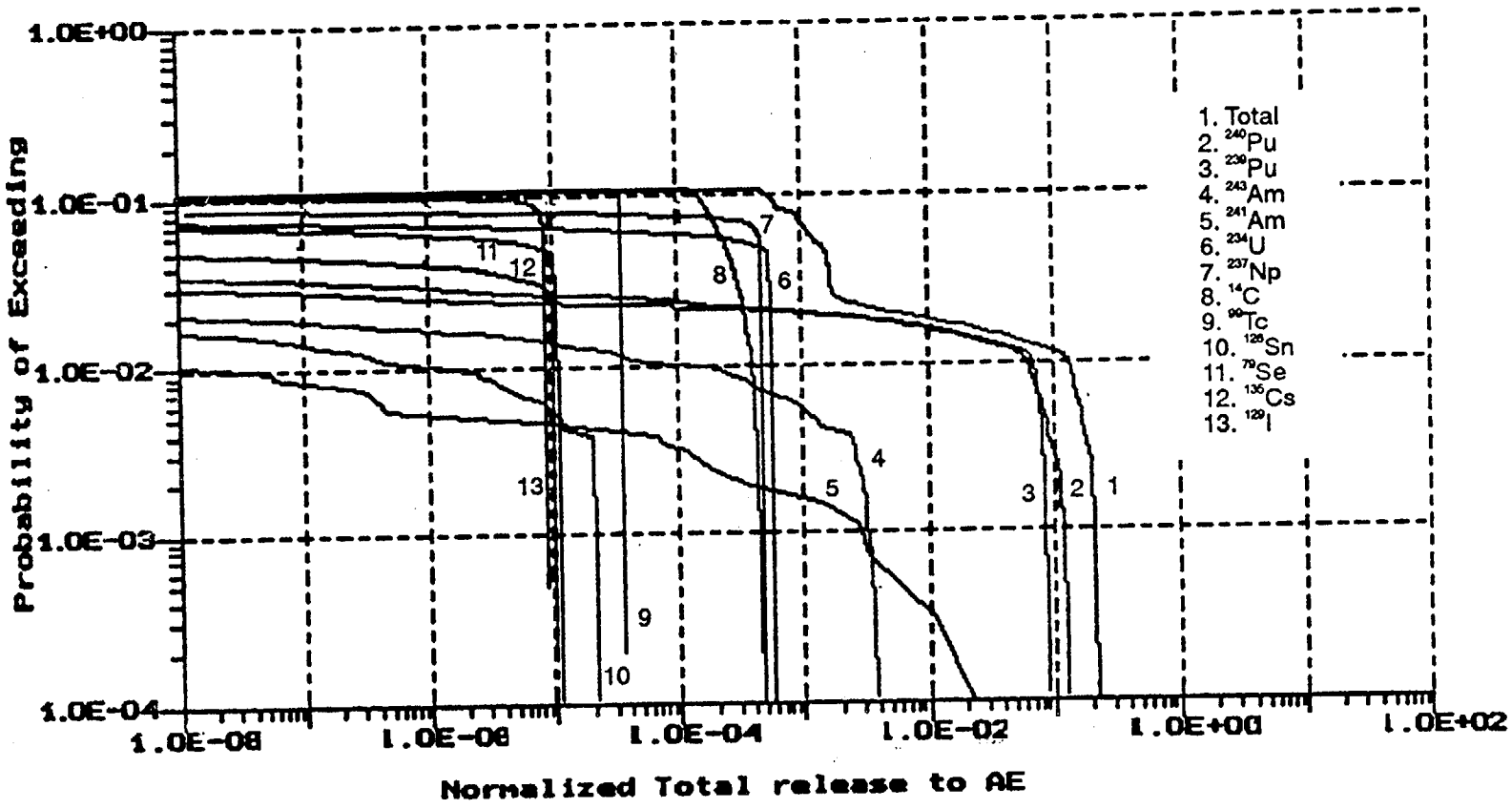

Figure 5-34. RIP Conditional CCDF for Normalized Total Release to the Accessible Environment for Human Intrusion into the Carbonate Aquifer, including the Probability of Occurrence

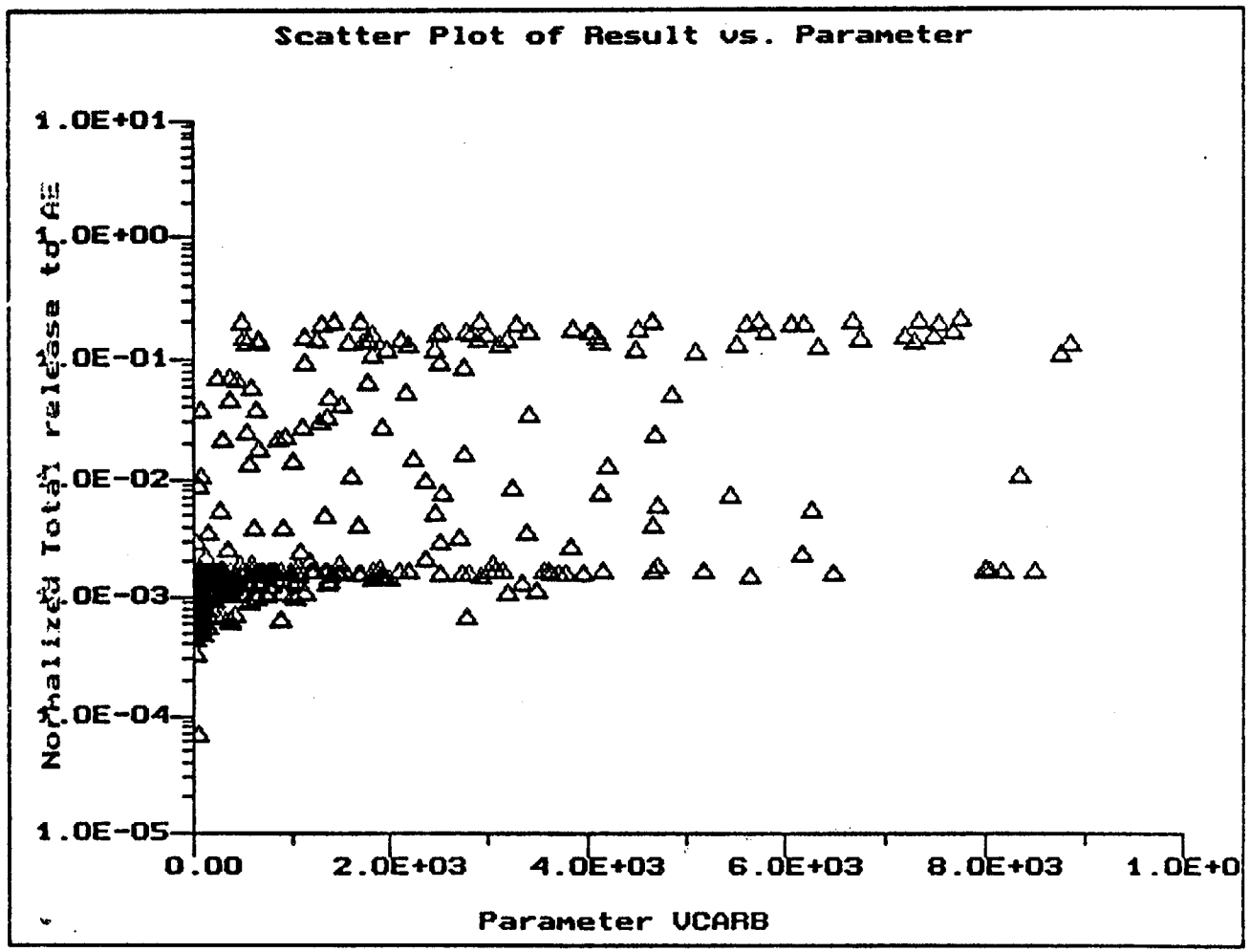

Figure 5-35. Scatter Plot of Ground-Water Velocity versus Total Normalized Release to the Accessible Environment for the Human Intrusion into the Carbonate Aquifer

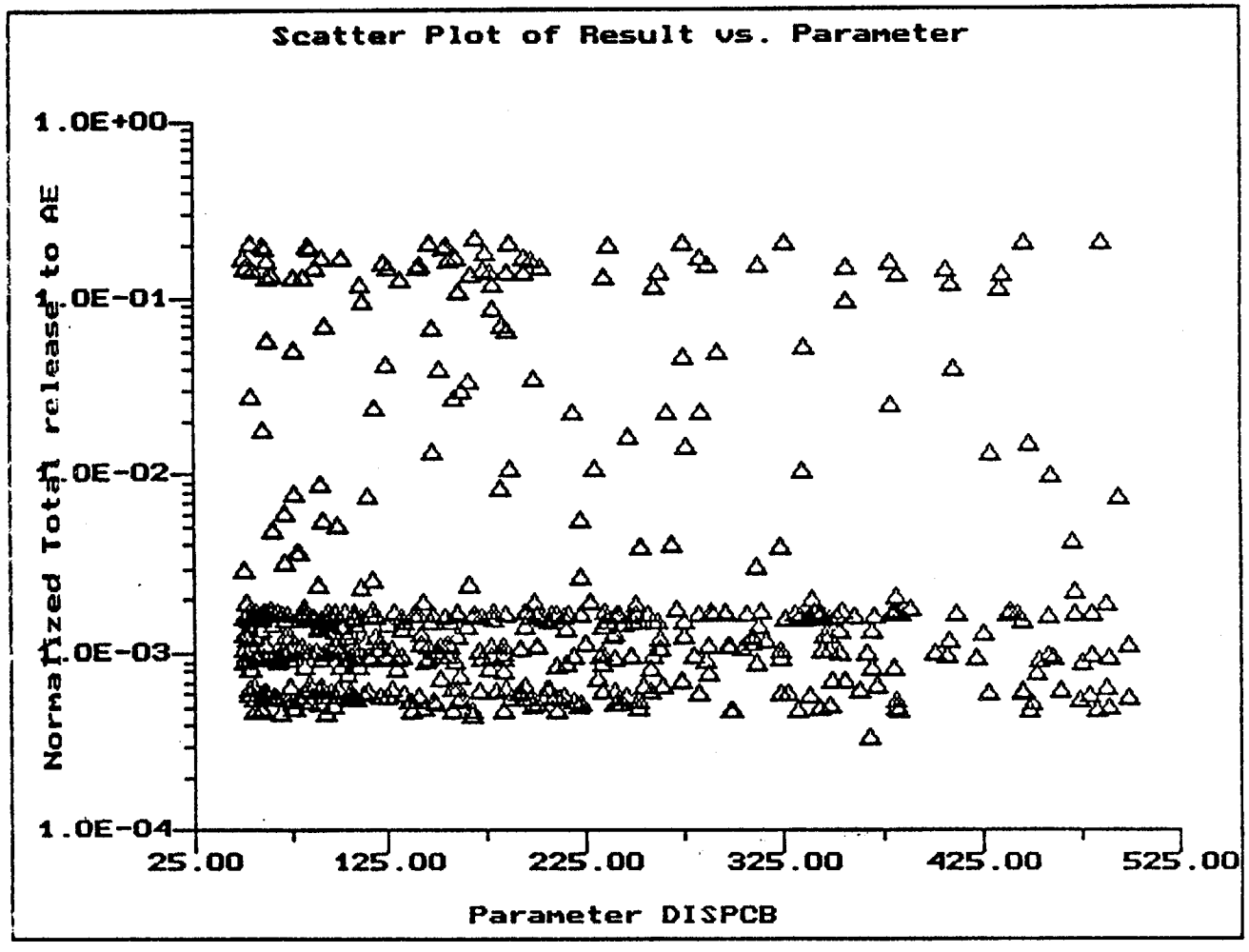

Figure 5-36. Scatter Plot of Longitudinal Dispersivity versus Total Normalized Release to the Accessible Environment for the Human Intrusion into the Carbonate Aquifer

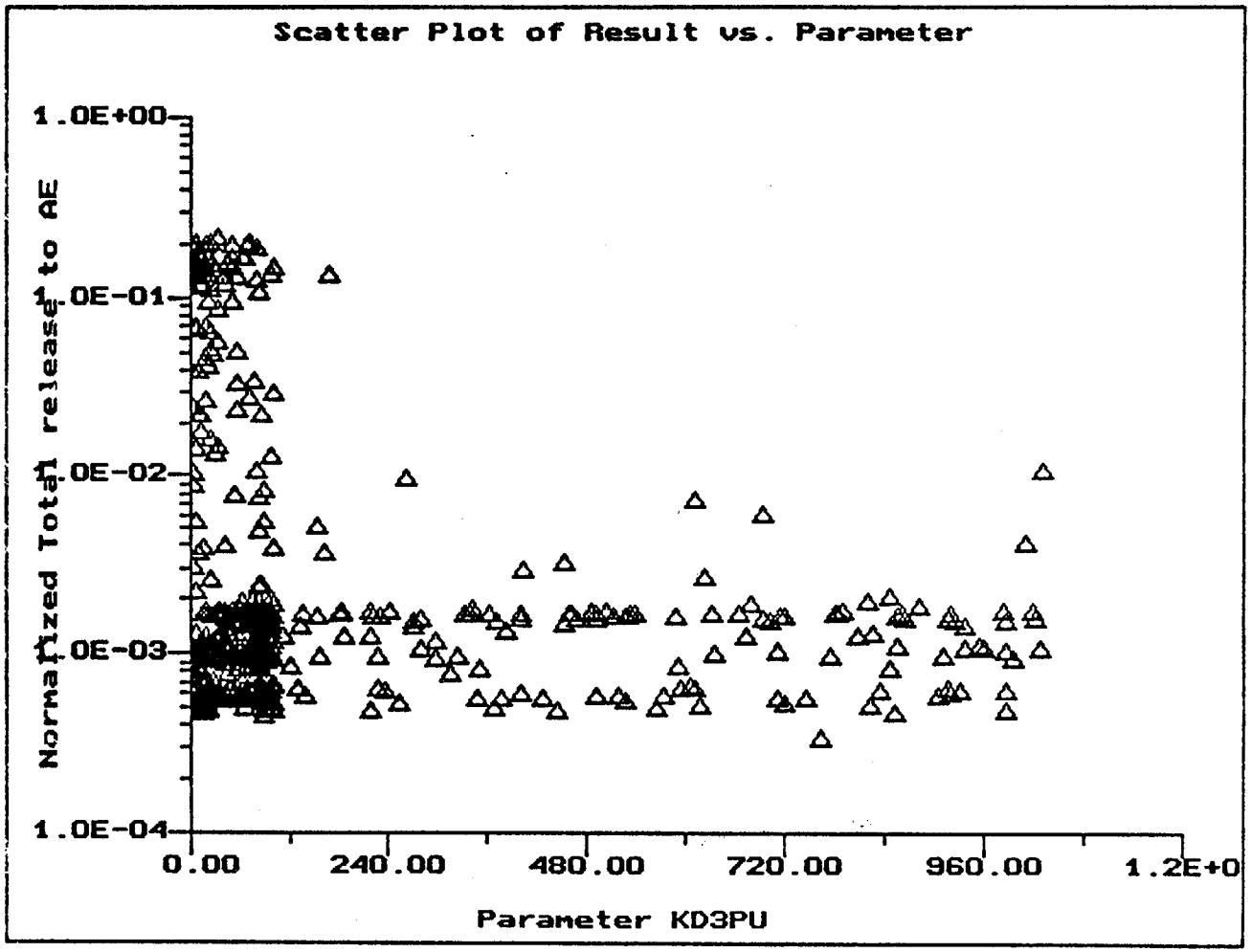

Figure 5-37. Scatter Plot of the Distribution Coefficient for Plutonium versus Total Normalized Release to the Accessible Environment for the Human Intrusion into the Carbonate Aquifer

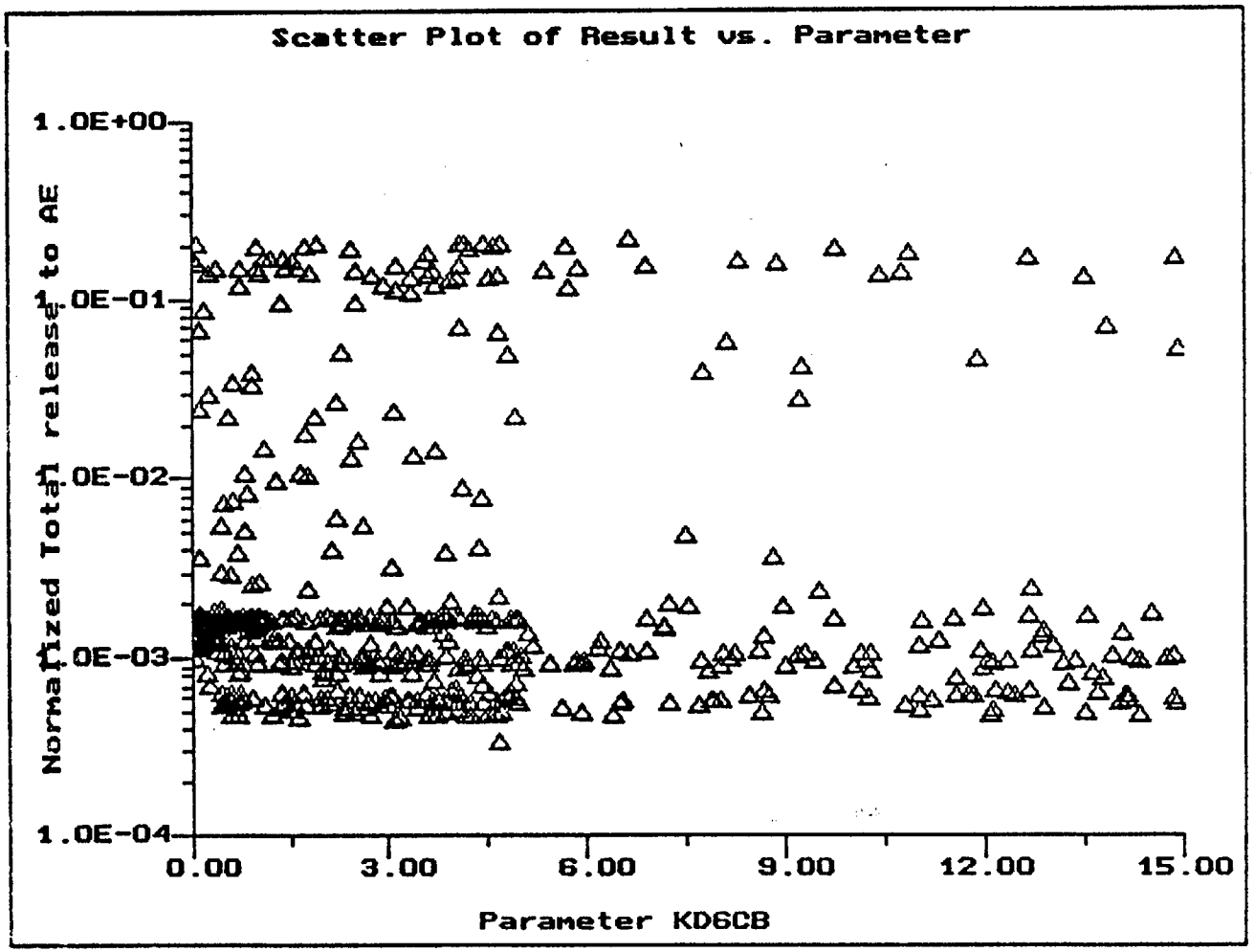

Figure 5-38. Scatter Plot of the Distribution Coefficient for Uranium versus Total Normalized Release to the Accessible Environment for the Human Intrusion into the Carbonate Aquifer

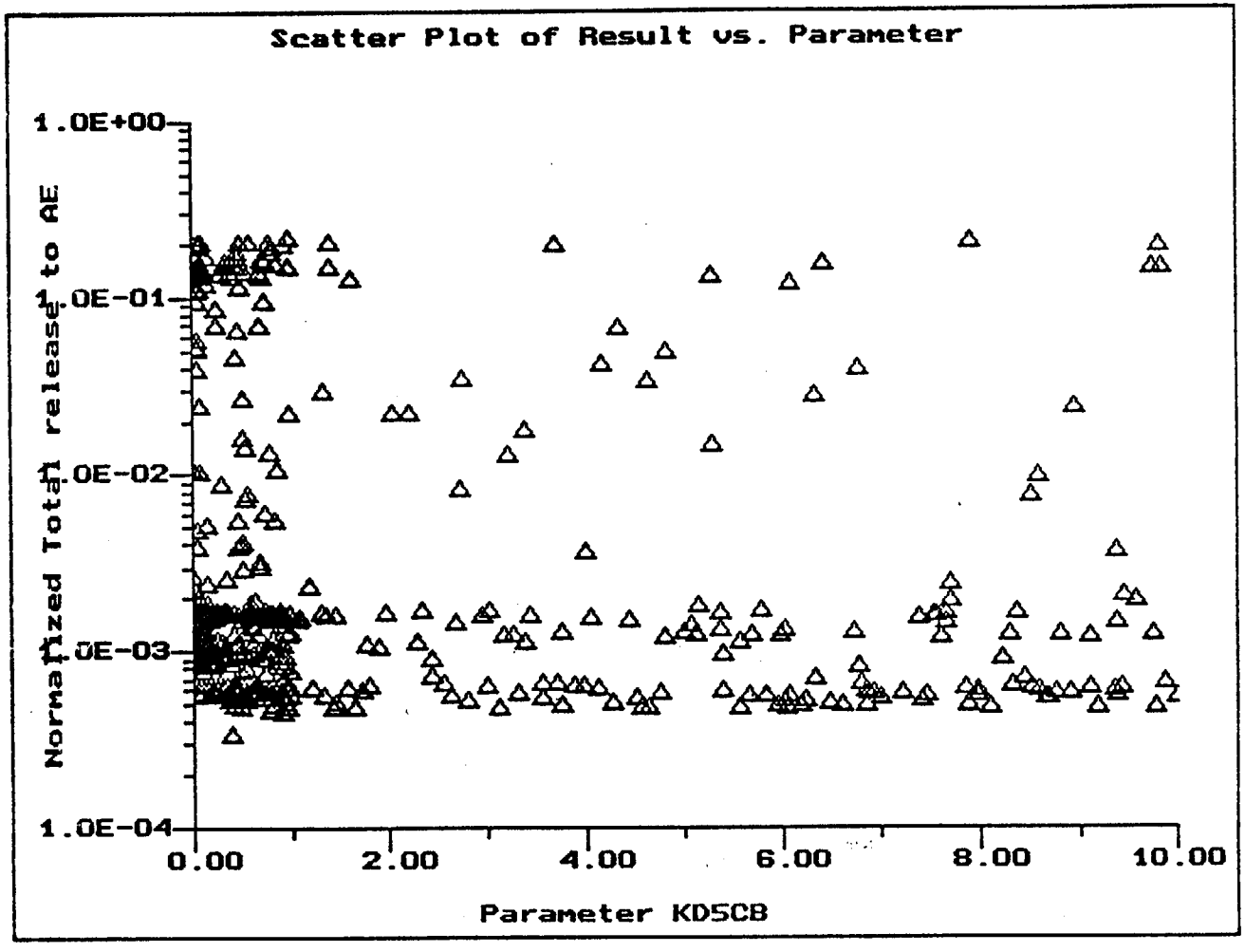

Figure 5-39. Scatter Plot of the Distribution Coefficient for Neptunium versus Total Normalized Release to the Accessible Environment for the Human Intrusion into the Carbonate Aquifer

Table 5-1. TSPA-1991 Volcanic Intrusion Method Two Parameters

Parameter	Distribution	Min, Max, Mean
Wall-rock fraction (*W*)	Beta	9.0×10^{-5}, 6.0×10^{-4}, 3.0×10^{-4}
Fraction of xenoliths (*R*)	Uniform	0.017, 0.033, 0.025
Portion of dike (*F*)	Uniform	0.0, 1.0, 0.5

Table 5-2. TSPA-1991 K_d Beta Distributions for the Tuff Aquifer (Barnard et al., 1992)

Nuclide	Expected Value	Coefficient of Variation	Minimum	Maximum
C, Tc, and I	0.0			
Sn, Pu, and Am	100.0			
Cs	50.0	0.20	20.0	100.0
Np	2.0	1.00	0.0	50.0
U and Se	2.5	0.58	0.0	4.0

Table 5-3. TSPA-1991 Distribution Coefficients (mg/l) for the Human Intrusion Scenario into the Carbonate Aquifer (taken from Barnard et al., 1992)

Percentile	Pu	Am, Sn	U, Se	Np	Cs	I, Tc, C
100%	1050	380	15	10	50	0
75%	100	200	5	1	20	0
50%	80	110	3	0.5	10	0
25%	25	100	1	0.1	5	0
0%	0	0	0	0	0	0
Mean	182	150	4	1.6	15	0

Table 5-4. TSPA-1991 Parameters for the Human Intrusion Scenarios (taken from Barnard et al., 1992)

Parameter	Value
General parameters	
Distance to accessible environment	5000 m
Typical number of trials in a simulation	1000
Source term	
Spent-fuel burnup (in MWD/MTHM)	33,000 (PWR)/27,500 (BWR)
PWR/BWR proportion	60/40
Number of radionuclides in source	12
Solubility of radionuclides	1000 kg/m^3
Probability factors	
Number of boreholes	17
Probability of hitting 1 waste package in 10,000 years with 17 boreholes	0.113
Hydrologic parameters (mean values)	
Saturated velocity (tuff aquifer)	4.07 m/yr
Saturated velocity (carbonate aquifer)	230 m/yr
Saturated porosity (tuff aquifer)	0.175
Saturated porosity (carbonate aquifer)	0.05
Saturated dispersivity (tuff aquifer)	195 m
Saturated dispersivity (carbonate aquifer)	195 m

Table 5-5. Comparison of TSPA-1991 and RIP Parameters for the Tuff Saturated Aquifer

TSPA-1991 Parameter	Distribution Type	Distribution Parameters (mean, min, max)	RIP Parameter	Distribution Type	Distribution Parameters (mean, min, max)
Flowpath: Length Depth Width	Constant	 5000 1000 3000	Flowpath: Length Depth Width	Constant	 5000 1000 3000
Ground-water velocity (m/yr)	Beta	4.07 3.2, 5.9	Ground-water velocity (m/yr)	Beta	4.07, 3.2, 5.9
Bulk porosity	Beta	0.175, 0.09, 0.29	Bulk porosity	Beta	0.175, 0.09, 0.29
			Volumetric flow rate (m^3yr)	Based on velocity and porosity distributions	Mean = 2.13×10^6
Distribution coefficient (ml/g)	Beta or constant	Dependent on nuclide*	Distribution coefficient (ml/g)	Beta or constant	Dependent on nuclide*
Bulk density (g/cm^3)	Constant	1.80	Bulk density (g/cm^3)	Constant	1.80
Longitudinal dispersivity (m)	Log-uniform	195, 50, 500	Longitudinal dispersivity (m)	Log-uniform	195, 50, 500

* See Table 5-2.

Table 5-6. Comparison of TSPA-1991 and RIP Parameters for the Carbonate Aquifer

TSPA-1991 Parameter	Distribution Type	Distribution Parameters (mean, min, max)	RIP Parameter	Distribution Type	Distribution Parameters (mean, min, max)
Flowpath: Length Depth Width	Constant	5000 1000 3000	Flowpath: Length Depth Width	Constant	5000 1000 3000
Ground-water velocity (m/yr)	Log-uniform	230.0, 6.0, 9000	Ground-water velocity (m/yr)	Log-uniform	230.0, 6.0, 9000
Bulk porosity	Uniform	0.05, 0.1, 0.09	Bulk porosity	Uniform	0.05, 0.1, 0.09
			Volumetric flow rate (m^3yr)	Based on velocity and porosity distributions	Mean = 1.35×10^7
Distribution coefficient (ml/g)	Histogram probability	Dependent on nuclide*	Distribution coefficient (ml/g)	Beta or constant	Dependent on nuclide*
Bulk density (g/cm^3)	Constant	2.80	Bulk density (g/cm^3)	Constant	2.80
Longitudinal dispersivity (m)	Log-uniform	195, 50, 500	Longitudinal dispersivity (m)	Log-uniform	195, 50, 500

* See Table 5-3.

6. CONCLUSIONS AND RECOMMENDATIONS

RIP is a tool for describing the relevant processes which may affect the postclosure performance of a repository. The present document describes an application of RIP to the potential repository for high-level radioactive waste at Yucca Mountain, Nevada. This application is derived entirely from the data set used to generate the cumulative releases to the accessible environment presented in the TSPA-1991 document (Barnard et al., 1992). The present study should not be inferred to be a separate total system performance assessment of Yucca Mountain; but instead it is an evaluation of the applicability of the RIP simulation approach to produce representative cumulative release distributions. In addition, this study may be considered an evaluation of the ability to abstract information from the TSPA-1991 document to independently reproduce the results of Barnard et al. (1992). We feel the results presented in this document represent a test of the RIP total system performance assessment model and a "verification" of the results of Barnard et al. (1992). We also present areas where the abstractions developed in RIP must be based on more physical understanding of the underlying processes, conceptual models, and parameters controlling the predicted releases.

RIP may be considered as the top of the performance assessment model hierarchy in terms of its high level of abstraction. It allows for all the relevant external initiating events and processes to yield a complete description of the postclosure behavior of the repository system. The approach followed in RIP is very different from that used by SNL in TSPA-1991 (Barnard et al, 1992), PNL (Eslinger et al., 1993), or by the NRC in their Iterative Performance Assessment. These organizations use relatively complex representations of each of the domains (waste package/engineered barrier system, unsaturated zone, saturated zone, external features, events, and process scenarios); solve these representations using numerical, semi-analytical or analytical methods; and combine the results using a statistical driver that samples from parameter probability density functions. In such an approach the results for each scenario must be subsequently weighted by the probability of the scenario occurring. RIP instead combines all the processes and events into a single simulation of likely alternate futures and evaluates the consequences (i.e., releases to the accessible environment) for each future state. The advantage of the approach used in TSPA-1991 is the added realism in the treatment of the complex processes (such as unsaturated zone flow). The advantage of the RIP approach is the flexibility, the ability to make numerous realizations very quickly, and the ability to directly combine all possible futures.

The following items summarize the principal comparison between RIP and TSPA-1991:

WASTE PACKAGE COMPARISON

- RIP can be used to approximate the waste package/EBS processes included in TSPA-1991.

- TSPA results for release from the waste package are higher than RIP for solubility-limited radionuclides, and lower for alteration-limited radionuclides. These two classes of radionuclides are treated differently in TSPA-1991, but treated in a similar manner in RIP.

- TSPA-1991 CCDF results are slightly higher than RIP. This discrepancy may be due to the slight differences in the waste package failure distribution and solubilities used in RIP and TSPA-1991.

- RIP contains capabilities not present in TSPA-1991 analyses including effective radionuclide solubilities, and creation of daughter products during simulations. These capabilities provide a more realistic simulation of expected waste package processes and resultant releases.

UNSATURATED ZONE GASEOUS RELEASE COMPARISON

- RIP can approximate the gaseous releases presented in TSPA-1991.

- Slight differences in RIP and TSPA-1991 results are likely due to small differences in the waste package failure distribution and the time-stepping algorithm used to approximate the breakthrough curve.

UNSATURATED ZONE AQUEOUS RELEASE COMPARISON

- RIP can approximate the unsaturated zone releases to the saturated zone presented in TSPA-1991.

- Differences between RIP and TSPA-1991 exist when the Markovian multi-mode transport algorithm is used with either no or full matrix-fracture coupling. For representative transition rates (about 1/L, where L is the layer thickness) good agreement exists. Also, when the matrix flow layers are treated as single-mode transport units, good agreement exists.

SATURATED ZONE RELEASE COMPARISON

- RIP can approximate the saturated zone radionuclide transport presented in TSPA-1991.

VOLCANIC/HUMAN INTRUSION SCENARIO RELEASE COMPARISON

- RIP can approximate the scenarios represented in TSPA-1991.

The principal differences between TSPA-1991 and our implementation of the same data set using RIP are enumerated below:

- RIP input has to be simplified to mimic the treatment of radionuclide inventories and solubilities adopted in TSPA-1991. RIP allows complete chains to be specified and tracked and allows for partitioning between radionuclides which compete for solubility-limited releases.

- Diffusive releases in RIP are assumed to be steady-state.

- RIP can approximate fracture-matrix coupling by a Markovian process, which requires definition of a Markov transition rate. Such an approach does not reproduce dispersive mass transport.

- Future states are simulated directly in RIP. We have conducted conditional simulations for comparison to TSPA-1991 by using the importance sampling option in RIP.

- RIP saves all results which allows for numerous post-processing capabilities, including scatter plots. *[Note: Graphic capabilities of RIP are being enhanced for better display of sensitivities.]*

Based on the experience gained in this study, we feel confident that the RIP approach is a viable method for use in future iterations of total system performance assessment. Its advantages (notably in flexibility in handling numerous types of functional relationships) far outweigh the simple representations required to make the model efficient for multiple realizations (in particular the Markovian approximation of multi-mode transport and the temporal approximation of theoretical break-through curves). The flexibility of the RIP approach should be used to advantage in the next TSPA iteration (TSPA-II) to account for temperature dependencies on water contact mode, waste package failure, waste form alteration and dissolution, radionuclide mobilization (solubility), the percent of water in contact with the waste, and the gaseous and aqueous phase velocities. These dependencies should be derived from expert judgement or more detailed process-oriented modeling.

We suggest several activities be conducted to build on the analyses presented herein. We feel it would be useful to conduct additional comparisons of the Lawrence Livermore National Laboratories (LLNL) waste package model used in TSPA-1991 with the waste package model used in RIP. While these models are similar (in fact, the RIP model was developed in consultation with LLNL and other waste package experts), their differences should be well understood prior to selecting one or the other for specific application. Additional "tests" of RIP's treatment of flow and transport should be conducted to evaluate how best to abstract results from more detailed process models. These "tests" may include the use of different spatial and temporal discretizations to evaluate the sensitivity of results to these model parameters (the latter would require a change in the current version of RIP). Those "tests" would increase our confidence further in the applicability of RIP to future TSPAs.

7. REFERENCES

Abramowitz, M., and I. Stegun, 1970. *Handbook of Mathematical Functions*. Dover Publications, Inc., New York.

Apted, M., W. O'Connell, K. Lee, A. MacIntyre, T. Veng, W. Lee, and T. Pigford, 1990. Preliminary Calculations of Release Rates of ^{99}Tc, ^{129}I, and ^{237}Np from Spent Fuel in a Potential Repository in Tuff. LBL-31069, Lawrence Berkeley Laboratory, Berkeley, California.

Barnard, R., M. Wilson, H. Dockery, J. Gauthier, P. Kaplan, R. Eaton, F. Bingham, and T. Robey, 1992. TSPA-1991: An Initial Total-System Performance Assessment for Yucca Mountain. SAND91-2795. Sandia National Laboratories, Albuquerque, New Mexico.

Chambre, P., T. Pigford, W. Lee, J. Ahn, S. Kajwara, C. Kim, H. Kimura, H. Lung, W. Williams, and S. Zavoshy, 1985. Mass Transfer and Transport in a Geologic Environment. LBL-19430, Lawrence Berkeley Laboratory, Berkeley, California.

Conca, J., 1990. Diffusion Barrier Transport Properties of Unsaturated Paintbrush Tuff Rubble Backfill. In: Proceedings of the International Topical Meeting on High-Level Radioactive Waste Management, American Nuclear Society, La Grange Park, Illinois, pp. 304-401 (NNA.900710.0198).

Czarnecki, J.B., 1985. Simulated Effects of Increased Recharge on the Ground-Water Flow System of Yucca Mountain and Vicinity, Nevada-California. USGS/WRI-84-4344, U.S. Geological Survey, Denver, Colorado (NNA.870407.0008).

Czarnecki, J.B., and R.K. Waddell, 1984. Finite-Element Simulation of Ground-Water Flow in the Vicinity of Yucca Mountain, Nevada-California, USGS/WRI-84-4349, U.S. Geological Survey, Denver, Colorado (NNA.870407.0173).

Doctor, P.G., P.W. Eslinger, D.M. Elwood, D.W. Engel, M.D. Freshley, A.M. Liebetrau, P.W. Reimus, D.L. Strenge, J.E. Tanner, and A.E. Van Luik, 1992. An Example Postclosure Risk Assessment Using the Yucca Mountain Candidate Site. PNL-8081, Pacific Northwest Laboratory, Richland, Washington.

Environmental Protection Agency (EPA), 1985. Environmental Radiation Protection Standards for Management and Disposal of Spent Nuclear Fuel, High-Level and Transuranic Radioactive Wastes. Code of Federal Regulations, Title 40, Part 191 (HQS.880517.3264).

Eslinger, P.W., L.A. Doremus, D.W. Engel, T.B. Miley, M.T. Murphy, W.E. Nichols, M.D. White, D.W. Langford, and S.J. Ouderkirk, 1993. Preliminary Total-System Analysis of a Potential High-Level Nuclear Waste Repository at Yucca Mountain. PNL-8444, Pacific Northwest Laboratory, Richland, Washington, January.

Golder Associates Inc., 1993. Application of RIP (Repository Integration Program) to the Proposed Repository at Yucca Mountain: Conceptual Model and Input Data Set. Golder Associates Inc., Seattle, Washington.

Johnson, G., and D. Montan, 1990. Thermal Calculations Pertaining to a Proposed Yucca Mountain Nuclear Waste Repository. UCRL-ID-10354, Lawrence Livermore National Laboratory, Livermore, California.

Kossik, R., and J. Hachey, 1993. Interim Document: RIP Repository Performance Assessment and Strategy Evaluation Model: User's Guide Version 2.00. Golder Associates, Inc., Seattle, Washington.

MacDougall, H.J., L.W. Scully, and J.R. Tillerson, 1987. Site Characterization Plan Conceptual Design Report. SAND84-2641. Sandia National Laboratories, Albuquerque, New Mexico.

Miller, I., R. Kossik, M. Cunnane, and J. Hachey, 1993. Interim Document: RIP Repository Performance Assessment and Strategy Evaluation Model: Theory and Capabilities Version 2.00. Golder Associates, Inc., Seattle, Washington.

Ross, B., S. Amter, and N. Lu, 1992. Numerical Studies of Rock-Gas Flow in Yucca Mountain, SAND91-7034. Sandia National Laboratories, Albuquerque, New Mexico.

Sinnock, S., Y. Lin, and J. Brannen, 1984. Preliminary Bounds on the Postclosure Performance of the Yucca Mountain Repository Site, Southern Nevada. SAND84-1492. Sandia National Laboratories, Albuquerque, New Mexico.

Travis, B., S. Hodson, H. Nuttal, T. Cook, and R. Rundberg, 1984. Preliminary Estimates of Water Flow and Radionuclide Transport in Yucca Mountain. LA-UR-84-40 (Rev.), Los Alamos National Laboratory, Los Alamos, New Mexico.

Ueng, T., and W. O'Connell. 1992. Diffusive Barrier Simplified Analysis — Design and Sensitivity Applications. In: Proceedings of the Topical Meeting on Nuclear Waste Packaging, Focus '91, American Nuclear Society, La Grange Park, Illinois, pp. 277-284.

U.S. Department of Energy, 1988. Site Characterization Plan, Yucca Mountain Site, Nevada Research and Development Area, Nevada. DOE/RW-0199, Washington, D.C.

Wilson, M., 1993. Personal communications with M. Wilson, Sandia National Laboratories: Las Vegas, Nevada, February 23-25.

APPENDIX A. DETAILED DESCRIPTION OF RIP WASTE PACKAGE IMPLEMENTATION

Several key functions in the RIP waste package data set are described in this appendix. These functions include: (1) the procedure for determining the number of WPs in each water contact mode, (2) the procedure for simulating the air gap, (3) the procedure for diffusive release, (4) the selection of an effective catchment area, and (5) special conditions for water contact mode 4—nominal (dry) case.

A.1 PROCEDURE USED TO DETERMINE THE NUMBER OF WASTE PACKAGES IN A PARTICULAR WATER CONTACT MODE

TSPA-1991 divided the waste packages into four categories depending on the water saturation of the waste packages. The saturation was directly related to the release mode of radionuclides from the containers. Four different modes of release were included: (1) advective only, (2) diffusive only, (3) advective and diffusive, and (4) none. Advective releases were assumed to occur if a waste package was in a locally wet (seepage area) part of the potential repository. A simple flow-through model was assumed in calculating the advective releases. Diffusive releases were assumed to occur if the air gap was partially filled with rubble. The height of the rubble in the air gap was assumed to be the same as the height of the water in the container, thus simplifying the estimate of the fraction of the spent fuel in a given container that contributes to diffusive releases. Advective and diffusive releases occurred when the containers were in locally wet areas and had rubble in the air gap. A fraction of the waste packages potentially were in dry areas with an intact air gap, and no release occurred from these packages.

The relative number of waste packages in each category was determined in the following manner. The fraction of containers in seepage areas is denoted by f_s and the fraction of containers with rubble filling at least part of the air gap is denoted f_r. The f_s fraction covers those containers experiencing advective releases, and the f_r fraction covers those containers with a failed air gap. The f_r fraction was a user supplied value. In TSPA-1991 (Barnard et al., 1992), half of the containers were assumed to be in the f_r fraction. The fraction of containers in the f_s fraction was calculated from the following equation:

$$f_s = P[q > q_0] = 0.5 \cdot \mathrm{erfc}\left(\frac{\ln q_o - u}{\sqrt{2}\,\sigma}\right) \qquad \text{(A-1)}$$

where: erfc = complementary error function (1 - error function)
- u = mean of the spatial flux distribution in log space
- σ = standard deviation of the spatial flux distribution in log space
- q = percolation rate
- q_0 = flux carried by porous matrix (assumed equal to the saturated matrix hydraulic conductivity of the Topopah Springs, a tuff unit of Yucca Mountain that is the potential repository host rock).

An approximation of the error function is taken from Abramowitz and Stegun (1970), p. 299:

$$\mathrm{erf}(x) = 1 - (a_1 \cdot t + a_2 \cdot t^2 + a_3 \cdot t^3) \cdot e^{-x^2} \qquad \text{(A-2)}$$

where $t = 1/(1+p \cdot x)$
$p = 0.47047$
$a_1 = 0.3480242$
$a_2 = -0.0958798$
$a_3 = 0.7478556$

The absolute value of the error of this approximation is less than or equal to 2.5×10^{-5}.

The average flux for those containers subjected to seepage flow is given by:

$$q' = q \cdot f_s^{-1} \cdot 0.5 \cdot \mathrm{erfc}\left(\frac{\ln q_0 - u - \sigma^2}{\sqrt{2}\,\sigma}\right) \qquad \text{(A-3)}$$

It is assumed that q_0 of that flux is carried by the porous matrix, so that the average flux available for seepage flow is given by:

$$q_s = q' - q_0 \qquad \text{(A-4)}$$

The implementation of this in RIP was included in the definition of water contact modes. The following details the parameter information (function, distribution) for the RIP representation of this conceptualization. Basically, the information is input to the RIP menu item called "Fraction of remaining waste packages in this contact mode" (Miller et al., 1993). The preliminary determination included the calculation of f_s, the fraction of containers with seepage.

A portion of the logic expressed in the definition of water contact mode fraction is required to circumvent a RIP criterion. For each water contact mode defined within RIP, there must be at least one container. Also, for each waste group within a contact mode there must be at least one container. We have defined four contact modes and two waste groups (spent fuel 1 (PWR) and spent fuel 2 (BWR)), and each mode must have at least one container. The "IF" statements (to be presented below) which define the lower and upper bound of the fraction for each water contact mode are established to meet this RIP criterion. An example is found in the definition of WC1CON (see Equation A-5), which constrains the fraction for water contact mode 1 between 0.0002 and 0.9996. Note that RIP deals with the fraction of remaining waste packages, so the remaining waste packages must be calculated prior to determining how many waste packages are in a particular water contact mode.

Water Contact Mode 1 -- Wet Feet:

The TSPA-1991 fraction for this water contact mode is equal to the fraction of containers in seepage areas times the fraction of containers with rubble filling at least part of the air gap ($f_s \cdot f_r$). Since this is the first water contact mode, 33,300 waste packages are available. The logic must ensure that more than one waste package is in each of the waste groups.

The fraction input to RIP (WC1CON) has a minimum value (WC1) of 0.0002 and a maximum value of 0.9996. Otherwise, the value (WC1) is equal to $f_s \cdot f_r$, This is incorporated into RIP using the following equations:

$$WC1CON = IF(WC1<=0.0002,0.0002,(IF(WC1>=0.9996,0.9996,WC1))) \quad \text{(A-5)}$$

and

$$WC1 = f_s \cdot f_r \quad \text{(A-6)}$$

where f_r = 0.5
f_s = $0.5 \cdot erfc$
erfc = 1 - erf
erf = $1 - (a_1 \cdot t_1 + a_2 \cdot t_1^2 + a_3 \cdot t_1^3) \cdot \exp(-x_{abs}^2)$
a_1 = 0.3480242
a_2 = -0.0958798
a_3 = 0.7478556
t_1 = $1/(1+p \cdot x_{abs})$
x_{abs} = If x is less than 0, change the sign; otherwise, x remains the same
P = 0.47047
X = $(\ln(K_0)-\ln(q)+0.49477)/1.406799$
K_0 (mm/yr) = beta distribution: mean = 0.63, S.D. = 0.61, min = 0, max = 25
q (mm/yr) = beta distribution: mean = 1, S.D. = 0.89, min = 0, max = 39

Under these conditions, the minimum number of waste packages is 6.66 packages and the maximum is 33286.68. This allows for waste packages to be assigned to the remaining 3 water contact modes each of which has 2 waste groups. The upper bound could be refined in future work to include all but 6 waste packages.

Water Contact Mode 2 -- Wet Drip:

The TSPA-1991 fraction for this water contact mode is equal to the fraction of containers in seepage areas times one minus the fraction of containers with rubble filling at least part of the air gap ($f_s \cdot (1-f_r)$).

This fraction must take into account the number of packages remaining and ensure at least one package per waste group, while leaving enough waste packages for the last two water contact modes.

The fraction input to RIP (of remaining waste packages) is set to 0.2 if the wet feet fraction is 0.9996. Otherwise, the fraction is constrained by the number of WPs already in water contact mode 1 (Equation A-7), and has a minimum of 0.0001 (Equation A-8).

$$WC2 = 33300 \cdot (f_s \cdot (1-f_r))/(33300-(f_s \cdot f_r \cdot 33300)) \quad \text{(A-7)}$$

$$WC2CON = IF(WC2<=0.0001,1/((1-WC1) \cdot 13320), (IF(WC2>=0.9996,0.9996,WC2))) \quad \text{(A-8)}$$

Under these conditions, the minimum number of waste packages for this water contact mode is 2.66 packages. This occurs if the water contact mode 1 fraction is 0.9996, leaving 13.32 packages.

Water Contact Mode 3 -- Moist Continuous:

The TSPA-1991 fraction for this water contact mode is equal to the fraction of containers with rubble filling at least part of the air gap times one minus the fraction of containers in seepage areas.

The fraction for this water contact mode is calculated similar to water contact mode 2, with a minimum of 0.0001 and a maximum of 0.9997 of the remaining waste packages. The fraction is also constrained by the number of WPs already in water contact modes 1 and 2.

Using Equation A-9, water contact mode 3 fraction

$$= 33300 \cdot ((1-f_s) \cdot f_r)/(33300-(33300 \cdot f_s \cdot f_r)-(33300 \cdot f_s \cdot (1-f_r))) \qquad \text{(A-9)}$$

Water Contact Mode 4 -- Nominal:

The fraction of WPs in this water contact mode is equal to one, all of the remaining WPs.

Q_s Evaluation:

The second phase of implementing the infiltration dependent grouping of waste packages required incorporation of q_s (see Equations A-3 and A-4). The infiltration rate in water contact modes 1 and 2 is altered according to the following equation:

$$q_s = \frac{q \cdot \frac{1}{2} \cdot \mathrm{erfc}\left(\frac{\ln K_0 - \ln q - 0.49477}{1.406799}\right)}{\frac{1}{2} \cdot \mathrm{erfc}\left(\frac{\ln K_0 - \ln q + 0.49477}{1.406799}\right)} - K_0 \qquad \text{(A-10)}$$

Otherwise, infiltration is selected from the original beta distribution of:

beta: mean = 0.001, S.D. = 0.0009, min = 0, max = 0.039.

The error functions are constrained so that if they are equal to 1, they are set to 0.99999.

A.2 PROCEDURE USED TO IMPLEMENT AIR GAP IN RIP

The air gap in TSPA-1991 was simulated as an integrated part of the diffusion release calculations. In RIP, the air gap was included in the following manner. A pathway of 3 cm length was included. Release only went to this pathway when the water contact mode was 3 by specifying the radionuclide inventory release pathway fraction definition as 1 if and only if the water contact mode was 3.

In other words, if the water contact mode was 3, all of the release went to the air gap pathway. If the water contact mode was other than 3, the release went to a fast path which did not delay the radionuclide transport at all.

The parameter information for the air gap pathway was:

Length = 0.03 m
Area of pathway = 1 m^2
Volumetric flow = 1 m^3/yr
Dispersivity = 1 m (arbitrary)
Poisson transition rate = 0
Velocity = moist diffusion coefficient
Retardation: sorption = 1; diffusion = 1
Moist diffusion coefficient = Log-uniform: 3.0×10^{-6} to 3.0×10^{-4} m^2/yr

The velocity in the air gap pathway was intended to simulate the diffusive mass transfer release through the 3 cm air gap.

The parameter information for the fast path was:

Length = 0.03 m
Area of pathway = 560000 m^2
Volumetric flow = 210 m^3/yr
Dispersivity = 1 m
Poisson transition rate = 0
Velocity = 100 m/yr
Retardation: sorption = 1; diffusion = 1

A.3 PROCEDURE TO IMPLEMENT DIFFUSIVE RELEASE INTO WASTE PACKAGE.

In RIP, the diffusive release occurs only from water contact modes 1 and 3. This is implemented in the radionuclide inventory where all radionuclides are given the same effective diffusion coefficient (m^2/yr), but diffusion is only allowed if water contact mode is equal to 1 or 3. The diffusion coefficient for water contact mode 1 was equal to TSPA-1991 wet diffusion coefficient, and for water contact mode 3 was equal to the TSPA-1991 moist diffusion coefficient. The geometric factor for diffusion was also constrained to zero for water contact modes 2 and 4. Otherwise, it was set to one. This is implemented in RIP as follows:

Geometric Factor for Diffusion (GDVAL):

```
IF((CONTAC==1) !! (CONTAC==3),GDVAL,0)
GDVAL = 1
```

A.4 EFFECTIVE CATCHMENT AREA

To ensure that only packages with advective release (water contact modes 1 and 2) had infiltration, logic was set up in RIP for the definition of effective catchment area to be equal to one only if water contact mode was 1 or 2. This is implemented in RIP as follows:

```
IF ((CONTAC==1) !! (CONTAC==2),1,0)
```

A.5 FAILURE FOR NOMINAL WATER CONTACT MODE (4)

It was assumed there were no releases from waste packages in water contact mode 4, so no WP failures could occur in this mode. To implement this in RIP, if water contact mode was equal to 4, then no infiltration was allowed, the effective catchment area was equal to zero, and the geometric factor for diffusion was zero. Each of these constraints was implemented using the logic statements in RIP.

APPENDIX B. RIP THEORY: NUMERICAL ILLUSTRATIONS

B.1 GENERAL

This appendix explains the algorithm for the flow and transport simulation in the RIP code with the aid of simple numerical examples. It may be recalled that the RIP code does not have a capability for flow simulation, but requires the velocity to be input directly or indirectly. Also, the transport simulation is based on a simplified version of the Markov process, as explained earlier. When there are two modes in a pathway, the method of apportioning the given flow rate in the matrix and fracture has also been explained earlier.

For purposes of illustration, individual vertical columns simulating the flow and transport in the unsaturated zones are considered. In particular, columns 1 and 6, used in the simulation of unsaturated flow and transport below the repository, are used for verification. These cases are single deterministic cases corresponding to the expected values in all the distributions. The hydrogeologic parameters for the layers in the columns are shown in Tables B-1 and B-2 for the matrix and fractures, respectively. The thicknesses of the layers are shown in Tables B-3 and B-4 for column 1 and column 6, respectively. For simplicity, a constant release rate of 238.84 Ci/yr has been used. The computations have been made under conditions of "full coupling" and "no coupling" between the matrix and the fracture. In the RIP model, full coupling is simulated by specifying the poisson transition rate λ to be very large, and no coupling is simulated by specifying λ to be close to zero. For example, when λ is very low, the mean length of travel in that mode is very large (greater than the length of the leg), effectively ensuring that the particle travels in the same medium without transition to the other medium. Simulations have been performed for 50,000 years. (There will be no release at 10,000 years at the bottom of layer 5 in column 1.)

In order to understand the RIP simulation, it would be necessary to compute the fluxes and velocities through the matrix and fracture in each of the five layers used in the discretization of the unsaturated flow and transport domain. Subsequently, travel times through the matrix and fracture need to be computed.

B.2 FLUXES AND VELOCITIES IN ALL LAYERS

B.2.1 Fluxes in Matrix and Fractures

Consider for example, layer 1 of column 1. The hydraulic conductivity of the matrix in this layer is 6.3×10^{-4} m/yr. The infiltration rate is 1.0×10^{-3} m/yr. Since the hydraulic conductivity of the matrix is lower than the infiltration rate, the matrix would carry a flux equal to its hydraulic conductivity (under a unit hydraulic gradient). Thus, the matrix would carry a flux of 6.3×10^{-4} m/yr and the balance of 3.7×10^{-4} m/yr would be carried by the fracture. The flow proportions for matrix (f_m) and fracture (f_f) in layer 1 would be 0.63 and 0.37, respectively.

As another example, consider layer 3, where the hydraulic conductivity is 2.5 x 10^{-3} m/yr, which is higher than the infiltration rate. Thus, the matrix in layer 3 can carry the full infiltration rate and none of the infiltration would go through the fracture. The fluxes through the matrix and the fracture would be 1.0 x 10^{-3} m/yr and 0, respectively. (The flow factors are 1.0 and 0.0 for the matrix and fracture, respectively, in layer 3.)

A similar situation as in layer 3 also prevails in layer 5, where the matrix would carry the entire infiltration. The fluxes in the matrix and the fracture for all the five layers in the unsaturated flow zone are computed in Tables B-1 and B-2, respectively, based on the hydrogeologic parameters.

B.2.2 Velocities in Matrices and Fractures

The interstitial velocity in the matrix (V_m) is derived by assuming full saturation in the matrix. Accordingly, it is derived by dividing the flux in the matrix (U_m) by the porosity (ϕ_m) of the matrix. In fractures, a saturation of 10 percent is assumed, based on the results of flow simulations by TOSPAC (presented in Appendix C). Accordingly, the effective velocity in the fractures is deduced by dividing the flux in fractures by the product of the fracture saturation and fracture porosity. The values for the velocities in the matrix and fractures are also shown in Tables B-1 and B-2, respectively.

B.3 TRAVEL TIMES IN MATRICES AND FRACTURES

If a particle travels exclusively in a matrix or exclusively in a fracture, the travel times are easily computed using the velocities in the matrix and fracture. The velocities depend merely on the hydrogeologic parameters and depend on the layer and not the column. However, the travel times depend on the thickness of the layer, which differs from column to column. Therefore, the travel times are given separately for column 1 (Table B-3) and column 6 (Table B-4). For example, in column 1 (Table B-3), the travel time through the fracture (T_f) in layer 1 is 65 years, and that through the matrix (T_m) in layer 1 is nearly 7,000 years.

For layer 1, the flow proportions for the matrix and the fracture are 0.63 and 0.37, respectively. These values may be interpreted as the probability for a particle to be in the matrix or the fracture. Thus, there is a 63 percent probability that a given particle would be in the matrix, and a 37 percent probability that it would be in the fracture.

In the case of "full" coupling between the matrix and the fracture, the particle transits with a high frequency between the fracture and the matrix. According to the algorithm in the RIP, the travel time for the full coupling case is given by the expected travel time (T^*), given by:

$$T^* = f_f T_f + f_m T_m$$

The values of T^* are shown in Table B-3 for column 1 and in Table B-4 for column 6.

B.4 NUCLIDE RELEASE RATES

B.4.1 Single Pathway Cases

For these illustrative examples, the nuclide (repository) source is taken to yield a constant release (Q) of 238.84 Ci/yr at the top of the column. For the simplest case, consider a single pathway, given by layer 1, column 1. If there is no coupling between matrix and fracture, it is clear that a fraction f_f (Ci/yr) of the source rate would break through the fracture at time T_f (65 years) and discharge at that rate till the matrix contribution breaks through at T_m (6,980 years), at which time the release rate would equal the source rate. This is illustrated in Figure B-1.

If, however, there is full coupling between the matrix and the fracture, the nuclides would break through layer 1 at the time T* (4,421 years) at the rate of Q (238.8 Ci/yr). This is shown in Figure B-2.

B.4.2 Two Pathways in Series

Consider, for example, layers 1 and 2 in column 1, and the special case of no coupling between the matrix and the fracture in both the layers. As already noted, 63 percent of the nuclides in layer 1 would go through the matrix and 37 percent through the fracture. Thus, 37 percent of the nuclides would reach the top of layer 2 in 65 years. In layer 2, 90.5 percent of these nuclides would travel through the fractures in 17 years. Thus, considering the nuclides traveling through the fracture in both the layers, 34 percent of the nuclides (= 0.37 · 0.905) would exit layer 2 in 82 (= 65 + 17) years. Similarly, of the 37 percent of the nuclides reaching the top of layer 2 in 65 years, 9.05 percent would travel through the matrix in layer 2 in 20,000 years. Thus, 3 percent (= 0.37 · 0.095) of the nuclides would exit layer 2 in 20,065 (= 65 + 20,000) years. Similar considerations of the nuclides reaching the top of layer 2 via the matrix in layer 1 indicate that 57 percent (= 0.63 · 0.905) of the nuclides would exit the fracture in layer 2 at 6,997 (6,980 + 17) years and 6 percent (= 0.63 · 0.095) of the nuclides would exit the matrix in layer 2 at 26,980 (6,980 + 20,000) years. These results are shown in Figure B-3.

In the case of full coupling between the matrix and the fracture in both the layers, nuclides would break through layer 2 at 6,336 (4421 + 1915) years, at a rate of Q (= 238.84 Ci/yr). This is shown in Figure B-4.

These considerations can be extended to predict the releases at the bottom of layer 5 in column 1. (This is not given here.)

B.5 OUTPUT FROM RIP

The results of the RIP simulations in column 1 and column 6, corresponding to the numerical illustrations cited above, are presented here and compared with the result expected from "theory" as given above.

B.5.1 Result for Column 1

Figure B-5 presents releases through layer 1 in column 1 for the uncoupled case. The RIP simulations are in close agreement with the RIP theory shown in Figure B-1. Figure B-6 shows the same results for the fully coupled case and is in good agreement with Figure B-2, which gives the result for RIP theory.

Figure B-7 shows the RIP simulations for the release rates at the bottom of column 1 (i.e., layer 5) for the "no coupling" case. Table B-3 shows that the earliest breakthrough should occur at 38,4876 years (65 + 17 + 13,655 + 1 + 24,760), by traveling through fractures in layers 1, 2, and 4 and in the matrix in layers 3 and 5. However, RIP simulations indicate that the breakthrough occurs at 25,000 years. Further, the fraction that would break through should be 30 percent (0.37 · 0.905 · 1.0 · 0.905 · 1.0), so that the coordinate should be (0.30 · 238.84) 72.37 Ci/yr, while the predicted release is about 130 Ci/yr. This discrepancy arises due to the coarseness of the time steps used in RIP. For example, with the time step Δt = 100 years, certain time windows (cells) span from 12,800 to 25,600 years and from 25,600 to 51,000 years. For example, if the earliest breakthrough occurs at 38,483 years, RIP starts to release the nuclides from 25,600 years, which is the starting point for that time window (cell). In general, this results in higher releases than those computed theoretically. This treatment of the releases is adequate for the purposes of this comparative performance assessment.

In the case of full coupling, Table B-3 indicates the breakthrough should be at 56,162 years. Figure B-8, which shows the RIP simulation, gives 37,000 years as the breakthrough time. The reason for this discrepancy is again due to the coarseness of the time windows, as explained above.

B.5.2 Results for Column 6, Layer 1

Figures B-9 and B-10 shows the release rates through layer 1 of column 6 for the "no coupling" and "full coupling" cases, respectively. Table B-3 shows that, for the no coupling case, the release through the fracture should occur at 108 years, and through the matrix at 11,692 years. Figure B-9 shows about 100 years and 7,000 years, respectively, for these breakthrough times using RIP. Although the agreement is not as good as in column 1 for breakthrough times, the proportions through the fracture (0.37) and the matrix (0.63) are correctly reproduced by RIP. For the fully coupled case, Table B-4 indicates that 7,405 years should be required for breakthrough. Figure B-10 shows close agreement with this value.

Figures B-11 and B-12 present the results for the release rates through the bottom of layer 4 in column 6 for "no coupling" and "full coupling" cases, respectively. Table B-4 indicates the earliest breakthrough should occur at 4,743 years (108 + 10.7 + 4,621 + 3) by traveling through the fracture in layers 1, 2, and 4 and through the matrix in layer 3. The corresponding fraction would be (0.37 · 0.905 · 1 · 0.905) 0.30, so that the release rate given should be 72 Ci/yr (0.30 · 238.84). Figure B-11 shows good agreement with these values. Subsequently, after 11,692 years, i.e., at a total time of (11,692 + 4,743) 16,435 years, the contributions from the matrix in layer 1 would reach the bottom of layer 4 and the total release would be 82 percent ((0.63 + 0.37) · 0.905 · 1 · 0.905). The release rate at 16,435 years should be (0.82 · 238.84) 196 Ci/yr. Figure B-11 shows agreement with these times and release rates. For certain theoretical

breakthrough times, as in this example, the RIP time windows yield more accurate results. (This is not generally the case.)

For the case of full coupling, Table B-4 shows the breakthrough time should be 46,349 years. Figure B-12 shows a value of 37,000 years. The reason for this discrepancy is due to the coarseness of time windows in RIP simulations.

B.6 RIP'S ABILITY TO MIMIC A DISPERSIVE FRONT

In the earlier illustrations presented, extreme values of λ were used, which gave rise to sharp release fronts. This section presents the results for intermediate values of λ and examines whether the dispersive fronts for the release given by other process models such as TOSPAC can be given by RIP simulations. Once again, for illustration, layer 1 of column 1 and the bottom of column 1 are used.

Layer 1 of Column 1:

In general, for very low values of λ, λ has been set to 10^{-8} m^{-1}, and for large values, λ has been set to 10^{8}. The results for λ = 1,0, 0.1, 0.05, 0.025, 0.01, and 10^{-3} m^{-1} are all presented in Figures B-13 through B-18. For values of $\lambda \geq 1$, the results do not change. Similarly, for $\lambda \leq 10^{-3}$ m^{-1}, the results do not change. They correspond respectively to large and small values of λ, in that they ensure full coupling and no coupling for this example. Values of λ between 0.01 and 0.1 m^{-1} bring about dispersive fronts. A rough guideline for λ to produce such dispersive fronts would be to use $\lambda \approx 1/L$, where L is the length of the pathway.

Column 1:

The release rates for $\lambda = 10^{4}$, 10^{2}, 10^{1}, 10^{0}, 10^{-1}, 10^{-2}, and 10^{-3} m^{-1} are shown in Figures B-19 through B-25. At the bottom of Column 1, where the flow and transport would take place through five layers (pathways), it is found that the dispersive front produced for layer 1 cannot be reproduced. This again is due to the travel times being large (30,000 to 50,000 years) and the extreme coarseness of the time windows used to simulate the release rates in that period.

Conclusions: RIP results were generally adequate for the purposes of this comparative performance assessment. Results were generally more "conservative" in actual runs than theoretical results, largely because of the large fixed time windows used in RIP.

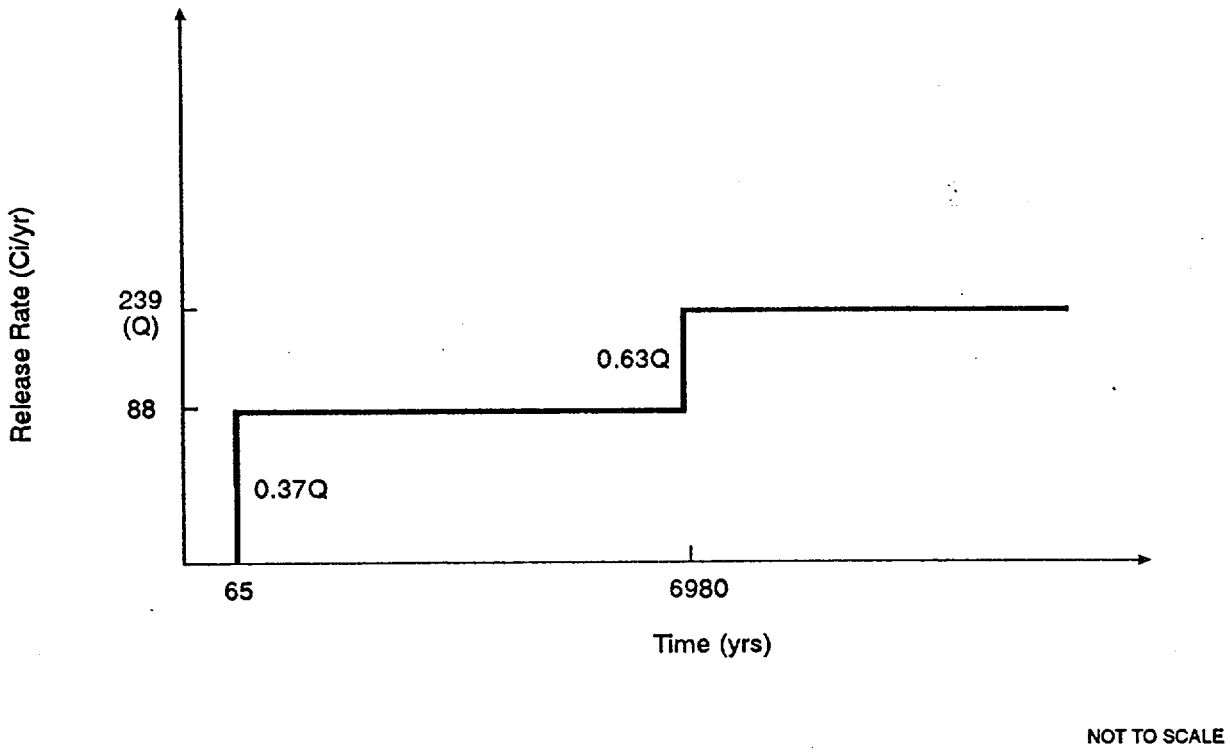

Figure B-1. Nuclide Release Rate for Layer 1, Column 1: No Coupling Case - RIP Theory

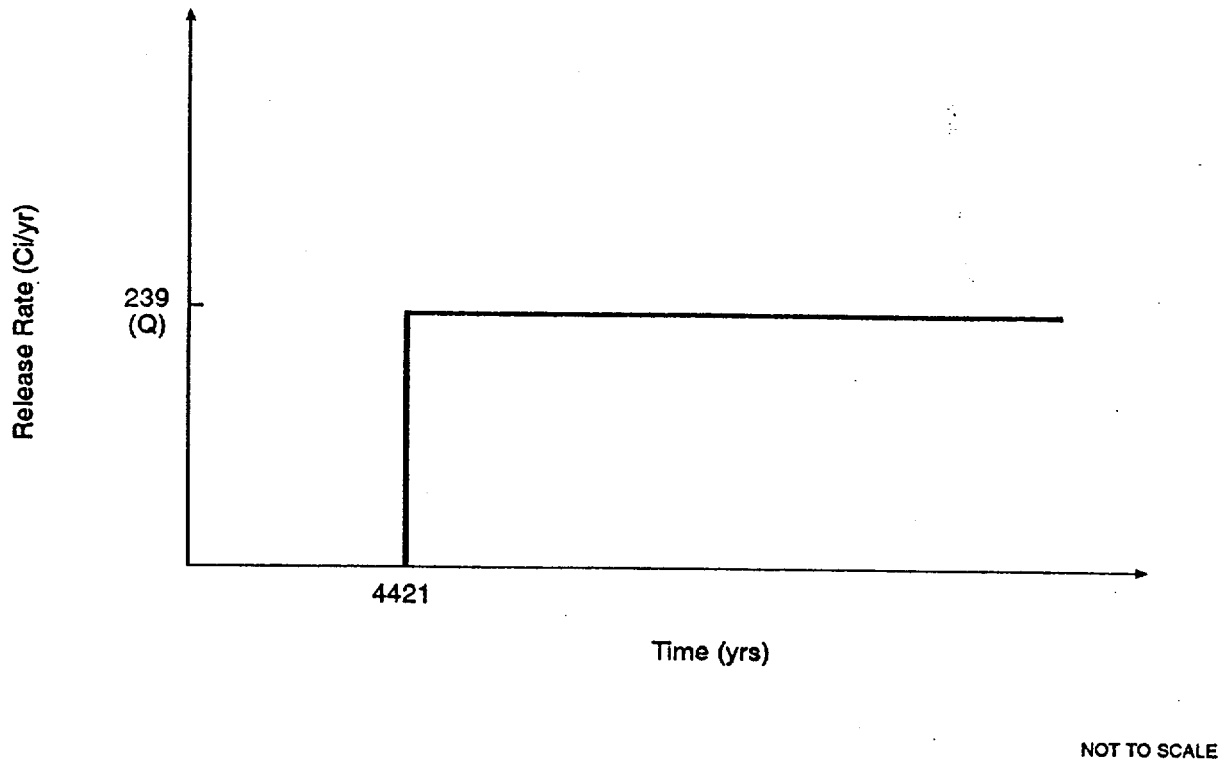

Figure B-2. Nuclide Release Rate for Layer 1, Column 1: Full Coupling Case - RIP Theory

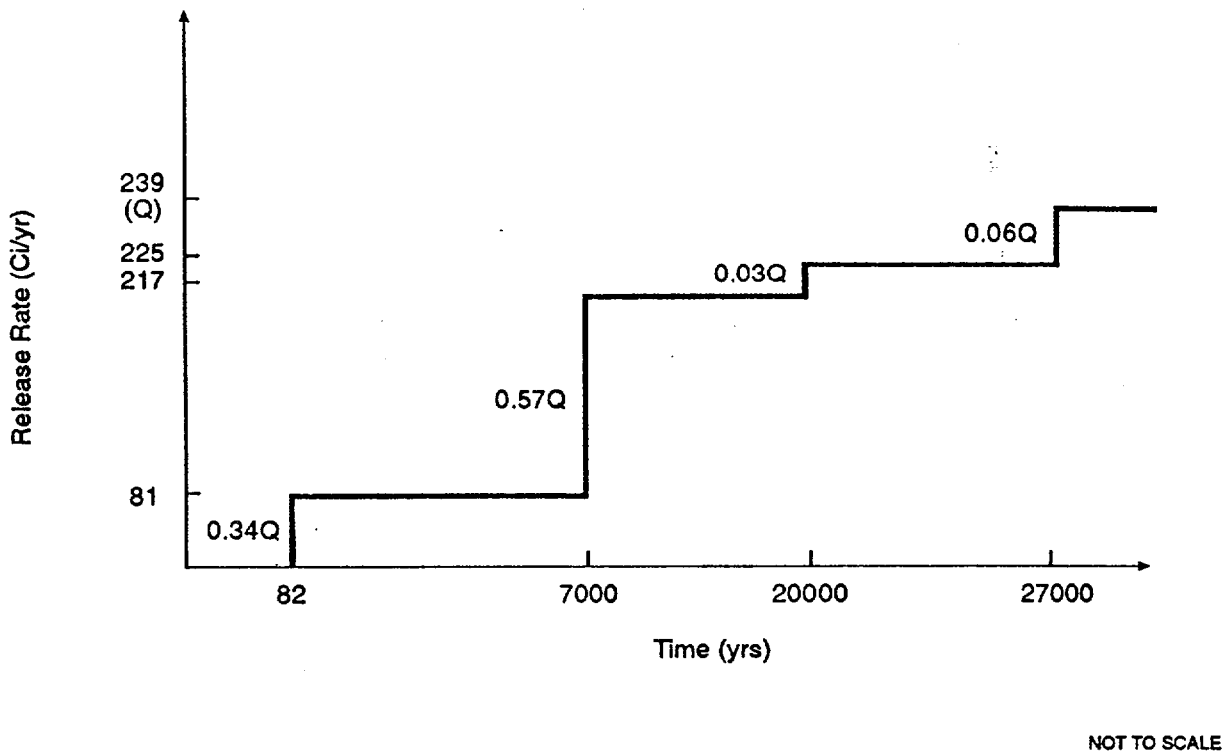

Figure B-3. Nuclide Release Rate Through Layer 2, Column 1:
No Coupling Case - RIP Theory

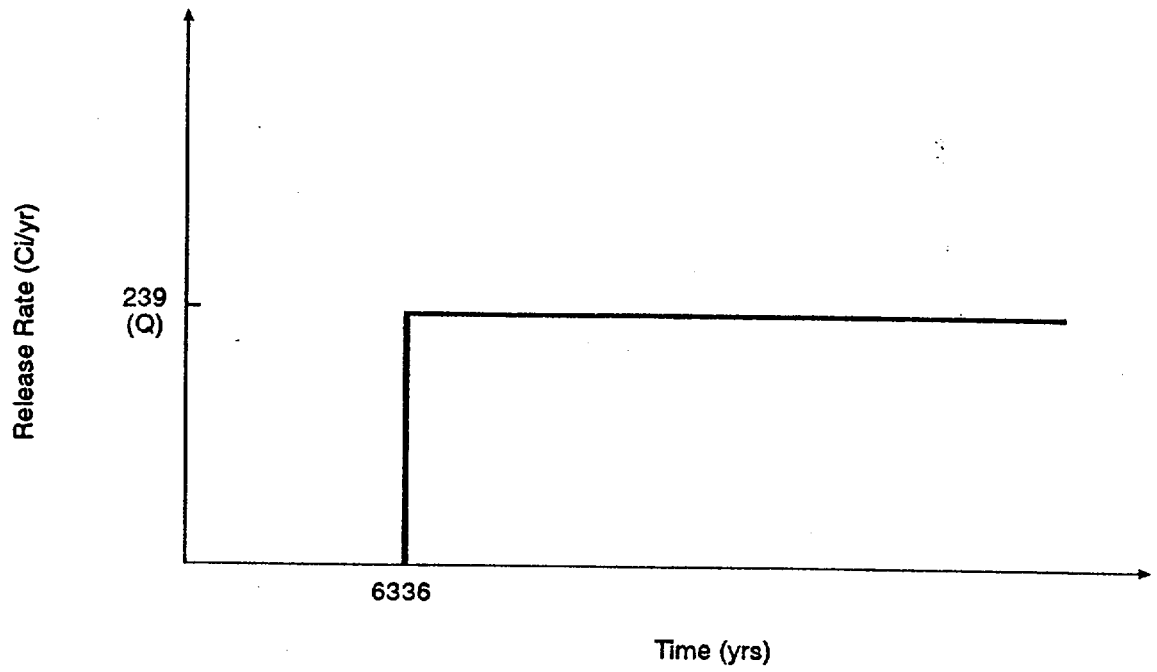

NOT TO SCALE

Figure B-4. Nuclide Release Rate Through Layer 2, Column 1:
Full Coupling Case - RIP Theory

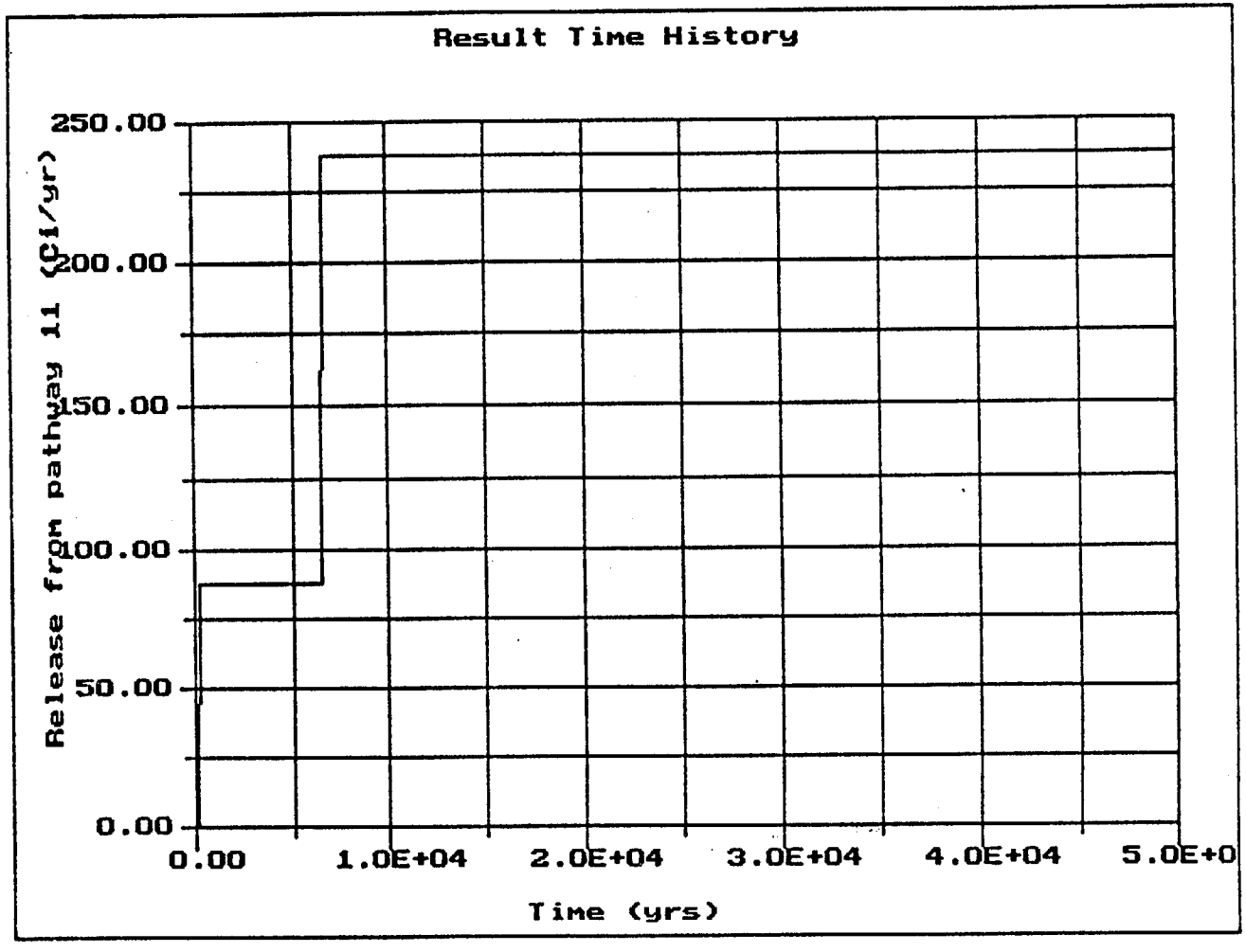

Figure B-5. Nuclide Release Rate Through Layer 1, Column 1: No Coupling Case - RIP Simulations

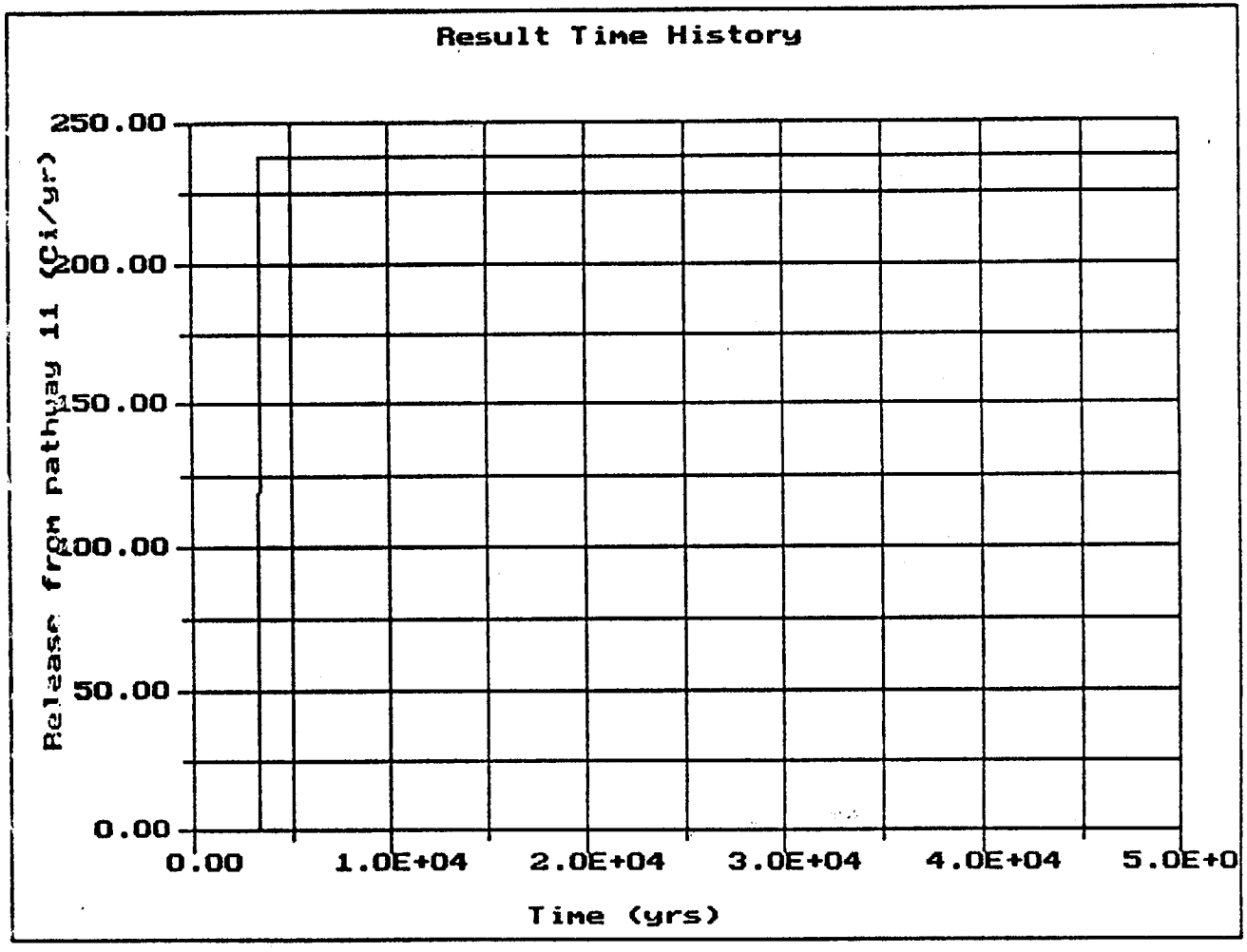

Figure B-6. Nuclide Release Rate Through Layer 1, Column 1: Full Coupling Case - RIP Simulations

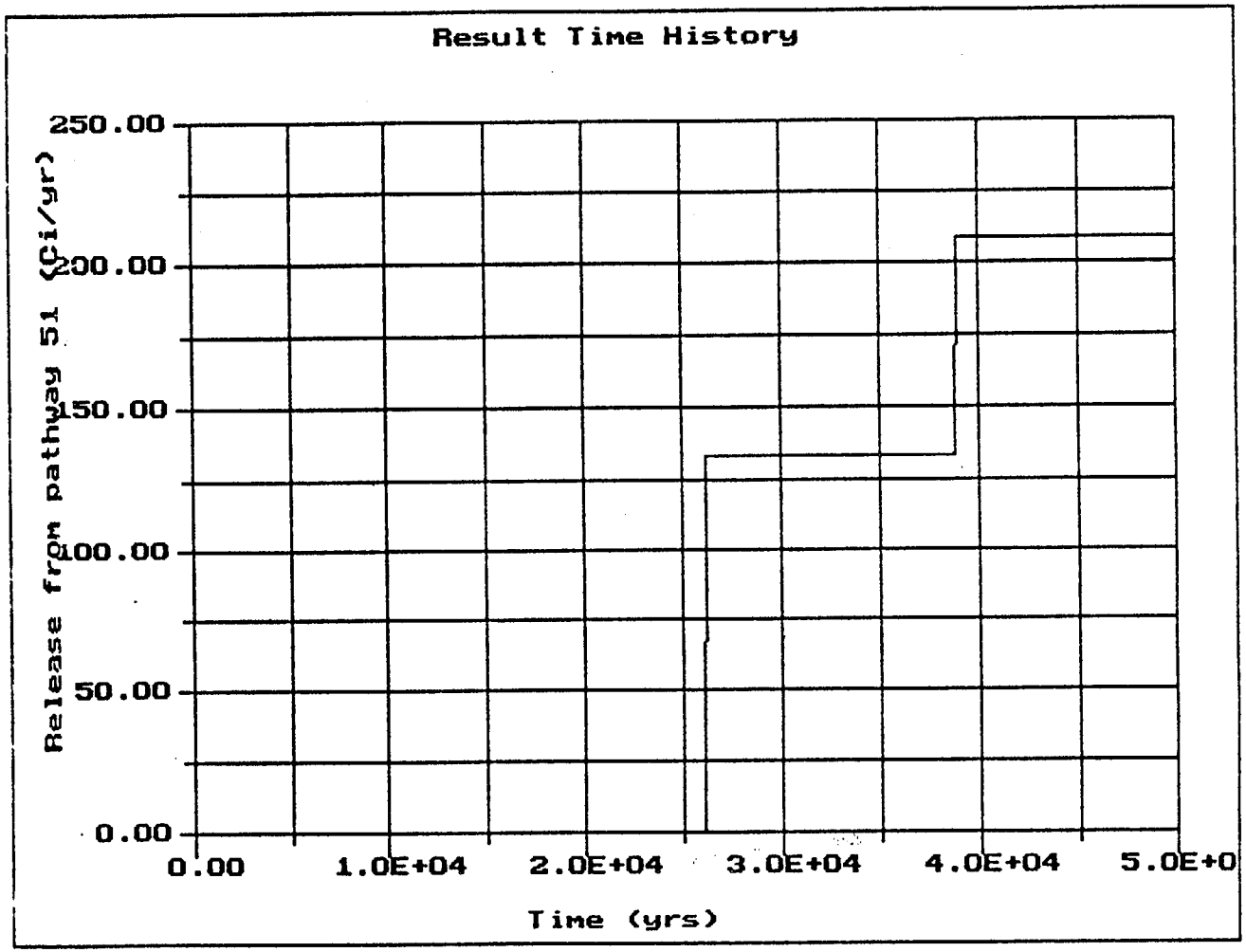

Figure B-7. Nuclide Release Rate at the Bottom of Column 1: No Coupling Case - RIP Simulations

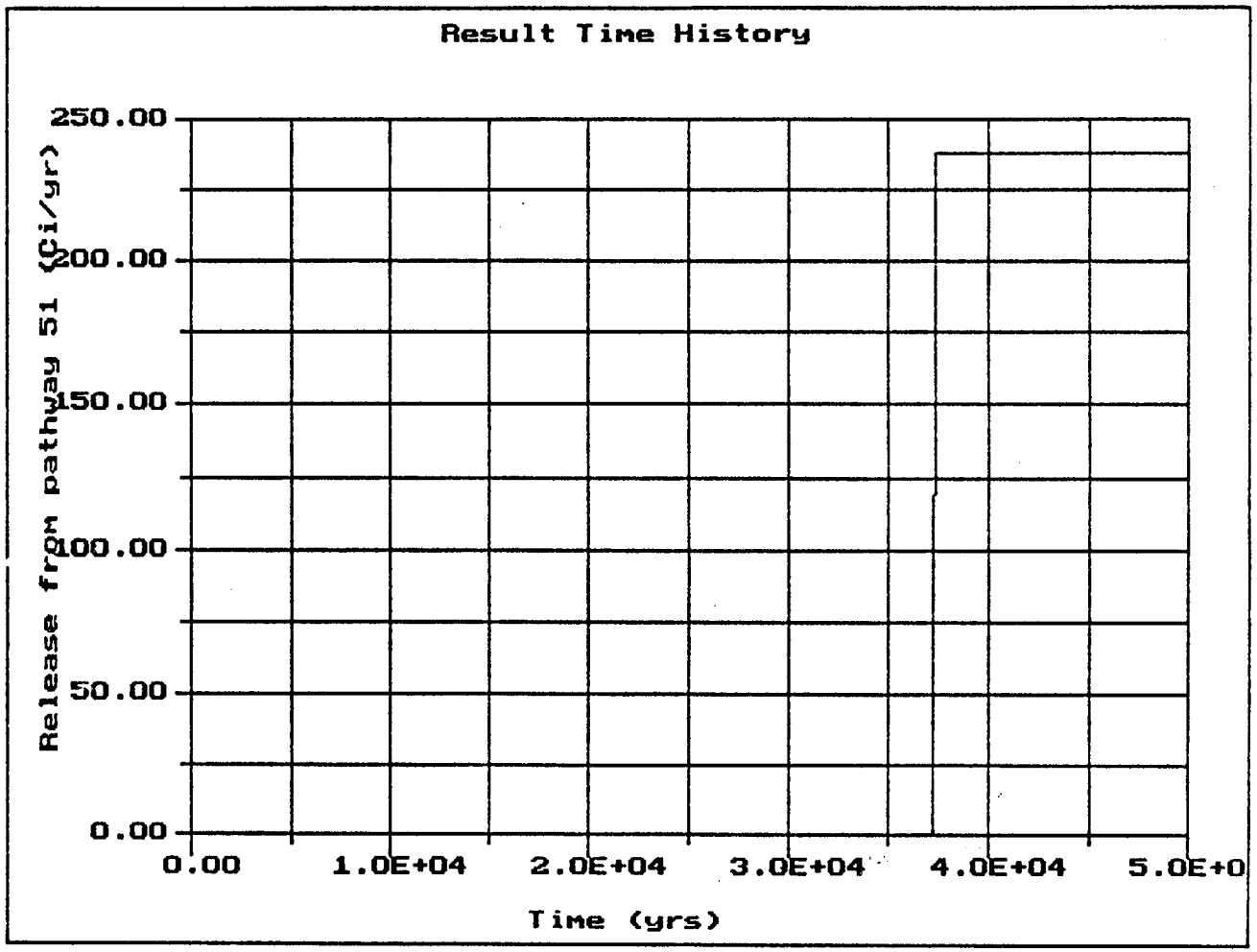

Figure B-8. Nuclide Release Rate at the Bottom of Column 1: Full Coupling Case - RIP Simulations

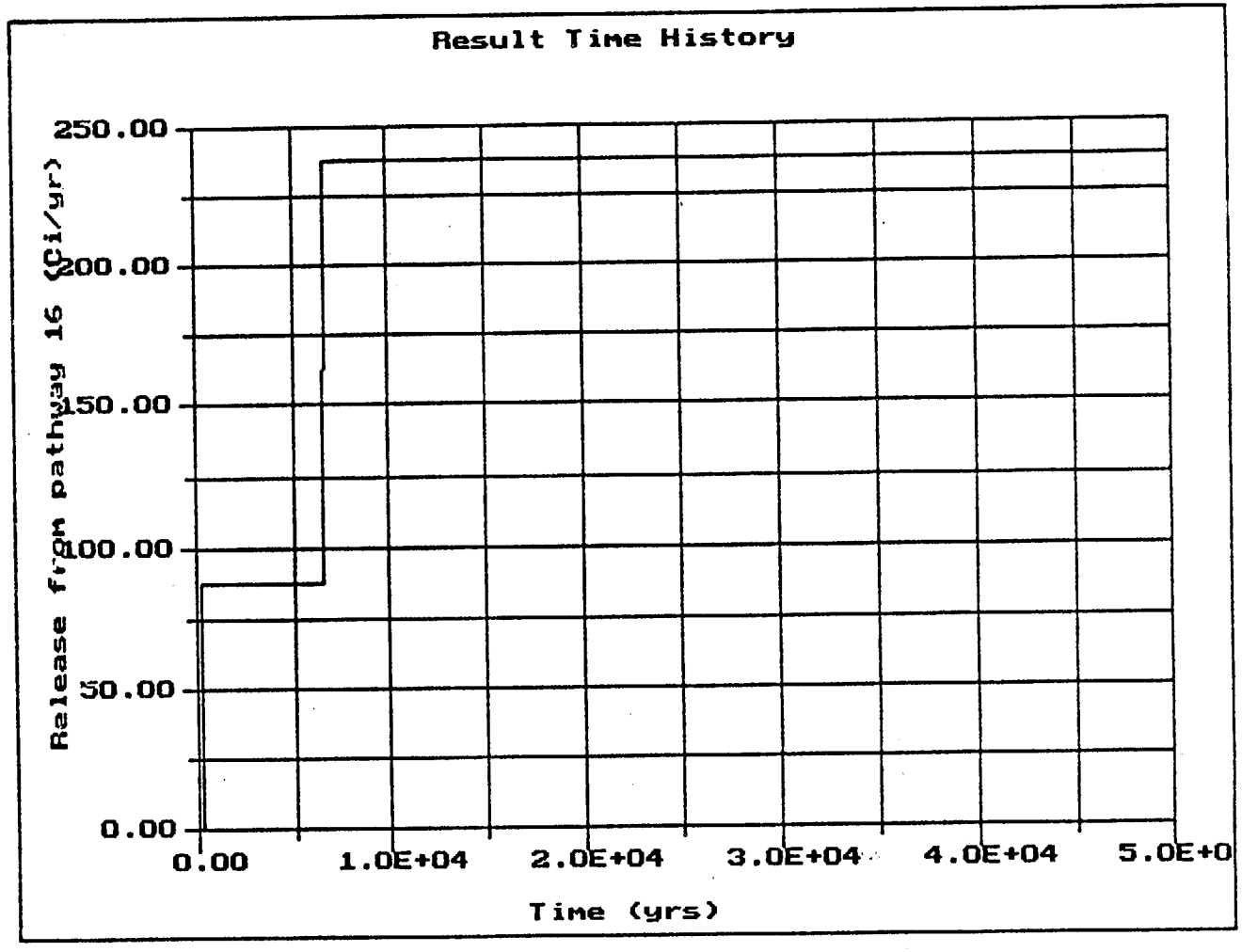

Figure B-9. Nuclide Release Rate Through Layer 1, Column 6: No Coupling Case - RIP Simulations

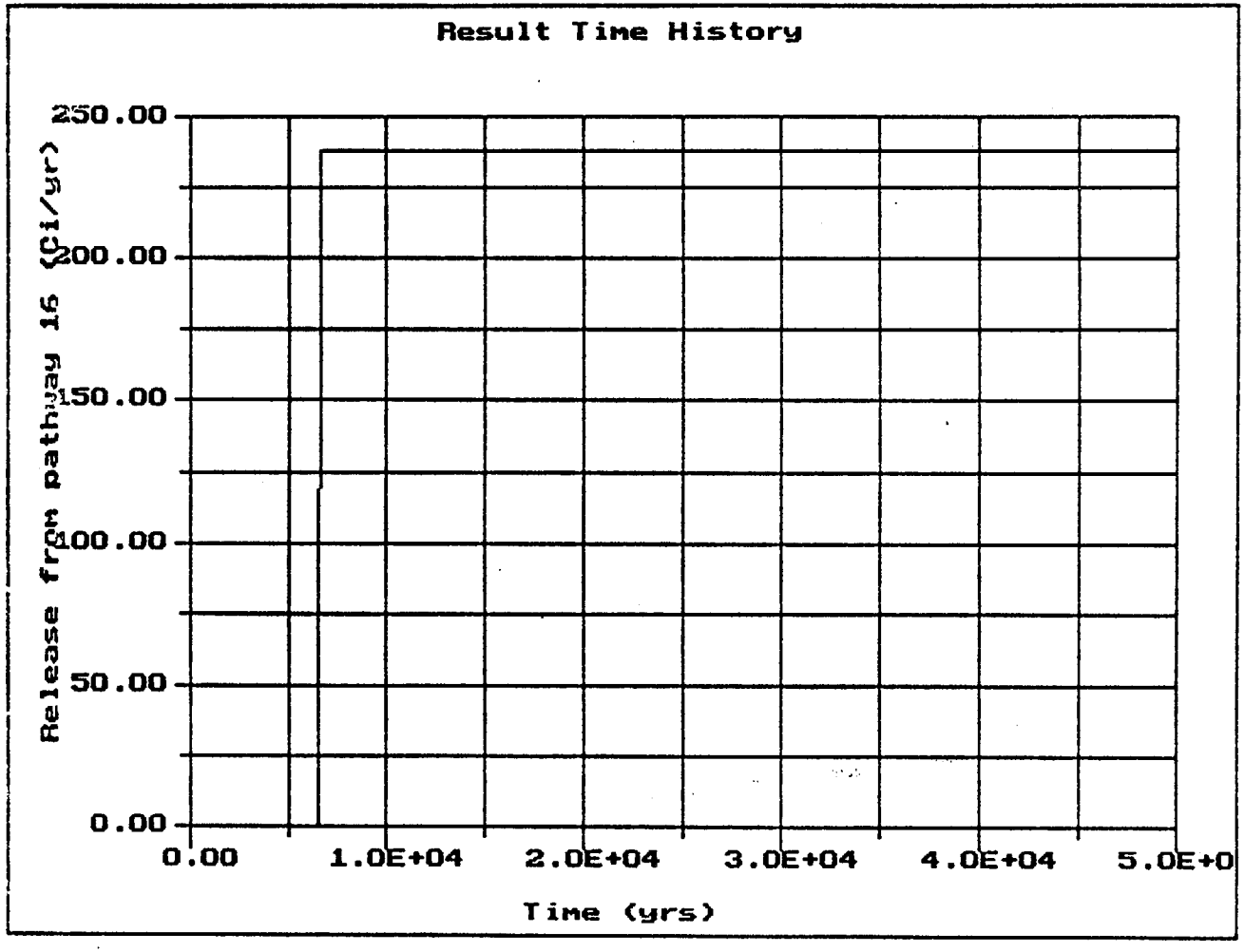

Figure B-10. Nuclide Release Rate Through Layer 1, Column 6: Full Coupling Case - RIP Simulations

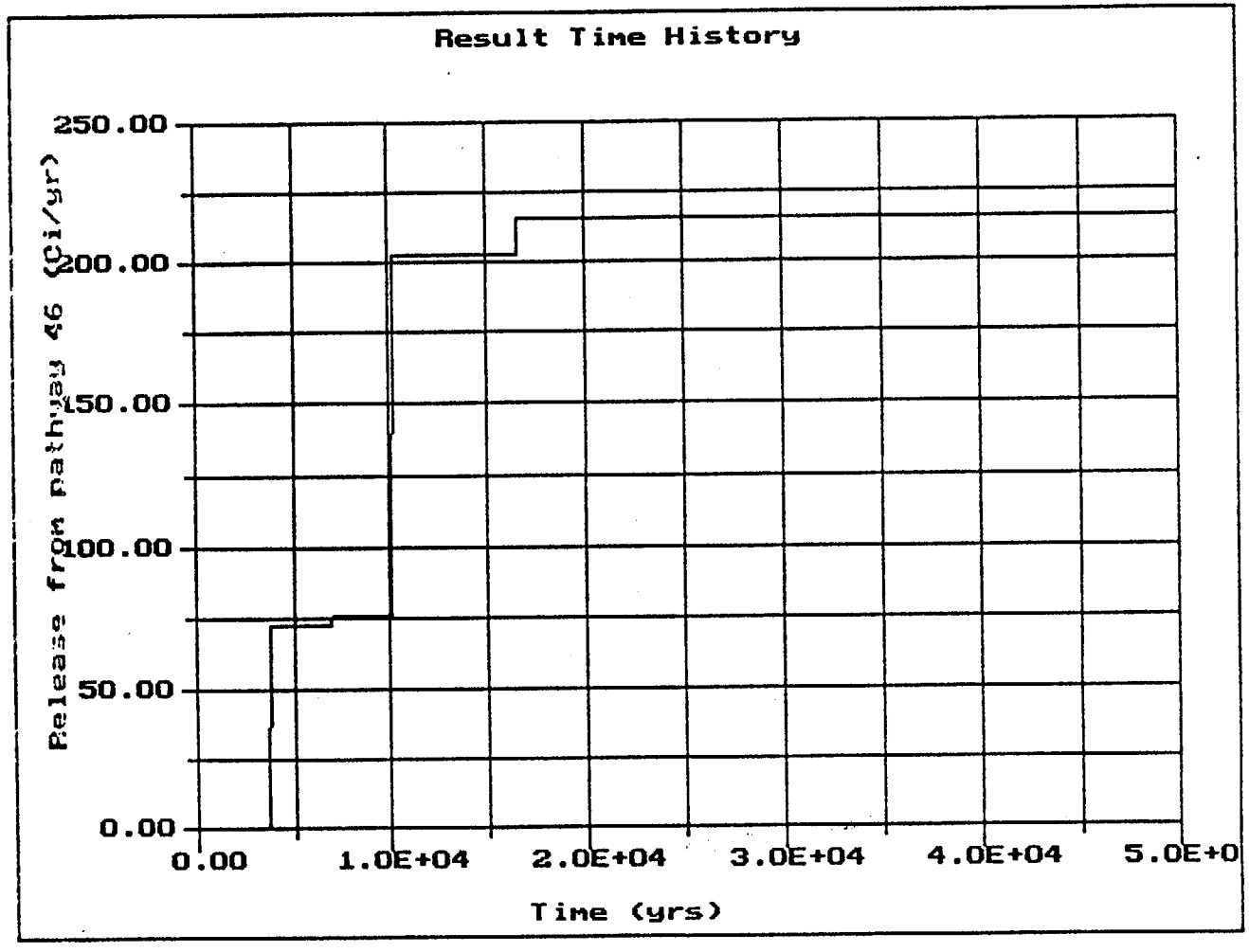

Figure B-11. Nuclide Release Rate at the Bottom of Column 6: No Coupling Case - RIP Simulations

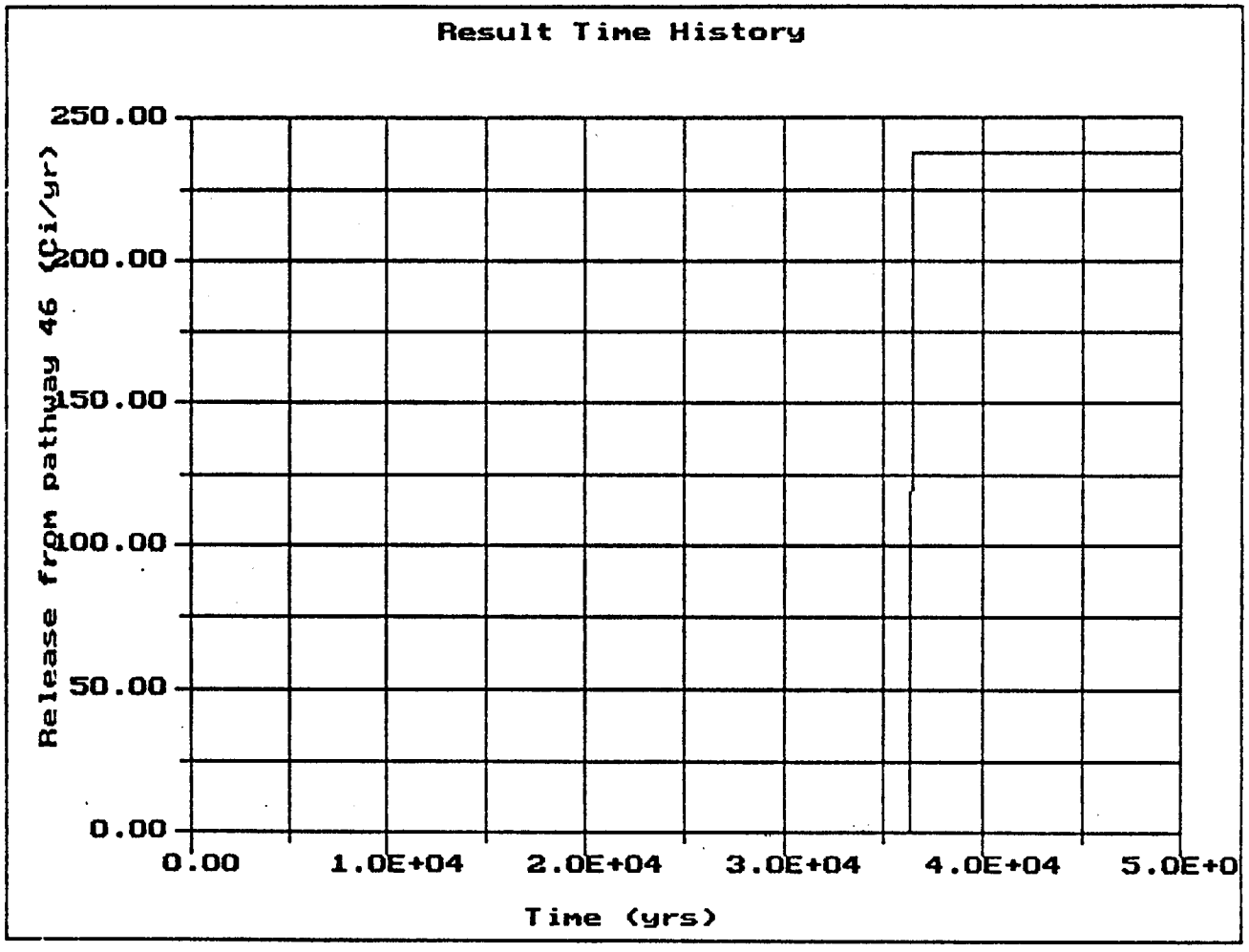

Figure B-12. Nuclide Release Rate at the Bottom of Column 6: Full Coupling Case - RIP Simulations

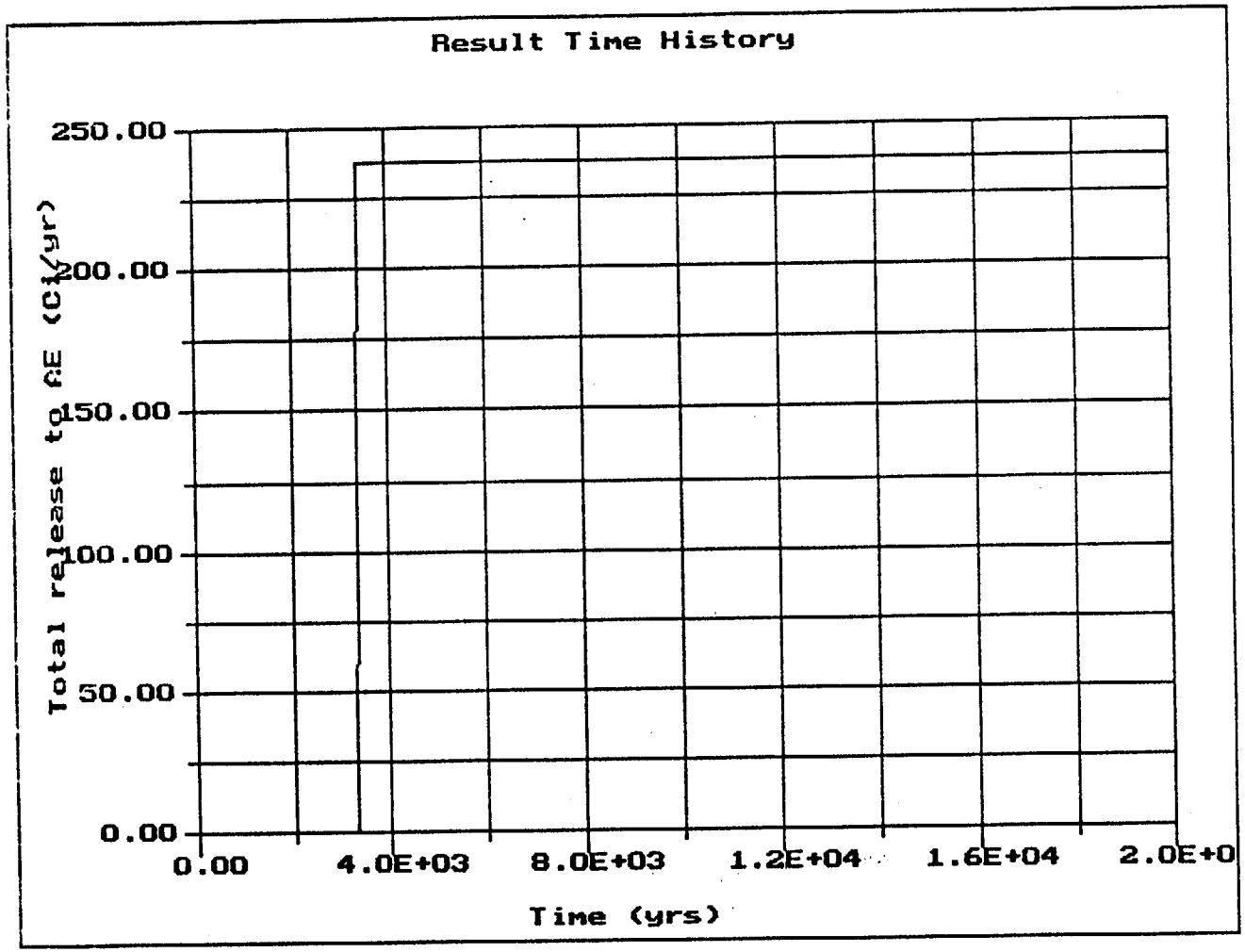

Figure B-13. Effect of λ on Breakthrough Curves at the Bottom of Layer 1: $\lambda = 1.0\ m^{-1}$

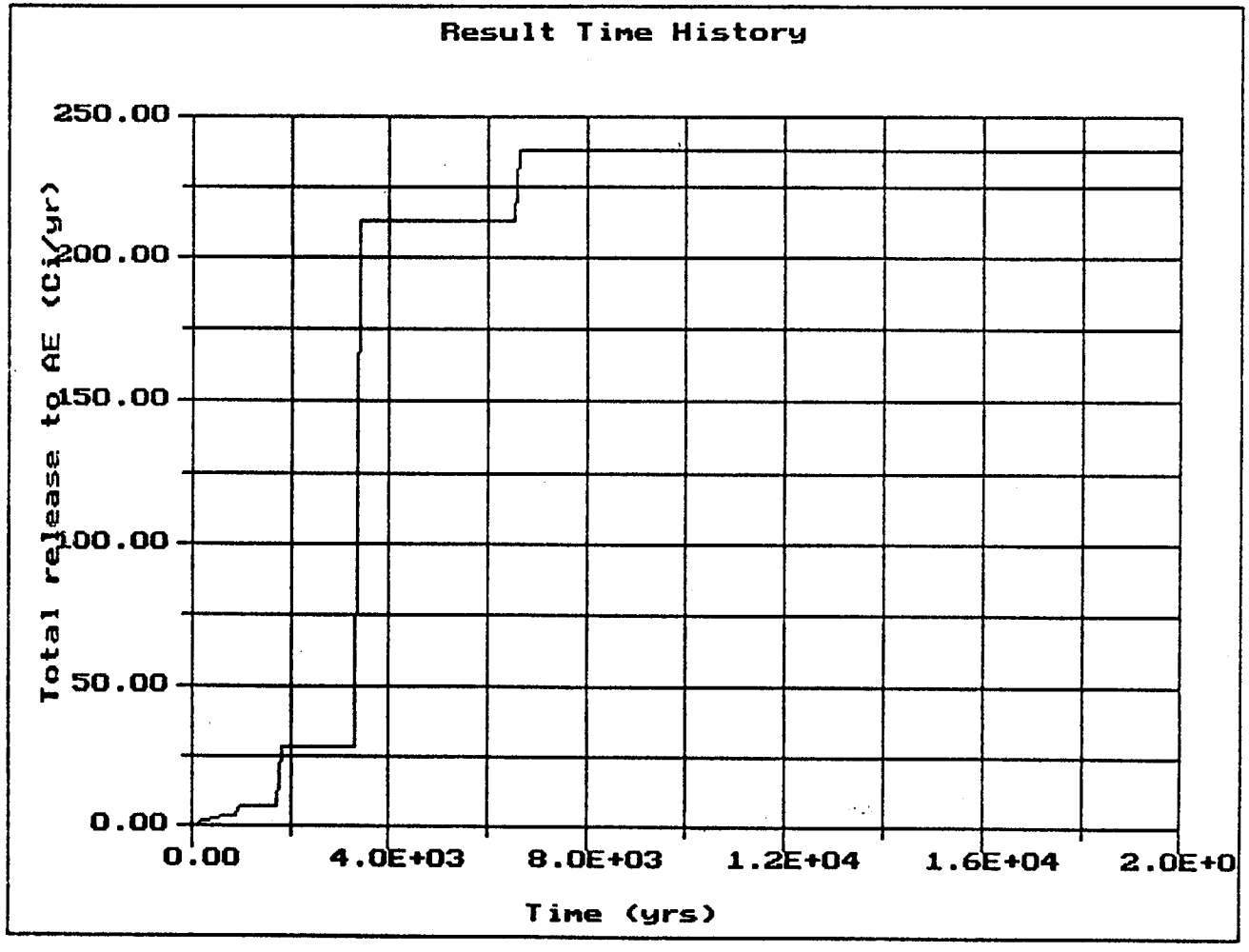

Figure B-14. Effect of λ on Breakthrough Curves at the Bottom of Layer 1: $\lambda = 0.1\ m^{-1}$

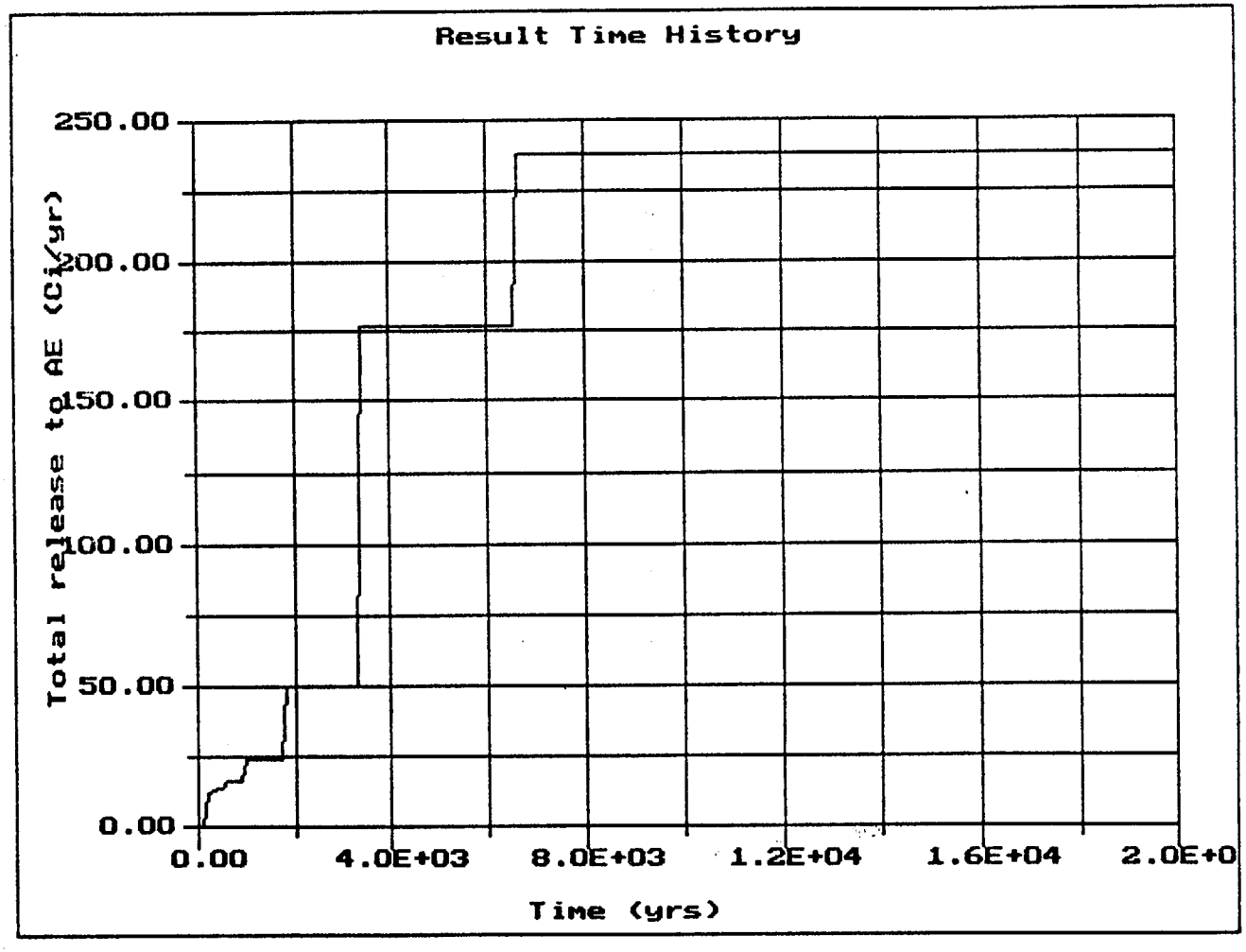

Figure B-15. Effect of λ on Breakthrough Curves at the Bottom of Layer 1: $\lambda = 0.05\ m^{-1}$

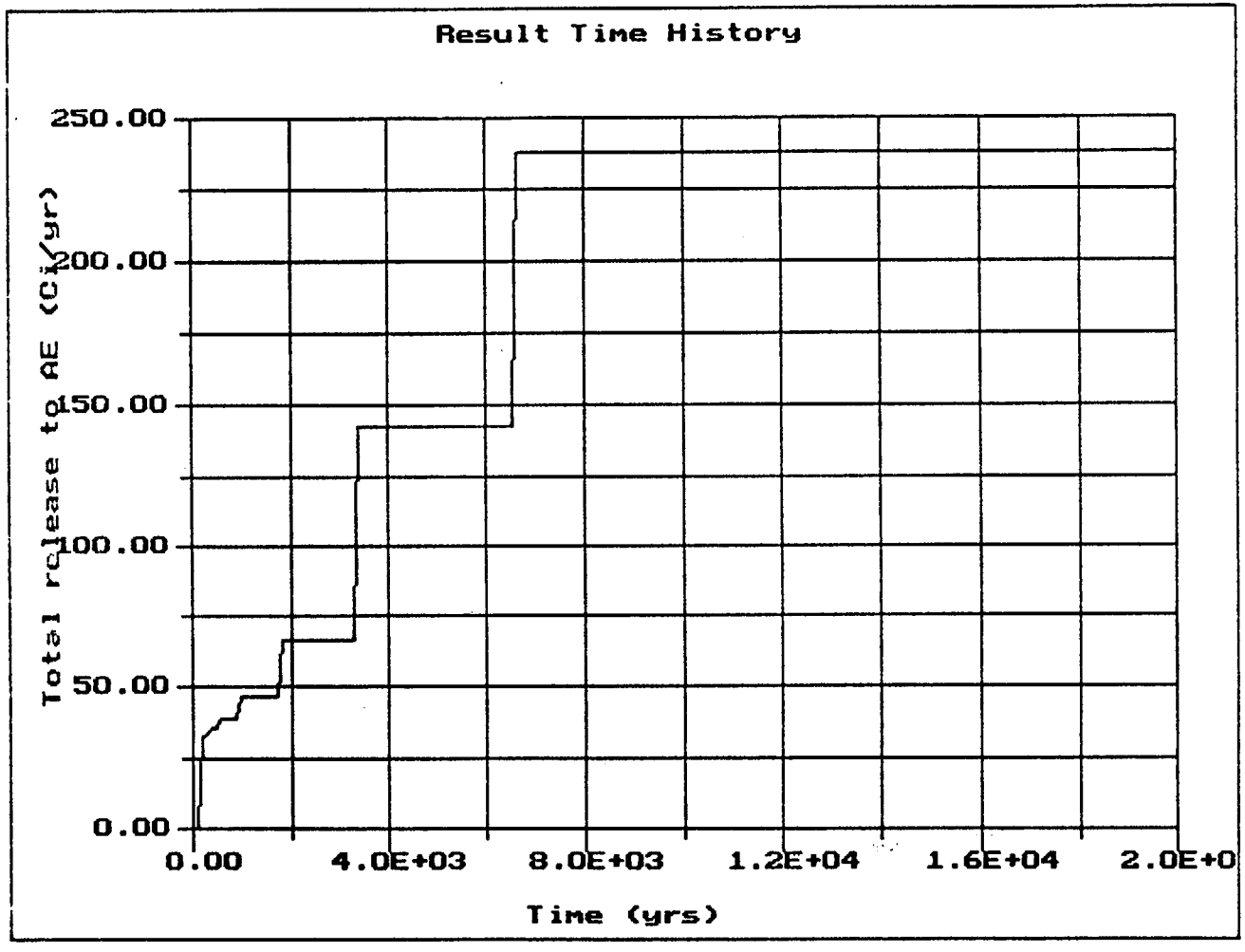

Figure B-16. Effect of λ on Breakthrough Curves at the Bottom of Layer 1: $\lambda = 0.025\ m^{-1}$

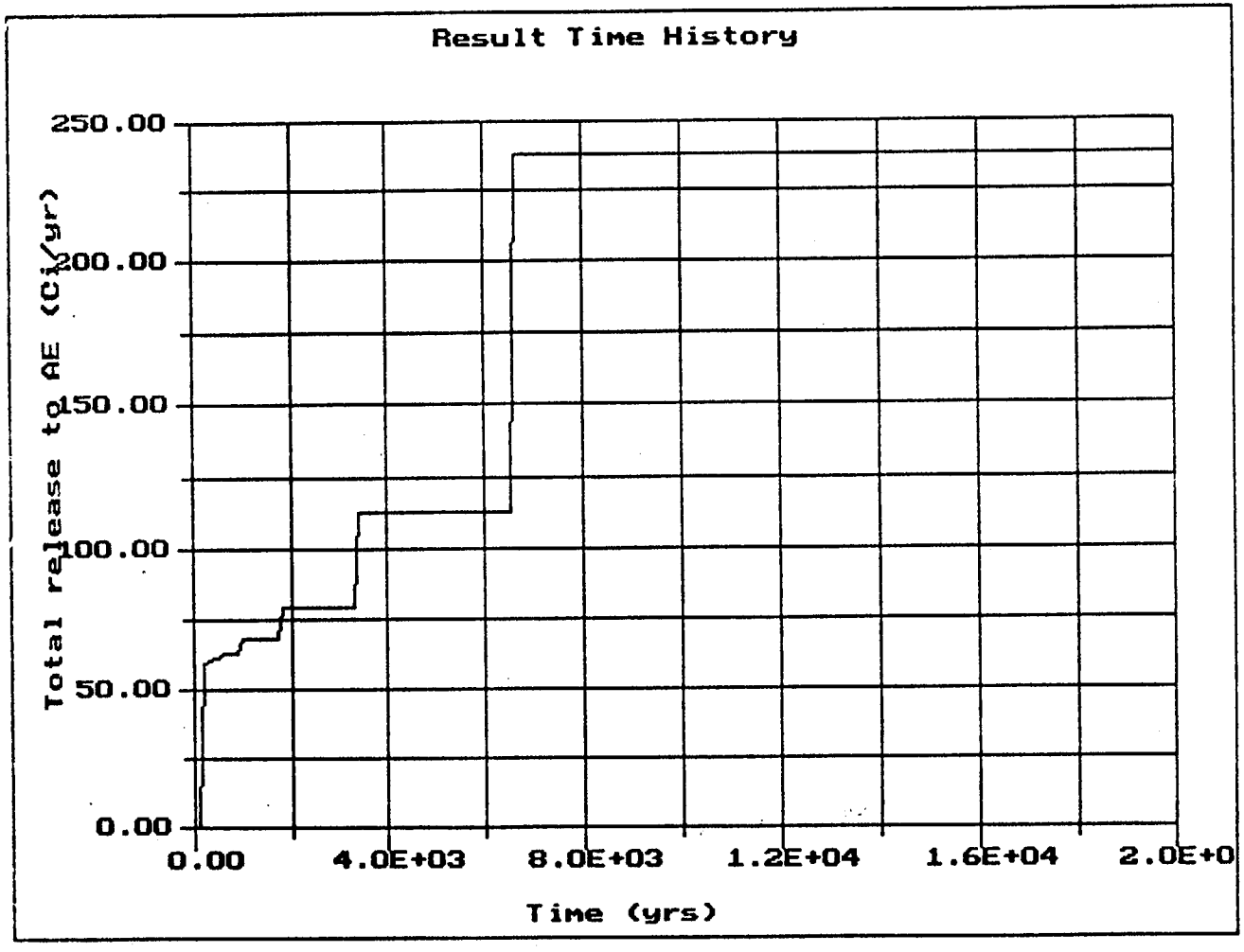

Figure B-17. Effect of λ on Breakthrough Curves at the Bottom of Layer 1: $\lambda = 0.01\ m^{-1}$

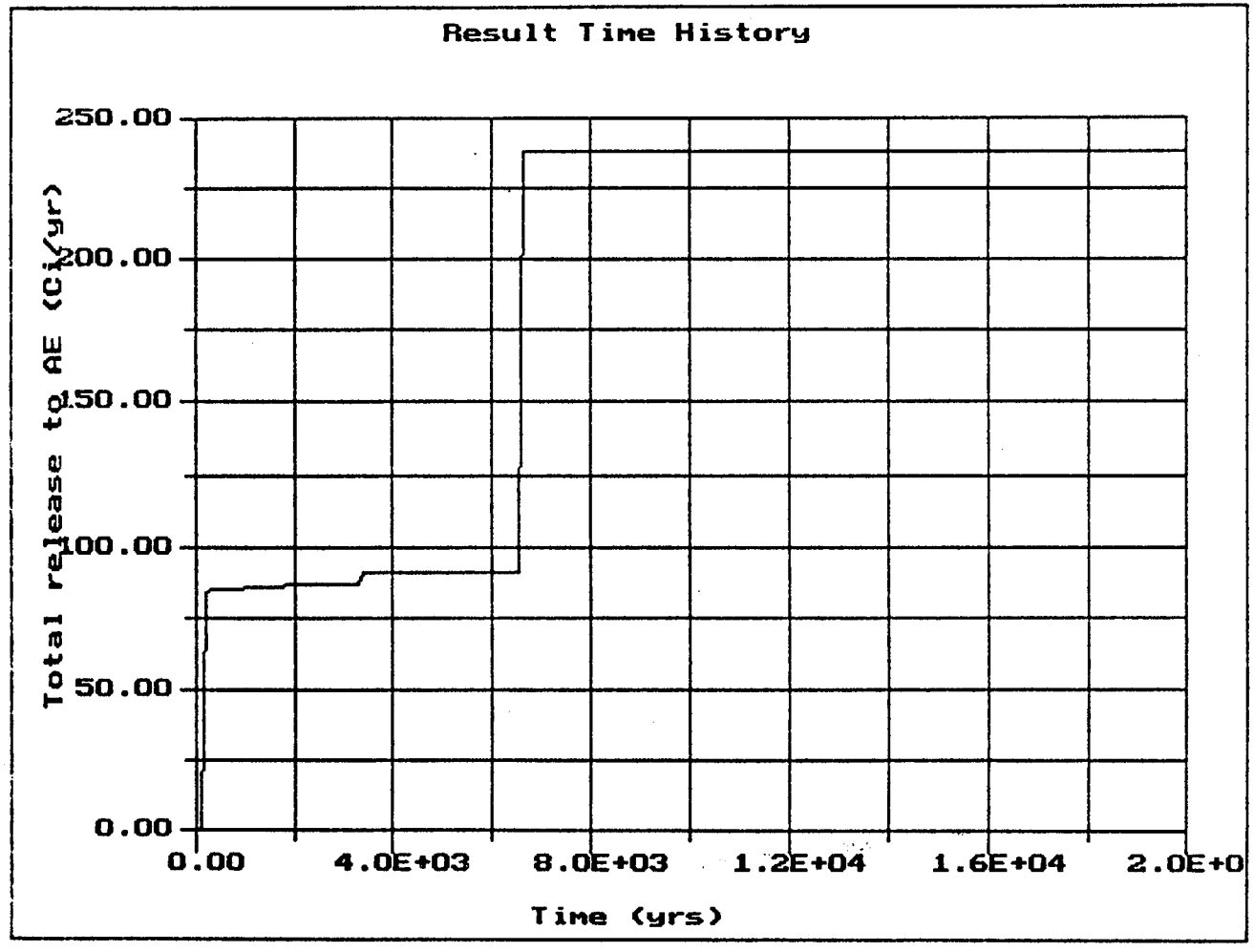

Figure B-18. Effect of λ on Breakthrough Curves at the Bottom of Layer 1: $\lambda = 10^{-3}\ m^{-1}$

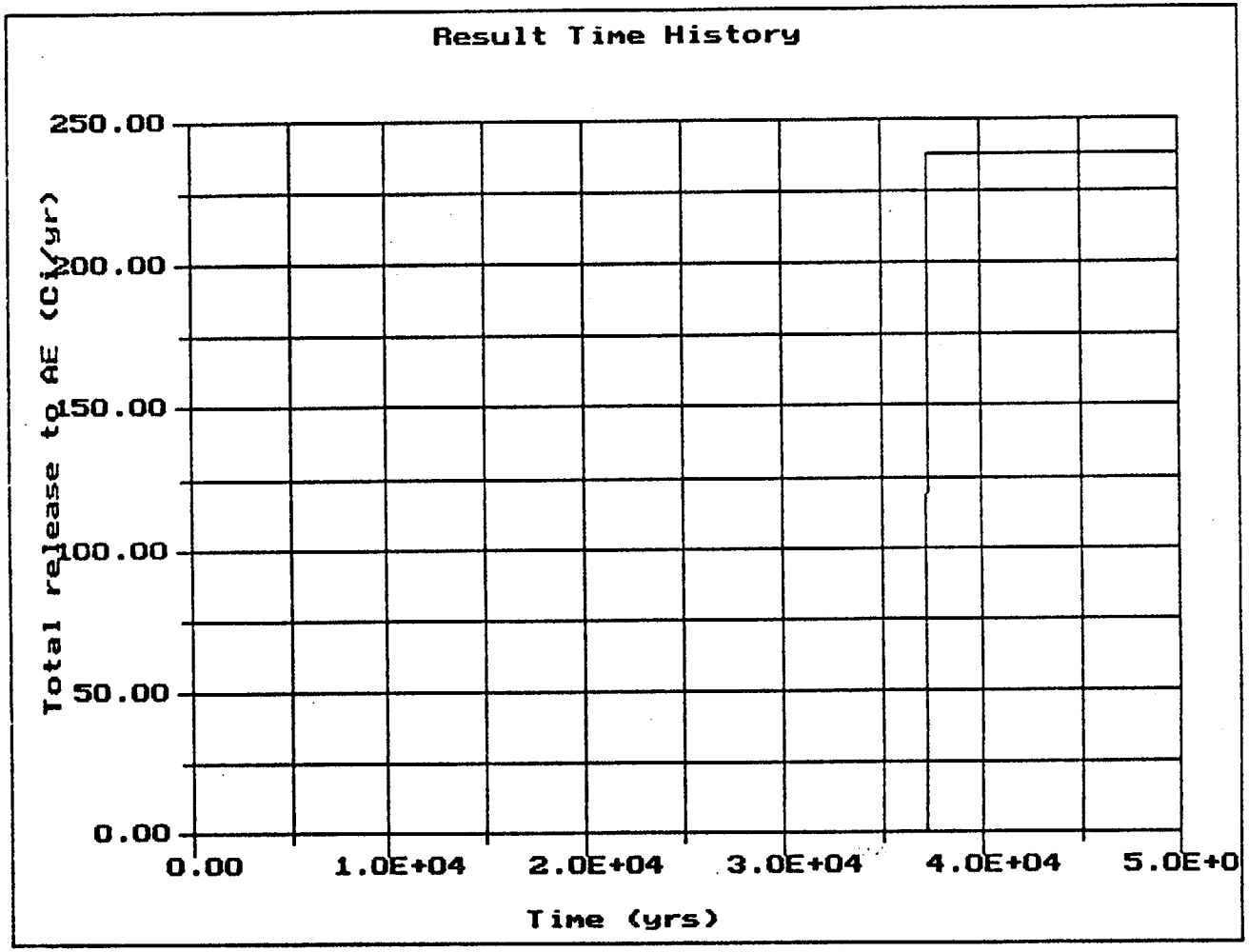

Figure B-19. Effect of λ on Breakthrough Curves at the Bottom of Column 1: $\lambda = 10^4\ m^{-1}$

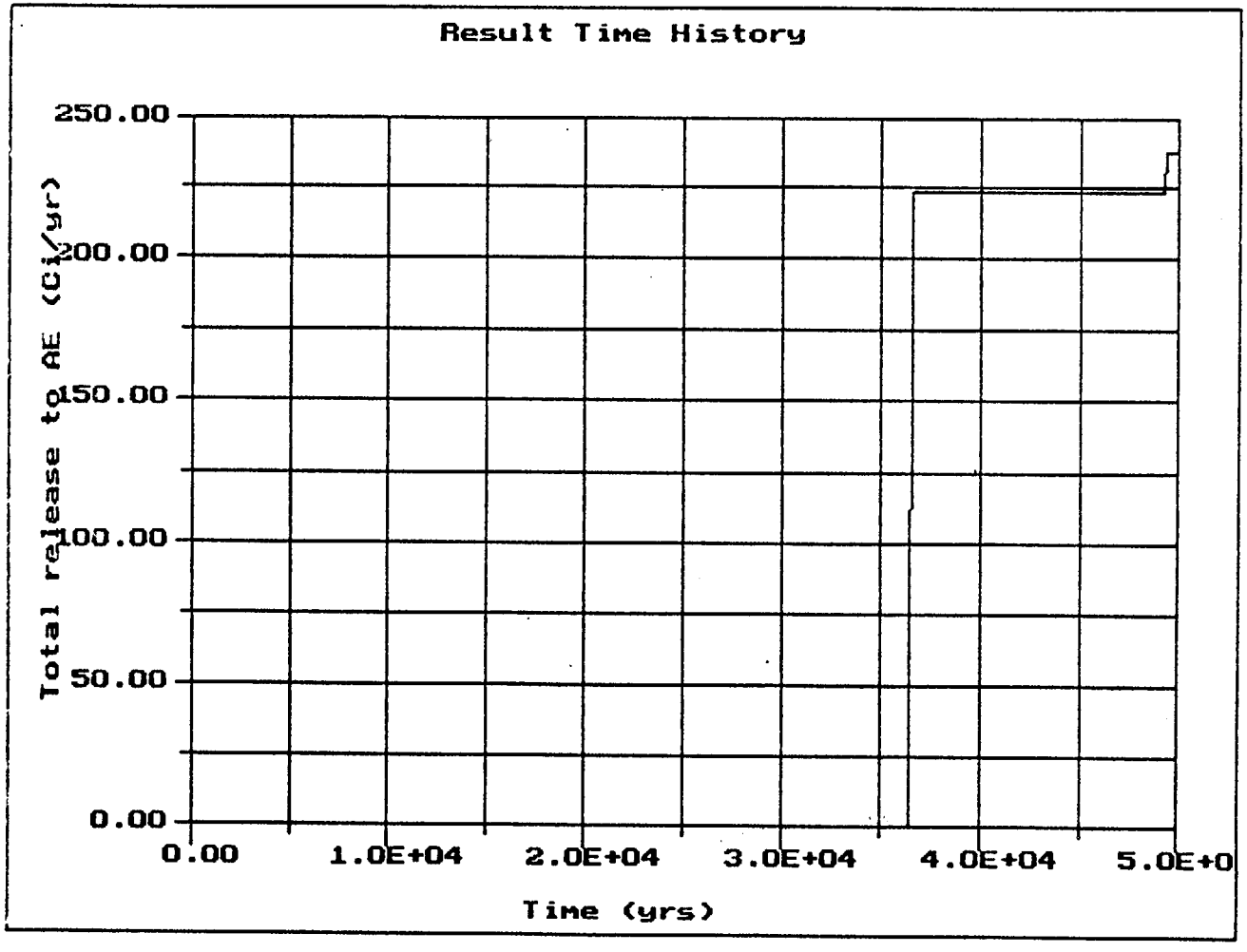

Figure B-20. Effect of λ on Breakthrough Curves at the Bottom of Column 1: $\lambda = 100\ m^{-1}$

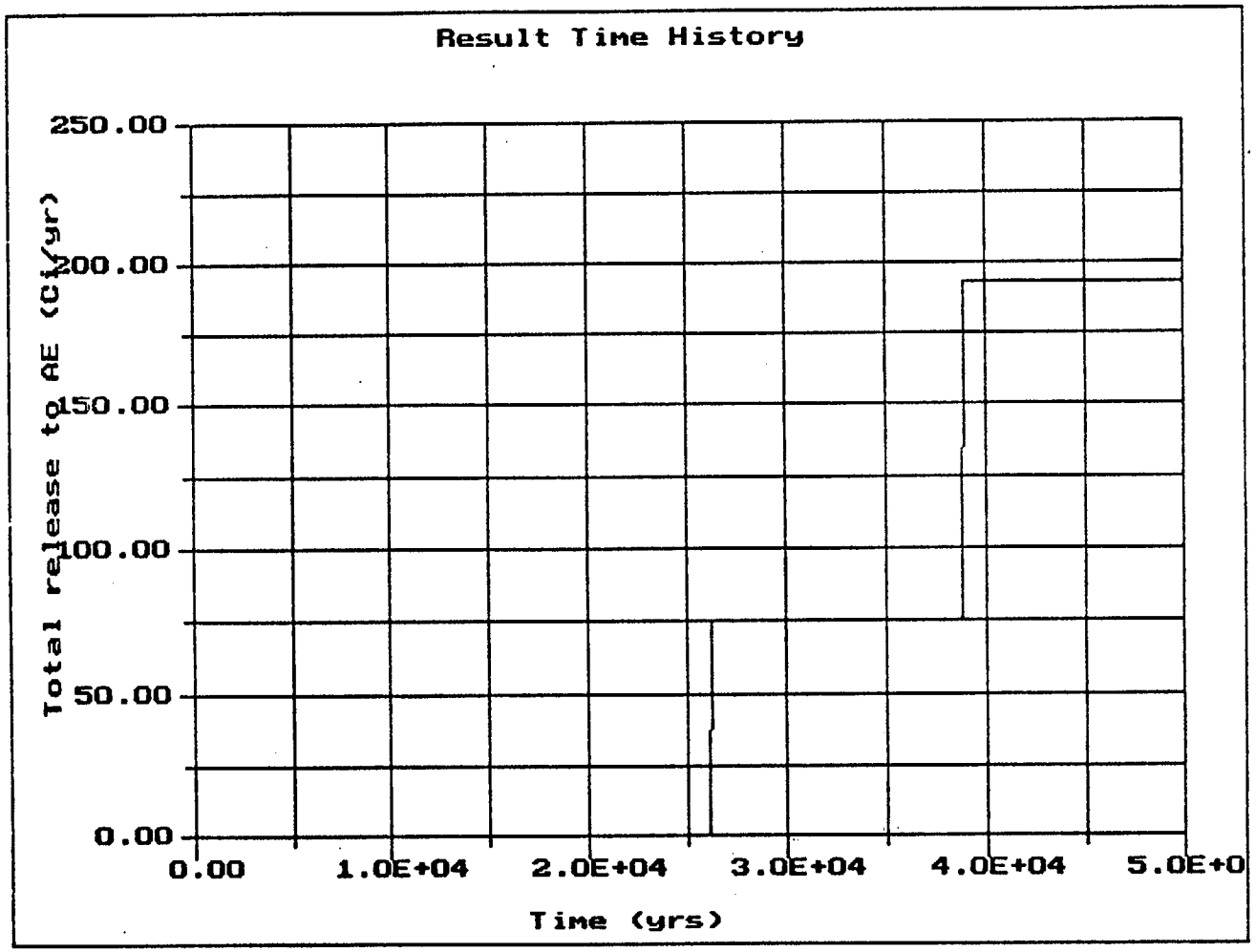

Figure B-21. Effect of λ on Breakthrough Curves at the Bottom of Column 1: $\lambda = 10\ m^{-1}$

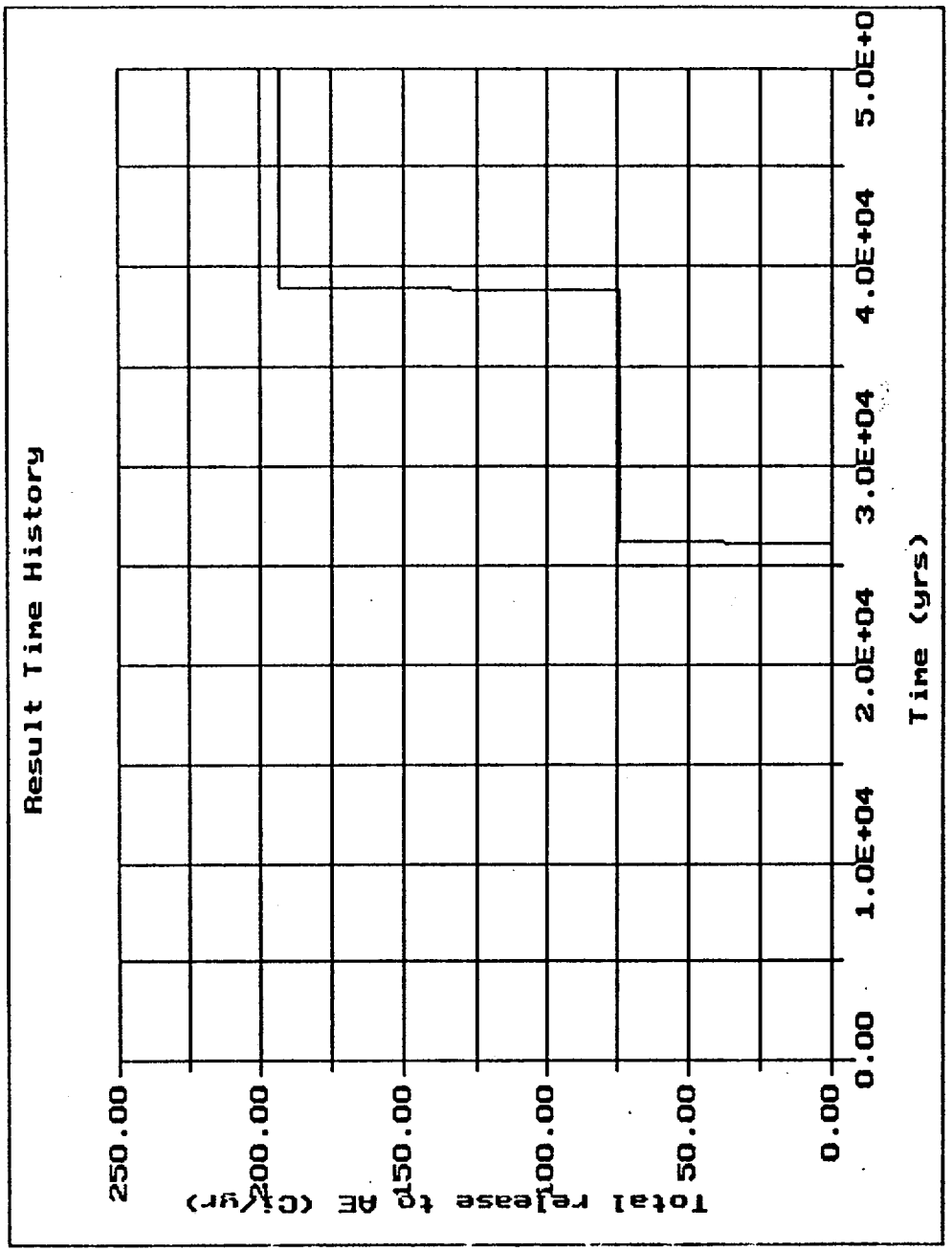

Figure B-22. Effect of λ on Breakthrough Curves at the Bottom of Column 1: $\lambda = 1.0\ m^{-1}$

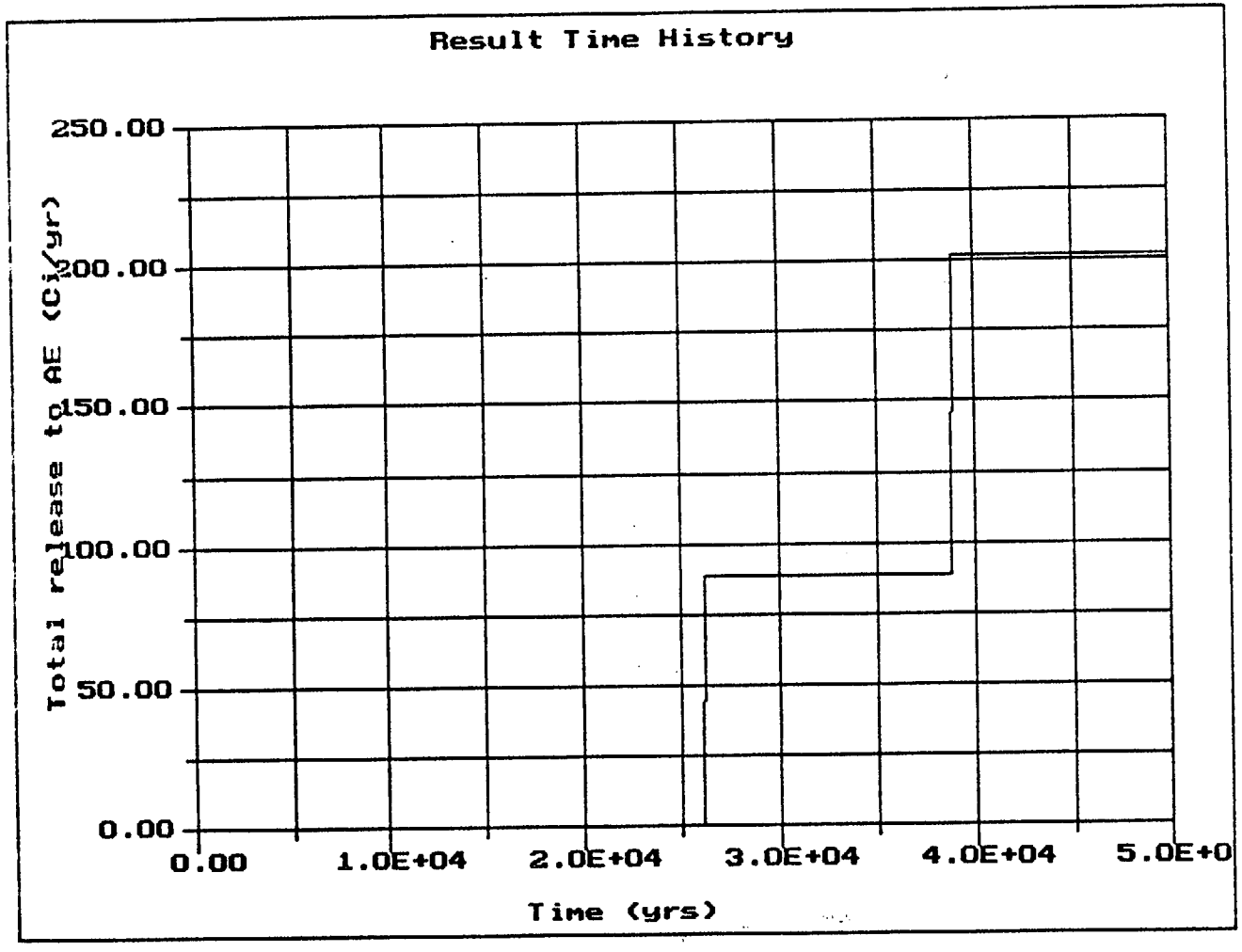

Figure B-23. Effect of λ on Breakthrough Curves at the Bottom of Column 1: $\lambda = 0.1\ m^{-1}$

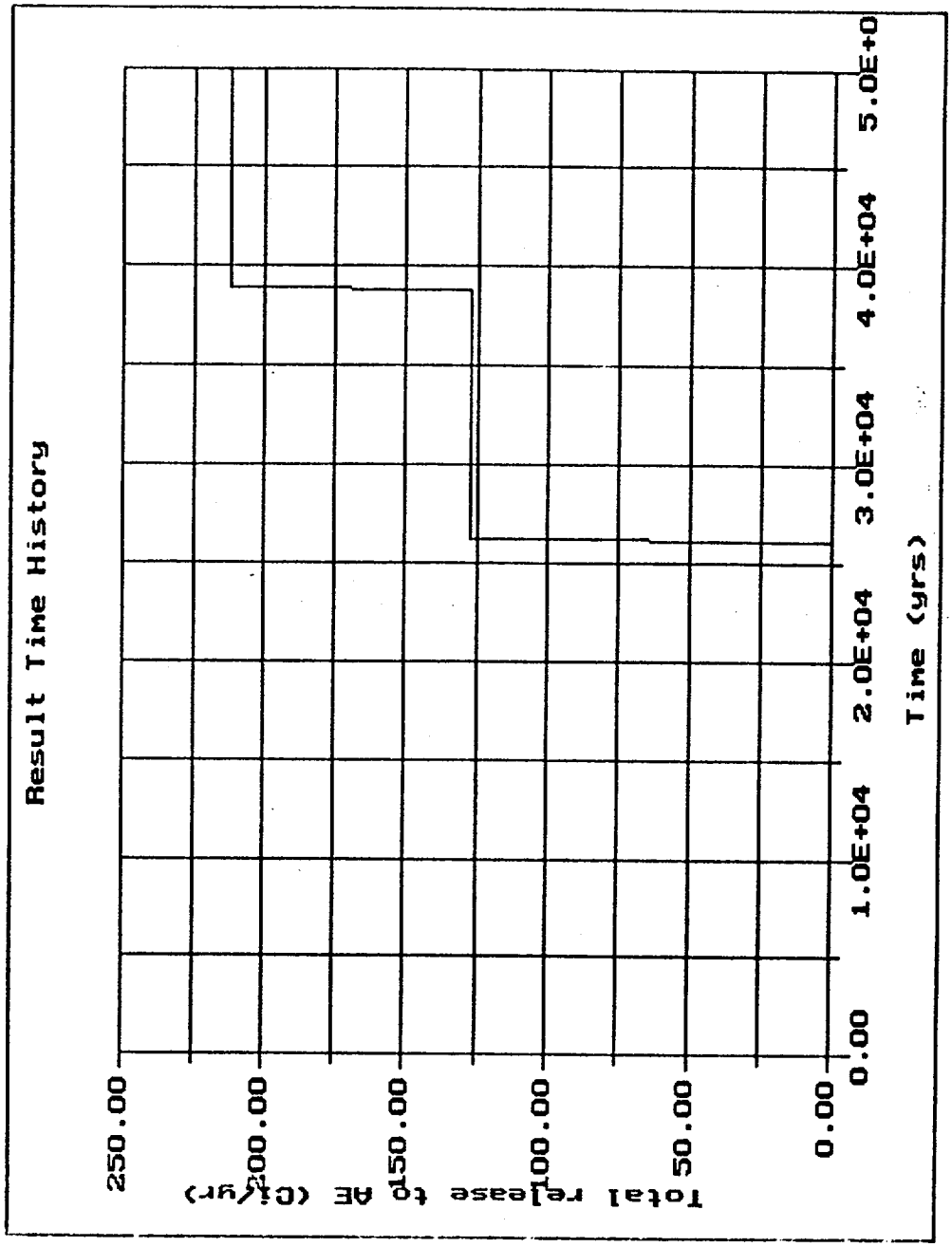

Figure B-24. Effect of λ on Breakthrough Curves at the Bottom of Column 1: $\lambda = 10^{-2}\ m^{-1}$

Table B-1. Fluxes and Velocities in Matrix* For All Layers

Layer	Infiltration Rate (m/yr) i	Matrix Hydraulic Conductivity (m/yr) K_m	Darcy Flux (m/yr) U_m $U_m = K_m$; $K_m < i$ $U_m = i$; $K_m \geq i$	Flow Proportion for Matrix $f_m = U_m/i$	Porosity ϕ_m	Interstitial Velocity (m/yr) $V_m = U_m/\phi_m$
1	1.0×10^{-3}	6.30×10^{-4}	6.30×10^{-4}	0.63	0.11	5.73×10^{-3}
2	1.0×10^{-3}	9.49×10^{-5}	9.49 c 10^{-5}	0.0949	0.09	1.05×10^{-3}
3	1.0×10^{-3}	2.50×10^{-3}	1.00×10^{-3}	1.0	0.21	4.76×10^{-3}
4	1.0×10^{-3}	9.49×10^{-5}	9.49×10^{-5}	0.0949	0.41	2.31×10^{-4}
5	1.0×10^{-3}	4.40×10^{-1}	1.00×10^{-3}	1.0	0.24	4.16×10^{-3}

* Assumed to be fully saturated

Table B-2. Fluxes and Velocities in Fractures for all Layers

Layer	Infiltration Rate (m/yr) i	Flow Proportion f_f $(1 - f_m)$	Flux (m/yr) U_f $U_f = f_f\, i$	Porosity ϕ_f	Saturation S_f	Effective Velocity (m/yr) $V_f = U_f/(\phi_f\, S_f)$
1	1.0×10^{-3}	0.37	3.70×10^{-4}	5.94×10^{-3}	0.10	0.62
2	1.0×10^{-3}	0.9055	9.06×10^{-4}	7.48×10^{-3}	0.10	1.21
3	1.0×10^{-3}	0.0	0.0	4.2×10^{-4}	0.10	--
4	1.0E x 10^{-3}	0.9051	9.06×10^{-4}	3.36×10^{-4}	0.10	26.94
5	1.0×10^{-3}	0.0	0.0	9.24×10^{-5}	0.10	--

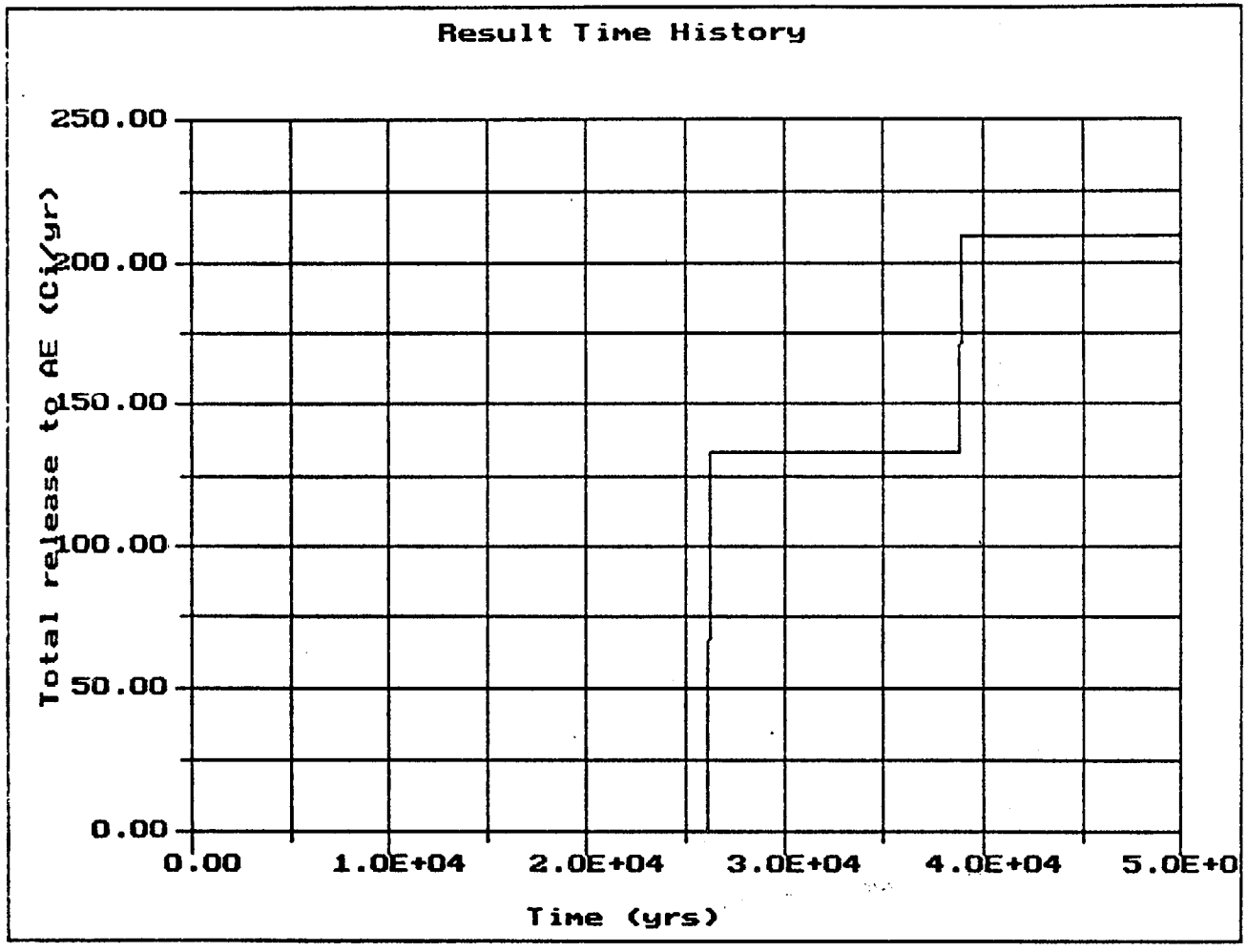

Figure B-25. Effect of λ on Breakthrough Curves at the Bottom of Column 1: $\lambda = 10^{-3}\ m^{-1}$

Table B-3. Travel Times Through Column 1

Layer	Thickness of Layer (m) L	Matrix and Fracture Uncoupled		Matrix and Fracture Fully Coupled		
		Travel Time Through Matrix T_m (yrs) (= L/V_m)	Travel Time Through Fracture T_f (yrs) (= L/V_f)	Flow Proportions		Travel Time Through Layer T* (yrs) (= $T_m f_m + T_f f_f$)
				Matrix (f_m)	Fracture (f_f)	
1	40	6,980	65	0.63	0.37	4,421
2	21	20,000	17	0.095	0.905	1,915
3	65	13,655	--	1.0	0.0	13,655
4	28	120,120	1	0.095	0.905	11,411
5	103	24,760	--	1.0	0.0	24,760
						56,152

Table B-4. Travel Times Through Column 6

Layer	Thickness of Layer (m) L	Matrix and Fracture Uncoupled		Matrix and Fracture Fully Coupled		
		Travel Time Through Matrix T_m (yrs) (= L/V_m)	Travel Time Through Fracture T_f (yrs) (= L/V_f)	Flow Proportions		Travel Time Through Layer T* (yrs) (= $T_m f_m + T_f f_f$)
				Matrix (f_m)	Fracture (f_f)	
1	67	11,692	108	0.63	0.37	7,405
2	13	12,381	10.7	0.095	0.905	1,186
3	22	4,621	--	1.0	0.0	4,621
4	83	359,307	3	0.095	0.905	34,137
						46,349

APPENDIX C: COMPARISON OF UNSATURATED ZONE FLOW AND MASS TRANSPORT MODELED USING RIP, TOSPAC, AND TRACR3D

In addition to comparing RIP's approximation of flow and transport in the unsaturated zone to simple problems with analytical solutions, it is also important to compare the results with numerical solutions. Numerical solutions of unsaturated flow and radionuclide transport generated by TOSPAC were used by SNL in TSPA-1991. Therefore, before comparing the cumulative releases generated by TOSPAC and RIP, it is worthwhile to look at the release rates calculated by the different conceptual models of flow and transport in the unsaturated zone embodied within the numerical and Markovian approximations.

As discussed in Appendix B, for purposes of verification, individual vertical columns 1 and 6 (Figure 3-3) were used for simulating the flow and transport in the unsaturated zone. The comparisons have been made under conditions of "full coupling" and "no coupling" between the matrix and the fracture. In the RIP model, full coupling is secured by specifying the Poisson transition rate λ to be very large, and no coupling is secured by specifying λ to be close to zero. TOSPAC, the model used for TSPA-1991 analyses, requires an input parameter specifying the degree of interaction between the matrix and the fracture. This parameter has been set to zero and one for no coupling and full coupling, respectively. Simulations have been performed for 50,000 years. (There will be no release at 10,000 years at the bottom of layer 5 in column 1.)

To facilitate a meaningful comparison, we have generated equivalent TOSPAC and TRACR3D data sets which represent column 1 of the TSPA-1991 flow and transport domain.

In our simulations with TOSPAC and TRACR3D, we have used the expected value of each parameter for each layer of the conceptual model as well as the applied infiltration flux. All five layers of column 1 are represented by composite media where the fracture and matrix characteristic curves are combined into a single curve. Figures C-1 and C-2 represent the relative permeability and capillary pressures for the Topopah Springs welded unit. It is apparent in these figures that, as the liquid saturation approaches about 0.95, the fractures start to saturate, causing a dramatic increase in the effective hydraulic conductivity and a corresponding decrease in the negative pressure head (suction). At lower liquid saturations, the bulk conductivity is controlled by the matrix conductivity and the water suction due to capillary forces is very high.

Simulated saturation-depth profiles for column 1 for an infiltration flux of 1.0 mm/yr are presented in Figures C-3a and C-3b for TOSPAC and TRACR3D, respectively. These results are analogous to Figure 4-14 presented in Barnard et al. (1992). Given that the residual fracture saturation is equal to 0.1, any saturation above this value indicates that some component of fracture flow is initiated. It is important to note that layers 3 and 5, which correspond to the non-welded vitric tuff and the partially welded tuff, are dominated by matrix flow for the expected conductivity and infiltration. Similar results exist for column 6 (with the exception that layer 5 is not present).

Simulated velocity-depth profiles for column 1, given an infiltration flux of 1.0 mm/yr, are presented in Figures C-4a and C-4b for TOSPAC and TRACR3D, respectively. These results are analogous to Figure 4-15 presented in Barnard et al. (1992). These figures illustrate the importance of fracture flow in the welded, vitrophyre, tuffs, and the zeolitic Calico Hills (layers 1, 2, and 4, respectively).

The above velocity and saturation profiles were used in TOSPAC-TRANS and TRACR3D to simulate the mass breakthrough of a non-retarded, non-decaying tracer. In this analysis, a constant release rate of 240 Ci/yr was used as the source at the top of the first layer. For TOSPAC-TRANS, we have simulated the transport under the assumption that either there is complete coupling between the matrix and fractures or there is no coupling between the two flow modes. TOSPAC-TRANS calculates the fracture and matrix breakthroughs independently, then adds them to get the cumulative mass breakthrough. TRACR3D calculates only the cumulative mass breakthrough (equivalent to TOSPAC's full coupling representation). The simulated results at the base of the top layer generated by TOSPAC-TRANS and TRACR3D are illustrated in Figure C-5. Figures C-5a and C-5b illustrate the TOSPAC-TRANS results for matrix and fracture mass breakthroughs for no coupling and coupling, respectively. Figures C-5c and C-5d depict the combined effects on mass breakthrough generated by TOSPAC and TRACR3D. The corresponding results generated by RIP are illustrated in Figure C-6. Figure C-6a depicts the no-coupling case ($\lambda = 10^{-8}$ m^{-1}), while Figure C-6b depicts the full coupling case ($\lambda = 10^{8}$ m^{-1}). These results indicate that RIP has difficulty reproducing the dispersive breakthrough when using the Markov approximation to transport in two modes.

The simulated mass breakthrough results at the base of the unsaturated column 1 are illustrated in Figure C-7. Figures C-7a and C-7b depict the combined effects of fractures and matrix on mass breakthrough generated by TOSPAC and TRACR3D. The corresponding RIP results for no coupling and full matrix-fracture coupling are illustrated in Figures C-8a and C-8b, respectively. Again, RIP has difficulty reproducing the dispersive breakthrough. Modifying the Markov transition rate can add some dispersive effects (see Figures B-13 through B-18), but still not to the extent that the numerical models predict. An additional simulation was conducted with the flow in the matrix-dominated units (layers 3 and 5) was replaced by a single advective-dispersive mode in RIP (the other layers maintaining their dual mode logic with $\lambda = 0.1$ m^{-1}). Using a dispersivity of 0.1 times the layer thickness resulted in a mass breakthrough, as illustrated in Figure C-8c. This curve closely approximated the TOSPAC-TRANS and TRACR3D breakthroughs.

Table C-1 summarizes the cumulative release results generated with TOSPAC and RIP.

TOSPAC results show smooth and gradually rising release rates, finally leveling at the input source rate, as expected. A comparison of the TOSPAC and RIP results indicates a good agreement between them, given a full cognizance of the workings of these models and their scope of application. It may be recalled that RIP does not actually simulate the flow and performs transport simulation by a simplified Markov process. In contrast, TOSPAC simulates unsaturated flow using a Van Genuchten model for water retention properties and simulates transport by a dual-porosity advective-dispersive model. Because of the larger time windows used in RIP, and because of its algorithm, very early breakthrough occurs. Also, because of constant input source rate, this involves larger total releases at the end of legs. These aspects are all clearly seen in the figures. In general, RIP predictions are higher than those of TOSPAC and may be considered conservative.

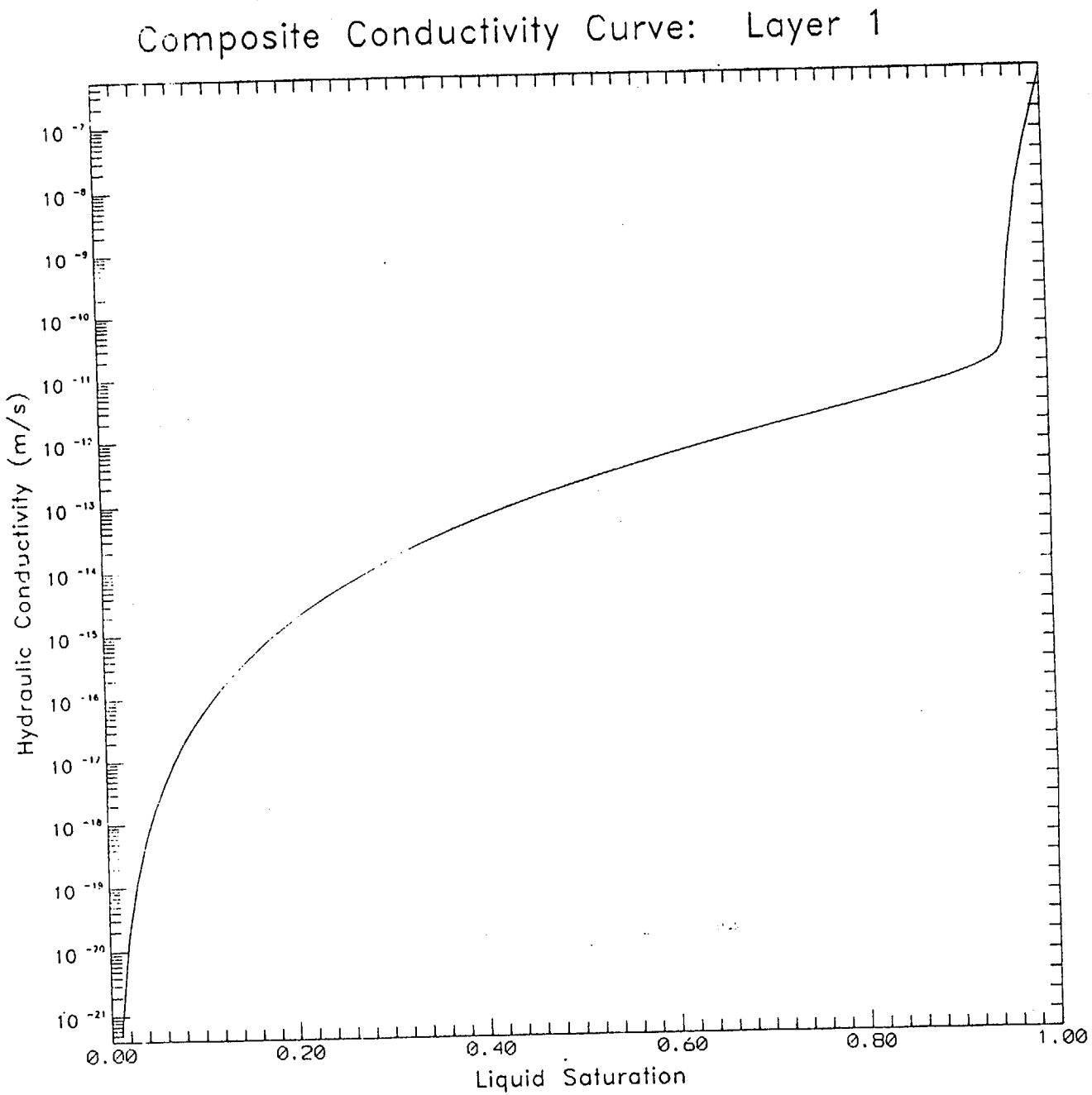

Figure C-1. Composite Hydraulic Conductivity of Topopah Springs Welded Unit

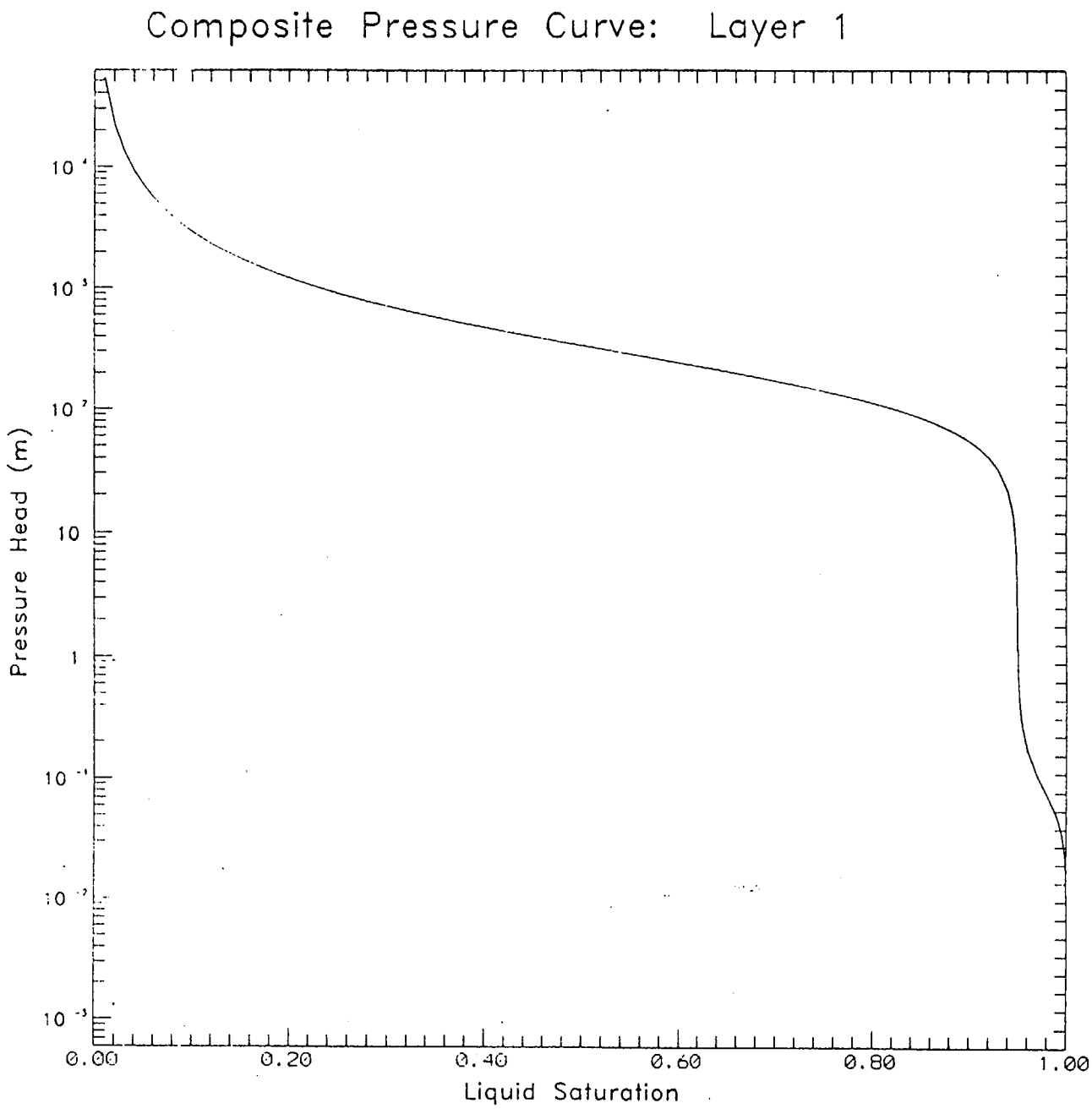

Figure C-2. Composite Capillary Pressure Head of Topopah Springs Welded Unit

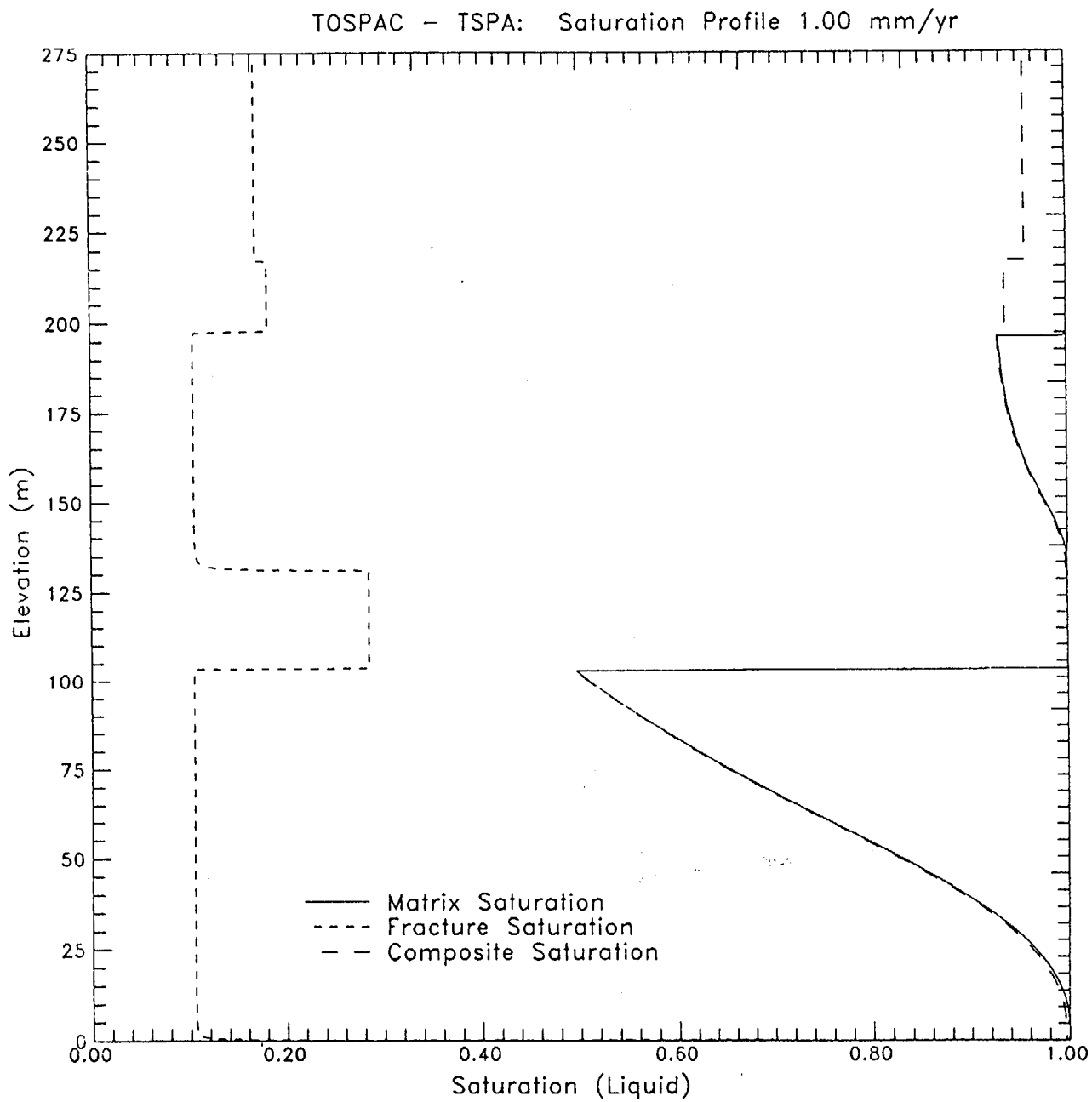

Figure C-3a. Saturation Profile for Column 1: TOSPAC Simulations

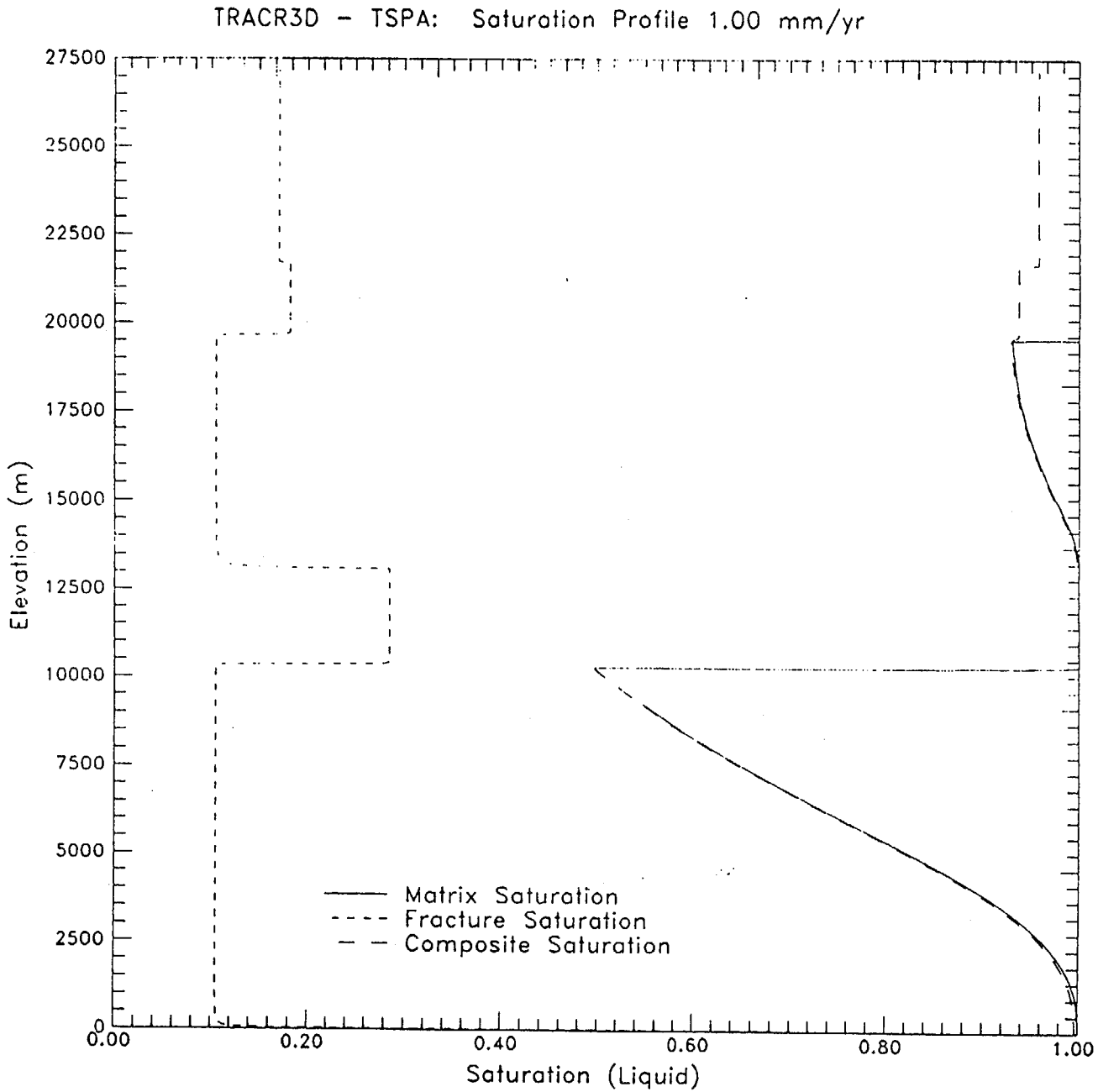

Figure C-3b. Saturation Profile for Column 1: TRACR3D Simulations

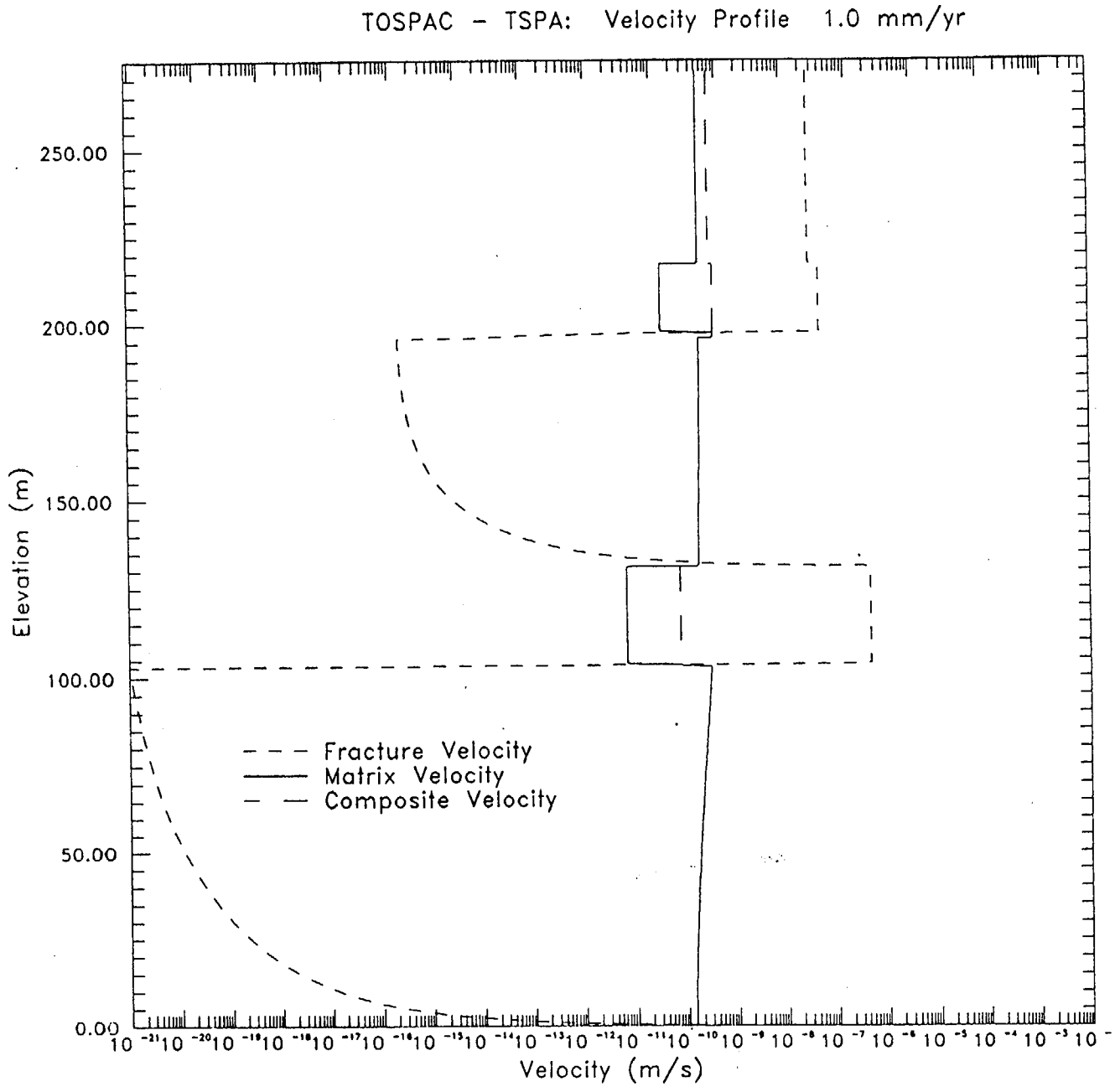

Figure C-4a. Velocity Profile for Column 1: TOSPAC Simulations

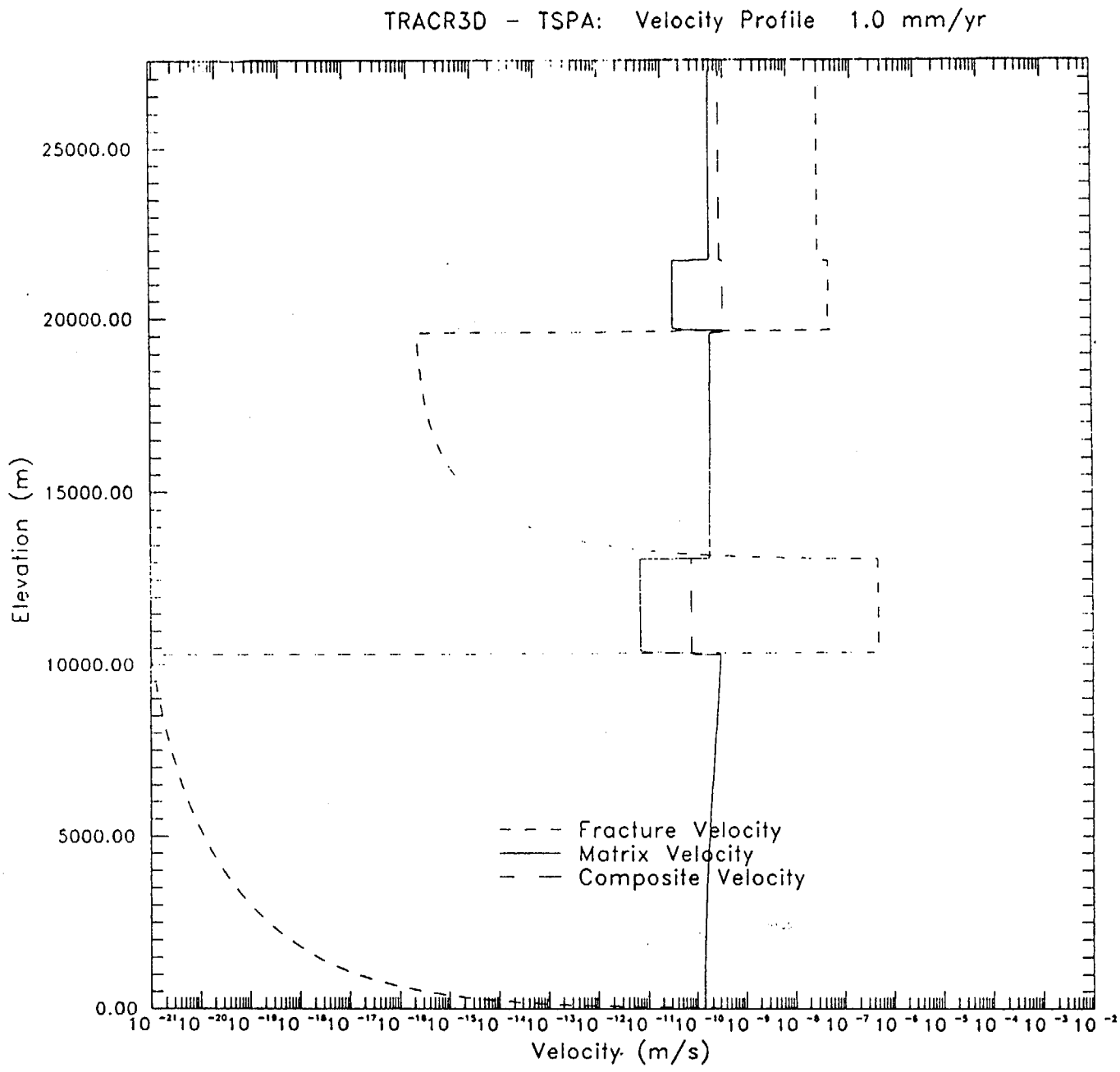

Figure C-4b. Velocity Profile for Column 1: TRACR3D Simulations

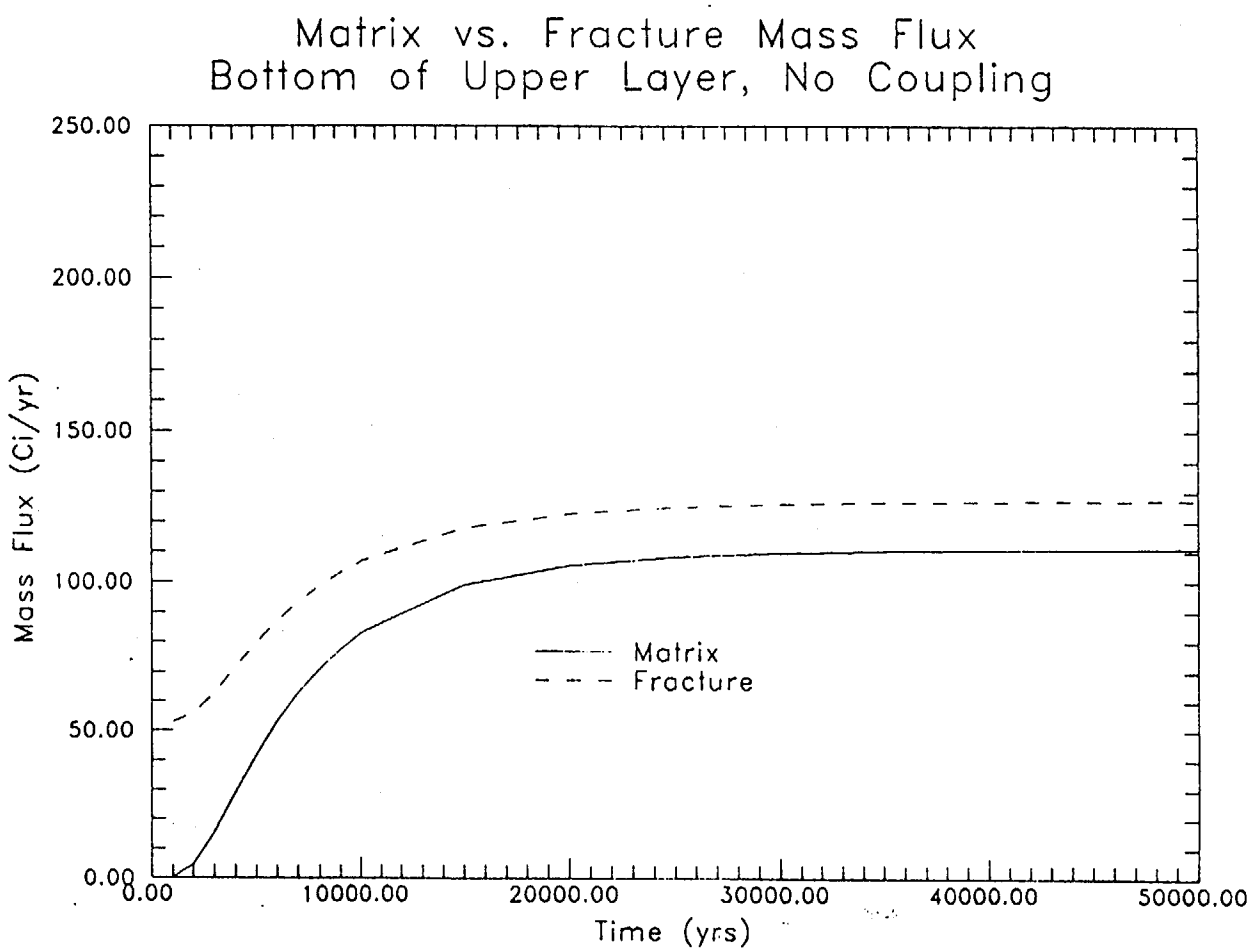

Figure C-5a. Nuclide Release Rate Through Matrix and Fracture at the Bottom of Layer 1, Column 1: No Coupling Case - TOSPAC-TRANS

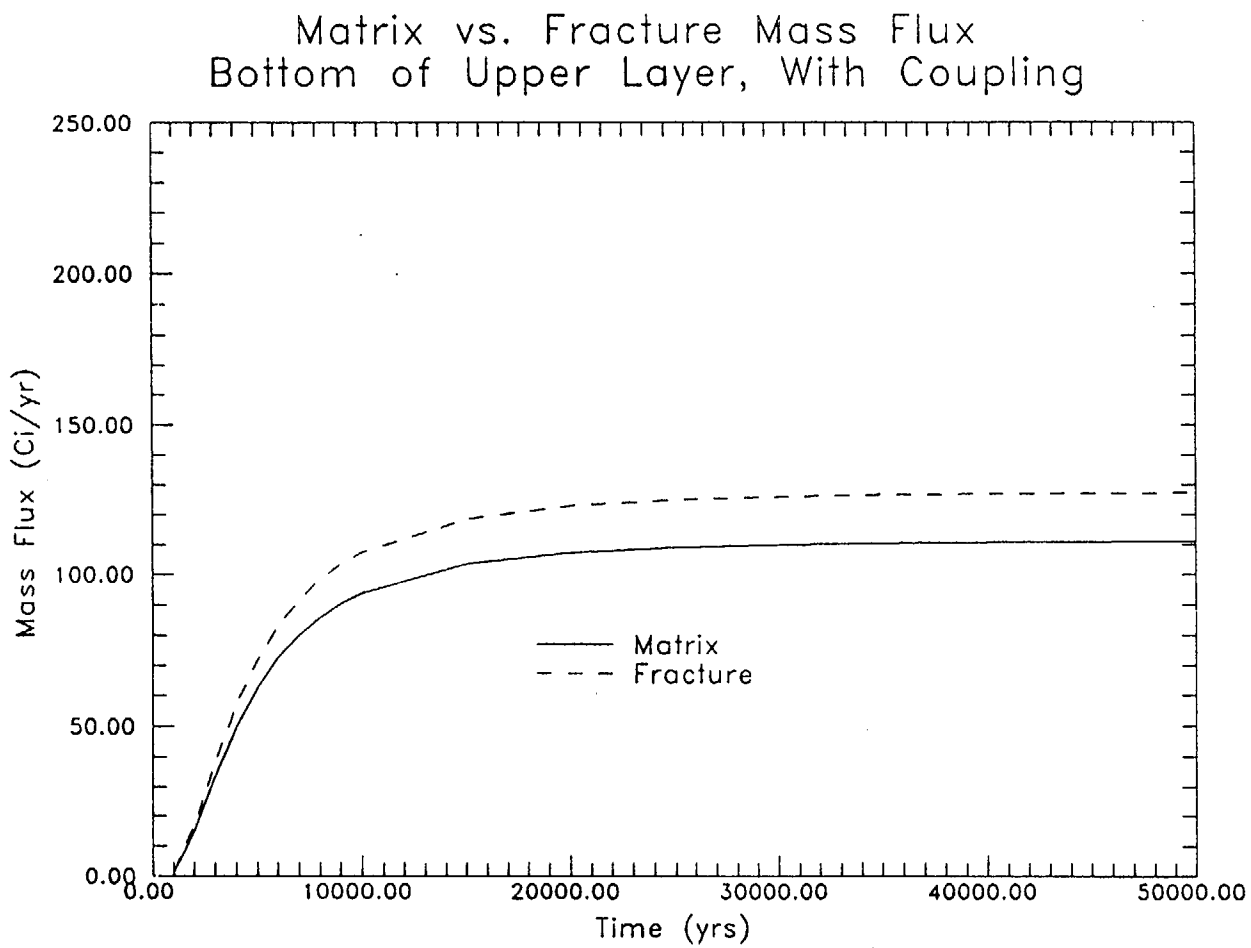

Figure C-5b. Nuclide Release Rate Through Matrix and Fracture at the Bottom of Layer 1, Column 1: Full Coupling Case - TOSPAC-TRANS

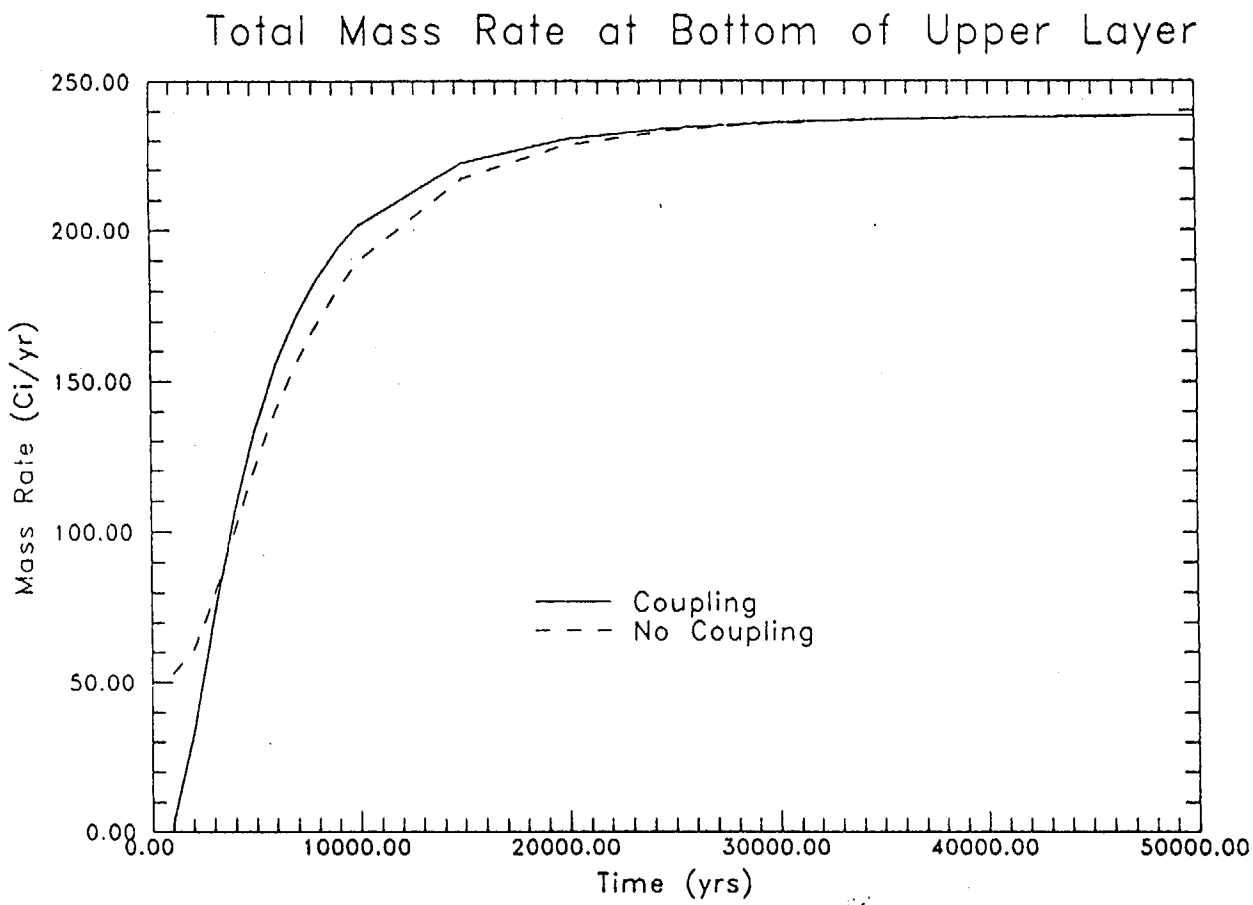

Figure C-5c. Total Nuclide Release Rate at the Bottom of Layer 1, Column 1: No Coupling Case - TOSPAC

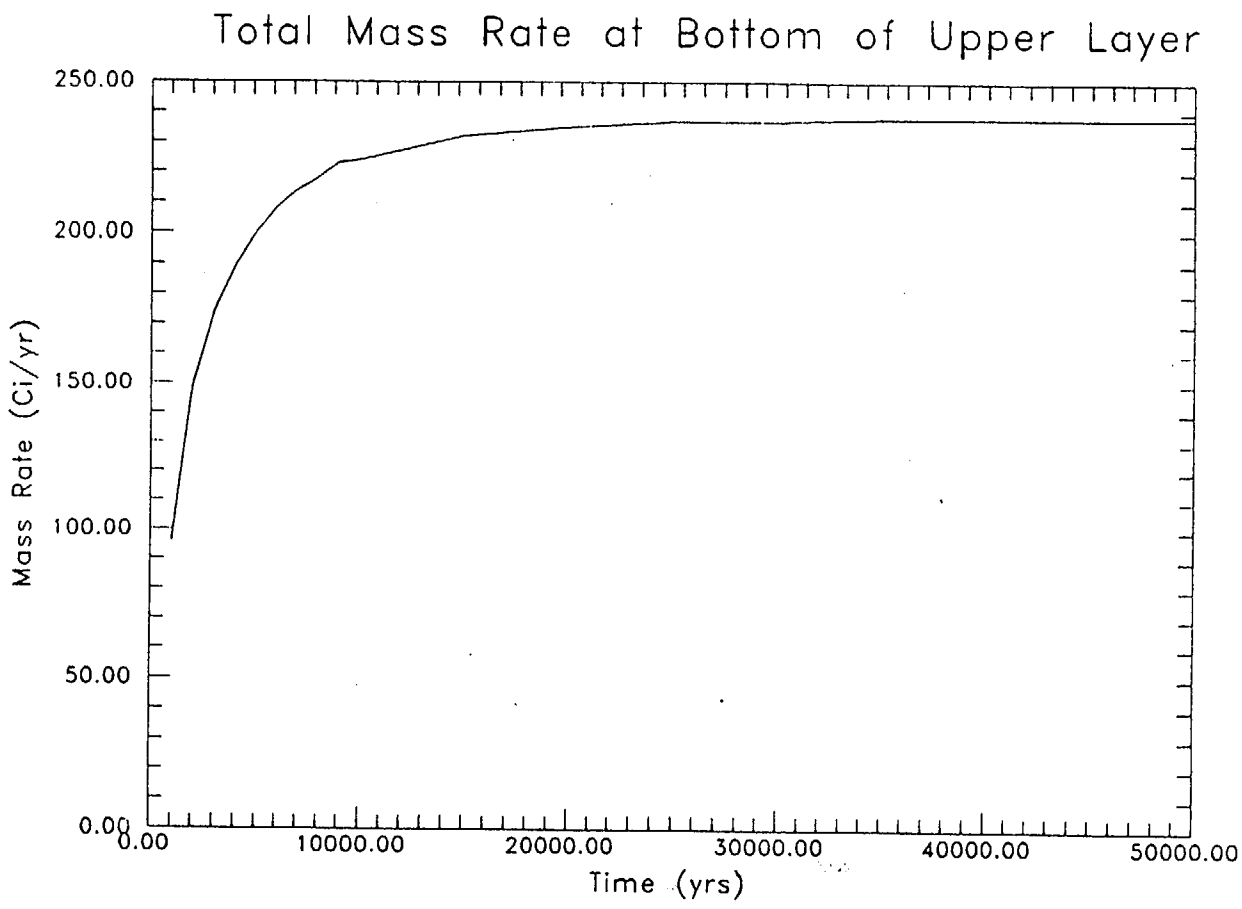

Figure C-5d. Total Nuclide Release Rate at the Bottom of Layer 1, Column 1: Full Coupling Case - TRACR3D

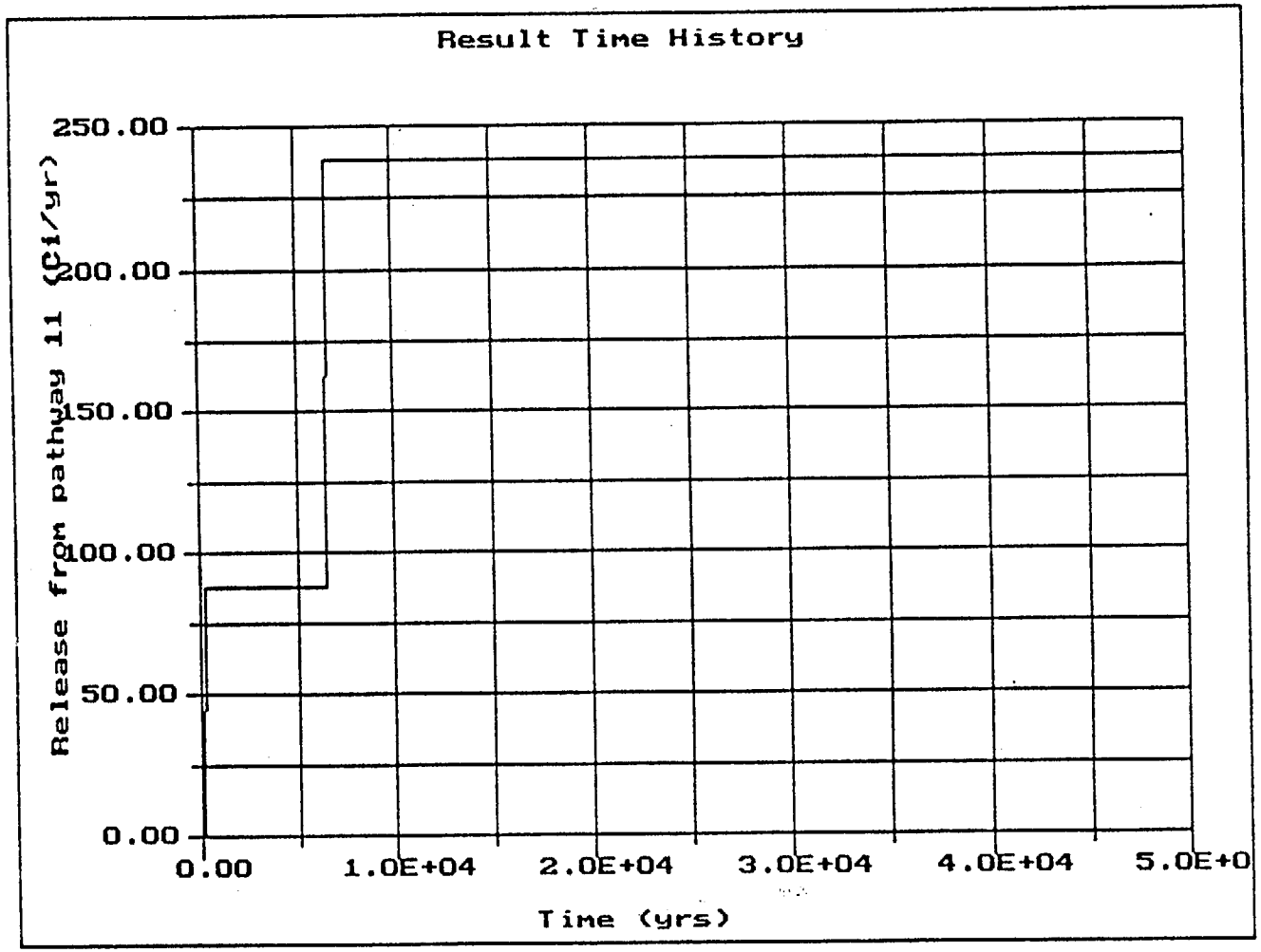

Figure C-6a. Nuclide Release Rate at the Bottom of Layer 1, Column 1: No Coupling Case - RIP

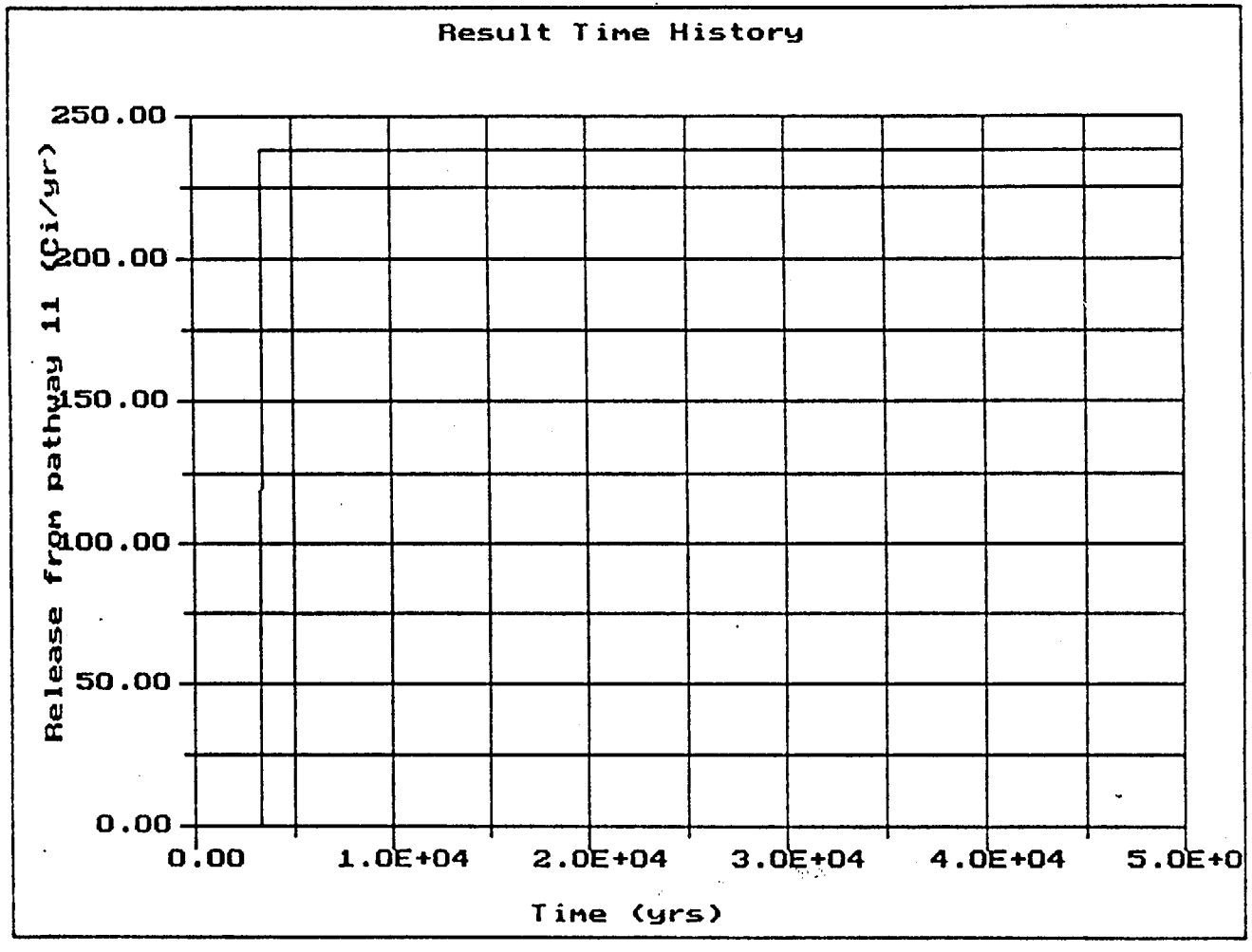

Figure C-6b. Nuclide Release Rate at the Bottom of Layer 1, Column 1: Full Coupling Case - RIP

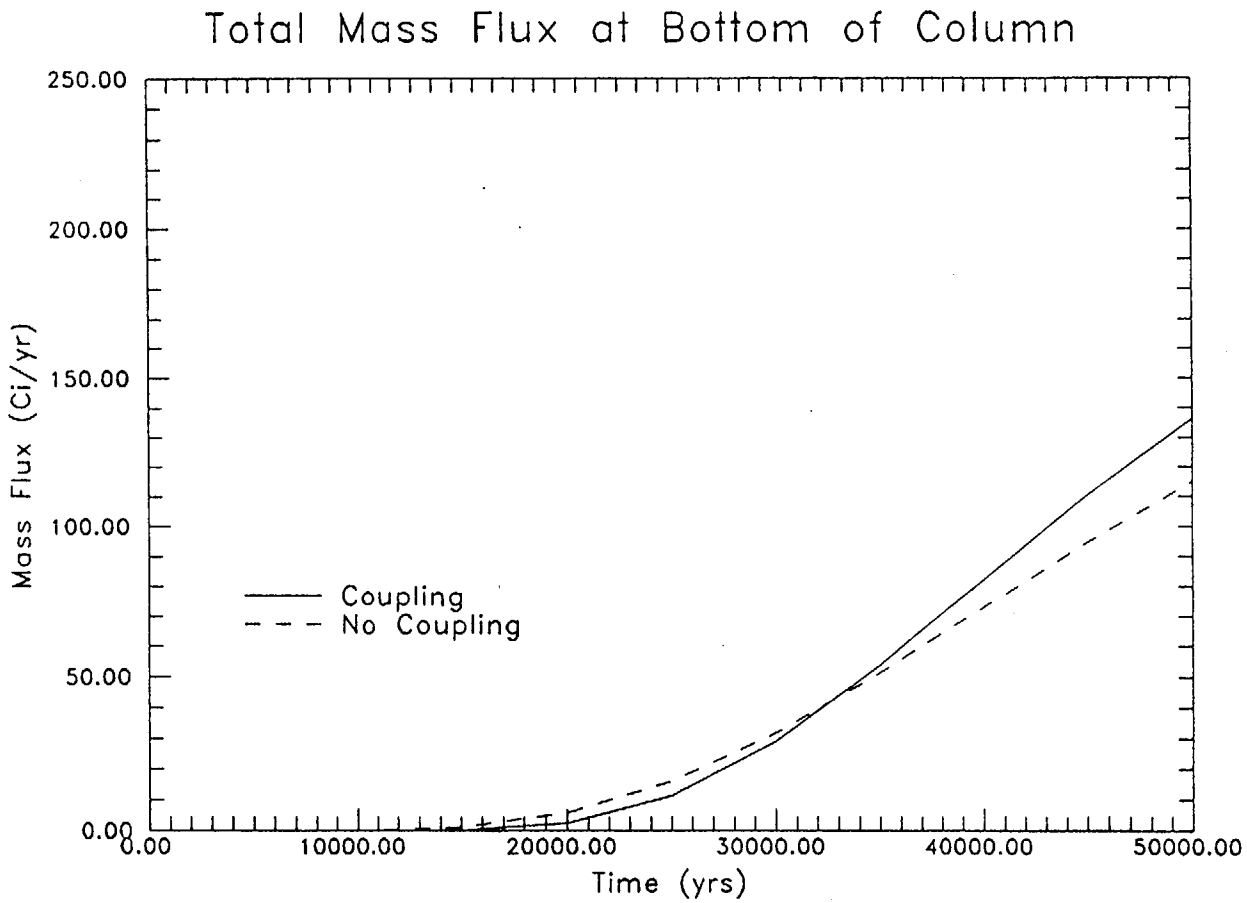

Figure C-7a. Total Nuclide Release Rate at the Bottom of Column 1: TOSPAC

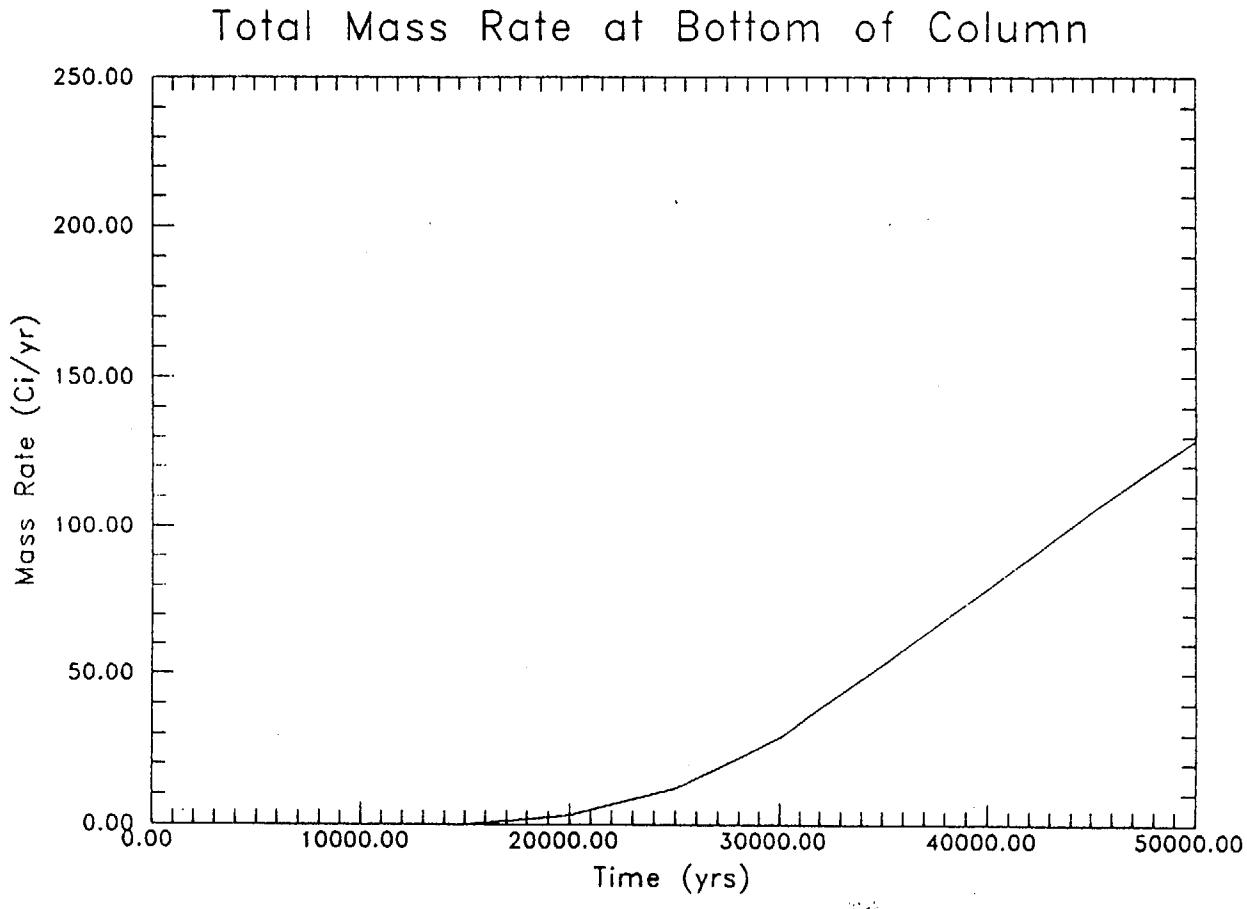

Figure C-7b. Total Nuclide Release Rate at the Bottom of Column 1: TRACR3D

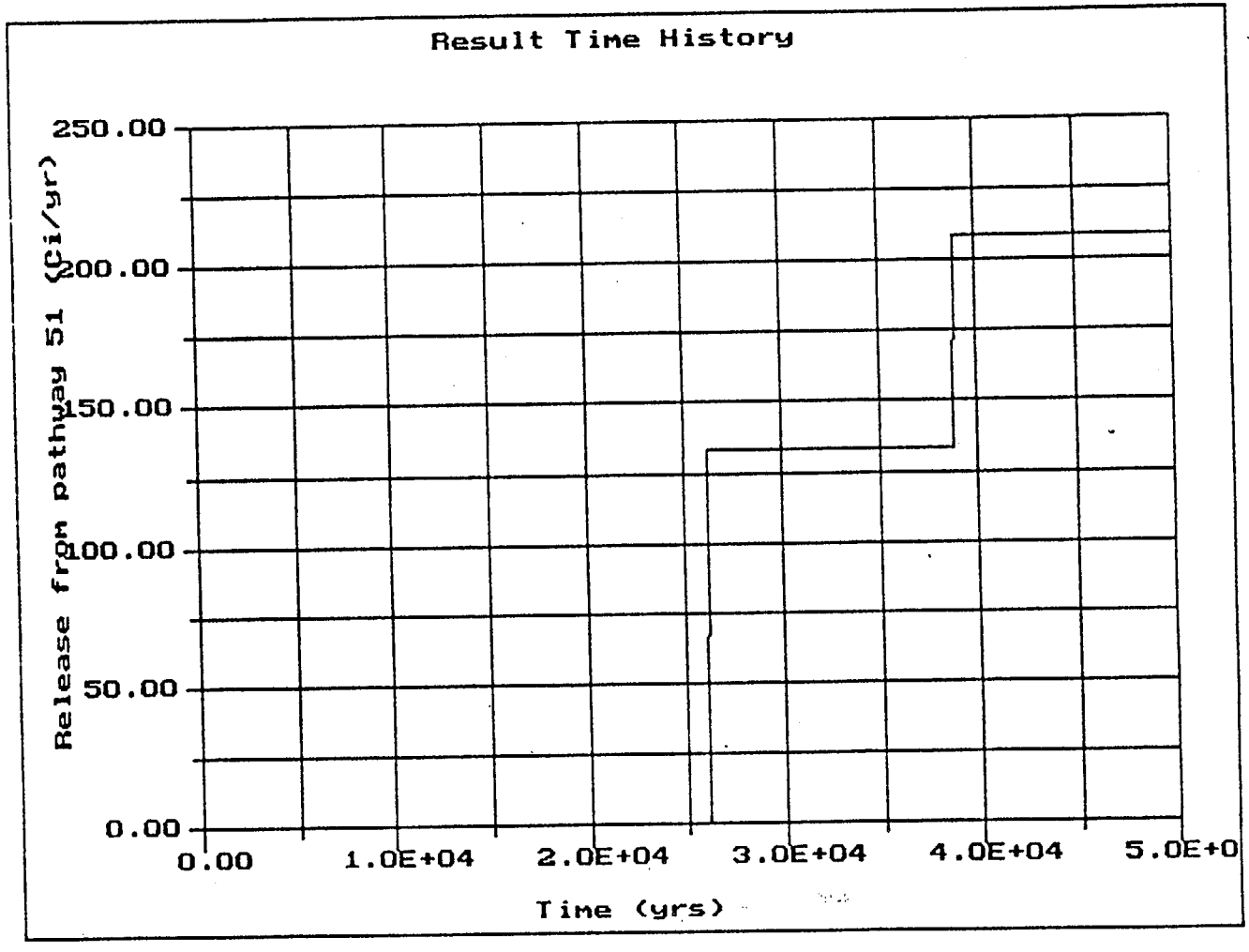

Figure C-8a. Nuclide Release Rate at the Bottom of Column 1: No Coupling Case - RIP

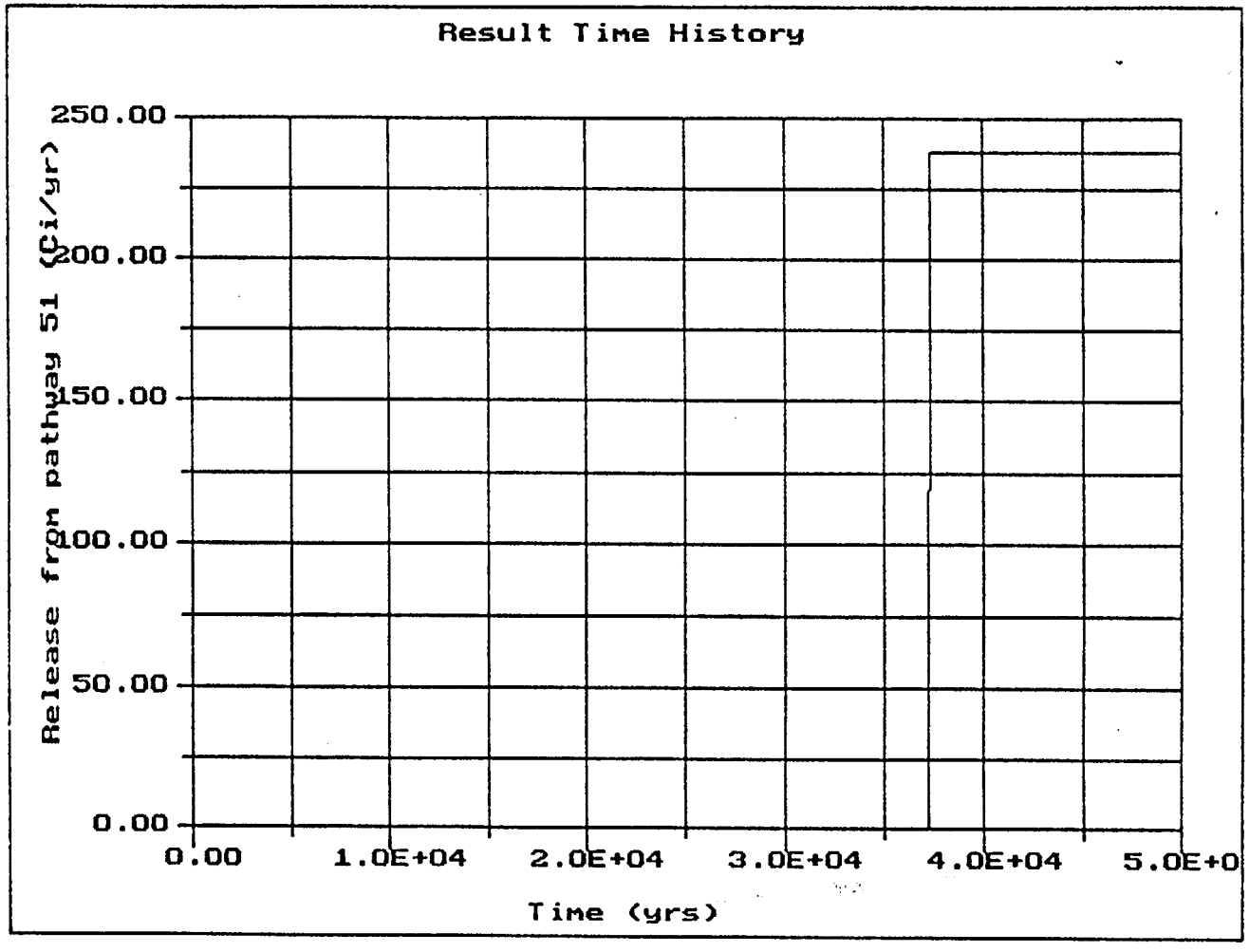

Figure C-8b. Nuclide Release Rate at the Bottom of Column 1: Full Coupling Case - RIP

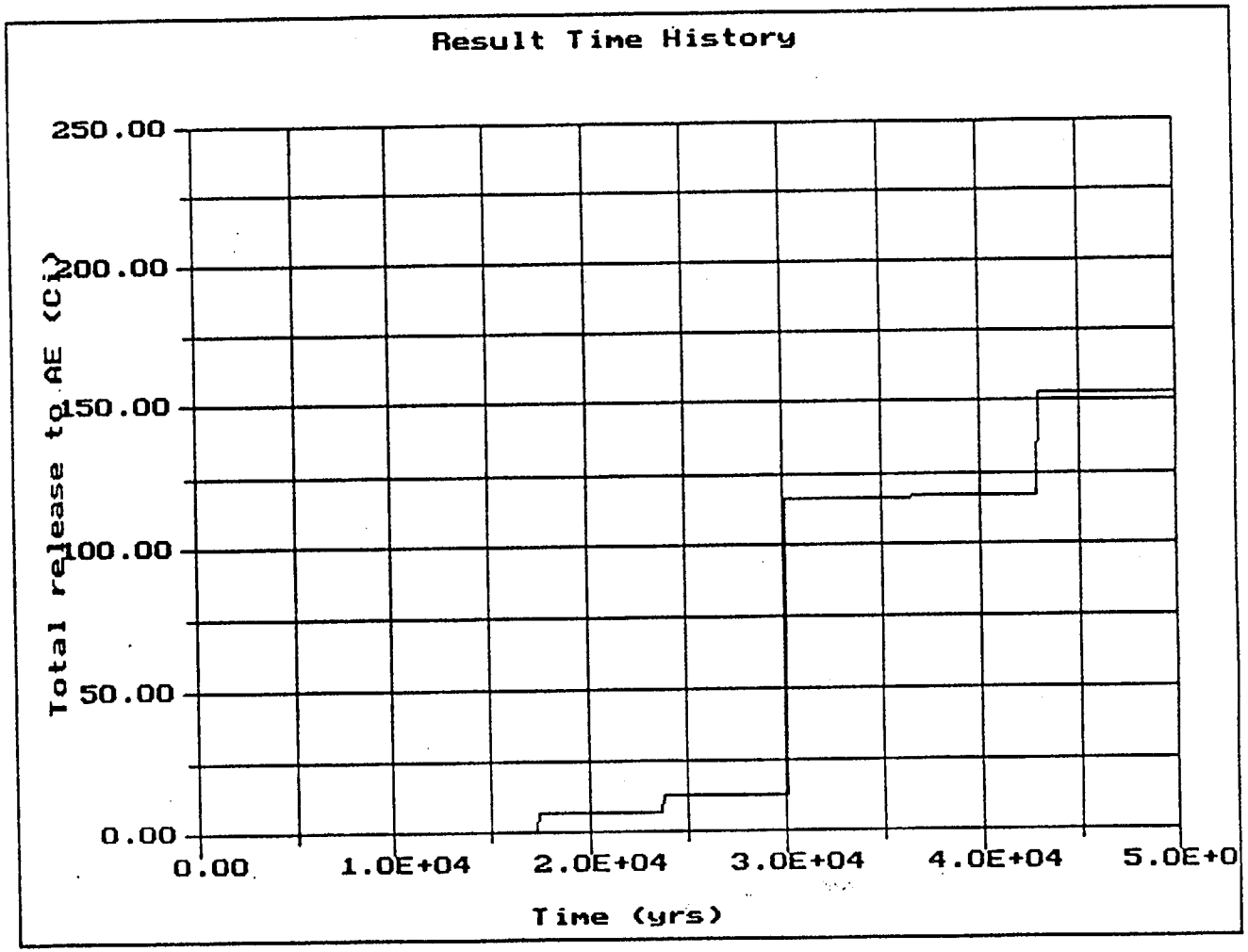

Figure C-8c. Nuclide Release Rate at the Bottom of Column 1 (Layers 3 and 5 in Single Mode): RIP Simulations

Table C-1. Total Releases at Bottom of Columns 1 and 6

Column	Total Releases (Ci)		
	Infiltration (mm/yr)	Coupled	Not Coupled
1	1	*1.85×10^6 +(4.56×10^6)	1.72×10^6 (4.47×10^6)

* TOSPAC
\+ RIP